1974

Hydrodynamic Properties Of Two And Three Phase Fluidized Beds

Sang Done Kim

HYDRODYNAMIC PROPERTIES OF TWO AND THREE PHASE FLUIDIZED BEDS

by

Sang Done Kim

Faculty of Engineering Science

Submitted in partial fulfillment
of the requirements for the degree of
Doctor of Philosophy

Faculty of Graduate Studies
The University of Western Ontario
London, Canada

April, 1974

ABSTRACT

The hydrodynamic properties of two (liquid-gas, liquid-solid) and three (liquid-gas-solid) phase fluidized beds have been studied in a large two dimensional column.

A wide variety of liquids and three different solids were employed. Air was used as the gas phase throughout the study.

The effects of liquid velocity (0.090-0.335 ft/sec), gas velocity (0.0-0.854 ft/sec), liquid viscosity (1-70 cp) and surface tension (39.8-72.8 dyne/cm) and particle size (1-6 mm) on the individual phase hold-ups, bed expansion, liquid phase axial mixing and bubble characteristics were measured.

Individual phase hold-ups were measured using a pressure profile technique. In liquid-gas beds, the liquid hold-up decreased with increasing liquid and gas velocity. The effect of liquid viscosity and surface tension on the individual phase hold-ups was found to be insignificant.

In liquid-solid beds, the liquid hold-up increased with increasing liquid velocity, viscosity and with decreasing particle size and was independent of liquid surface tension.

In three phase beds, the liquid hold-up increased with increasing liquid velocity, viscosity and surface tension and with decreasing particle size, whereas it decreased with increasing gas velocity. The gas hold-up increased with gas velocity and decreased with liquid surface tension. However, in general, the gas hold-up was nearly independent of liquid velocity and viscosity.

The bed porosity increased with increasing liquid velocity,

viscosity and decreased with increasing particle size. For solids having a minimum fluidizing velocity below around 0.042 ft/sec in the liquid, the bed contracted upon injection of small amounts of gas. However, the reverse trend was found for beds of solids having a minimum fluidizing velocity above 0.042 ft/sec.

Liquid phase axial mixing coefficients were measured using two tracer techniques, namely pulse and step injection. Liquid phase axial mixing increased with increasing gas velocity and decreased with increasing liquid flowrate in liquid-gas beds. In liquid-solid beds, it increased with increasing liquid velocity and decreasing particle size. In three phase beds, it increased with increasing liquid and gas velocity and with decreasing particle size.

Bubble rising velocity and size were measured by movie photography. In liquid-gas beds, the bubble size and rising velocity increased with increasing gas velocity and decreased with increasing liquid velocity. The bubble size distribution narrowed with increasing liquid velocity; the reverse trend was observed with increasing gas velocity. The effect of liquid viscosity on bubble size and rising velocity was minimal. However, decreasing surface tension was found to increase both the bubble size and rising velocity. In three phase beds, these parameters increased with increasing gas velocity and decreasing surface tension but were nearly independent of liquid velocity. The bubble size distribution widened somewhat with increasing liquid velocity in the beds of larger particles. In contrast, the reverse trend was observed in the beds of smaller particles.

Bubble size decreased with increasing particle size.

The wake volume was determined from a material balance in three phase beds. It increased with decreasing bubble size, gas velocity and particle size. Plots of the ratio of the wake to gas volume against liquid velocity went through a maximum. The liquid velocity at which the maximum value of this ratio occurred increased with increasing particle size.

The existence of two distinct types of three phase fluidization is proposed, namely "bubble-coalescing" and "bubble-disintegrating". The former occurs with particles smaller than a critical size and with high viscosity liquids; the latter is observed with larger particle sizes.

Correlations are given for individual phase hold-ups, bed expansion, liquid phase axial mixing coefficient and bubble characteristics. These are applicable to industrially realistic flow conditions.

ACKNOWLEDGEMENTS

The author wishes to express his sincere gratitude to Dr.C.G.J. Baker and Dr. M.A. Bergougnou to whom he is deeply indebted for their valuable guidance and continuous encouragement throughout the period of this study.

Appreciation is also expressed to many others who offered encouragement and interest in the project.

Finally, thanks are owed to the Ontario Provincial Goverment for a fellowship and the National Research Council of Canada for a grant in aid of research to Dr. C.G.J. Baker.

TABLE OF CONTENTS

LIST OF TABLES

LIST OF FIGURES

LIST OF APPENDICES

NOMENCLATURE

a	empirical constant
A	column cross sectional area
A_b	bubble area
C	concentration
d	diameter
D	diffusion coefficient
D_L	axial diffusion coefficient
D_{mo}	average bubble diameter immediately above the nozzle
D_{mzz}	average bubble diameter at a distance z from the nozzle
F	tracer response to unit step input
Fr	Froude number, $V^2/d_p g$
g	gravitational acceleration
g_c	dimensional constant
G	volumetric gas flowrate
H	expanded bed height or height of test section
HMU	height of liquid phase axial mixing unit
Ho	unfluidized bed height
k	empirical constant
K	empirical constant or fluid consistency index
ℓ	average individual bubble length
L	liquid volumetric flowrate
m	empirical constant
M	empirical constant
n	empirical constant or fluid behaviour index

N	empirical constant
P_b	bed pressure
Pe	Peclet number , VH/D
P_i	power input
Q	volumetric flowrate
R	rate of production
Re	Reynolds number
Re_t	Reynolds number based on particle terminal velocity
R_ℓ	specific weight of pure liquid
Ro	specific weight of liquid-solid beds
t	time
V	velocity
V_B	bed volume
V_{br}	relative bubble rising velocity
V_t	particle terminal velocity
V'_ℓ	actual velocity of the liquid flowing through the interstices of particles
W	weight of solid particles
We	Weber number, $V_g \gamma / \sigma$
We_m	modified Weber number , $V_g^2 \rho_\ell d_h / \sigma$
X_1	height of the top of the column
X_m	sampling point
X_o	height of injection point

Greek letters

γ	generalized viscosity constant, $g_c K 8^{n-1}$
ϵ	average bed porosity defined as the volume of gas and liquid phases

ε_i	average volume fraction (or hold-up) of phase i in the column
μ	abosolute viscosity of liquid
μ_a	apparent viscosity of liquid
ρ_i	density of phase i
σ	surface tension of liquid
σ^2	second moment about mean

Subscripts

b	bubble
c	continuous phase or column
f	fluid
g	gas phase
h	hydraulic
i	dummy index or refer to system i, i=1 liquid-gas beds, i=2 liquid-solid beds, i=3 liquid-gas-solid beds
ℓ	liquid phase
mf	minimum fluidization
p	particle
s	solid phase
w	wake phase

Superscripts

-	mean value

CHAPTER 1

INTRODUCTION

1.1. TWO PHASE FLUIDIZATION

When a fluid flows upwards through a bed of solid particles, several different flow regimes are observed as the velocity of the fluid is increased. At low flowrates, the fluid merely percolates through the interstices between stationary particles in the bed. In this, the fixed bed regime, the pressure drop across the bed increases proportionally with the fluid velocity. With increasing flowrate, the particles move apart and a few vibrate and move about in restricted regions. At a still higher fluid velocity, a point is reached where all the particles are just suspended in the upward flowing gas or liquid. At this point the frictional force between the particles and fluid counterbalances the effective weight of the particles and the pressure across the bed becomes equal to the effective weight of the particles per unit area. This condition is referred to as the point of incipient fluidization and the velocity at which it occurs is termed the minimum fluidizing velocity. An increase in the fluid velocity above this point results in an expansion of the bed. This continues with increasing velocity until the latter attains the terminal velocity of the smallest particles which are entrained by the fluid and form a dilute phase above the main bed.

As the velocity is increased still further, the surface of the bed becomes diffuse as it enters the pneumatic transport regime.

The above discussion is applicable when the fluid phase is either a liquid or a gas. However, the characteristics of both the solid and the fluid determine whether the fluidization is "Particulate" or "Aggregative". A description of these states is given below.

1.1.1. Particulate and Aggregative Fluidization

Aggregative fluidization (figure 1.1.A), which normally occurs when a bed of solids is fluidized by a gas, is characterized by the formation of large bubbles in the bed. The particles appear to act not as individual units but rather as aggregates having no discernible free path. At higher gas flowrates, the bubbles may grow in size until their frontal diameters become essentially equal to the diameter of the containing vessel. This state, which is termed "slugging", is especially pronounced in beds having large height to diameter ratios.

In particulate fluidization (figure 1.1.B), which typically occurs when particles are fluidized by a liquid or a gas under high pressure, the bed height increases smoothly with fluid velocity but large scale bubbling and fluctuations are not observed. Under such conditions the particles are discretely separated from each other and

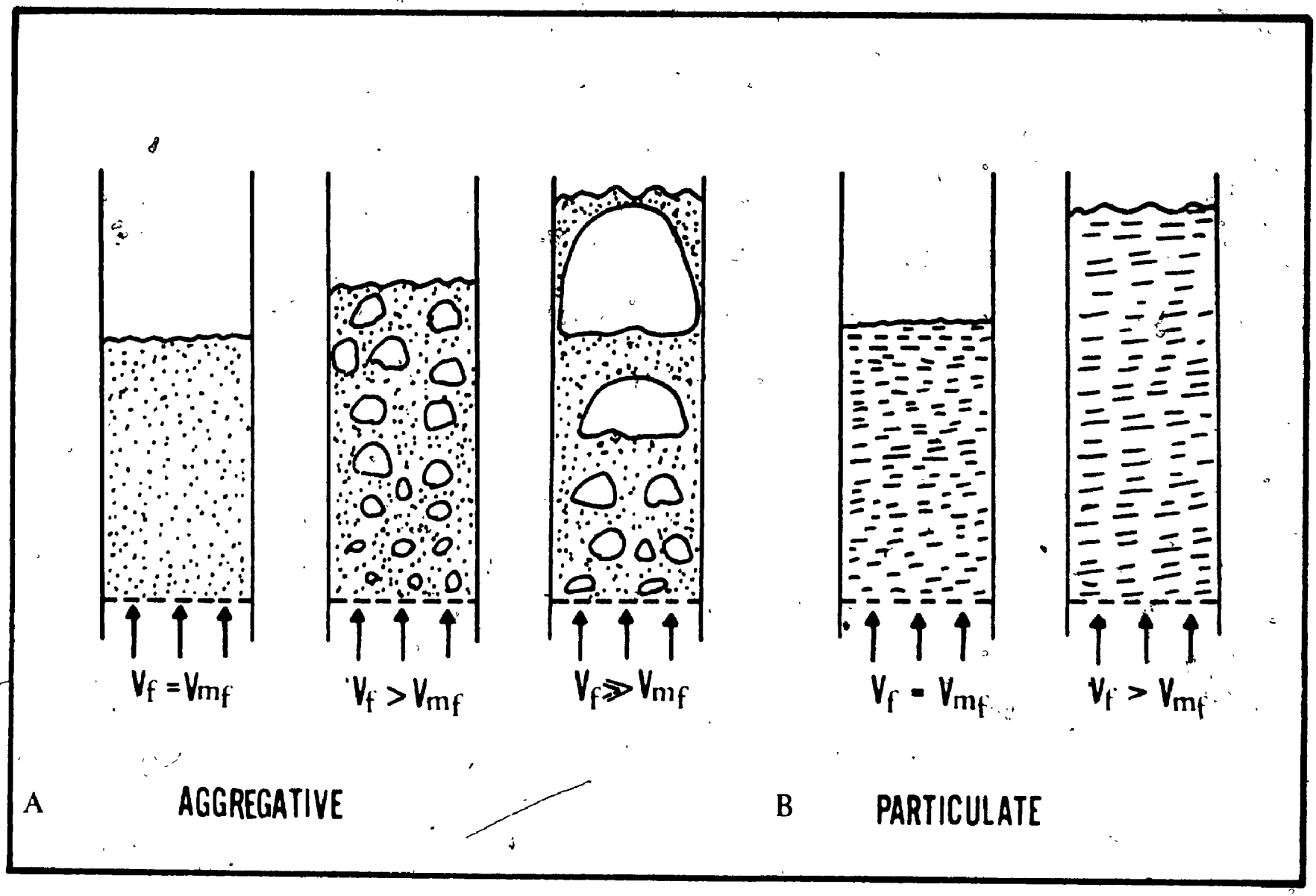

Figure 1.1. States of Fluidization

exhibit a mean free path, which appears to increase with fluid velocity (30,32).

On the basis of empirical data, Wilhelm and Kwauk (71) suggested that the value of the Froude number, $V_f^2/d_p g$, in which V_f is the superficial velocity of the fluid, d_p is the particle average diameter and g is the gravitational constant, is indicative of the type of fluidization.
For Froude numbers less than unity, fluidization is said to be particulate. Froude numbers exceeding unity are said to be characteristic of aggregative fluidization. However, there does not appear to be a sharp demarkation between these two types of fluidized bed behaviour.

After extensive studies on both aggregative and particulate fluidization, Simpson and Rodger (58) found that there was no fundamental mechanical difference between a liquid fluidized bed and a gas fluidized bed. A gas bed normally contains a comparatively small number of large bubbles and appears to fluidize aggregatively. In contrast, a liquid bed may contain a large number of small bubbles and exhibit particulate fluidization characteristics. The question of precisely what causes the differences between aggregative and particulate fluidization is still largely unanswered. However, generally speaking, there is a tendency towards aggregative fluidization in systems in which there is a large solid-fluid density difference. For small differences, the trend is toward particulate fluidization.

1.1.2. Advantages and Disadvantages of Fluidization

Fluidized beds, which are employed largely as chemical reactors in industry, have both desirable and undesirable characteristics.

The advantages are:

1) The smooth, liquid-like flow of fluidized particles permits easy handling of solids
2) The rapid mixing of solids leads to almost perfectly isothermal conditions throughout the reactor.
3) Heat and mass transfer rates between the fluid and the particles are high compared to other modes of contacting.
4) The circulation of solids between two fluidized beds makes it possible to transport the vast quantities of heat produced or required in large reactors.
5) It is suited to large scale operations.
6) The rate of heat transfer between a fluidized bed and internals, such as cooling coils, is high.

The disadvantages are:

1) Large variations from plug flow and the bypassing of solids by bubbles readily occur.
2) The rapid mixing of solids in the bed leads to a nonuniform distribution of particle residence times in the reactor.
3) Because of solids carry over by the gas bubbles, known as entrainment, the installation of devices such as cyclones to recover the fines is normally necessary.

4) Errosion of internals and the vessel by particles can be serious.

5) A catalyst may undergo attrition, or size reduction.

6) For non-catalytic operations at high temperature, the agglomeration and sintering of the fine particles can necessitate a lowering of the operating temperature thereby reducing the reaction rate considerably.

Despite some of its serious drawbacks, the compelling advantages and overall economy of fluidized bed contacting have been responsible for its successful use in many industrial operations. However, operating success does not come easily and is only achieved by a thorough understanding of these deficiences and by a deliberate effort to overcome them so that the advantages prevail. The successful use of the fluidized beds in a wide variety of industrial operations is evidence that this can be done.

1.2. THREE PHASE CONTACTING OPERATIONS

For reaction systems in which the liquid is not readily vaporized, the gas is not easily liquefied, and a catalyst is required to enhance the rate of reaction, three phase contacting is necessary.

A number of types of industrial unit may be employed to obtain the desired contact between the three phases. These may be grouped into two main classes, depending upon the state of motion of the solid particles.

In the first class, the particles form a fixed bed, and the fluid phases move either cocurrently or countercurrently through the bed. Two types are of industrial interest here, namely trickle flow and bubble flow reactors. In trickle flow reactors, a film of liquid flows downwards over the surface of the particles and the gas forms the continuous phase. A typical example of this type of operation (hydrodesulphurization) is described by Van Deemter (63).
In bubble flow reactors, the liquid hold-up is relatively high, and the gas forms the dispersed bubble phase.

In the second class of operations, the particles are suspended in the liquid by the transfer of momentum from the liquid or gas phase. In one example, the bubble column slurry reactor, momentum is transferred to the liquid phase by the movement of gas bubbles alone. The liquid medium is stationary in most instances, and the operation is usually carried out in columns having a large height to diameter ratio. This technique is normally employed for the batchwise conversion of a liquid reactant, or for promoting a continuous reaction between gaseous reactants. A typical example of this type of operation is the hydrogenation of topped crude oil (28).
In stirred-slurry reactors, momentum is transferred to the liquid phase by mechanical stirring as well as by the movement of gas bubbles. Small particles are used in most cases, and the operation is usually carried out in tank reactors having small height to diameter ratios. The operation is in widespread use in both batch and continuous processes involving

liquid reactant such as the hydrogenation of unsaturated fats and fatty oils (4).

Other types of three phase contacting devices in this category are the turbulent bed contactor and the spouting bed. In turbulent bed contactors, spherical particles of low density, typically made of hollow polystyrene foam, are fluidized by the upward flow of gas and irrigated by downward flowing liquid. This operation is used industrially for the absorption of gases in liquids, for the scrubbing of gases containing particles, and for the cooling and dehumidification of gases (21,22). In spouting beds, the liquid and gas enter the column through an opening in the apex of a conical inlet. The entrance is so abrupt that there is essentially no opportunity for the fluids to distribute themselves over the total cross section of the column. Hence a central channel is formed in which the solids are entrained upward. They disengage at the top of the bed and recirculate downwards in the region of the column wall. Recent research on spouted three phase beds has been reported by Vukovic et al.(69).

Yet another type of reactor in this category, the gas-liquid (or three phase) fluidized bed, is the subject of this research. In three phase fluidization, the particles are fluidized by the cocurrent flow of liquid and gas. The gas forms a discrete bubble phase and the liquid a continuous phase containing the solid particles as shown in figure 1.2. The operation may be used for the continuous processing of liquid as well as gaseous reactants and relatively large

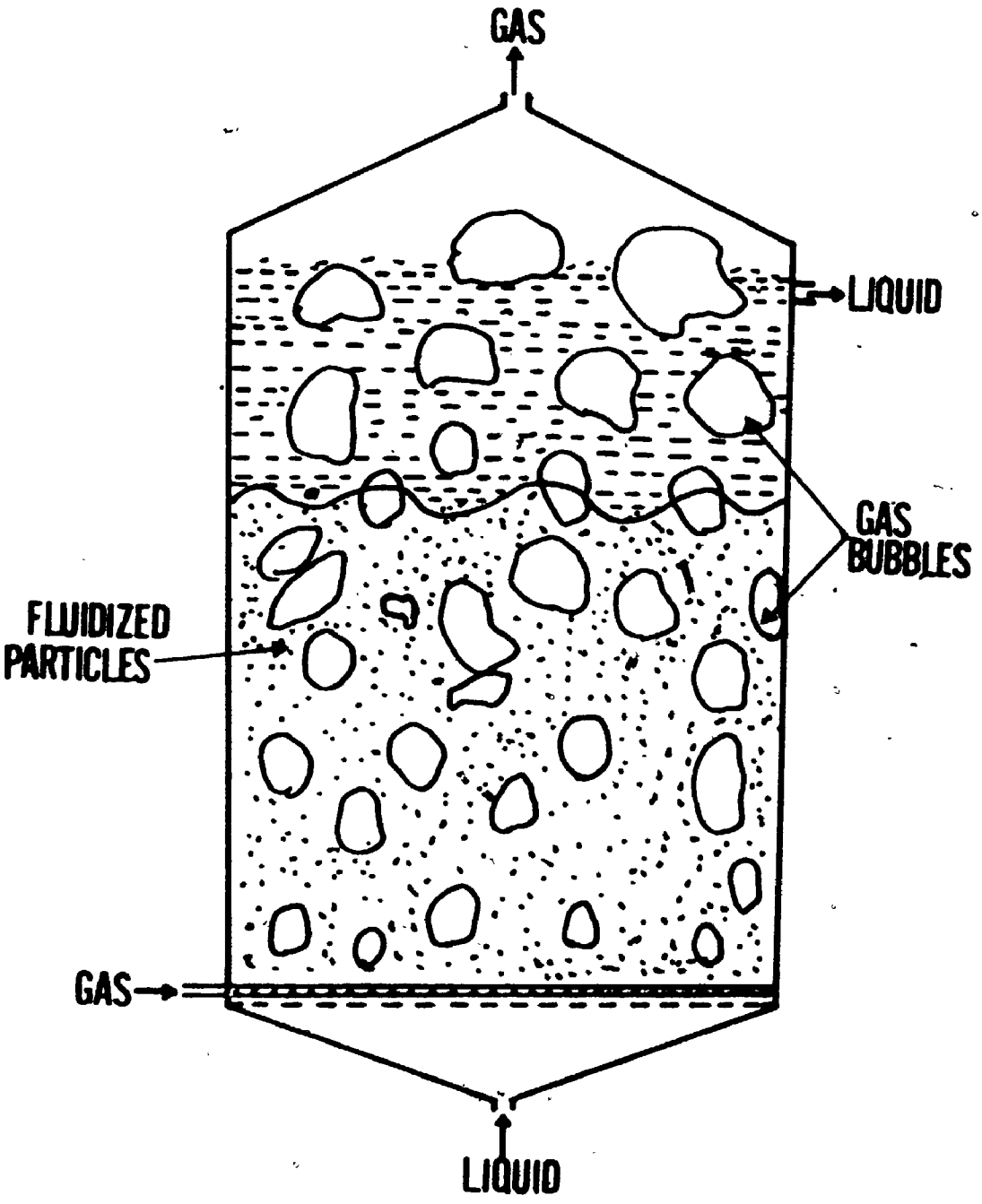

Figure 1.2 THREE PHASE FLUIDIZED BED

particles can be employed. Three phase fluidization has been examined to a considerable lesser extent than most of the other liquid-gas-solid operations, presumably because of its relatively recent development and industrial application.

Under certain circumstances, three phase fluidization has several advantages over the other types of reactor described above. There is excellent contacting between reactants and catalyst due to the turbulent mixing inside the reactor, and a relatively low pressure drop across the bed even at high flowrates. As the liquid flow is increased the bed height increases but there is a negligible increase in the pressure drop. Equilibrium of temperature is easily maintained and controllable throughout the bed because of the high hold-up of liquid which act as a heat sink. Exothermic reactions can be conveniently controlled by cooling recycled liquid. Catalyst can be added or withdrawn continuously, thereby eliminating the need for costly shutdowns for catalyst replacement. Attrition of the catalyst is insignificant since the particles are cushioned by the liquid. The unit is very flexible in operation; particles with different physical and chemical properties can be usually handled sucessfully by modifying the process conditions.

1.3. INDUSTRIAL APPLICATIONS OF THREE PHASE FLUIDIZATION

Three phase fluidized beds have been developed by Hydrocarbon Research Inc. and Cities Service Oil Co. (11-14, 26, 56, 65) for the treatment of residual feedstocks and

other heavy fractions using the H-Oil and Hy-C cracking processes. In these, residuum and distillate stocks are catalytically hydrogenated and desulphurized to yield distillates. Basically the two processes are very similar. A fixed amount of catalyst contained within a chemical reactor is expanded somewhat in excess of its settled volume by the cocurrent flow of oil and hydrogen. One of the differences between the two processes is in selection of the catalyst used. Employing generally cleaner feedstocks, Hy-C cracking justifies the use of conventional catalysts of somewhat higher unit cost, usually having a more highly developed acidic function than those used in the H-Oil process. The catalysts normally used are cobalt molybdate and nickel molybdate particles 0.08 mm in diameter. Characteristic reaction conditions in both processes are a temperature of 650-1100°F and a pressure of around 1500 psig.

Adlington and Thomson (1) also described a pilot plant study on a hydrodesulphurization process for the treatment of residual fuel oils in a small, high temperature, high pressure three phase fluidized bed reactor. Experiments were carried out in a 1 in. diameter column with cobalt molybdenum alumina catalyst at temperatures between 720 and 800°F and a pressure of 500 to 1000 psig. Two runs were carried out, the first with a low space velocity, high gas rate and high oil recycle ratio and the second with a high space velocity, low gas rate and no liquid recycle. From this study, they determined

rates of mass transfer and derived a relationship between the fractional desulphurization and the oil recycle ratio.

Volpicelli and Massimilla (67,68) have proposed the use of a three phase fluidized bed in the production of "calcium bisulphite" for the pulp and paper industry. They investigated the chemical behaviour of fluidized limestone (0.6-10 mm), sulphur dioxide, and water in model reactors having internal diameters of 45 and 140 mm. From the experiments, they found that the rates of limestone dissolution per unit volume of bed were about two orders of magnitude greater than those obtained in a conventional Jenssen tower. The latter is a fixed bed absorber in which the limestone packing promotes contact between the gas and the liquid as well as providing the base for partially salting the acid solution.
The more numerous industrial applications of trickle flow reactors, bubble flow reactors, stirred-slurry reactors and turbulent bed contactors have been reviewed by Østergaard (40,41).

1.4. OBJECTIVES OF THIS STUDY

The effectiveness of a three phase fluidized bed as a chemical reactor may be determined largely by its hydrodynamic properties. Most of the studies reported to date have been carried out using small particles in small diameter beds, even though it is well known that small and large beds behave so differently that extrapolation up to the commercial scale can be quite unreliable. This is particulary true in the

case of reactors. The present work was therefore undertaken to obtain additional information on the hydrodynamics in a comparatively larger bed and to attempt to clarify apparently conflicting information in the literature.

In the design of catalytic reactors, a knowledge of the hold-up of individual phases, the degree of mixing of each phase and the gas bubble behaviour is necessary to estimate the rates of both the chemical reaction and physical operations such as mass and heat transfer.

In the present study, the effects of liquid and gas velocity, particle size, and liquid surface tension and viscosity on the liquid and gas phase hold-ups, the bed expansion, axial mixing of the liquid phase, and the bubble characteristics in three phase beds have been investigated. For the sake of comparison , experiments were also carried out in liquid-gas and liquid-solid fluidized beds.

CHAPTER 2

PREVIOUS STUDIES

In contrast to the field of gas, and to a lesser extent, liquid fluidization, there have been relatively few studies on three phase fluidization over the past ten years. However, the following properties of three phase fluidized beds have been studied in some depth: liquid and gas hold-ups, bed expansion, bubble characteristics, mass transfer across the gas-liquid interface, mixing of the liquid and gas phases, and heat transfer between the wall and the bed. In the majority of these studies, which are reviewed in this chapter, model systems with air as the gas phase, tap water as the liquid phase and either sand or glass beads as the solid phase were used.

2.1. BED EXPANSION AND BED POROSITY

Since bed expansion and bed porosity (or fraction of the bed volume occupied by both liquid and gas) are directly related, both these topics are reviewed in the same section.

2.1.1. Liquid-Solid Fluidized Beds

The height of an expanded particulate (liquid-solid) fluidized bed may be calculated from a knowledge of the liquid hold-up. The latter may be estimated from the empirical

correlation of Richardson and Zaki (51):

$$\varepsilon_{\ell_2} = (V_\ell / V_t)^{1/n} \qquad .....(2.1)$$

where V_ℓ is the superficial velocity of the liquid, and V_t is terminal velocity of the average particle. The exponent n is dependent on the particle Reynolds number Re_t based on the terminal velocity, $V_t d_p \rho_f / \mu$, and the ratio of the particle and column diameters (d_p/d_c) :

$$n = [4.35 + 17.5(d_p/d_c)]\ Re_t^{-0.03} \qquad 0.2 < Re_t < 1 \quad ..(2.2)$$

$$n = [4.45 + 18.0(d_p/d_c)]\ Re_t^{-0.1} \qquad 1 < Re_t < 200..(2.3)$$

$$n = 4.45\ Re_t^{-0.1} \qquad 200 < Re_t < 500..(2.4)$$

$$n = 2.39 \qquad Re_t > 500..(2.5)$$

The above equations were derived from the results of experiments carried out in columns 1.5 and 2.4 in. in diameter containing particles ranging in size from 0.253 to 6.35 mm fluidized by a wide variety of liquids.

2.1.2. Liquid-Gas-Solid Systems

In many instances three phase fluidized beds containing fine particles exhibit rather surprising expansion characteristics. In a bed of particles fluidized by a liquid only, the bed height increases progressively with increasing liquid flowrate. However, if the liquid velocity is maintained constant

and a small amount of gas is injected into the bed, its height may initially diminish.

Stewart and Davidson (59) studied this phenomenon in two dimensional beds of 0.46 mm glass ballotini, and iron and lead shot fluidized by water and air. They observed that when a bubble rose through the liquid fluidized bed, it was followed by a certain volume of liquid which was almost free of particles. This liquid may be thought of as a wake, or a stabilized liquid bubble, rising with the air at a velocity much greater than that of the liquid passing through the interstices in the bed. Thus the liquid in the bubble wakes has a much smaller residence time than that passing through the bulk of the bed. This results in a reduction of the average superficial liquid velocity and a consequent reduction in the liquid hold-up which, at low gas velocities, more than offsets the added hold-up of the gas. However, at high gas rates, the bed again expands as a result of increased gas hold-up.

Østergaard and Theisen (43) also studied the expansion of beds of glass ballotini fluidized by air and water in 2 and 4 in. diameter columns. Particle diameters were varied from 0.28 to 2.2 mm. The reduction of bed porosity upon injection of gas was observed for all particle sizes studied. This was again explained by the presence of wakes as described

above. From their experimental observations, they noted that the contraction increased as the particle size was reduced and the height to diameter ratio of the bed was increased.

In deriving a semi-theoretical model of three phase fluidized beds, Østergaard (44) assumed that the wakes move at the same velocity as the bubbles and contain the same concentration of solids as the continuous liquid phase. The bed porosity ε is related to liquid and gas hold-ups:

$$\varepsilon = \varepsilon_{\ell_c} (1 - \varepsilon_g) + \varepsilon_g \qquad .....(2.6)$$

in which the liquid hold-up in the continuous phase $\varepsilon_{\ell c}$ can be calculated from Richardson and Zaki's correlation, equation (2.1). The gas hold-up ε_g was calculated from the following expression obtained from a material balance in bubbly flow:

$$\varepsilon_g = V_g / V_b \qquad .....(2.7)$$

where V_g is the superficial gas velocity and V_b is the bubble rising velocity. The latter was obtained from a modified version of Nicklin's equation for stagnant liquid-gas beds(36):

$$V_b = 21.7 - 4.6 \ln V_g + V'_\ell \qquad .....(2.8)$$

In equation (2.8), V'_ℓ is the actual velocity of the liquid flowing through the interstices of the bed and was calculated from a material balance on the liquid flowing across unit area of the cross section:

$$V_\ell = V'_\ell \ (1 - \varepsilon_g - \varepsilon_w) + V_b \ \varepsilon_w \ \varepsilon_{\ell c} \qquad ....(2.9)$$

where ε_w is the fraction of the bed volume occupied by the bubble wakes. This was empirically correlated by the equation:

$$\varepsilon_w = 0.14 \ \varepsilon_g^{1/2} \ (V'_\ell - V_{mf}) \qquad ....(2.10)$$

where V_{mf} is the minimum fluidizing velocity of in the liquid. Values of bed porosity predicted from the above equation (2.6) were compared with the experimental data of Turner (60) and of Stewart and Davidson (59). The agreement between the calculated values of ε and Turner's experimental data was better than 6 %. However, there was a discrepancy between the calculated values of bed porosity and Stewart and Davidson's results for 30-36 mesh glass beads of more than 10 %. The data obtained by these authors for beds containing lead and iron shot did not fit the above equations.

The same line of approach to predict the wake volume, in three phase fluidized beds, was employed by Rigby and Capes (53). Experiments were carried out in a 15 cm x 45 cm x 0.7 cm two dimensional bed containing 0.775, 0.47 or 0.29 mm particles fluidized by air and water. The bed porosity was calculated from measurements of the expanded bed height. Since Østergaard assumed that the solid content of the wakes was identical to that of the continuous liquid phase and Stewart and Davidson found the wakes to be almost free of solids, these authors derived the following equations

for calculating the hold-up of wakes.

For wakes containing solids:

$$\epsilon_w = \frac{V_\ell(1 - \epsilon_g) - V'_\ell}{V_\ell - V_b\epsilon_\ell} \qquad .....(2.11)$$

For solids-free wakes

$$\epsilon_w = \frac{V'_\ell - V(1-\epsilon_g)}{V_b - V_\ell} \qquad .....(2.12)$$

Values of ϵ_w calculated from equations (2.11) and (2.12) were compared to those obtained experimentally by photographic observations and found to be substantially in agreement. They found that the ratio of wake volume to bubble volume increased with increasing particle size and liquid velocity and with decreasing gas flowrate, all of which correspond to a decrease in the bubble size. The bubble wakes were found to consist not only of a stable portion carried upward by the bubbles but also of vortices shed by the bubbles. They again concluded from this study that the contraction of a liquid fluidized bed on introducing small amounts of gas was caused by the presence of wakes.

Recently, Bhatia and Epstein (8) reported a generalized wake model for three phase fluidized beds. Experiments were carried out to test the model in beds of solids having a diameter range of 0.25 - 3 mm and a density range of 2.5 - 11.1 g/cm^3. The fluidizing medium was a cocurrent flow of air and either water, aqueous glycerol (2.1 cp) or aqueous polyethylene (63 cp). The experiments were performed in 2 cm

and 5.1 cm diameter transparent columns. The expanded bed height was obtained from longitudinal pressure drop profiles measured along the column wall.

Gas hold-ups were determined by direct volumetric measurements using fast closing valves. For the larger column these were supplemented by measurements of the static pressure drop gradient, and in a few cases, by electro-resistivity probe measurements.

In the model developed by Bhatia and Epstein (8), the solids content of the wakes was allowed to vary from zero to the value prevailing in the particulate phase based on the assumptions of Østergaard and of Stewart and Davidson. In order to calculate the gas hold-up and the bed porosity using this model, eight equations were proposed to solve eight unknowns. Using a numerical trial and error technique, in general, the best agreement with experiment was obtained by assuming that the wakes were solids-free. However, some initially dense beds proved to be an exception at high gas rates. The agreement between the experimental data for 1 mm glass beads and the model was better than 10 % even though the model was not strictly applicable to beds of small light particles. From their experimental observations, the following general conclusions were drawn: fluidized beds of small light particles were found to contract on the introduction of gas, the degree of contraction depending mainly on the initial bed height. At high gas flows, a dilute phase above the main region of the bed was formed, the height of which increased

with gas flowrate, until it ultimately reached the top of the column. At this point a systematic elutriation of solid particles was recorded. With light solids increasing the particle size reduced the degree of bed concentration. For large, heavy particles, introduction of gas caused the liquid fluidized bed to expand. The transition from bubbly to slug flow at higher gas flowrates gave rise to a measureable reduction in the bed height, but subsequent increases in gas flowrate caused the bed to expand again. The three phase fluidization of particles in the Stokes's law regime failed to produce a steady bed, since a systematic elutriation was observed for gas flowrates as low as 1 cm/sec. However, the experimental results did indicate that these beds also expand on introduction of the gas phase.

Efremov and Vakhushev (23) also measured the bed porosity in three phase fluidized beds using a pressure drop technique. Experiments were carried out with beds of 0.32, 0.61, 0.97, 1.47 and 2.15 mm glass beads having a density of 2.46 g/cm^3 fluidized by the cocurrent flow of water and air in a 10 cm diameter column. The following empirical equation was proposed to calculate the bed porosity in three phase fluidized beds:

$$\varepsilon = \left(\frac{V_\ell - KW}{V_t}\right)\left(1 - \varepsilon_g - K\varepsilon_g\right)^{1-n} + \varepsilon_g(1+K) \qquad \ldots(2.13)$$

in which V_ℓ, V_t, and W are the liquid flowrate, the particle terminal velocity, and the weight of solid particles, respectively. K is an empirical coefficient defined by the

equation:

$$K = 5.1\ \varepsilon_{\ell 2}^{4.85}\ [1 - \tanh(40\frac{W}{V_\ell}\varepsilon_{\ell_2}^{10} - 3.32\ \varepsilon_{\ell 2}^{5.45})]\ ..(2.14)$$

where $\varepsilon_{\ell 2}$ is the liquid hold-up in liquid-solid system. The deviation between their experimental data and equation (2.13) was within 5 %.

Dakshinamurty et al.(15,16) measured the bed porosity of three phase fluidized beds of rockwool shot, glass beads, iron shot and sand. Water and kerosene were used as the liquid phase, air as the gas phase, and experiments were carried out in a 5.6 cm diameter glass column.

The effect of particle size and density, liquid surface tension and viscosity, and the flowrates of both gas and liquid on the bed porosity were studied. The size and density of the particles were varied from 1 to 6.8 mm and 2.4 to 7.7 g/cm^3. The gas and liquid flowrates ranged from 0.1 to 7.5 cm/sec, and from 1 to 20 cm/sec, respectively. The reduction in bed porosity of the bed on injection of a swarm of gas bubbles was observed in the beds of rockwool shot and small glass beads fluidized both by water and kerosene. In beds of 1.0 and 2.1 mm sand particles, the contraction was observed only with water while with the other particles, no such contraction occurred.

Two correlations were developed to predict the bed porosity in three phase fluidized beds:

For $Re_t \geq 500$

$$\varepsilon = 2.65\ (V_\ell/V_t)^{0.6}\ (\mu\ V_g/\sigma)^{0.08}\ \ ....(2.15)$$

For $Re_t < 500$

$$\epsilon = 2.12 \left(V_\ell / V_t \right)^{0.41} \left(\mu \, V_g / \sigma \right)^{0.08} \quad \ldots(2.16)$$

where V_t, V_ℓ, μ , and σ are the particle terminal velocity, liquid superficial velocity, liquid viscosity and surface tension, respectively.

Equations (2.15) and (2.16) showed average deviations of 4.6 and 4.4 % from the experimental data, respectively.

It is of interest to note that the authors claimed that Østergaard's correlation only fitted their data for particles smaller than 3.3 mm at low gas flowrates.

Recently, Bhatia et al.(7) reported the effect of solid wettability on bed porosity. Experiments were carried out in a 2 cm diameter glass column using air as the gas phase, distilled water as the liquid phase, and 1 mm glass beads as the solid phase. In order to render the particles non-wettable, they were coated with a Teflon spray. With the uncoated glass beads, the bed exhibited the familiar contraction upon injection of gas. In contrast, the bed containing the Teflon-coated beads expanded. It was suggested that this was the result of the non-wettable solids being able to contact the gas phase instead of being wholly immersed in the liquid.

From the above studies, the following general observations may be made. An initial contraction in bed volume occurs on injection of air into beds of wettable particles smaller than about 2.5 mm fluidized by water. This effect becomes more marked as the particle size is decreased. With particle

sizes larger than 2.5 mm, the bed expands. However, small non-wettable particles exhibit anomalous behaviour in that they initially expand on introducing gas into the bed.

2.2. LIQUID AND GAS PHASE HOLD-UPS

The hold-up of a phase in a mutiphase bed is defined as the fraction of the bed volume occupied by that phase. In the case of a three phase bed, the phases are liquid, gas and solid.

Adlington and Thompson (1) reported values of the gas hold-up in three phase beds of aluminum particles having sizes ranging from 0.3 to 2.75 mm fluidized by air and either water or white spirit. Experiments were carried out in a 3 in. diameter column. They observed that the gas hold-up was independent of the liquid flowrate, increased with height above the column base, and increased markedly with gas rate. The presence of solids had little effect on the gas hold-up below a superficial velocity of 0.05 ft/sec. At higher gas velocities, it was decreased by the presence of solids, particulary in the denser beds prevailing at lower liquid rates.

Gas hold-ups at constant expanded bed height were measured by Viswanathan et al. (66) in beds of 0.469 and 0.928 mm quartz particles and 4 mm glass beads fluidized by tap water and air. These authors also measured the gas hold-up in water-air bubbling beds for comparison with the three phase systems. They observed that, at the same fluid velocities,

the gas hold-up in the beds of glass beads was higher than that in the liquid-gas system whereas the reverse was true in the beds of quartz particles. The hold-up data in three phase beds were correlated using Bankoff's model (5) which was derived for a liquid-gas bed:

$$(\varepsilon_\ell + \varepsilon_g) / \varepsilon_g = (Q_\ell / KQ_g) + (1 / K) \quad \ldots.(2.17)$$

where Q_ℓ and Q_g are the liquid and gas volumetric flowrates and K is an empirical parameter.

Sherrard (37) also measured the hold-up of gas emerging from the expanded bed using a γ-ray absorption technique. In his experiments, 6 mm glass beads, 6 mm acrylic spheres, 12-14 mesh lead shot and 12-14 and 36-44 mesh glass beads were fluidized by the cocurrent flow of water and air in a 2.5 in. square perspex column. He found that the gas hold-up decreased with increasing liquid flowrate in the beds of 6 mm glass beads and lead shot whereas it was independent of liquid flowrate in the beds of 12-14 and 36-44 mesh glass beads.

Michelson and Østergaard (36,37) investigated the effect of the fluid velocities and particle size on the hold-ups of liquid and gas in liquid-gas and three phase systems. Their experiments were carried out with beds of 0.25, 1.0, 3.0, and 6.0 mm glass beads fluidized by water and air in columns of 6 in. and 8.5 in. diameter. As tracers they employed Bromine-82 in the liquid phase and Argon-41 in the gas phase. They observed that the gas hold-up increased

with increasing gas velocity. For the solids-free system and for beds of 3 and 6 mm glass beads, the gas hold-up was nearly proportional to the superficial gas velocity, whereas in beds of 0.25 and 1 mm particles, the hold-up increased somewhat more slowly. The gas hold-up also decreased with increasing liquid velocity in the beds of 6 mm glass beads and in the solids-free bed. However, in beds of small particles, it increased with increasing liquid velocity. The influence of liquid velocity was more marked in the beds of 6 mm particles than in the solids-free bed. The liquid hold-up decreased with increasing gas flowrate in all cases.

Efremov and Vakhrushev (21) measured the gas hold-up in beds of 0.32, 0.61, 0.97, and 2.15 mm glass beads, also fluidized by water and air, in a 10 cm diameter column using a pressure drop technique. They found that the gas hold-up did not depend on the diameter or the total cross sectional area of the nozzles used to introduce the gas into the bed. When the gas and liquid flowrates were maintained constant, the gas hold-up decreased as the quantity of particles charged to the bed increased. The gas hold-up in the three phase fluidized beds was correlated with the gas hold-up in liquid-gas bubble beds, ε_{g1}, and the ratio of the specific weights of the pure liquid and the bed fluidized by liquid alone, R_l/R_o. The resulting equation was:

$$\varepsilon_g = \varepsilon_{g1} \, (R_l/R_o)^{1.22} \qquad .....(2.18)$$

Vail et al. (61) also studied the gas content of three phase fluidized beds. Experiments were carried out in a column 14.6 cm in diameter containing either glass beads (0.73 mm), aluminum silicate (0.77 mm) or alumocobalt-molybdenum (0.74 mm) particles fluidized by air and water. The gas hold-up was determined by simultaneously cutting off the water and air flows and subsequently recording the steady-state height established by the liquid surface. The gas hold-up was correlated with the liquid and gas superficial velocities and the solids hold-up in three phase fluidized bed as follows:

$$\varepsilon_g = K\ (1 - \varepsilon_s)^M\ (V_g/V_\ell)^N \qquad \ldots.(2.19)$$

In this equation, K,M and N are empirical constants which varied with the properties of the solids and ranged from 0.0526 to 0.1026, 0.63 to 0.78, and 1.69 to 2.09, respectively. The value of these constants increased as the ratio of the gas to liquid superficial velocities increased, and decreased with increasing solids hold-up. These authors also found that the gas hold-up in three phase fluidized beds was independent of the live cross sectional area of the distributing screens.

Recently Razumov et al. (50) reported measurements of the liquid and solid hold-ups in three phase fluidized beds. Experiments were carried out in beds of 0.82 mm quartz particles fluidized by air and water in a 30 cm diameter column. The concentration of the solid phase was determined by means of a capacitance probe attached to one of the arms of a capacitance

bridge. The hold-up of the liquid phase was determined in a column 9 cm in diameter by simultaneously cutting off the liquid and gas flows. Two empirical correlations were proposed for predicting the solid and liquid hold-ups in three phase fluidized beds. The equations are as follows:

$$\varepsilon_s = 0.578 - 3.198\ V_\ell - 0.538\ V_g \qquad \ldots(2.20)$$

and

$$\varepsilon_{\ell s} = 0.422 + (0.135\ V_\ell / d_p^{0.562}) - 1.82\ V_g \qquad \ldots(2.21)$$

where V_ℓ, V_g are the liquid and gas superficial velocities and d_p is the particle diameter.

The deviation between the experimental and calculated results were less than 7 % and 10 % for equations (2.20) and (2.21), respectively. From the above two equations, it can be noted that the solid hold-up decreased with increasing liquid and gas velocities, and the liquid hold-up increased with increasing liquid velocity and decreasing particle size and gas velocity.

Bhatia (9) also measured the gas hold-up in the three phase fluidized beds described above (p.19). From the experimental observations, the following general conclusions were reported. The gas hold-up increased with increasing gas flowrate. However, the effect of liquid flowrate on gas hold-up appeared to be either small or negligible. Comparison of the data for liquid-gas beds with that of three phase beds indicated that the presence of solids reduced the gas hold-up.

2.3. BUBBLE CHARACTERISTICS

Among the earlier works on bubble characteristics in three

phase fluidized beds is that of Massimilla et al. (33). These authors investigated the dependency of bubble size, rising velocity and coalescence on the initial and expanded bed heights, particle diameter and density, gas flowrate, bed porosity, and gas nozzle diameter. Experiments were carried out with atmospheric air as the gas phase, tap water as the liquid phase, and 0.026 mm iron sand, glass beads (0.077 and 0.11 mm) and 0.022 mm silica sand as the solid phase. Two air injection nozzles having internal diameters of 0.04 in. and 0.015 in. were tested. Experiments were performed in two columns. For photographic studies, a 4 ft high bed of 3.4 in. x 2.4 in. rectangular cross section was used. Measurements of bubble rising velocity were carried out in a 3.5 in. diameter bed 5.2 ft high.

The average size of the bubbles emerging from the fluidized bed was determined from the still photographs of the bed surface. For the bubble rising velocity measurements, a stopwatch was used to measure the time interval between bubble injection and emergence from the fluidized bed. The coalescence of two rising bubbles was also investigated.

Their results showed that the mean bubble diameter increased as the gas flowrate, the distance from the nozzle, and the expanded bed height increased. The bubbles reached an equilibrium size which was not dependent on the injection nozzle diameter. The following correlation was obtained:

$$\frac{D_{mzz} - D_{mo}}{z} = a \left(\frac{Ho}{\Delta H}\right)^b \qquad \ldots\ldots(2.22)$$

in which D_{mzz} is the average bubble diameter at a distance z from the nozzle, D_{mo} is the average bubble diameter immediately above the nozzle, Ho/ΔH is the reciprocal of the fractional bed expansion. The experimental values of the numerical coefficient a and b were 0.0027 and 1.3 respectively. The rate of coalescence decreased with increasing bed expansion and the bubble rising velocity increased with increasing bubble diameter in all the beds.

The growth of air bubbles at a single orifice in a 25 x 25 x 50 cm^3 bed of sand particles fluidized by tap water was studied by Østergaard (42). Experiments were carried out with a 3 mm i.d. orifice with air flowrates varying from 9 to 63 cm^3/sec. The bubble frequency at the orifice was measured by an electrical resistance probe connected to an oscilloscope. The oscilloscope screen was photographed and the bubble frequency determined by counting the number of peaks.
The rate of coalescence, markedly dependent on bed porosity, was relatively high near the point of minimum fluidization and decreased as the liquid flowrate was increased. The bubble frequency at the bed surface did not change significantly with bed height, and it was concluded that coalescence occurs mainly within a relatively short distance from the orifice.
This is in agreement with the results of Massimilla et al.(33). Visual observation indicated that the shape of the emerging bubble was markedly dependent on the liquid velocity. At lower liquid rates, the bubbles leaving the bed were spherical, but were transformed above the surface, with or without disintegration, to a spherical cap form. The bubble was accompanied by a

turbulent wake of liquid and solids. At higher liquid rates, the emerging bubbles had a spherical cap form which was either not tranformed at all above the bed surface, or transformed only by a small reduction of the included angle. Again, the bubbles were accompanied by extensive wakes containing solid particles, the concentration of which was lower than that observed at the lower liquid velocities.

Further studies on bubble size in three phase fluidized beds have been carried out by Sherrard (57) who employed a light transmission technique for the purpose.
Five different beds of particles having widely differing properties were used. He claimed that a particle Weber number

$$We_p = \frac{\rho_p V_b^2 d_p}{\sigma} \qquad \ldots\ldots(2.23)$$

greater than 3 will bring about bubble breakage rather than coalescence provided the bubble diameter is larger than that of particles. Two correlations were derived from the experimental data.

For particles larger than the bubbles ($d_p > d_b$):

$$d_b = 0.7 \frac{\sigma^{0.6}}{\rho_\ell^{0.2} (P_i/V_B)^{0.4}} \qquad \ldots(2.24)$$

where ρ_ℓ, P_i and V_B are the liquid density, power input to the bed and bed volume, respectively.

For bubble sizes approximately equal to the particle size ($d_p = d_b$) :

$$V_b^2 d_{b_o} = 10980/Re_p^{0.5} \qquad \ldots.(2.25)$$

where Re_p is the Reynolds number based on particle diameter.
His results showed that the bubble size decreased with increasing liquid flowrate and with increasing particle diameter.

Rigby and co-workers (52) measured the size, frequency, rising velocity, and size distribution of gas bubbles in a 10 cm three phase fluidized bed containing one of three different sizes of glass beads or Ottawa sand. The fluidizing media were atmospheric air and tap water. The bubble characteristics and the local gas hold-up were measured by an electro-resistivity probe. Bed viscosity was also determined to assess its effect on the bubble rising velocity. Their results led to the following conclusions. In the lower region of the bed, bubble frequency distributions exhibit a peak in the region between $x/r = 0.4-0.75$ where x is the radial distance from the bed axis and r is the bed radius. At higher levels, the peak moves towards the centre of the bed and coalescence of bubbles occurs as they pass through the bed resulting in an increase in bubble size with height.

An increase in liquid flowrate resulted in a decrease in bubble size. The rising velocity of a bubble in a freely bubbling bed increased with bubble size and was found to be dependent mainly on the expanded bed height.

A satisfactory correlation of the data was obtained using the following equation:

$$V_b - \left(\frac{G}{A} + \frac{L}{A}\right)\left(\frac{1-\varepsilon}{\varepsilon}\right)^2 = 32.5(\ell)^{1.53} \quad \ldots\ldots(2.26)$$

where G/A and L/A are volumetric gas and liquid flowrates per unit cross sectional area of the column, ε is the bed porosity and ℓ is the average individual bubble length.

Recently Page and Harrison (48) measured the size distribution of gas bubbles leaving a three phase fluidized bed by photography. They investigated the influence of changes in liquid and gas flowrates and in gas distributor design on the size of the bubbles. The experiments were carried out in a circular glass column 22.8 cm in diameter containing 0.5 mm sand particles fluidized by water and air.
Two types of gas distributor were used to produce bubbles of different initial size. They found experimentally that the size of bubbles leaving the surface of the bed was reduced by an increase in liquid velocity and, at lower values of the latter, was reduced by an increase in gas flowrate. Away from the gas distributor, its design did not effect the bubble size distribution.

Generally all of above researchers found that the bubble size increased with increasing gas velocity. However, the effect of liquid flowrate on bubble size is not well defined, presumably because of the unusual expansion characteristics of three phase fluidized beds.

2.4. GAS AND LIQUID PHASE MIXING

Liquid and gas phase mixing is of importance in determining the rate of heat, mass and momentum transfer in three phase fluidized beds. A knowledge of these factors is essential for the good engineering design of liquid-gas-solid reactors.

Schügerl (55) reported the results of mixing experiments carried out in two and three phase fluidized beds. Helium, carbon dioxide and sodium chloride solution were

used as tracers. The intensities of diffusive and convective mixing in the radial direction in both fluid phases were estimated. The interaction between phases in air-solid, water-solid, and air-water-solid fluidized beds was also determined. A 13.5 cm diameter column and five different particles having mean diameters in the range 0.04-0.5 mm were employed. In the bubble columns, axial mixing in the gas phase was caused solely by the non-uniformity of the bubble velocities. It was also influenced by the rate of coalescence and redistribution of the bubbles, which caused a convective lateral mixing and diminished the non-uniformity of the flow velocity perpendicular to the flow direction. There was no diffusive backmixing in the flow direction since the gas phase was dispersed in the liquid phase. In the three phase systems, axial mixing in the gas phase was also caused by non-uniformity of the bubble velocities. Bubble coalescence and redistibution which occur perpendicular to the direction of flow diminished the non-uniformity of the gas velocity. In the liquid phase of the bubble columns axial mixing is very intensive and governed by diffusion. In the liquid phase of three phase fluidized beds the axial mixing was also very pronounced and also caused mainly by diffusion.

In both bubble columns and three phase fluidized beds, the apparent diffusive mixing coefficients in the gas phase were about a hundred times greater than those in the liquid phase. However, the gas and liquid phase Peclet (or Bodenstein) numbers were nearly equal, since the gas flowrates were much

higher than those of the liquid. Liquid and gas phase Peclet numbers increased with increasing liquid and gas velocities in both beds. The presence of the solid particles increased the relative intensity of mixing in the liquid phase but had little effect on gas mixing.

A further study on liquid and gas phase mixing in three phase fluidized beds was reported by Afschar and Schügerl (3). Their experiments were carried out in a bench scale column 13.5 cm in diameter and 311 cm high. Water, air and 0.25 mm quartz particles comprised the three phases. The longitudinal and radial concentration profiles of carbon dioxide tracer in both fluid phases were measured upstream of a stationary source. Employing a two phase diffusion model, Peclet numbers describing backmixing and mass transfer between the phases were evaluated. The mass transfer coefficient and the intensity of backmixing were found to decrease with increasing gas flowrate in both two and three phase systems. However, they increased with increasing liquid flowrate in the three phase beds.

Michelson and Østergaard (36,37) also investigated liquid and gas phase mixing in two and three phase fluidized beds. They employed beds of 6 and 8.5 in. internal diameter using air, water and four different sizes of glass beads ranging from 0.25 to 6 mm in diameter. Bromine 82, in the form of ammonium bromide solution, and argon 41 were used as the liquid and gas phase tracers respectively. The tracer response was measured by two pairs of symmetrically arranged scintillation

detectors shielded by lead mantles. Correlations were derived from the experimental data for each particle size with liquid and gas superficial velocities as parameters. They observed that particle size played an important role in governing the intensity of axial mixing in three phase fluidized beds. The beds of 6 mm particles were characterized by a very low degree of liquid phase mixing which was independent of the gas flowrate and increased slightly with increasing liquid velocity. Also the gas phase axial mixing was rather small except at very high gas flowrates which resulted in slug formation. In the beds of 3 mm glass beads, the degree of mixing in the liquid phase was also very low and decreased with increasing gas velocity. At increased gas velocities bubble coalescence became important and a sharp increase in the degree of mixing was observed. Gas phase mixing was pronounced in the coalescence regime, but was very low in the break-up regime. The beds containing 0.25 and 1 mm particles were characterized by a high degree of mixing. Its intensity increased rapidly with decreasing liquid flowrate and increasing gas flowrate.

Vail et al. (61) studied turbulent mixing of the liquid phase in two and three phase fluidized beds in a column 3.75 ft. in diameter and 4.9 ft. high. Air was used as the gas phase, tap water as the liquid phase, and spheres having a density of 2.7 g/cm^3 and an average diameter of 0.87 mm as the solid phase. Sodium chloride solution was used as a tracer and the response was determined

by titration of the chloride ion. They observed that the tracer concentration profile in the axial direction was approximately logarithmic in form in the zone of observation and that an increase in the gas velocity intensified longitudinal mixing whereas an increase in the liquid velocity reduced it. The presence of solid particles considerably reduced longitudinal mixing of liquid phase. An increase in the kinetic energy of the jets of the liquid and gas entering the working zone of the reactor increased longitudinal mixing but not proportionally to the velocity. The irregularity of the concentration field of the tracer over the diameter of the bed in the three phase bed increased with increasing liquid flowrate but decreased with increasing gas rate. These effects became less marked as the live cross section of the grid was increased.

2.5. MASS TRANSFER

The main application of three phase fluidization appears to be in promoting heterogeneous catalytic reactions involving liquid and gases. Mass transfer across the liquid-gas interface is one of the possible rate controlling mechanisms and as such is of fundamental interest.

A study on mass transfer in three phase fluidized beds has been carried out by Massimilla et al. (34) who used silica sand particles having an average diameter of 0.22 mm and glass ballotini of average diameter 0.5 and 0.8 mm.

Columns of 30 and 90 mm internal diameter having heights ranging from 100 to 1200 mm were used. The rate of absorption of carbon dioxide in water from a mixture of carbon dioxide and nitrogen was measured. They found that the absorption rate increased with increasing particle size at all liquid velocities. The absorption rates were lower in three phase beds than in liquid-gas beds. The difference was explained as being due to a higher rate of bubble coalescence and, consequently, to a lower gas-liquid interfacial area in the three phase fluidized beds.

Østergaard and Suchozebrski (45) studied the effects of particle size and of liquid and gas flowrates on gas-liquid mass transfer. Their experiments were carried out in a bed 4 in. in diameter, using tap water as the liquid phase, and a mixture of carbon dioxide and nitrogen as the gas phase. Volumetric mass transfer coefficients were calculated for liquid-gas fluidized beds and for bubble columns by assuming that axial mixing of the fluid phase was negligible. Beds of 6 mm particles were characterised by high rates of gas-liquid mass transfer, beds of 1 mm particles by low rates, and bubble columns by rates of intermediate magnitude. The volumetric mass transfer coefficients increased with increasing gas flow-rate, but were relatively insensitive to liquid flowrates. The latter finding contrasts with that of Massimilla et al. (34). The reason for this difference could be the different particle sizes which may have different effect on bubble

characteristics. They also found that the mass transfer coefficients decreased with increasing distance from the distributor plate in bubble columns and in beds of 1 mm particles. However, in beds of 6 mm particles they passed through a maximum at different heights above the distributor.

Østergaard and Fosbøl (46) recently reported measurements of the rate of mass transfer of oxygen across the gas-liquid interface in three phase fluidized beds.
Tap water was used as the liquid phase, pure oxygen as the gas phase, and 1 mm and 6 mm diameter glass ballotini as the solid phase. The column diameter and height were 4 in. and 9.54 ft, respectively. High values of the absorption coefficient were obtained in the beds of 6 mm particles, low values in the beds of 1 mm particles, and values of intermediate magnitude in bubble columns. The superficial liquid velocity had no significant effect on the absorption rate in the beds of 6 mm particles and in bubble columns. However, in beds of 1 mm particles, an increase in the liquid velocity caused a marked increase in the absorption coefficient. Shallow beds of large particles exhibited particulary high mass transfer rates. The above findings are generally in good agreement with previous studies (34,45).

Most recently, Dakshinamurty et al. (17) again measured rates of absorption of oxygen in water in three phase fluidized beds containing particles of different size (2.1 to 6.8 mm) and density (2.4 to 11.2 g/cm^3) contained in a glass column 5.6 cm in diameter and 68 cm in length. It was observed that the

mass transfer coefficient increased with increasing particle size and density due to bubble disintegration. Their data also showed that the mass transfer coefficient increased with increasing gas flowrate and was independent of the liquid velocity. The data were correlated by Reynolds and Weber numbers. From the results of this study, they claimed that higher mass transfer coefficients were obtained under conditions favoring bubble disintegration. In general, above findings are in good agreement with those of Østergaard et al. (45,46). However, the effect of liquid velocity on mass transfer differs from the findings of Massimilla et al. (34). Again this discrepancy could be due to the different particle sizes employed in these studies or a difference in the rate-controlling resistance.

2.6. HEAT TRANSFER

Since chemical reactions frequently involve the evolution or absorption of large amounts of energy, a knowledge of heat transfer characteristics is extremely important in reactor design. The small number of studies on heat transfer in three phase fluidized beds are reviewed below.

Østergaard (47) measured the rate of heat transfer between the wall and the bed in a 3 in. diameter column containing 0.5 mm glass ballotini. The fluidizing media were air and water. It was observed that the heat transfer coefficient for a liquid fluidized bed operated close to the point of minimum fluidisation could be approximately doubled by the

injection of gas. However, at higher liquid velocities, only small increases in the heat transfer coefficient were obtained.

Viswanthan et al. (66) also measured heat transfer coefficients in a 2 in. diameter bed of quartz particles (0.649 and 0.928 mm mean diameter). The particles were fluidized by the cocurrent flow of water and air. The amount of solids as well as the liquid and gas velocities were varied in such a manner as to maintain the same expanded bed height throughout the experiments. From plots of the heat transfer coefficient against the ratio of the mass flowrates of gas and liquid, they observed that the heat transfer coefficient increased sharply to a maximum at low values of this parameter and then fell off again as the gas-liquid ratio was increased. They also observed from experiments on beds containing 0.928 mm quartz particles that for a given set of conditions, there existed a critical bed weight of solid that gave a maximum transfer coefficient.

Van Driesen and Stewart (65) measured the temperature at various locations in a commercial-scale two stage catalytic desulphurization and hydrocracking unit. The maximum temperature difference in the first reactor was only $4^{o}F$ and in the second reactor was only $2^{o}F$. These results indicated that three phase fluidized bed reactors are characterized by high internal heat transfer rates.

CHAPTER 3

EXPERIMENTAL

3.1. MATERIALS

The solids used in this study were 6.0 mm glass beads (Fisher Scientific Co.), 2.6 mm gravel and 1.0 mm glass beads (B. Braun Melsungen), the properties of which are summarized in Table 3.1. The weights of the different solids loaded into the column are also shown in this table.

Details of the fluidizing liquids are given in Table 3.2. In order to determine the effect of liquid viscosity on the bed hydrodynamics, tap water and various strength solutions of sugar and of sodium carboxymethyl cellulose (CMC) were employed. The solutions were prepared by dissolving commercial grade sugar and CMC in tap water.

The viscosities of the Newtonian sugar solutions were measured with a falling ball viscometer (Hoeppier Viskometer BH 59223) fitted with a glass ball having a density of 2.39 g/cm^3. A Brookfield Synchrolectric viscometer model LVT was used to determine the apparent viscosity of the pseudoplastic CMC solutions. The viscometer was fitted with a Brookfield U.L. adapter to determine the shear stress at a given shear rate for the lower viscosity solutions (3.7 - 20 cp). An LV-1

TABLE 3.1.

PROPERTIES OF THE SOLIDS

MATERIAL	PARTICLE DIAMETER (mm)	APPARENT DENSITY (g/cm^3)	WEIGHT OF SOLIDS IN BED (lbs)
GLASS BEADS	1.0	2.95	17.5
GRAVEL	2.6 (7-8 mesh)	2.52	34.0
GLASS BEADS	6.0	2.30	29.0

TABLE 3.2

PROPERTIES OF THE LIQUIDS

SOLUTIONS	Density (g/cm^3)	Viscosity (cp)	n	Surface tension (dyne/cm)
Water	1.00	1.00	1.00	72.8
Water-Acetone (10 Vol.%)	0.99	1.11	1.00	60.0
Water-Acetone (20 Vol.%)	0.98	1.26	1.00	50.2
Water-Acetone (40 Vol.%)	0.96	1.43	1.00	39.8
Water-Sugar (25 Wt. %)	1.09	2.37	1.00	72.9
Water-Sugar (36 Wt. %)	1.15	4.64	1.00	75.5
Water-Sugar (42 Wt. %)	1.17	7.60	1.00	75.9
Water-Sugar (50 Wt. %)	1.23	12.77	1.00	68.8
Water-CMC (0.09 Wt. %)	1.004	*5.70	0.976	72.8
Water-CMC (0.10 Wt. %)	1.004	*6.30	0.971	72.8
Water-CMC (0.15 Wt. %)	1.003	*13.00	0.927	73.0
Water-CMC (0.17 Wt. %)	1.002	*20.00	0.916	73.3
Water-CMC (0.35 Wt. %)	1.001	*70.00	0.914	73.8

*Apparent Viscosity

spindle was used for measurements on the higher viscosity solutions. The solutions exhibit power law behaviour throughout the concentration range studied as shown in figure 3.1. The temperature of the solutions was maintained at 22°C during all viscosity measurements by means of a Neslab temperature controller.

Technical grade acetone-water mixtures were employed to examine the influence of liquid surface tension which was measured by a capillary rise method (24).

The minimum fluidizing velocities of the solids were measured using the technique described in Appendix A. The results of these experiments are given in Table 3.3.

3.2. EQUIPMENT

Experiments were carried out in the 96 in. high x 26 in. wide x 1 in. thick two dimensional column shown in figures 3.2 and 3.3. The main section of the column was constructed from 0.75 in. plexiglass sheets separated by 1 in. square aluminum formers and indented O-ring seals. An approximately constant dynamic liquid level was maintained in the column by means of an outlet weir situated 78 in. above the grid. The liquid flowed over the weir into a 25 in. wide x 6 in. high x 3 in. thick box from which it exited through a 1.25 in. diameter outlet pipe. A brass screen (4,8 or 16 mesh, depending on particle size) was attached across the weir to prevent the loss of particles.

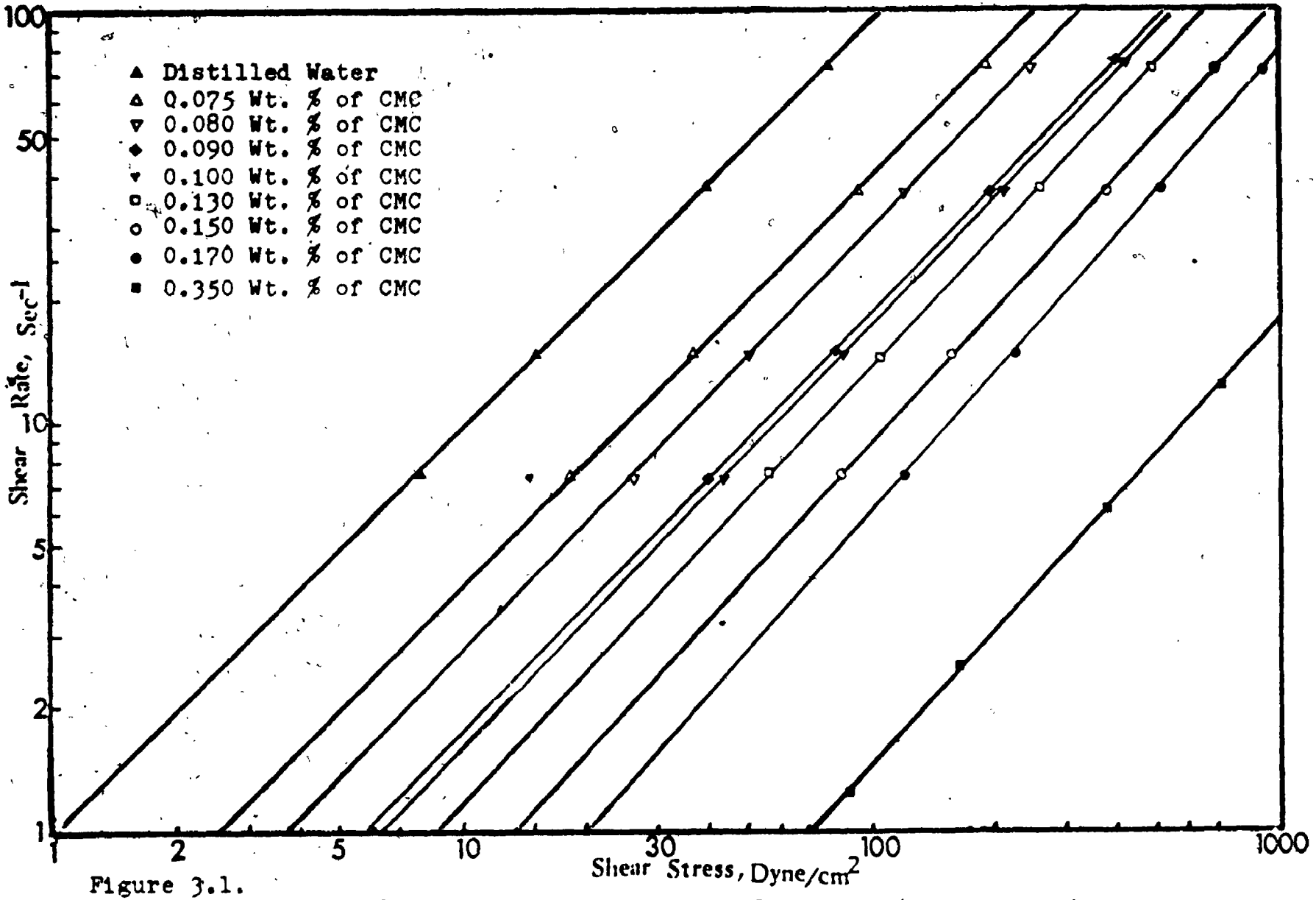

Figure 3.1.

Fluid-flow Curves for CMC Solutions (logarithmic)

TABLE 3.3.

MINIMUM FLUIDIZING VELOCITY

LIQUIDS	PROPERTIES	6 mm GLASS BEADS	2.6 mm GRAVEL	1 mm GLASS BEADS
WATER	μ_ℓ= 1.0	0.170	0.065	* 0.042
	σ_ℓ= 72.8			
ACETONE-	σ_ℓ= 39.8	0.169	0.064	* 0.042
WATER	σ_ℓ= 50.2	0.170	0.065	* 0.042
	σ_ℓ= 60.0	0.170	0.065	* 0.042
SUGAR-	μ_ℓ= 2.37	0.158	0.056	* 0.019
WATER	μ_ℓ= 4.64	0.125	0.042	* 0.015
	μ_ℓ= 7.60	0.118	* 0.034	* 0.010
	μ_ℓ=12.77	0.091	* 0.026	-
CMC-	μ_ℓ= 3.70	-	-	* 0.023
WATER	μ_ℓ= 5.70	-	-	* 0.017
	μ_ℓ= 6.30	-	-	* 0.014
	μ_ℓ= 8.50	0.128	* 0.042	-
	μ_ℓ=13.00	0.104	-	-
	μ_ℓ=20.00	0.083	* 0.018	-
	μ_ℓ=70.00	* 0.041	-	-

where V_{mf} is ft/sec, μ_ℓ ; cp σ_ℓ ; dyne/cm

* Bed contraction upon injection of gas.

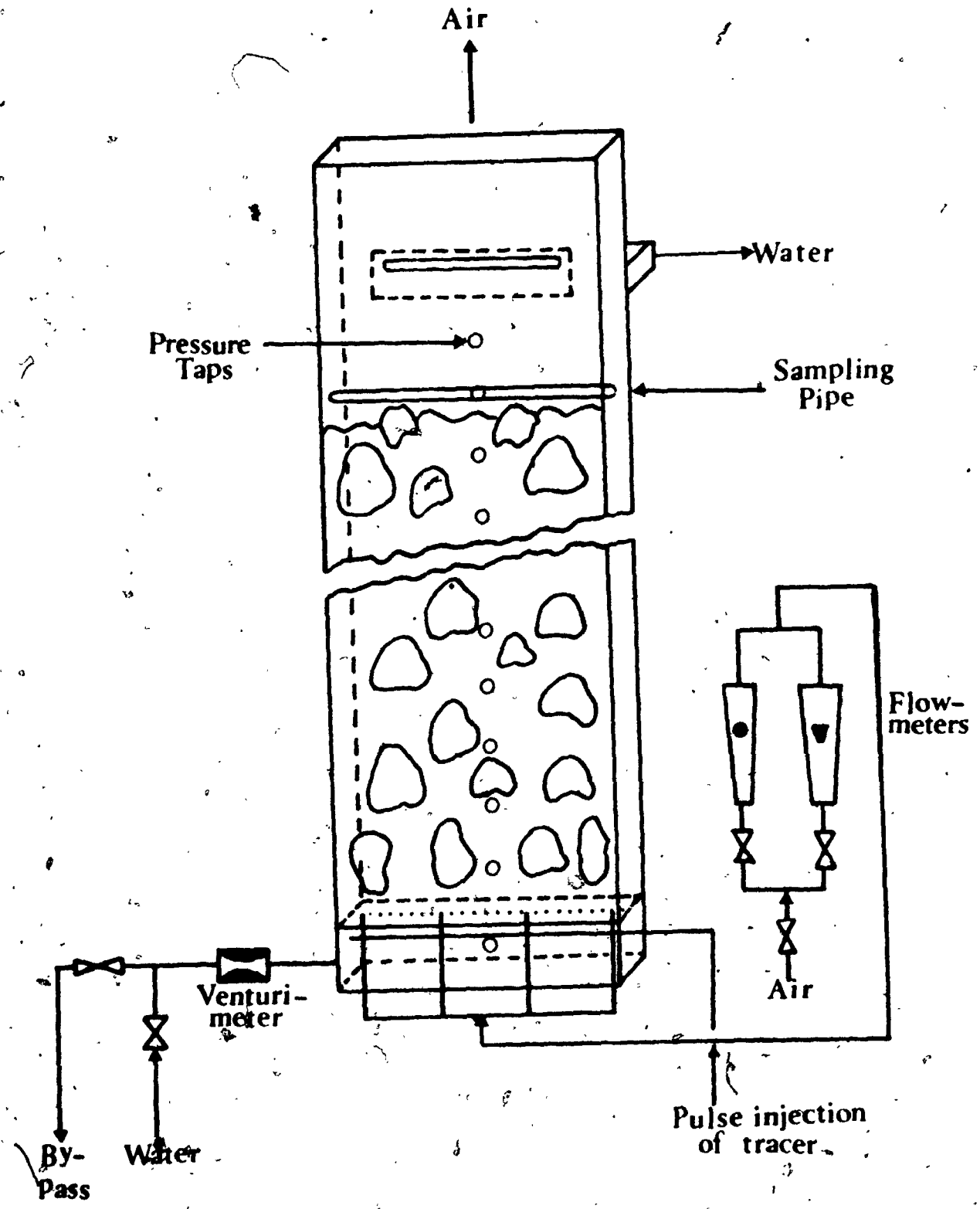

Figure 3.2. THE COLUMN

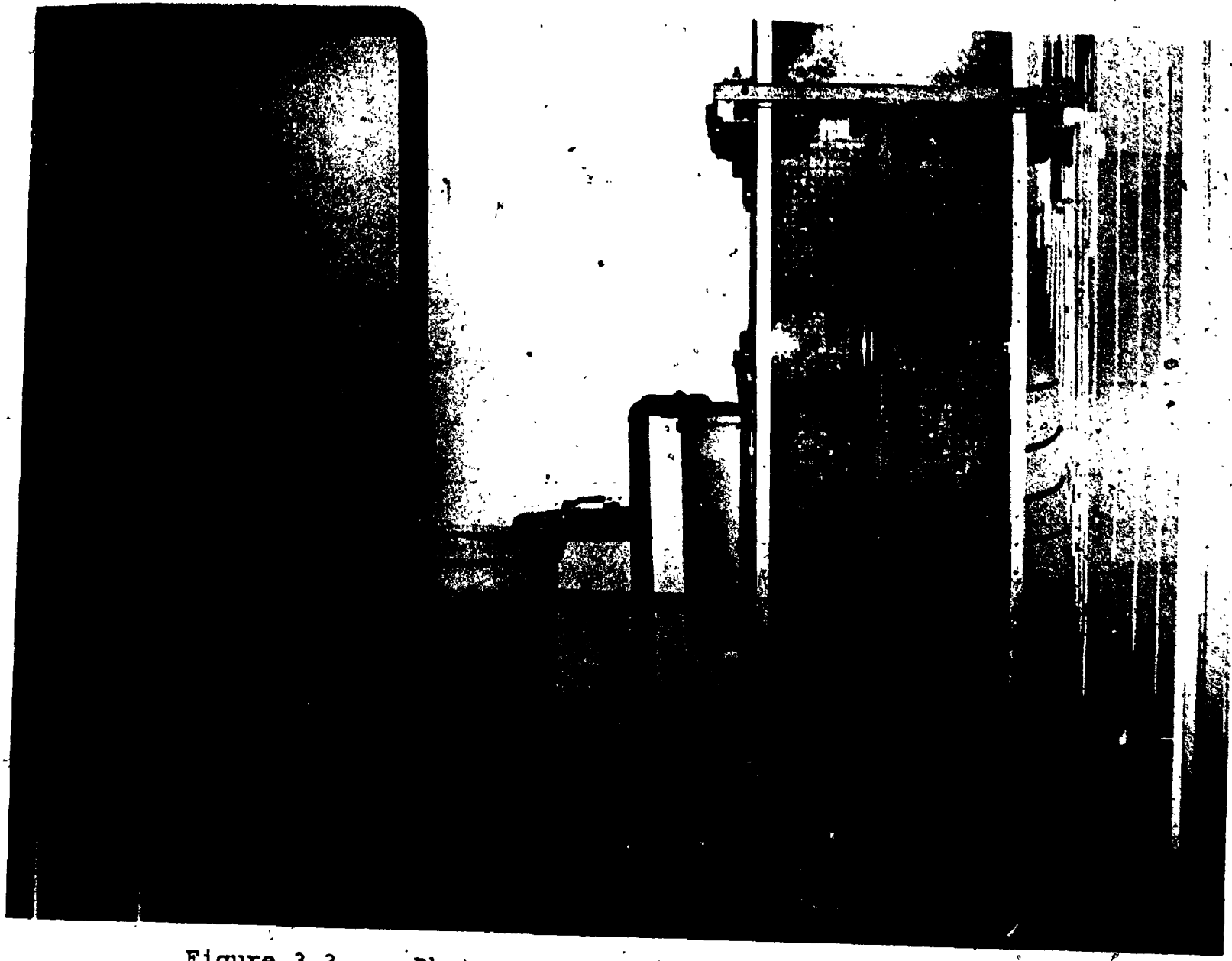

Figure 3.3 - Photograph EXPERIMENTAL EQUIPMENT

The solids were supported on a perforated plate grid which contained 38 evenly spaced holes 1/8 in. in diameter and served as the liquid distributor. The grid was situated between the main column section and a 4 in. high x 26 in. wide x 1 in. thick aluminum distributor box into which liquid was introduced through three 1/4 in. i.d. manifolds. The distributor box was packed with 0.8 lb of glass beads to promote further an even distribution of liquid over the cross section. The liquid was pumped through the system (figure 3.4) by a Duro 1/3 H.P. self-priming centrifugal pump having a capacity of 10 gpm. It was stored in a 60 gallon plastic reservoir and passed through a 1.25 in. diameter feed pipe to the manifolds at the bottom of the bed. Its flowrate was measured with a venturi-meter (Figure 3.5)which was connected to a differential manometer containing mercury. The venturi-meter was calibrated before use by measuring the weight of each liquid collected during a given time as shown in Appendix B.1. The liquid flowrate was regulated by means of globe valves on the 1.25 in. diameter main feed line and the 1 in. diameter bypass line.

Oil-free compressor air was fed to the column through a filter (Safe Vau Bowl), a pressure regulator (Watts model M-67125), and one of two rotameters (Brook's Sho-Rate) which were initially calibrated against a wet test meter (Precision Scientific Co.). Details of these calibrations are given in Appendix B.2.

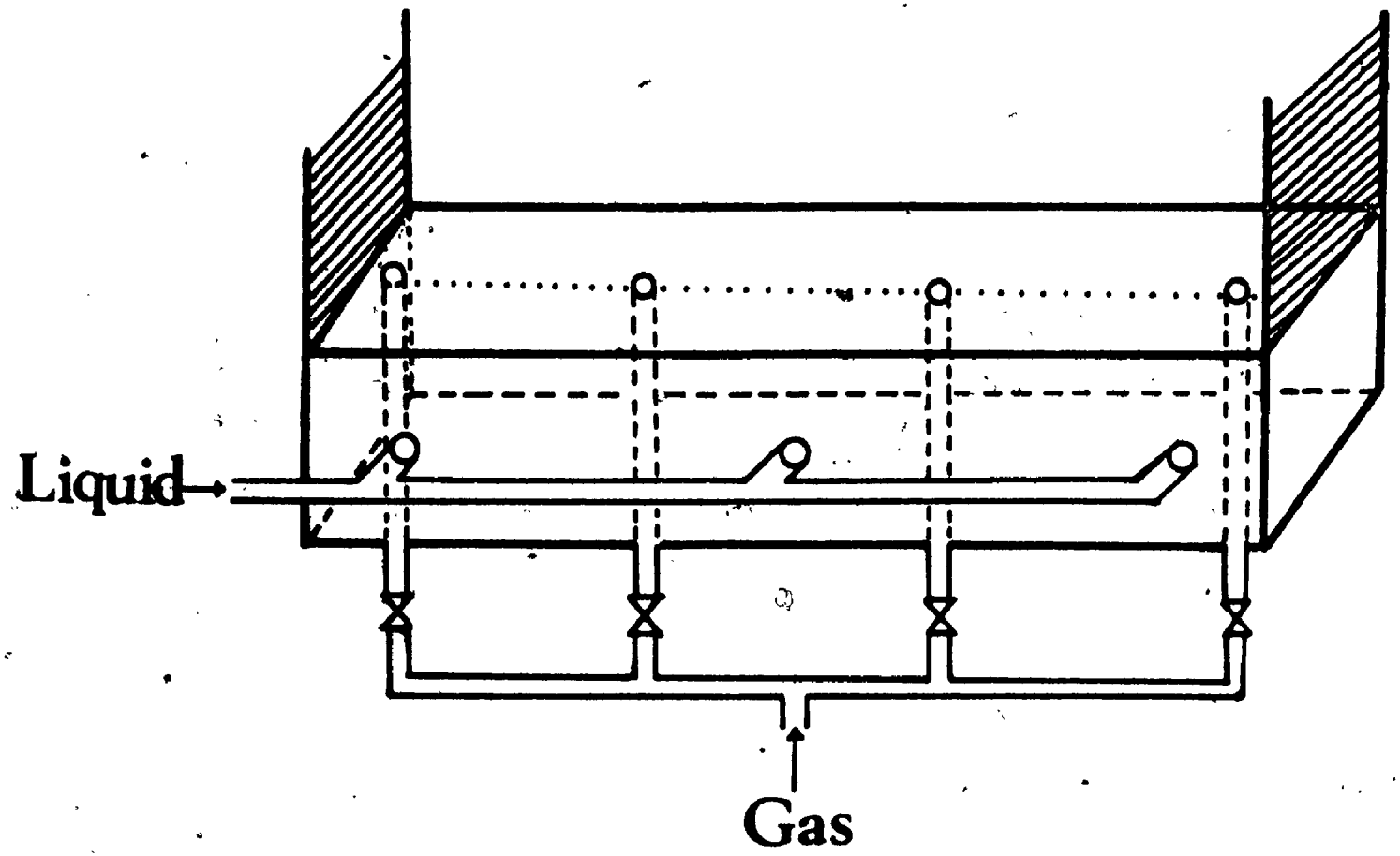

Figure 3.4. FLUID INLET SYSTEM

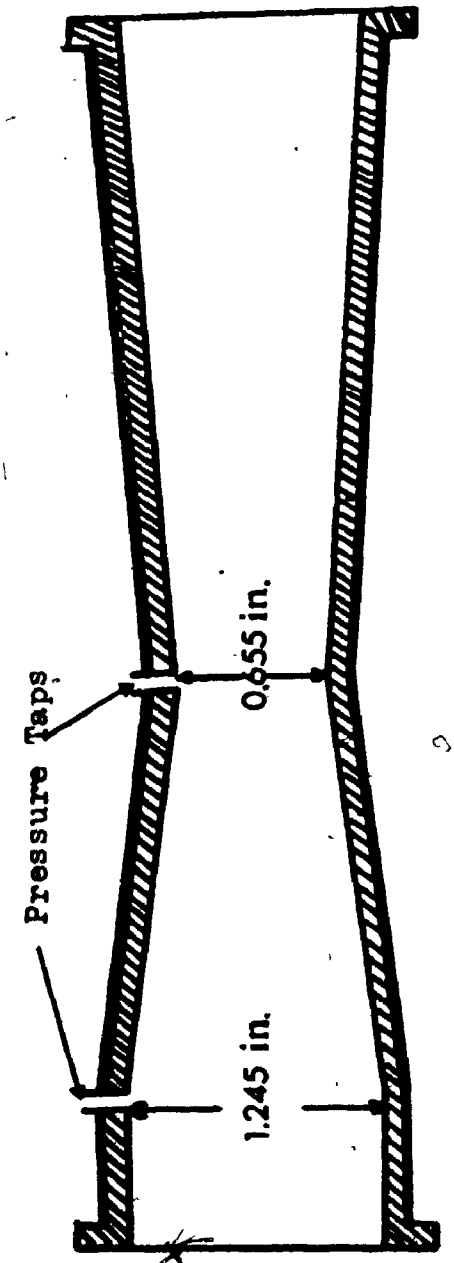

Figure 3.5. VENTURI METER

Since it was desired to inject the air into the fluidized bed with the minimum possible disturbance to the liquid flow, vertical nozzles rather than a sparger were selected. In this way the flat velocity profile of the liquid at the base of the column would be least affected. Thus the air was admitted to the bed through four 0.25 in. nozzles (figure 3.4) having a constriction and a gate valve in them to equalize the flow through each. These nozzles were evenly spaced across the width of the column and projected a short distance through four holes in the distributor plate.

Twelve centrally located brass pressure taps, 7/16 in. in diameter, were mounted flush with the rear wall of the column at 6 in. height intervals.
Each tap was connected to a manometer containing the same liquid as the column. The front of the column was marked with a 1 in. square grid.

In the liquid axial mixing study, two tracer techniques were employed, namely pulse and step injection. In the former, the tracer was contained in 2 in. diameter x 6 in. high reservoir pressurized by 40 psi compressed air as shown in figure 3.6. This reservoir was connected by way of a solenoid valve (ASCO-826223) controlled by an automatic timer (Bliss Eagel Signal Model 91) to a 0.25 in. pipe which contained eight evenly spaced holes 1/8 in. in diameter (49) located inside the distributor box.
In the step injection experiments, the tracer was contained

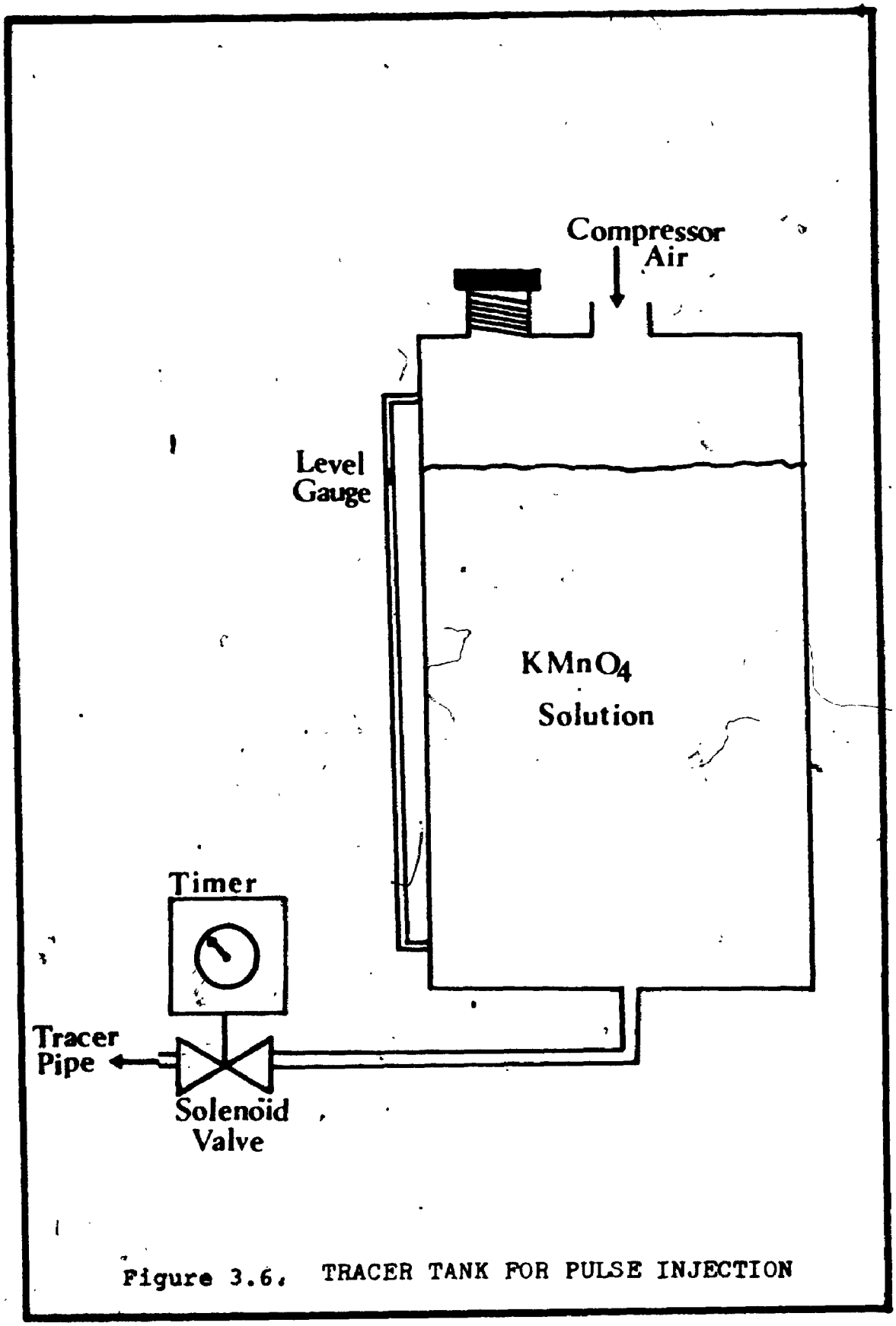

Figure 3.6. TRACER TANK FOR PULSE INJECTION

in a 20 gallon open reservoir. Two on-off valves (Jamesbury Type 353) were installed in the tracer and water reservoir feed lines. A 0.25 in. diameter tracer sampling pipe containing twelve evenly spaced 3/16 in. hole was installed horizontally across the whole width of the column. The sampled liquid flowed under gravity through a teflon tube which passed through one of the holes drilled to accomodate a pressure tap and was collected.

3.3. PROCEDURE

In the present study, the superficial velocities of the liquid and gas ranged from 0.090 to 0.335 ft/sec, and from 0.0 to 0.854 ft/sec, respectively.
In experiments on the liquid-solid and liquid-gas-solid systems, a weighed amount of solids (Table 3.1) was loaded into the column to give an initial bed height of 21.5 in. with the 6 mm glass beads and the gravel and 10 in. with the 1.0 mm glass beads.

3.3.1. Hold-up and Bed Expansion Measurements

In the liquid-gas experiments, the fluids were introduced into the column at the desired superficial velocities. The pressure profile up the entire height of the column was measured several times with the manometers which contained the same liquid as that in the column. When the pressure drop across the bed became constant, the bed was assumed to have reached steady-state. The pressure profile up the entire

column was then measured three or more times and the results recorded. Typical pressure profiles are shown in figure 3.7. The liquid hold-up was measured independently in the water-air system by simultaneously cutting off the air and water flows and subsequently recording the height established by the liquid surface.

The expanded bed height H was taken as the point at which a change in the slope of the plot of static pressure against height above the grid was observed (figure 3.7). The expanded bed height was also measured independently by visual observation.

The liquid hold-up, that is the fraction of the bed volume occupied by liquid, was calculated from the static pressure gradient up the column.

In the liquid-gas systems, the pressure drop between the distributor and a point 6 ft.above it was determined from the pressure profile. In the liquid-solid and liquid-gas-solid systems, the difference in static pressure between the distributor and the top of the bed was used to calculate the hold-ups.

The sum of the liquid, gas and solid hold-ups ϵ_ℓ, ϵ_g, and ϵ_s, in the three phase systems is unity:

$$\epsilon_\ell + \epsilon_g + \epsilon_s = 1.0 \qquad \text{.....(3.1)}$$

In the case of the liquid-solid systems, ϵ_g is zero and equation (3.1) reduces to

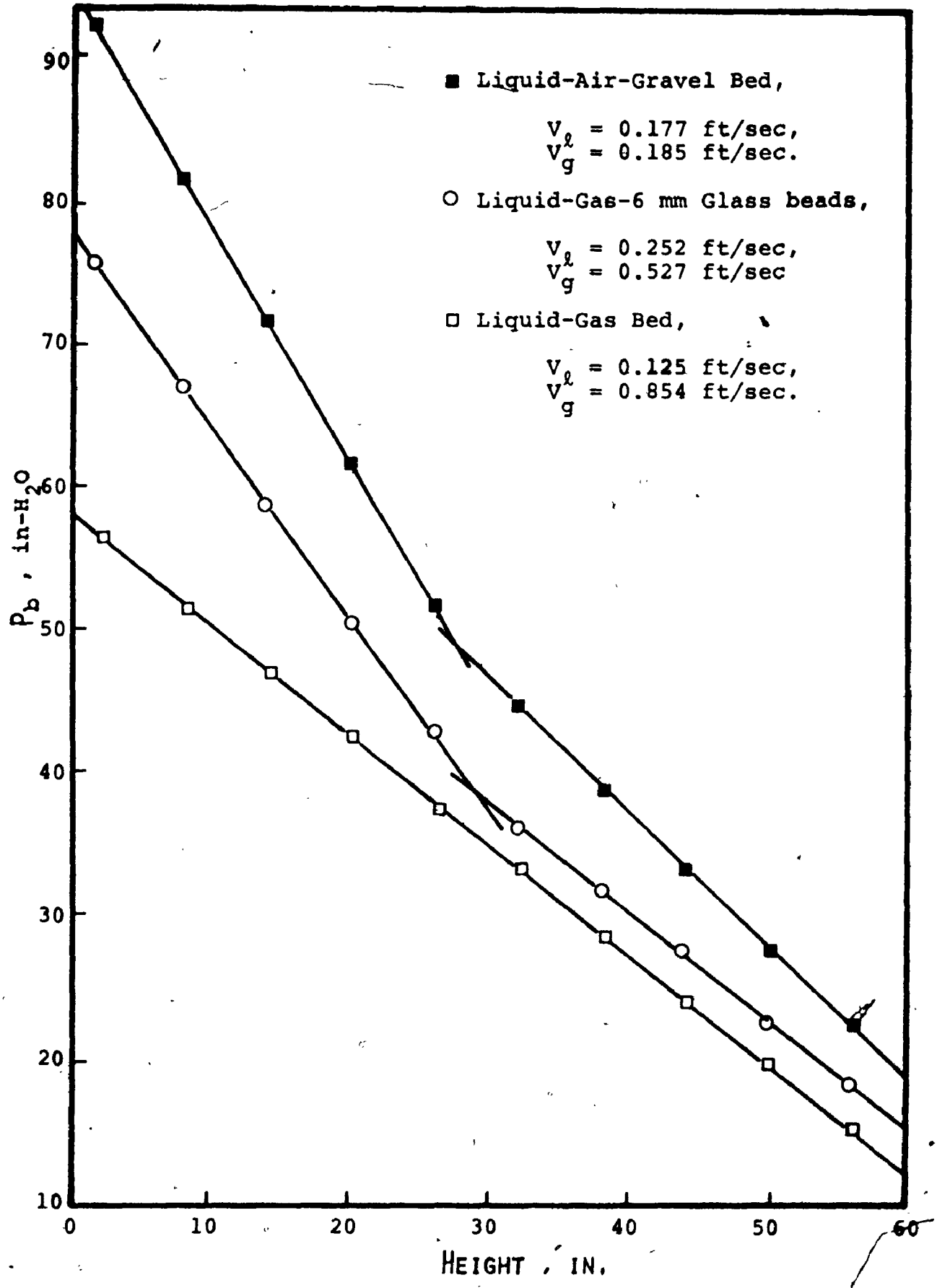

Figure 3.7 Typical Pressure Profiles

$$\varepsilon_\ell + \varepsilon_s = 1.0 \qquad \text{.....(3.2)}$$

Similarly, for the liquid-gas systems, ε_s is zero and

$$\varepsilon_\ell + \varepsilon_g = 1.0 \qquad \text{.....(3.3)}$$

The static pressure drop P_b across height H of the three phase bed can be expressed as

$$P_b = H\ (\varepsilon_\ell\ \rho_\ell + \varepsilon_g\ \rho_g + \varepsilon_s\ \rho_s) \qquad \text{.....(3.4)}$$

where ρ_ℓ, ρ_g, and ρ_s are the densities of the liquid, gas, and solid respectively.

Equation (3.4) reduces to

$$P_b = H\ (\varepsilon_\ell\ \rho_\ell + \varepsilon_s\ \rho_s) \qquad \text{.....(3.5)}$$

in the liquid-solid systems, and to

$$P_b = H\ (\varepsilon_\ell\ \rho_\ell + \varepsilon_g\ \rho_g) \qquad \text{.....(3.6)}$$

in the liquid-gas systems.

The hold-up of liquid phase in liquid-gas-solid systems is obtained from equations (3.1) and (3.4):

$$\varepsilon_{\ell_3} = [\ (P_b/H) - \varepsilon_s\ \rho_s - \rho_g(1-\varepsilon_s)]/[\ \rho_\ell - \rho_g\ ] \qquad \text{..(3.7)}$$

In the liquid-solid systems, ε_g is zero and equation (3.7) reduces to

$$\varepsilon_{\ell_2} = [\ (P_b/H) - \varepsilon_s\ \rho_s]\ /\ \rho_\ell \qquad \text{.....(3.8)}$$

From equations (3.3) and (3.6), the liquid phase hold-up in liquid-gas systems can be expressed as

$$\varepsilon_{\ell_1} = [\ (P_b/H) - \rho_g\ ]/[\ \rho_\ell - \rho_g\ ] \qquad ....(3.9)$$

where H is taken as the height of the column test section, 6 ft. In the above equations (3.7) to (3.9), ε_ℓ and ε_g are the only unknown quantities since ε_s can be calculated from a knowledge of the weight and density of the solids in the bed and the bed height and may be expressed as

$$\varepsilon_s = W / \dot{\rho}_s\ H\ A \qquad ....(3.10)$$

where W is weight of solids, and A is cross sectional area of the column.

The validity of this approach is dependent on the fact that the dynamic component of the measured pressure and the friction losses are minimal. In order to ensure that this was the case, pressure profiles were recorded with the column filled with liquid only. The superficial velocity of liquid was varied from zero up to the maximum values employed in the hold-up measurements.

As may be seen in Appendix C. , the measured pressures were essentially independent of velocity, confirming the validity of the above assumption.

3.3.2. Liquid Phase Axial Mixing

In order to obtain as much information as possible on axial liquid mixing in the bed, two tracer techniques were

employed, namely pulse and step injection. In the former, a one second pulse of tracer, potassium permanganate solution of known concentration, was injected into the column. The volume of tracer injected was measured by noting the change in liquid height in the reservoir by means of the level gauge attached to it. With step injection, the potassium permanganate solution was circulated at the desired flowrate through the open reservoir and the bed until its concentration was uniform throughout the system. This was checked by measuring the concentration of potassium permanganate in the reservoir three or more times before starting the measurements. The tracer was then abruptedly switched off and the water switched on simultaneously by means of the two on-off valves, thereby maintaining the same liquid velocity in the column.

In all experiments, tracer samples were taken at four second intervals by means of the sampling pipe described above. In the liquid-solid and liquid-gas-solid systems, the pipe was positioned just above the top of the expanded bed. In the liquid-gas systems, it was installed at a height of 6 feet above the distributor. The tracer samples were collected in photo tubes and analysed with a spectrophotometer (Baush & Lomb - Spectronic 20) which had been previously calibrated at a wave-length of 525 mμ using potassium permanganate solution of known concentration as shown in Appendix B.3. Only step injection was employed in the beds of 1 mm glass beads.

In this type of experiment, tailing of the response curves can result in a large error in calculating the first and second moments of the tracer concentration against time curve. This problem was overcome by correcting the tracer response curves using the exponential decay technique of Sater and Levenspiel (54), in which the curves are plotted on semilogarithmic graph paper and a corrected tail obtained by linear extrapolation as shown in figures 3.8 and 3.9. The first moment of the concentration distribution about the origin $\bar{t}$ and second moment about the mean σ^2 were then computed from the corrected response curves using the following relationships:

For pulse injection:

$$\bar{t} = \frac{\int_0^\infty t\,C(t)\,dt}{\int_0^\infty C(t)\,dt} = \frac{\sum_0^\infty t\,C(t)\,\Delta t}{\sum_0^\infty C(t)\,\Delta t} \qquad \ldots(3.11)$$

$$\sigma^2 = \frac{\int_0^\infty (t-\bar{t})^2 C(t)\,dt}{\int_0^\infty C(t)\,dt} = \frac{\sum_0^\infty (t-\bar{t})^2 C(t)\,\Delta t}{\sum_0^\infty C(t)\,\Delta t} \qquad \ldots(3.12)$$

where C(t) is the tracer concentration at time t.

For step injection:

$$\bar{t} = \int_0^\infty t\,dF = \sum_0^\infty t\,\Delta F \qquad \ldots(3.13)$$

$$\sigma^2 = \int_0^\infty t^2\,dF - \bar{t}^2 = \sum_0^\infty t^2 \Delta F - \Delta\bar{t}^2 \qquad \ldots(3.14)$$

where F is the fraction of the inlet tracer concentration in

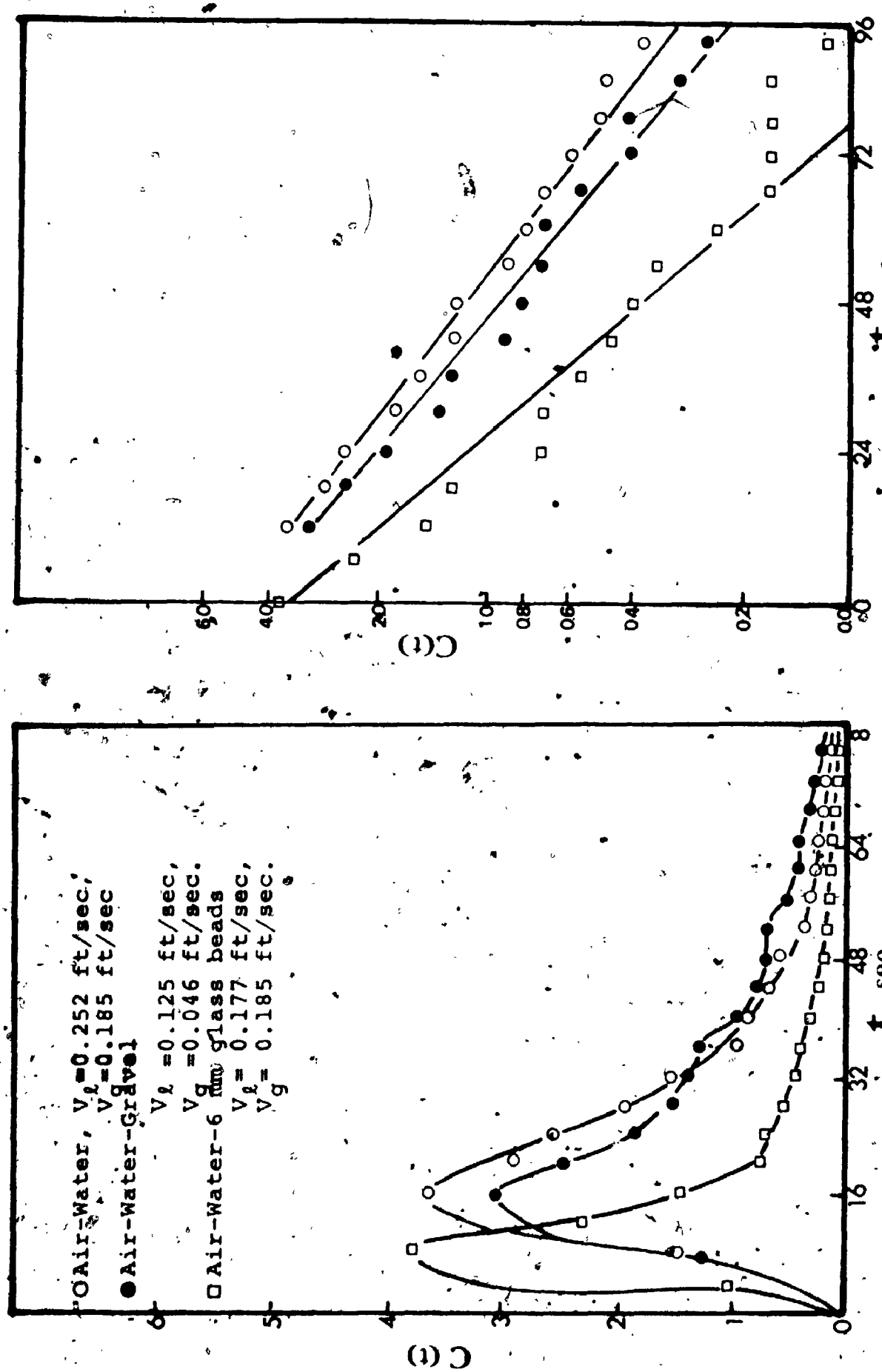

Figure 3.8 Pulse Tracer Response and Corrected Response Curves.

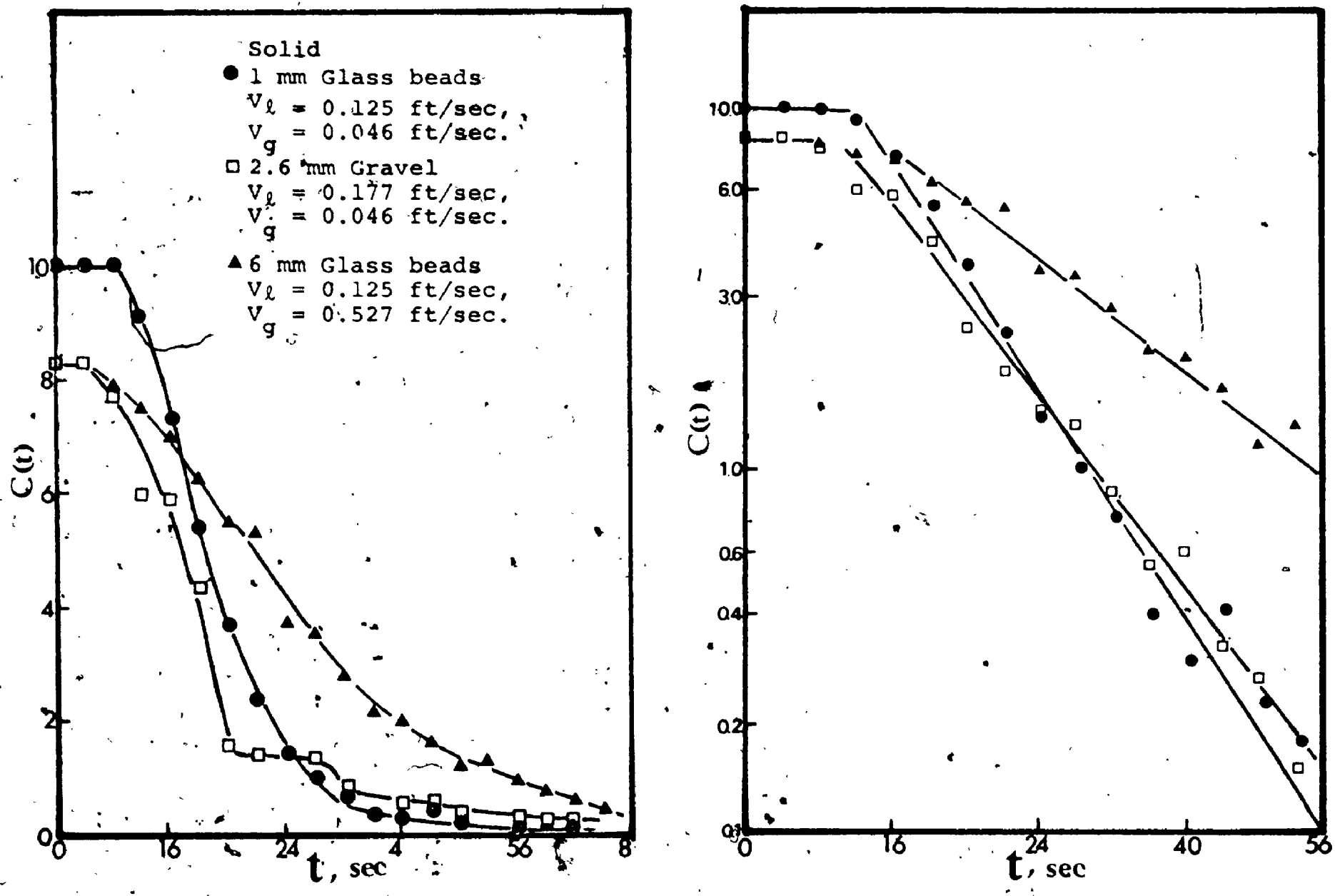

Figure 3.9. Step tracer Response Curves and Corrected Tracer Curves In Three Phase Fluidized Beds.

the outlet stream. Simpson's rule was used to integrate the above equations.

Axial liquid mixing in a fluidized bed is normally represented by the axially dispersed piston flow model illustrated in figure 3.10. In general terms, a mass balance yields the continuity equation in rectangular co-ordinates for any component i :

$$\frac{\partial C_i}{\partial t} + \frac{\partial}{\partial x}(V_x C_i) + \frac{\partial}{\partial y}(V_y C_i) + \frac{\partial}{\partial z}(V_z C_i) = \frac{\partial}{\partial x}(\rho D_{ix} \frac{\partial}{\partial x} \frac{C_i}{\rho}) + \frac{\partial}{\partial y}(\rho D_{iy} \frac{\partial}{\partial x} \frac{C_i}{\rho}) + \frac{\partial}{\partial z}(\rho D_{iz} \frac{\partial}{\partial x} \frac{C_i}{\rho}) + R_i \quad \ldots(3.15)$$

where C, V, ρ, D and R are the concentration, velocity, density, diffusion coefficient, and rate of production by chemical reaction of component i respectively.

Several simplifications to this equation can be made in the present case. Firstly, there are no chemical reactions, and therefore $R_i = 0$. Secondly, if the inlet concentration is uniform across the cross section of the column, only gradients in the axial direction are important and the x and y derivatives of the concentration can be ignored. Thirdly, since we are considering liquids and relatively slow moving gases the densities can be assumed constant. With these three simplifications, equation (3.15) reduces to

$$\frac{\partial C_i}{\partial t} + V_z \frac{\partial C_i}{\partial z} = D_L \frac{\partial^2 C_i}{\partial z^2} \quad \ldots\ldots(3.16)$$

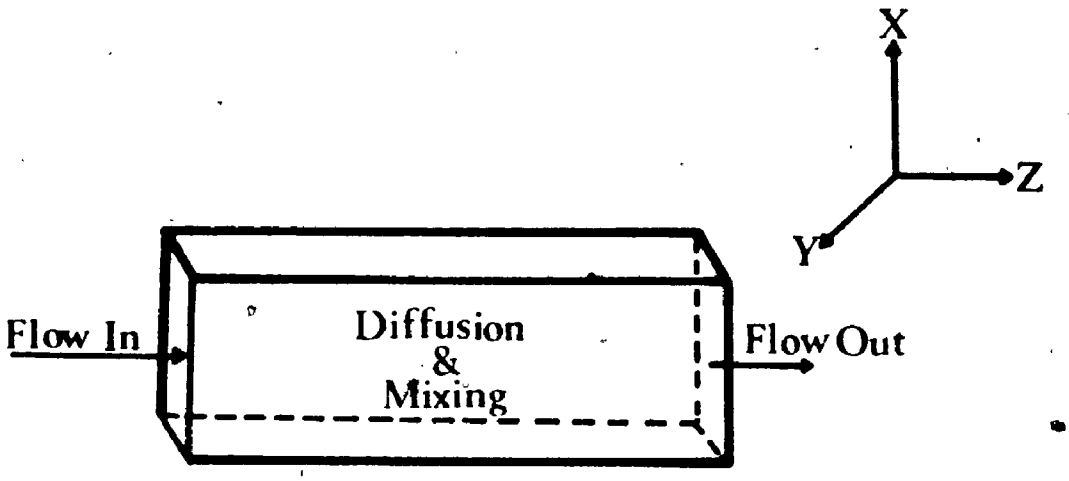

Figure 3.10. Schematic Representation of Flow System

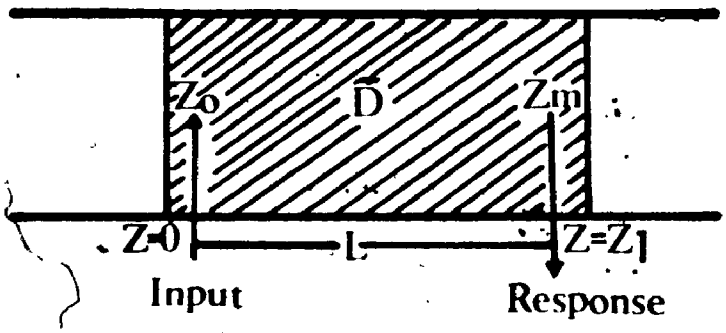

Figure 3.11. Schematic Description of Tracer Input and Response Corresponding to equation (3.18).

Equation (3.16) describes what is commonly termed the axially dispersed piston flow model. The axial diffusion coefficient quantitatively describes liquid mixing in the bed. It can be expressed in dimensionless form as the Peclet number,

$$P_e = V_z H / D_L \qquad \text{.....(3.17)}$$

In this study, the experimental data were interpreted using the above model. Since the solutions of equation (3.16) are quite complex, it would be difficult to evaluate the Peclet number from the concentration versus time data. It is far simpler to obtain Peclet numbers from the first and second moments of these plots using the method of Van der Laan (64). The equation used was

$$\sigma^2 = \frac{1}{P_e^2}\left[2 P_e + 8 + 2 e^{-P_e Z_1} - e^{-P_e Z_o} (4 Z_o + 4 + e^{-P_e Z_o}) - e^{-P_e (Z_1 - Z_m)} (4(Z_1 - Z_m) P_e + 4 + e^{-Pe(Z_1 - Z_m)}) \right]$$

$$\text{.....(3.18)}$$

which is applicable to the system illustrated in figure 3.11. In equation (3.18),

$$Z_o = X_o / (X_m - X_o) \qquad \text{.....(3.19)}$$

$$Z_1 = X_1 / (X_m - X_o) \qquad \text{.....(3.20)}$$

$$Z_m = X_m / (X_m - X_o) \qquad \text{.....(3.21)}$$

where X_o, X_1, and X_m are the heights of the injection point,

the top of the column, and the sampling point above the grid.

Peclet numbers obtained from equation (3.18) were used to calculate the height of the liquid phase axial mixing unit, HMU, defined as;

$$HMU = 2H / P_e \qquad \ldots\ldots(3.22)$$

HMU is equal to zero for plug flow and is infinite for perfect mixing conditions.

3.3.3. Bubble Characteristics

Liquid and gas were introduced into the column at the desired superficial velocities. When steady-state was reached, as indicated by the constancy of the static pressure profile, cine films were taken with a Bolex H 16 reflex movie camera for 10 - 20 seconds duration at 16 frames per second for each set of conditions.

The negatives were read by projecting single frame stills onto a large sheet of graph paper using an L-W Motion Analyser 900. The projected bubbles were transcribed onto the graph paper, together with the 1 in. square grid marked on the front of the column. The bubble areas were determined using the grid as a reference. Six frames of film were analysed for each set of experimental conditions. The bubble size distributions in all systems could be represented quite adequately by straight lines on logarithmic probability paper as shown in figure 3.12. From such plots, the mean bubble size and the geometric standard deviation of the distribution were determined.

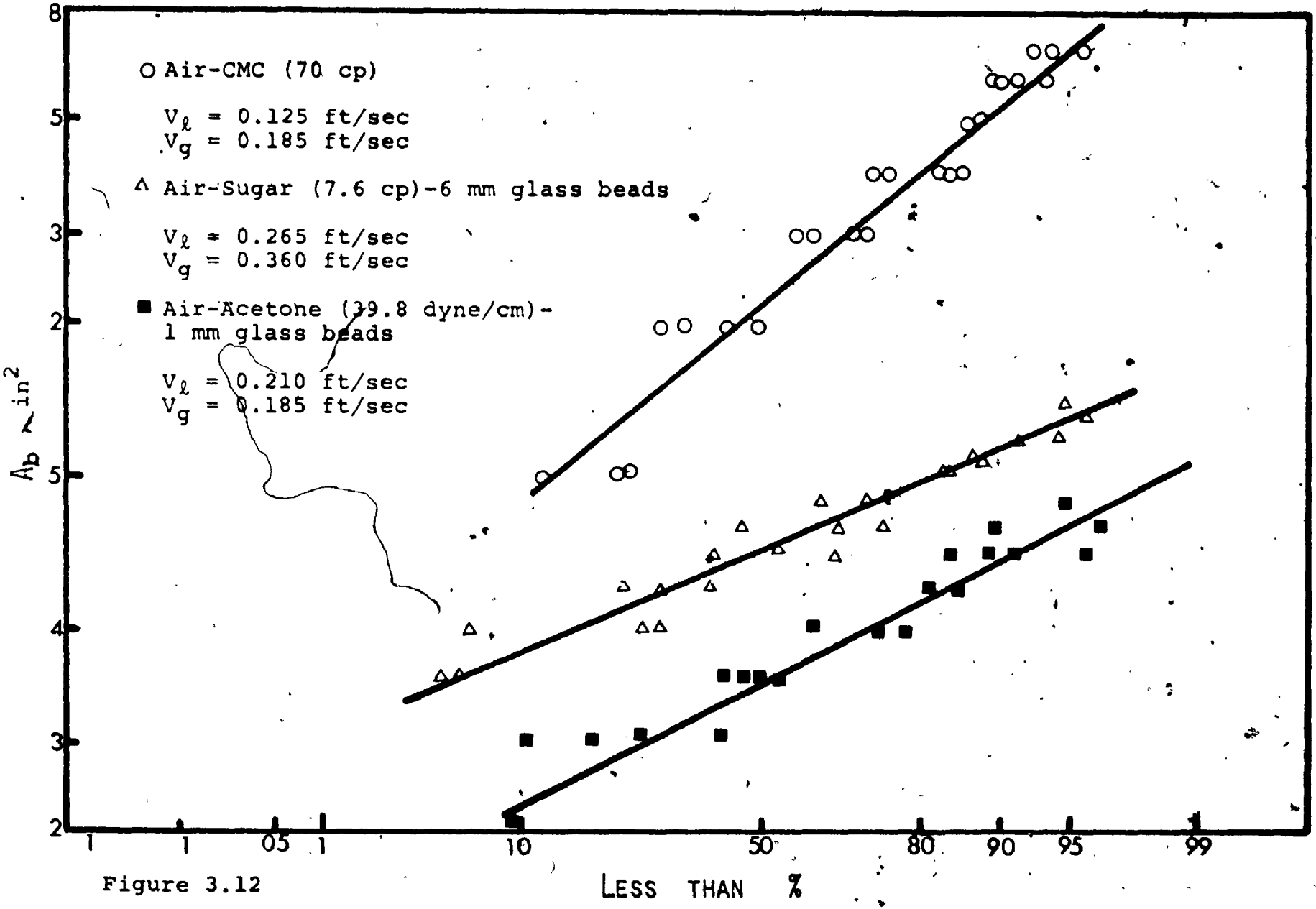

Figure 3.12

Typical Bubble Size Distribution

The mean bubble rising velocity was calculated by averaging the individual rising velocities of ten or more bubbles for each set of conditions. The grid marked on the front of the column enabled the height of the bubble in the bed to be determined. The time taken by the bubble to rise a given vertical distance could therefore be determined from the number of elapsed frames and the camera speed. The bubble rising velocities quoted in this study are relative to that of liquid phase. The relative rising velocity V_{br}, was determined from the absolute rising velocity of the bubbles V_b by equation;

$$V_{br} = V_b - (V_\ell / \varepsilon_\ell) \quad \text{.....(3.17)}$$

where V_ℓ is the superficial velocity of liquid.

CHAPTER 4

EXPERIMENTAL RESULTS

4.1. INTRODUCTION

In the present study, the liquid and gas hold-ups, the bed expansion, liquid phase axial mixing coefficients, and bubble characteristics were measured in two and three phase fluidized beds. The number and scope of the experiments are summarized in Table 4.1.

The liquid and gas phase hold-up data were obtained from the pressure profiles, typical examples of which are given in figure 4.1. The linearity of these profiles indicated that the individual phase hold-ups did not vary significantly with height in the main region of the bed. However, small deviations from linearity were observed close to the grid and in frothy region near the top of the column. These deviations were neglected in determining the slopes of the lines. At any given sets of conditions, at least three sets of measurements were made.

The expanded bed height in the liquid-solid and liquid-gas-solid beds were also obtained from the pressure profiles. There was some fluctuation in the manometer readings and the mean values were estimated by visual observation. At the lower gas flowrates, the fluctuations were very small for all the beds, but they increased markedly with gas rate up

TABLE 4.1

SCOPE OF EXPERIMENTS

SYSTEMS	EXPERIMENTAL PARAMETERS	NUMBER OF CONDITIONS	RANGE OF LIQUID VELOCITY (ft/sec)	RANGE OF GAS VELOCITY (ft/sec)	RANGE OF VISCOSITY (cp)	RANGE OF SURFACE TENSION (dyne/cm)
LIQUID-GAS BEDS	Liquid and Gas Hold-ups	250	0.125-0.335	0.046-0.854	1 - 70	39.8-72.8
	Liquid Phase Mixing	33	0.125-0.335	0.046-0.854	1	72.8
	Bubble Size and Rising Velocity	95	0.125-0.335	0.046-0.854	1 - 70	39.8-72.8
LIQUID-SOLID BEDS	Liquid Hold-up and Bed Expansion	147	0.090-0.335	0.0	1 - 70	39.8-72.8
	Liquid Phase Mixing	22	0.090-0.335	0.0	1	72.8
LIQUID-GAS-6 mm Glass beads	Liquid and Gas Hold-ups	199	0.125-0.335	0.046-0.854	1 - 70	39.8-72.8
	Bed Expansion	199	0.125-0.335	0.046-0.854	1 - 70	39.8-72.8
	Liquid Phase Mixing	36	0.125-0.335	0.046-0.854	1	72.8
	Bubble Size and Rising Velocity	72	0.125-0.335	0.046-0.854	1 - 70	39.8-72.8

...continued

TABLE 4.1. (continued)

LIQUID-GAS-2.6 mm Gravel	Liquid and Gas Hold-ups	141	0.125-0.335	0.046-0.185	1 - 20	39.8-72.8
	Bed Expansion	141	0.125-0.335	0.046-0.185	1 - 20	39.8-72.8
	Liquid Phase Mixing	20	0.125-0.335	0.046-0.185	1	72.8
	Bubble Size and Rising Velocity	65	0.125-0.335	0.023-0.185	1 - 20	39.8-72.8
LIQUID-GAS-1 mm Glass beads	Liquid and Gas Hold-ups	197	0.090-0.335	0.023-0.185	1 - 7.6	39.8-72.8
	Bed Expansion	197	0.090-0.335	0.023-0.185	1 - 7.6	39.8-72.8
	Liquid Phase Mixing	17	0.090-0.252	0.023-0.185	1	72.8
	Bubble Size and Rising Velocity	53	0.090-0.252	0.023-0.185	1 - 7.6	39.8-72.8

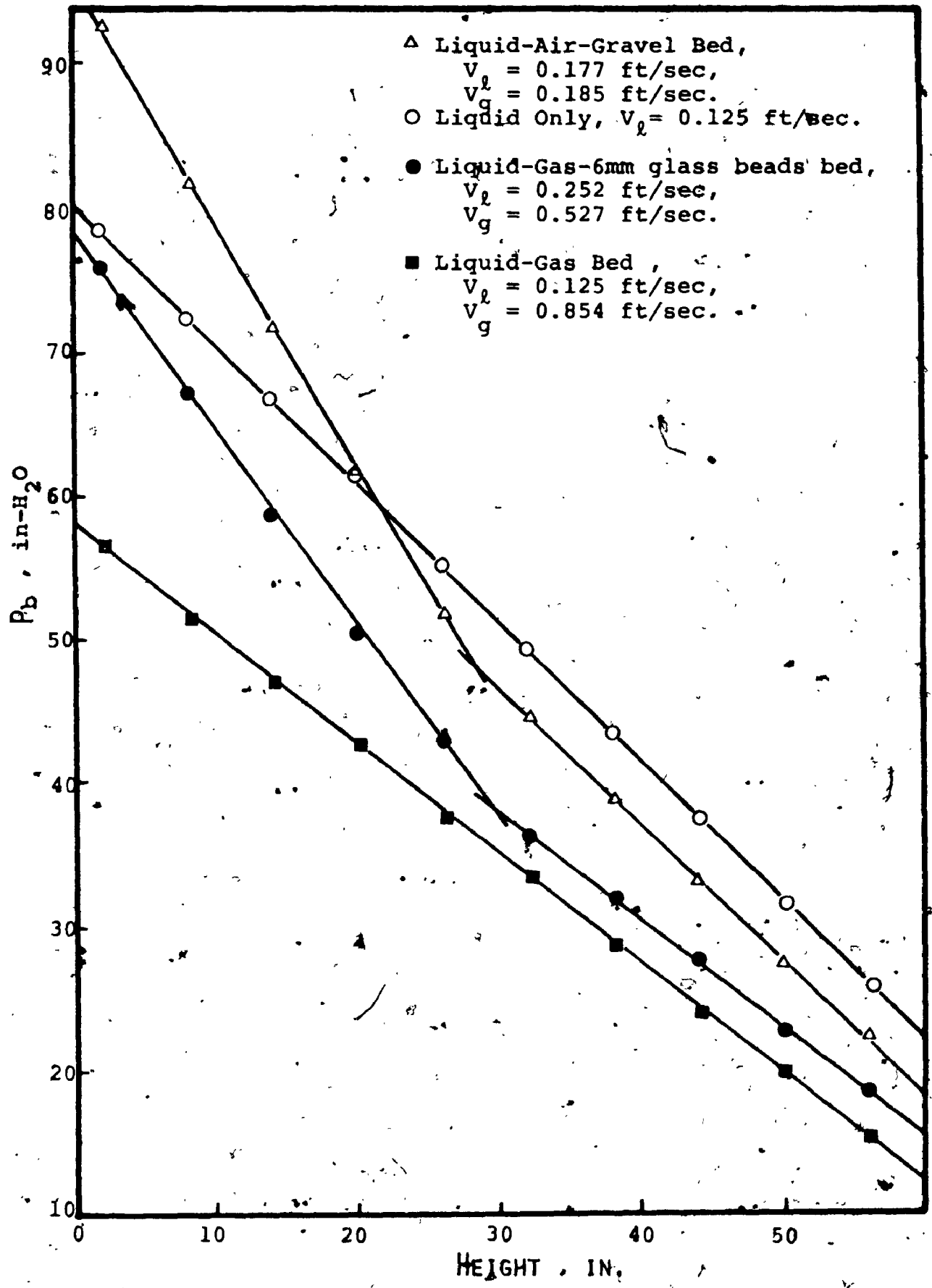

Figure 4.1. Typical Pressure Profiles

to a maximum of about ± 4 in., or ± 6 % of the manometer reading. However, the precision of the liquid hold-up and expanded bed heights was better than 10 % due to the constancy of the slopes of the pressure profiles regardless of the fluctuations.

Good agreement was also obtained between these values and those estimated by visual observation, even at high gas flowrates. The liquid and gas phase hold-ups and expanded bed height data obtained in two and three phase beds are given in Appendices E,F and G.

Axial mixing in the liquid phase was studied by two tracer techniques, namely pulse and step injection. The mean values of the first and second moments of the corrected response curves were obtained from seven or more experimental observations at the given operating conditions. The maximum deviation of the first and second moments from the mean values was around 15 %. The data were interpreted by the axially dispersed piston flow model and expressed in terms of the height of the mixing unit. The experimental data are summarized in Appendix H.

For given sets of conditions, cine films of the bed were taken from which the bubble size distribution, mean size and mean rising velocity were determined. Six frames of film were analysed in each case. The detailed results of these observations are given in Appendix I.

2 4

OF/DE

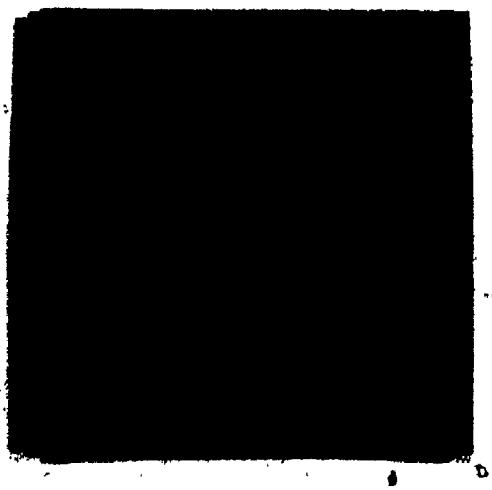

4.2. LIQUID-GAS BEDS

4.2.1. Liquid and Gas Phase Hold-ups

The effect of liquid and gas flowrate, and liquid surface tension and viscosity on the individual phase hold-ups in liquid-gas beds were determined. The results are summarized below.

Typical plots of liquid hold-up against liquid flowrate are shown in figure 4.2. The liquid and gas flowrates were varied from 0.125 to 0.335 ft/sec, and from 0.046 to 0.854 ft/sec, respectively. It should be pointed out that the data presented in this and other figures represents only a small fraction of the data obtained in this study. However, the trends indicated are typical of those observed throughout.

It can be observed from figure 4.2. that the liquid hold-up decreased only slightly with increasing liquid velocity in the different beds. The rate of decrease was more pronounced at high gas flowrates and low liquid viscosities. The sum of the liquid and gas hold-ups is unity in the solids-free beds. Consequently, it may be deduced that the gas hold-up increased slightly with increasing liquid velocity. However, the rate of increase was again relatively small in all cases studied.

As may be seen in figure 4.3 the liquid hold-up decreased with increasing gas flowrate. The influence of this parameter

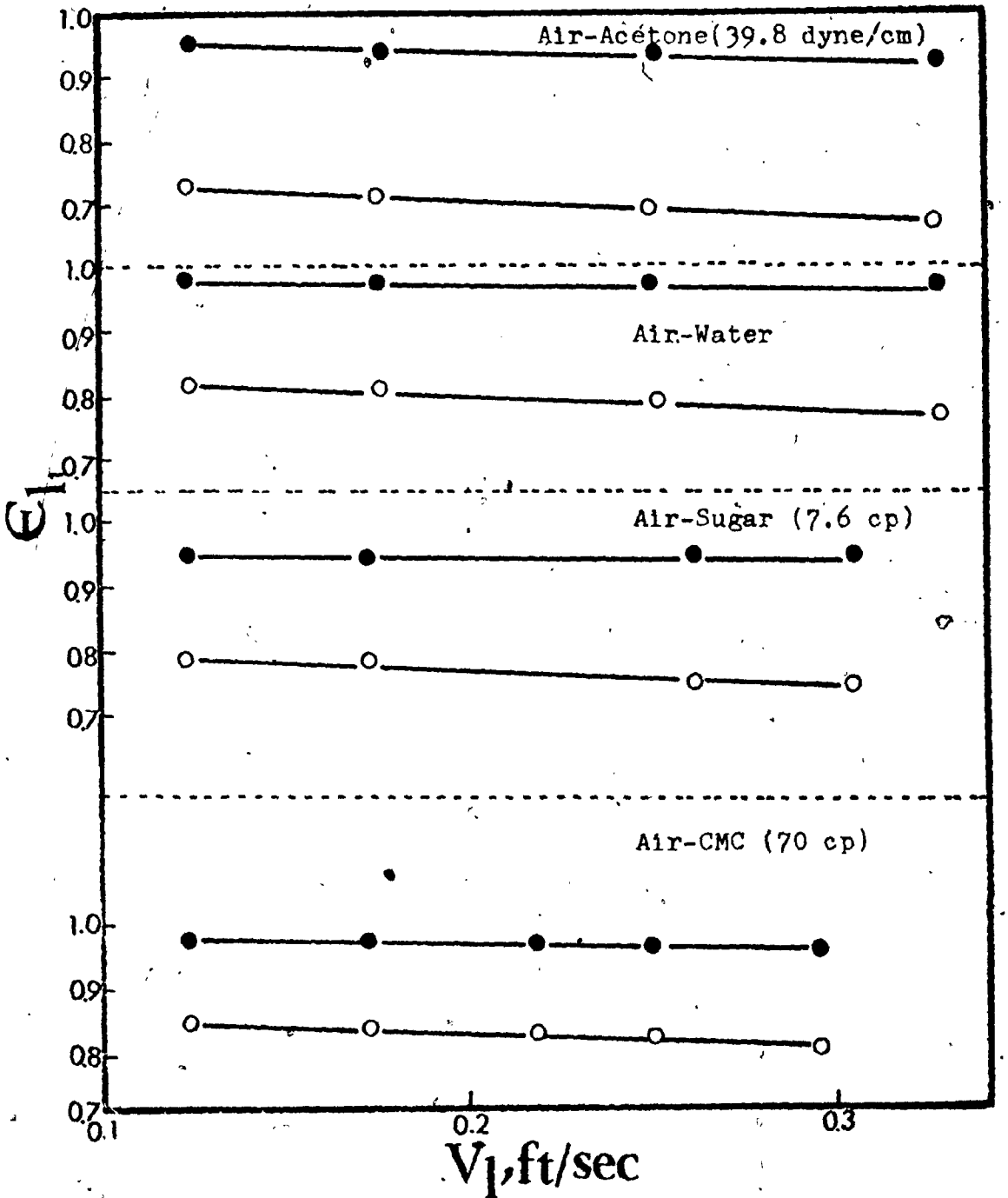

Figure 4.2. Effect of Liquid Velocity on Liquid Hold-up in liquid-gas beds. V_g : ●; 0.046 ft/sec. ○; 0.527 ft/sec.

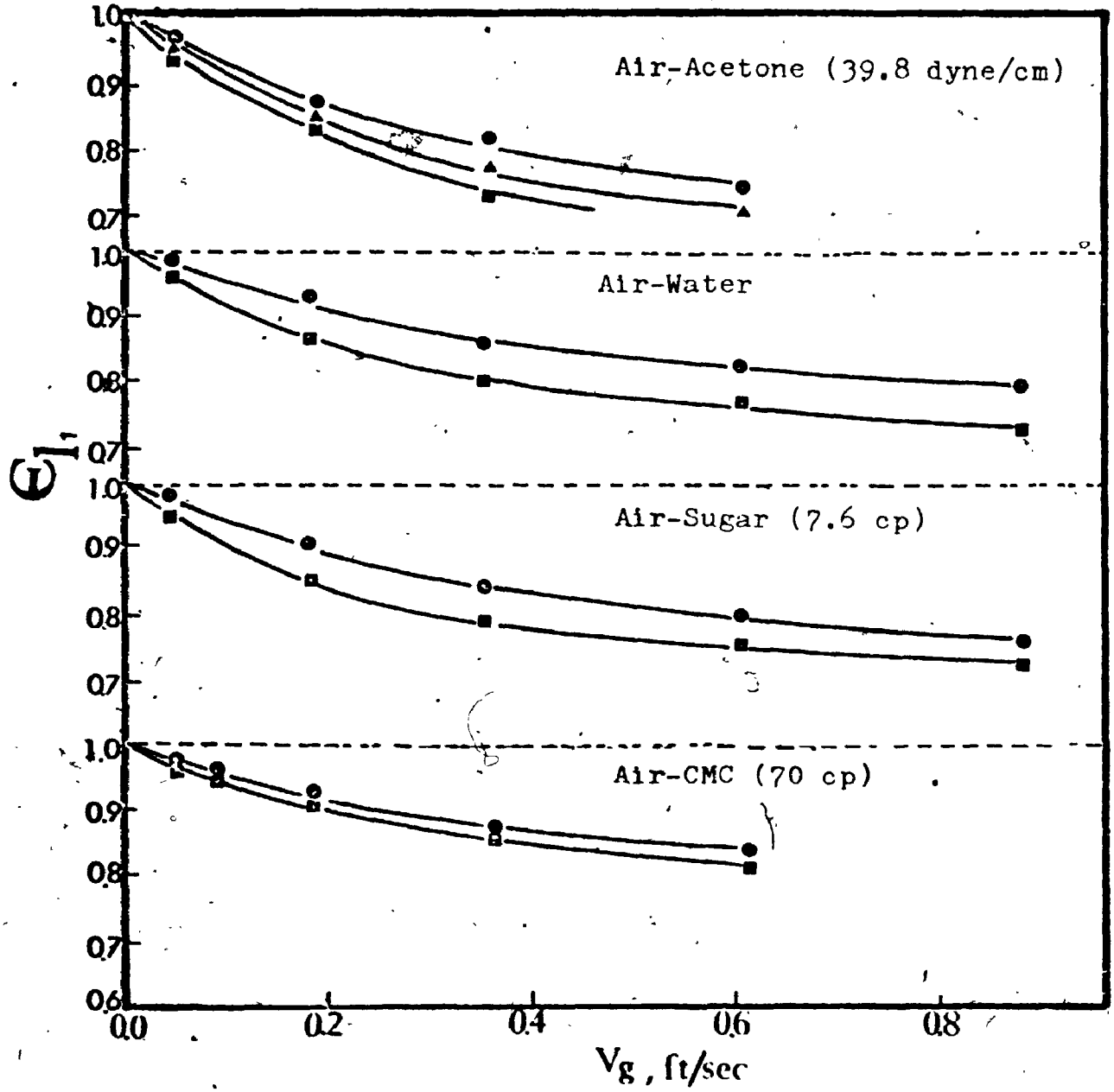

Figure 4.3. Effect of Gas Velocity on Liquid Hold-up in gas-liquid beds. V_l : ● ; 0.125 ft/sec.
▲ ; 0.252 ft/sec.
■ ; 0.312 ft/sec.

was considerably more marked than that of the liquid rate. Conversely, the gas hold-up increased with increasing gas velocity.

The liquid surface tension was varied between 39.8 and 72.8 dyne/cm using acetone-water mixtures of different concentration. Its effect on liquid hold-up at different liquid and gas velocities is shown in figure 4.4. The liquid hold-up increased slightly with increasing surface tension and, correspondingly, the gas hold-up decreased slightly.

The liquid viscosity was varied from 1 to 70 cp using sugar and CMC solutions of different concentration. Since the CMC solution exhibits pseudoplastic behaviour, its apparent viscosity μ_a can be defined as follows(35):

$$\mu_a = K/(du/dr)^{1-n} \qquad \ldots\ldots(4.1)$$

where K, (du/dr) and n are the fluid consistency index, shear rate, and the fluid behaviour index which characterises the extent of the deviation of the solution from Newtonian behaviour. For the CMC solutions the values of n ranged between 0.914 and 0.976 indicating that over the concentration range employed they exhibited essentially Newtonian behaviour. Consequently, the apparent viscosity of these solutions were taken as 3.7, 5.7, 6.3, 8.5, 13.0, 20.0, and 70.0 cp at zero shear rate.

The effect of liquid viscosity on liquid hold-up is illustrated in figure 4.5. The liquid and gas flowrates were varied from 0.125 to 0.335 ft/sec and from 0.046 to

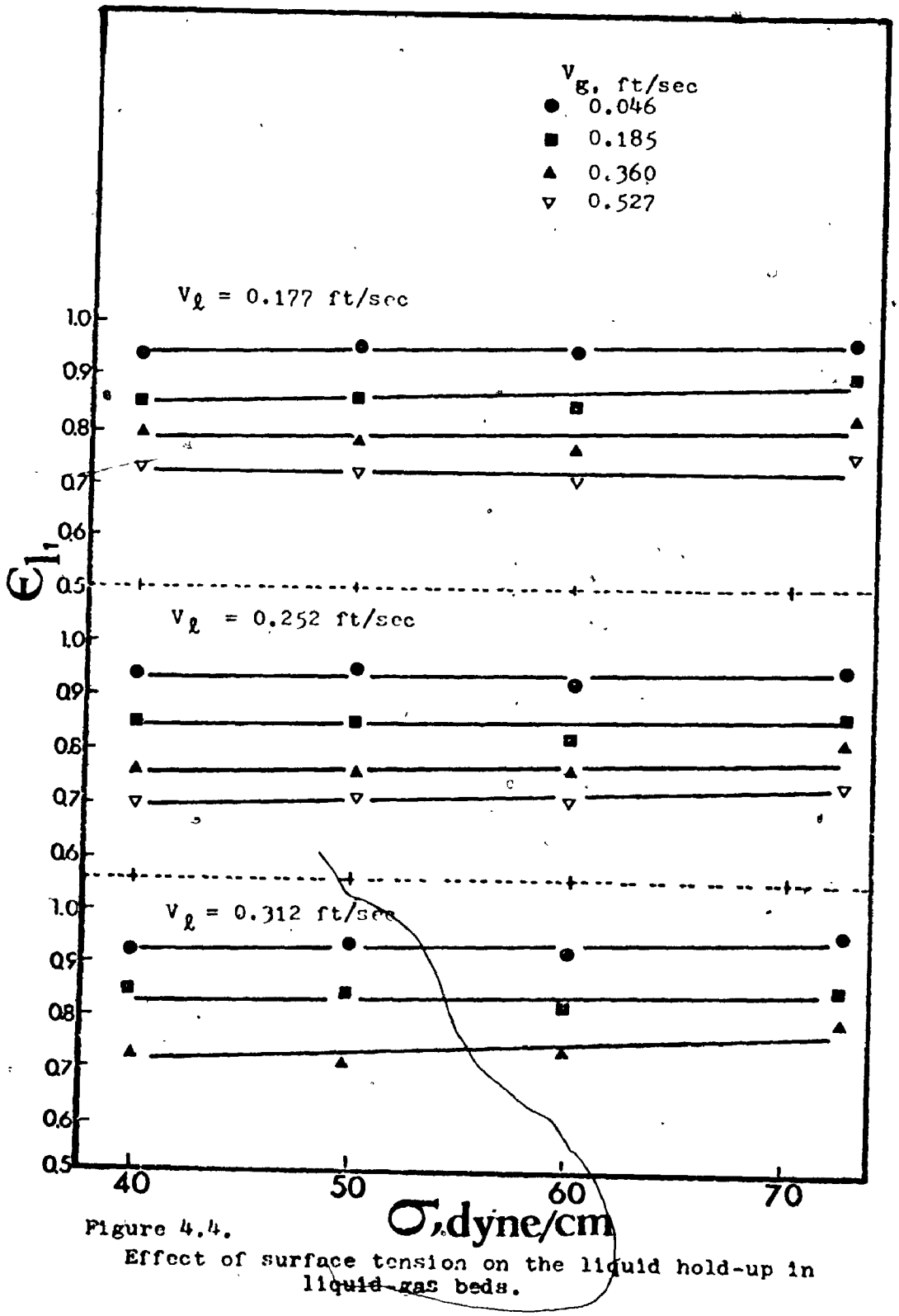

Figure 4.4.
Effect of surface tension on the liquid hold-up in liquid-gas beds.

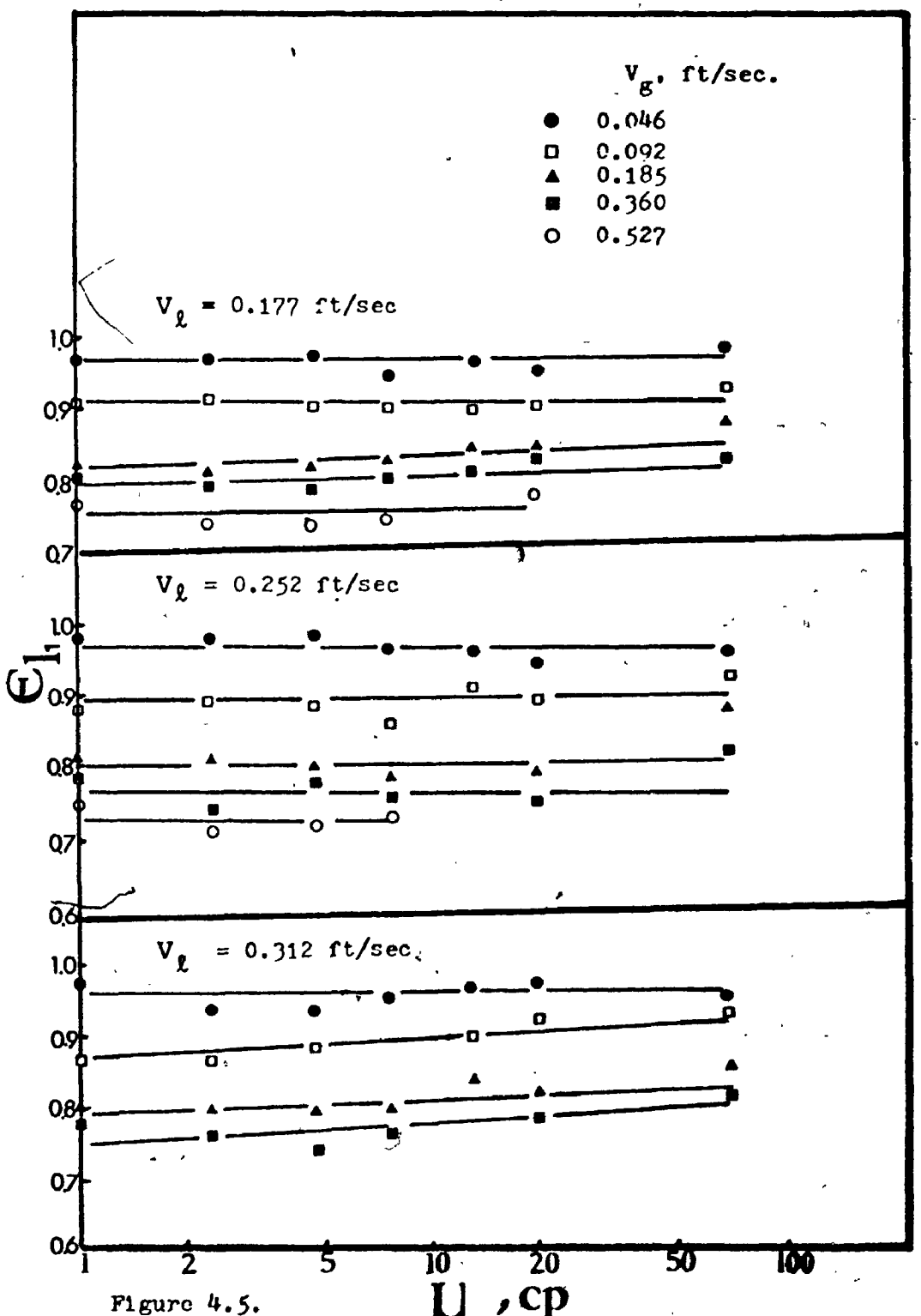

Figure 4.5.
Effect of Viscosity on Liquid Hold-up in Liquid-Gas Beds.

0.527 ft/sec, respectively in these experiments.
As may be seen, the liquid hold-up was virtually independent of viscosity in the range 1 to 70 cp. However, at the higher liquid rates, liquid hold-up was observed to increase marginally with increasing liquid viscosity. Again, since the sum of the liquid and gas hold-ups is unity, it follows that the gas hold-up was also essentially independent of liquid viscosity.

4.2.1.1. Correlation of The Liquid Phase Hold-up Data

A statistical analysis was performed on the liquid phase hold-up data for liquid velocities V_ℓ between 0.125 and 0.335 ft/sec, gas velocities V_g between 0.046 and 0.854 ft/sec, liquid viscosities μ between 1 and 70 cp and for liquid surface tensions σ between 39.8 and 72.8 dyne/cm.
The following relationship resulted:

$$\varepsilon_{\ell 1} = 0.890\ V_\ell^{-0.030}\ V_g^{-0.085}\ \gamma^{0.015}\ \sigma^{0.068} \quad ..(4.1)$$

where V_ℓ, V_g are in ft/sec, σ is in lb/sec^2 and γ ($lb/ft\ sec^{2-n}$) is defined as (33):

$$\gamma = g_c\ K\ 8^{n-1} \quad .....(4.2)$$

In equation (4.2), g_c is the dimensional constant in $lb_m/lb_f\ ft^2$, K is the fluid consistancy index in $lb_f sec^n/ft^2$, and n is the dimensionless flow behaviour index.
The standard error of estimate between the experimental and calculated values of $\varepsilon_{\ell 1}$ is 0.029 for 250 data points.

Equation (4.1) can be expressed in dimensionless form as follows:

$$\varepsilon_{\ell 1} = 0.899 \left(We_m \right)^{-0.043} \quad \ldots.(4.3)$$

where We_m is the modified Weber number $V_g^2 \rho_\ell d_h / \sigma$. In this equation, V_ℓ and γ are excluded since their contributions to variations in the liquid hold-up are small as may be seen in equation (4.1). The standard error of estimate between the experimental and calculated values of equation (4.3) is 0.035 for 250 data points. Figure 4.6 illustrates how well this equation fits the data for all experimental conditions. The procedures and the computer program used in this analysis are given in Appendix D.

A comparison was made between the present experimental data and that of Michelson and Østergaard (36) for liquid-gas beds. The latter were correlated by the equation:

$$\varepsilon_{\ell_1} = 1.0 - 0.025 \left(0.193\ V_\ell\right)^{-0.16} \left(1.2\ V_g\right)^{1.05} \quad \ldots.(4.4)$$

There was reasonable agreement between the present values and those calculated from equation (4.4) at lower gas flow-rates (0.046-0.185 ft/sec) but the agreement was poor at higher gas rates. This difference may be explained by the fact that the maximum gas rate employed by Michelson and Østergaard was 0.072 ft/sec which is considerably lower than that in the present study.

The present values of liquid hold-up were found to be

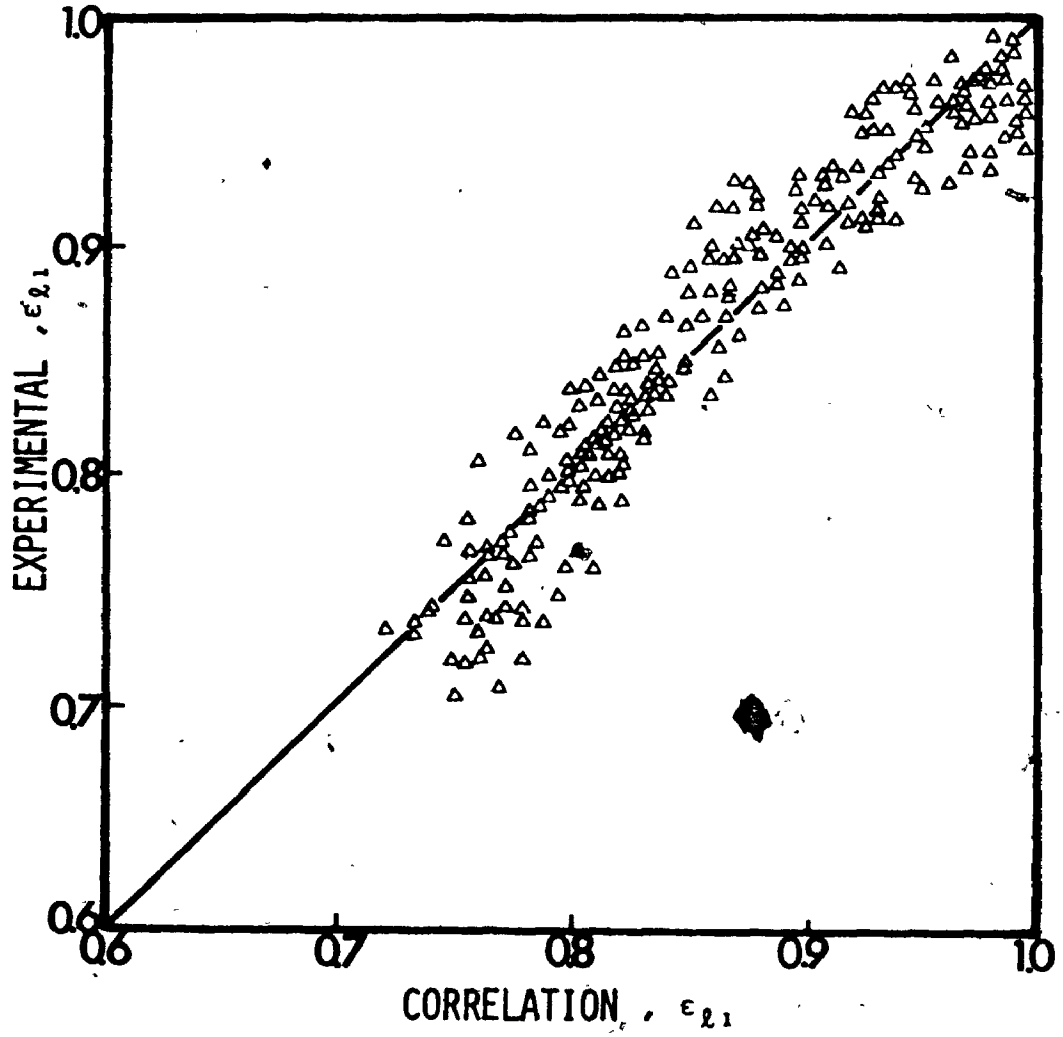

Figure 4.6 Comparison between Experimental and Calculated Values of $\varepsilon_{\ell 1}$ in Liquid-Gas Beds. (Equation 4.3)

about 35 % higher than those calculated by Bankoff's correlation (5):

$$\varepsilon_{\ell_1} = 1.0 - [0.89\ V_g/(V_\ell+V_g)] \qquad ....(4.5)$$

Since the equation (4.5) was formulated for systems having maximum gas hold-ups of 0.8, it can be expected to apply in the slug and froth flow regimes. It is therefore not surprising that this correlation did not accurately describe the present data which were obtained at much lower gas rates.

4.2.2. Liquid Phase Axial Mixing

The effect of liquid and gas flowrates on liquid phase axial mixing are shown in figure 4.7 in which the height of the mixing unit HMU is plotted against these variables. The values obtained by the pulse and step tracer techniques, plotted separately in the figure, are generally in good agreement. As may be seen in figure 4.7, HMU decreased with increasing liquid velocity. Increasing the liquid flowrates from 0.125 to 0.335 ft/sec resulted in a reduction of about 35 % in HMU. The height of the mixing unit increased with gas velocity in contrast to the trend exhibited with liquid velocity. Increasing the gas velocities from 0.046 to 0.854 ft/sec resulted in a 40 % increase in HMU. The above findings are qualitatively in accord with those of Michelsoñ and Østergaard (36) and Diboun and Schügerl (20). Longitudinal mixing of the liquid phase was also found to increase with

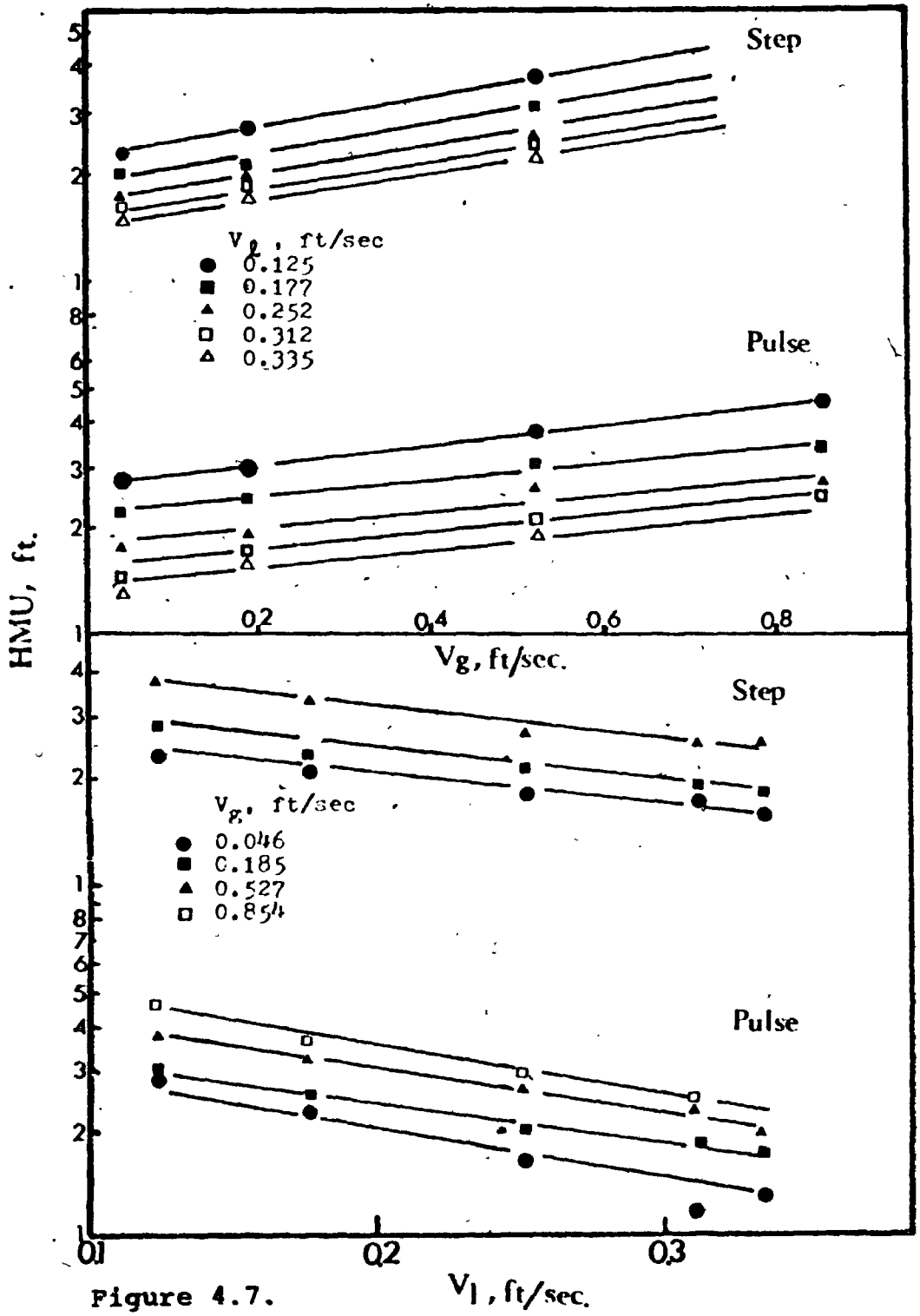

Figure 4.7. Effect of Liquid and Gas Velocity on HMU in Liquid-Gas Bed.

with gas flowrate in stagnant liquid columns (39).

4.2.2.1. Correlation of the Liquid Phase Axial Mixing Data

The axial mixing data was correlated with liquid flowrate V_ℓ (0.125 - 0.335 ft/sec) and gas flowrate V_g (0.046-0.854 ft/sec) using the technique described in Appendix D. The following relationship resulted:

$$HMU = 1.385 \; V_\ell^{-0.543} \; V_g^{0.185} \quad ....(4.5)$$

where V_ℓ and V_g are in ft/sec.

The standard error of estimate between the experimental values of HMU and those calculated from equation (4.5) was 0.033 for 33 data points. Figure 4.8 shows a plot of the experimental values against the fitted values calculated from equation (4.5). Since only the liquid and gas velocities were varied in this study, it was not considered meaningful to express equation (4.5) in dimensionless form.

Michelson and Østergaard (36) correlated their axial mixing data by equation (4.6) :

$$HMU = 56.0 \; (0.179 \; V_\ell)^{-0.73} . 10^{0.08(V_g - 1)} \quad .....(4.6)$$

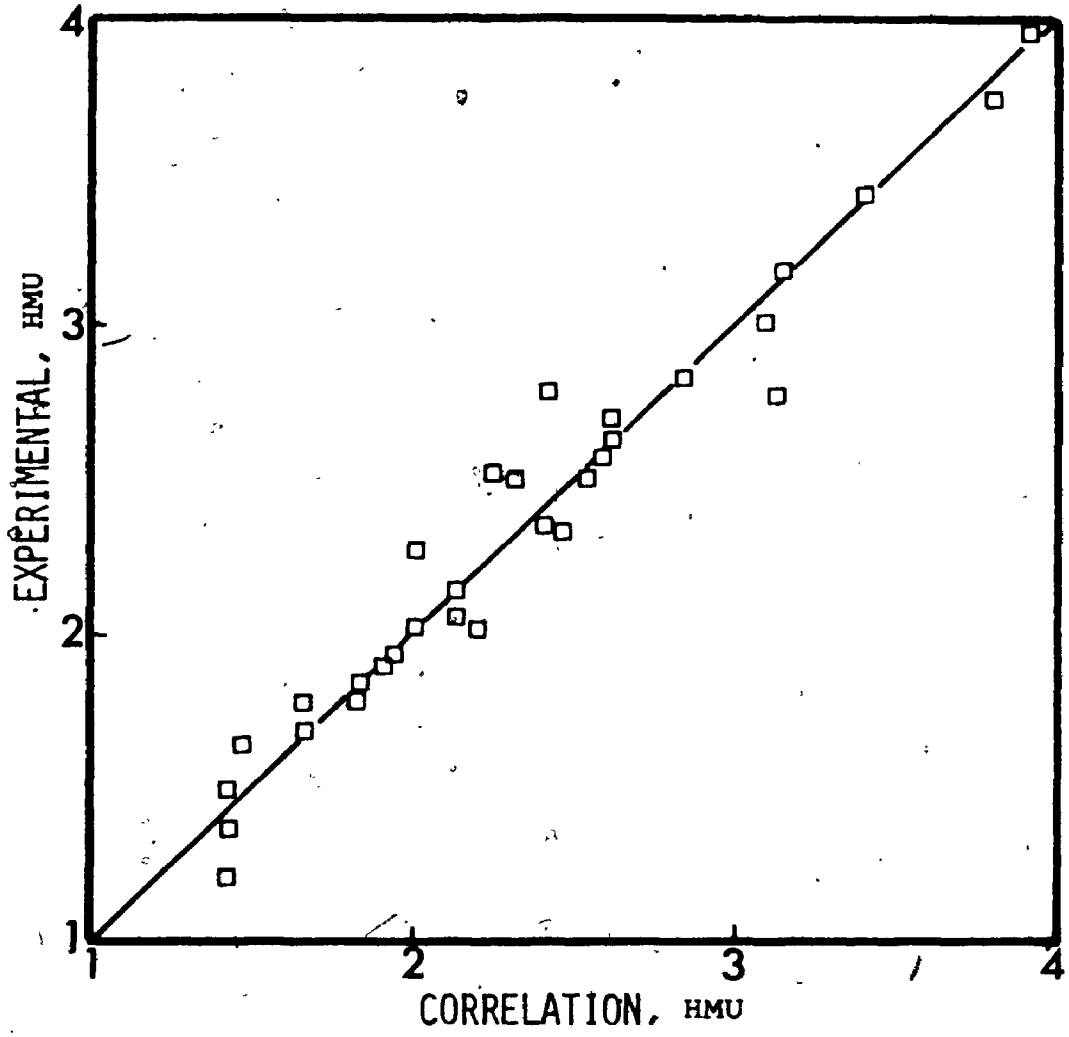

Figure 4.8 Comparison between Experimental and Calculated Values of HMU in Liquid-Gas Beds. (Equation 4.5)

There was good agreement between the present values of HMU and those of these authors at lower liquid and gas velocities. However, the values obtained from equation (4.6) were much lower than those obtained in the present study at higher liquid and gas velocities. This is again due to the fact that the higher gas flowrates employed in this work were outside the range of those studied by the above authors.

4.2.3. Bubble Characteristics

To complement the hold-up and axial mixing experiments the effects of liquid and gas velocity, liquid surface tension and viscosity on the bubble size distribution, mean size, and rising velocity were studied. The detailed data are given in Appendix I.

4.2.3.1. Mean Bubble Size, Size Distribution and Rising Velocity

Again, liquid flowrates were varied from 0.125 to 0.335 ft/sec. The effect of liquid velocity on bubble size is shown in figure 4.9 for different gas rates. It can be observed that the bubble size decreased noticeably with increasing liquid velocity in the beds of acetone (39.8 dyne/cm) and water. However, liquid velocity had no effect on the bubble size in the beds of higher liquid viscosity.

The bubble size distribution narrowed with increasing liquid velocity in all the gas-liquid beds (figure 4.10A).

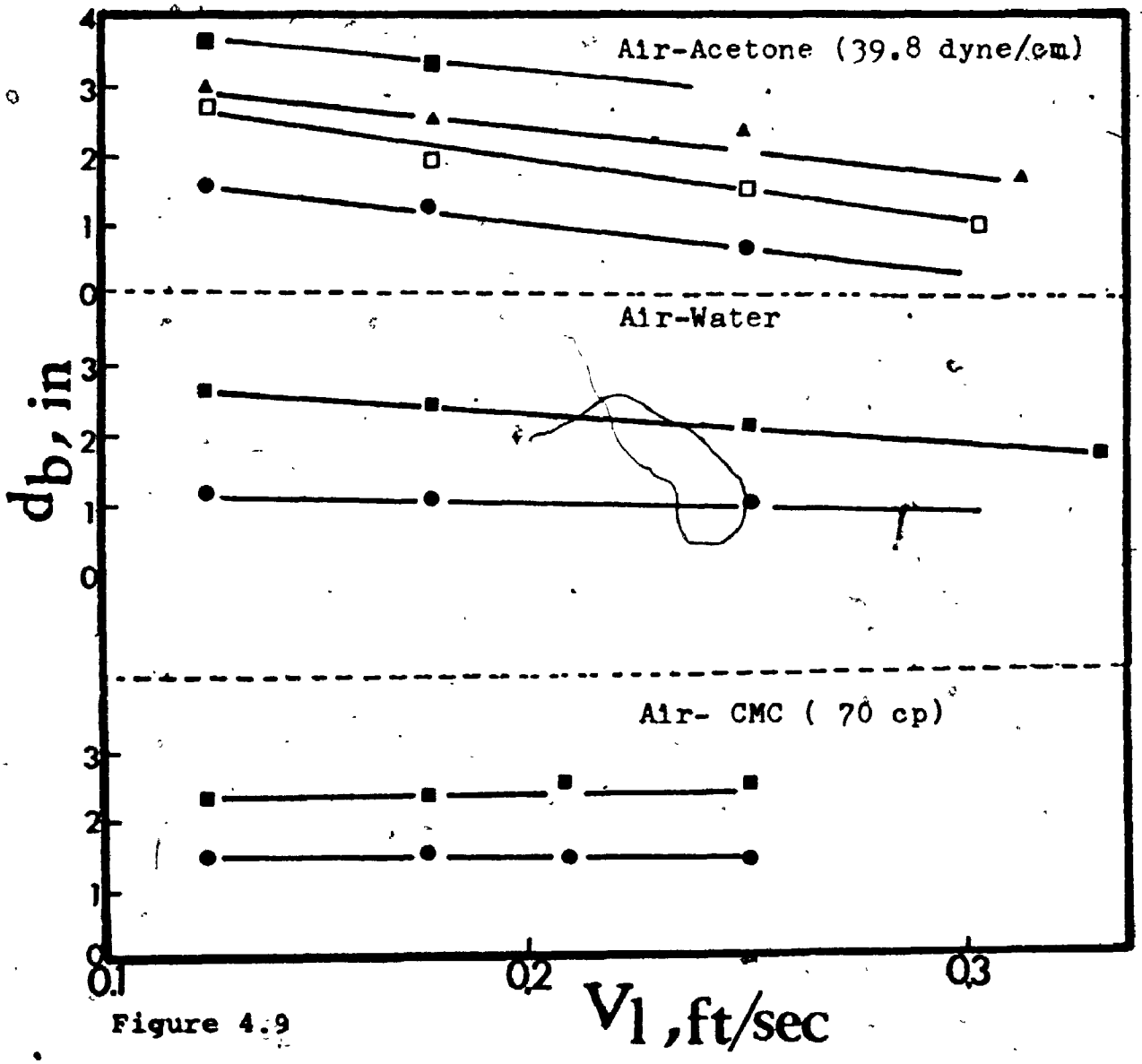

Figure 4.9

Effect of Liquid Velocity on Bubble Size in Liquid-Gas Beds. ●: V_g = 0.043 ft/sec, □: V_g = 0.185 ft/sec, ▲: V_g = 0.360 ft/sec, ■: V_g = 0.527 ft/sec.

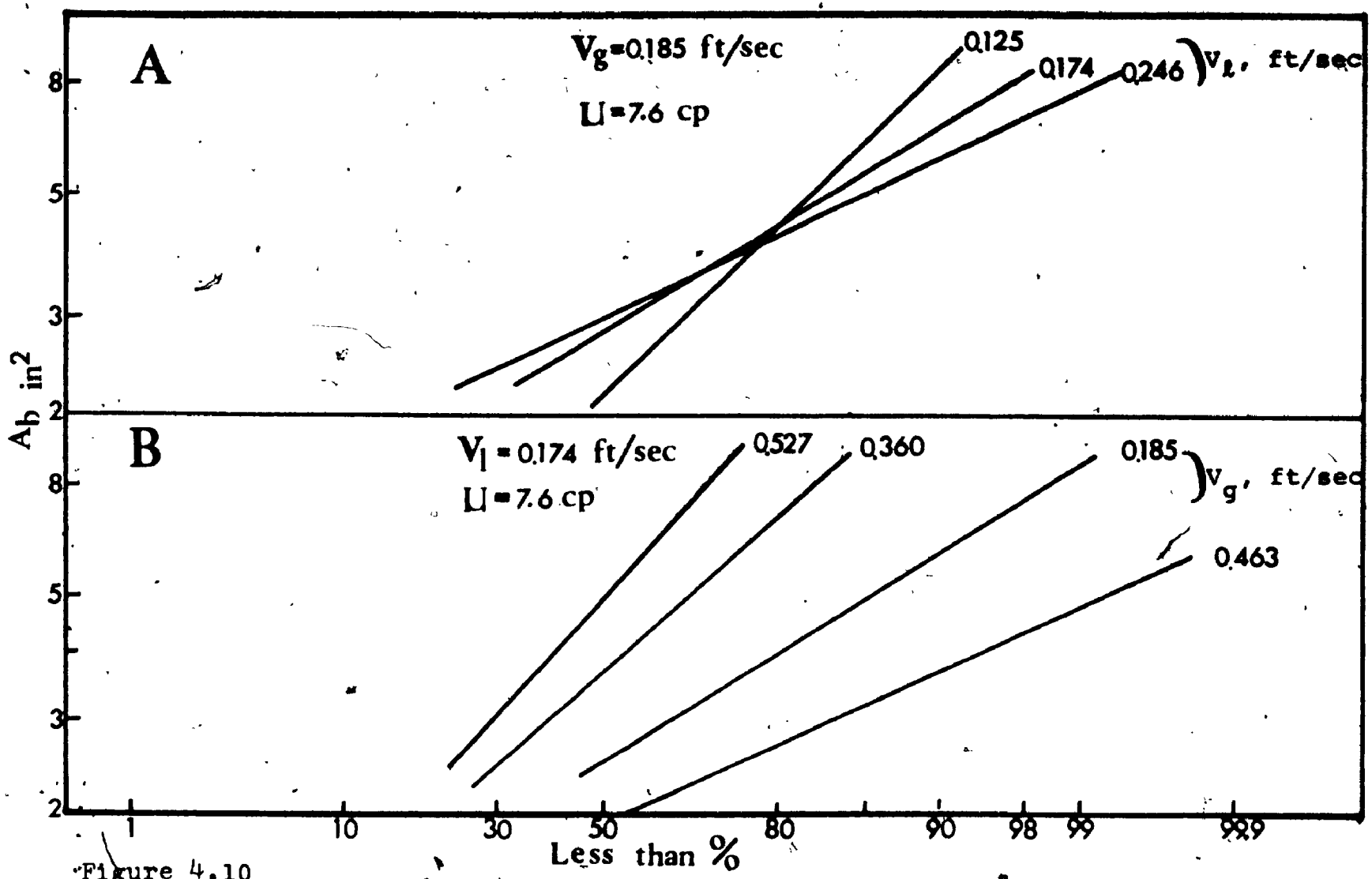

Figure 4.10

Effect of Liquid and Gas Velocity on Bubble Size Distribution in Liquid-Gas Beds. (log probability plot)

Typical plots of bubble size and rising velocity against gas velocity are shown in figure 4.11. It can be observed from this figure that both these parameters increased with increasing gas velocity in all the system studied. Again, this effect was less marked in the beds of higher viscosity. The effect of gas velocity on the size distribution can be observed in figure 4.10B. The latter widened with increasing gas velocity in all the liquid-gas beds studied.

The surface tension of the liquid may be expected to affect both the initial size of the bubbles formed at the orifices and also the degree of coalescence in the bed. In figure 4.12, it can be observed that the mean bubble size and rising velocity in the solids-free systems decreased with increasing surface tension. The effect appears to be most marked at the higher gas rates.

Viscosity changes had essentially no effect on the bubble size and rising velocity (figure 4.13). This finding is in accord with that of Davenport et al. (18) who studied the effect of viscosity on bubble size and rising velocity in gas-stagnant liquid beds.

4.2.3.2. Correlation of Bubble Rising Velocity and Bubble Size Data

A statistical analysis was performed on the bubble size and rising velocity data using the program listed in Appendix D. The following relationships resulted:

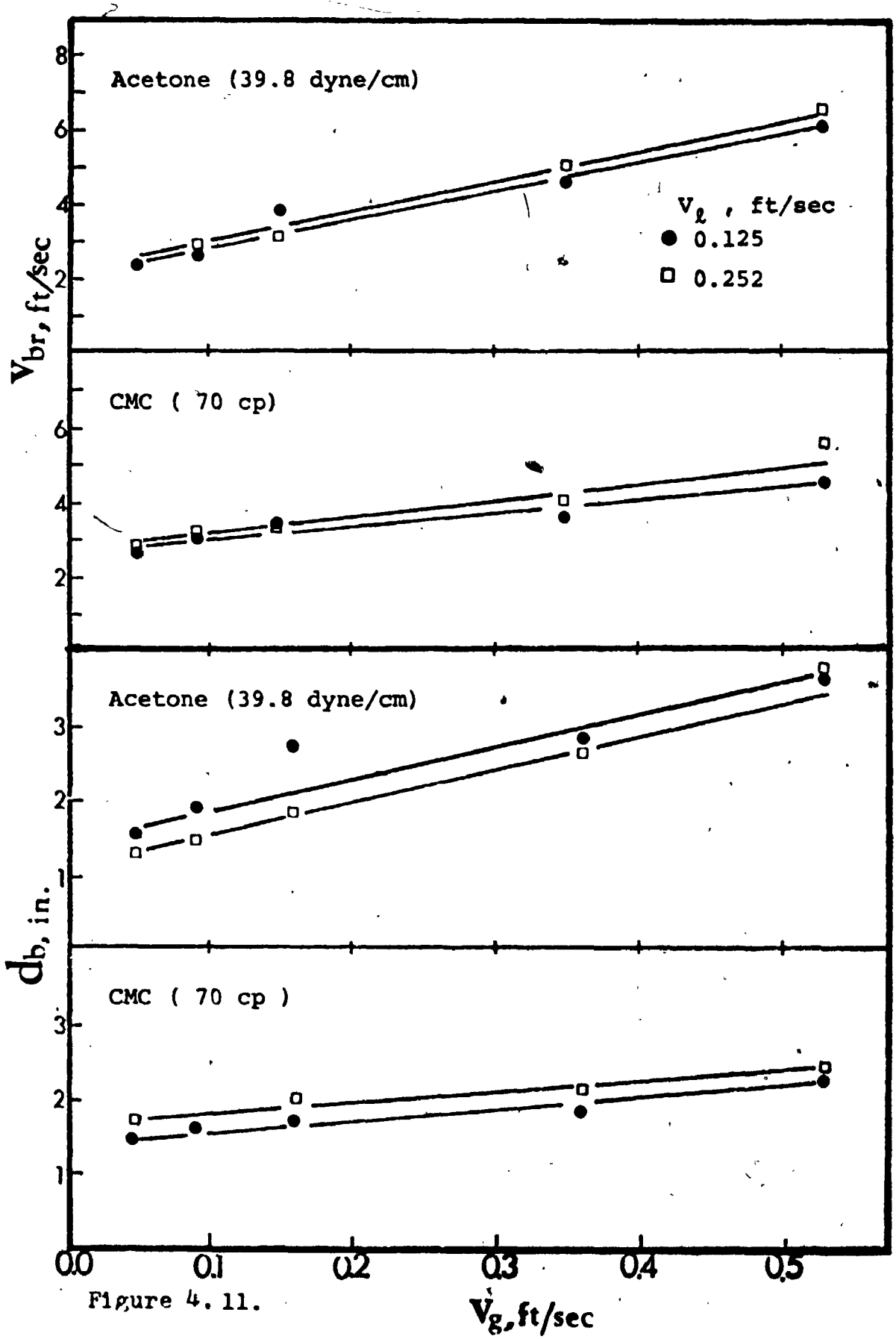

Figure 4.11.

Effect of Gas Velocity on Bubble Size and Rising Velocity in Liquid-Gas Beds.

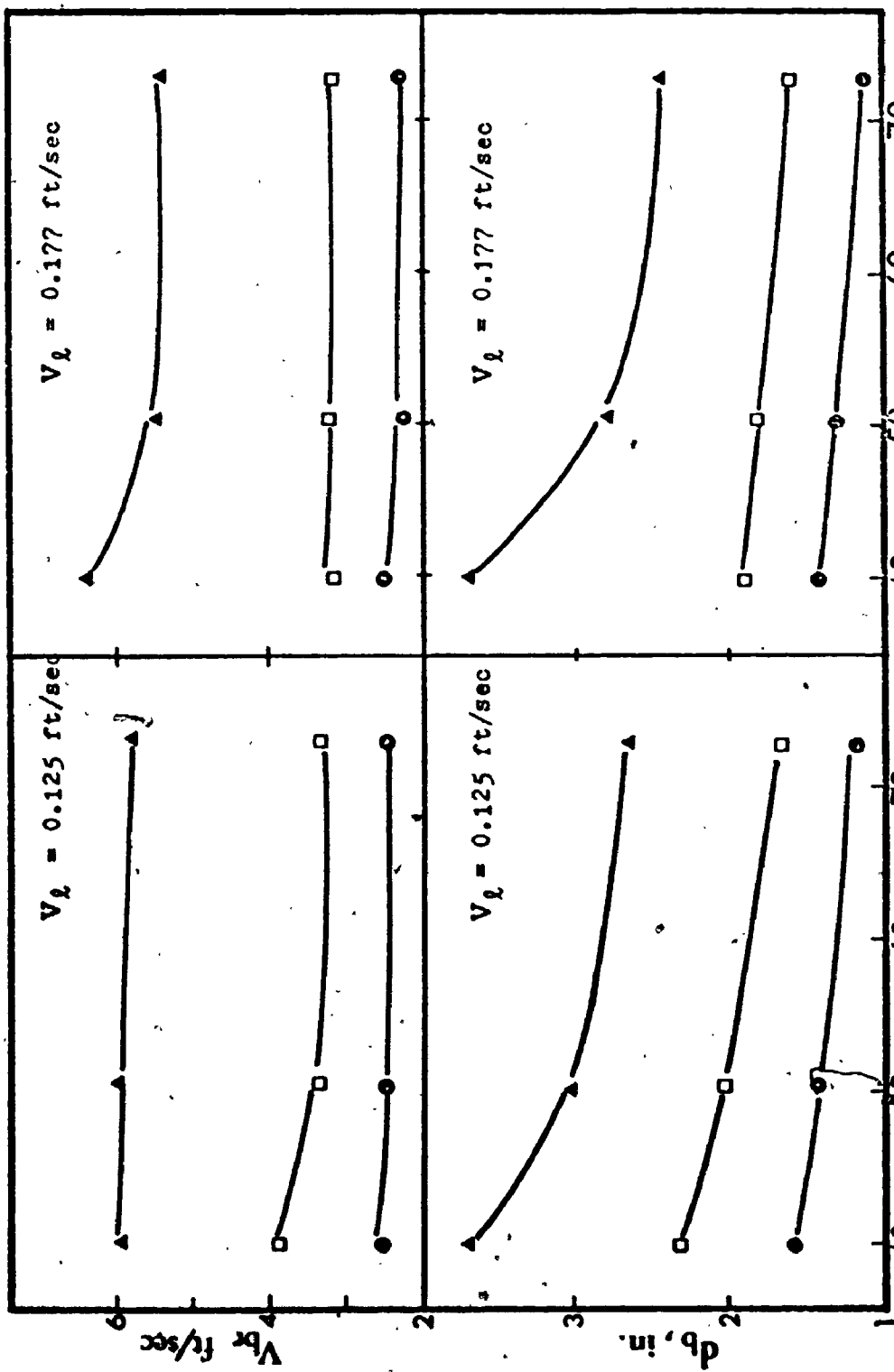

Figure 4.12. Effect of Surface Tension on Bubble Size and Rising Velocity in Liquid-Gas Beds.
●: V_g = 0.046 ft/sec □: V_g = 0.185 ft/sec ▲: V_g = 0.527 ft/sec

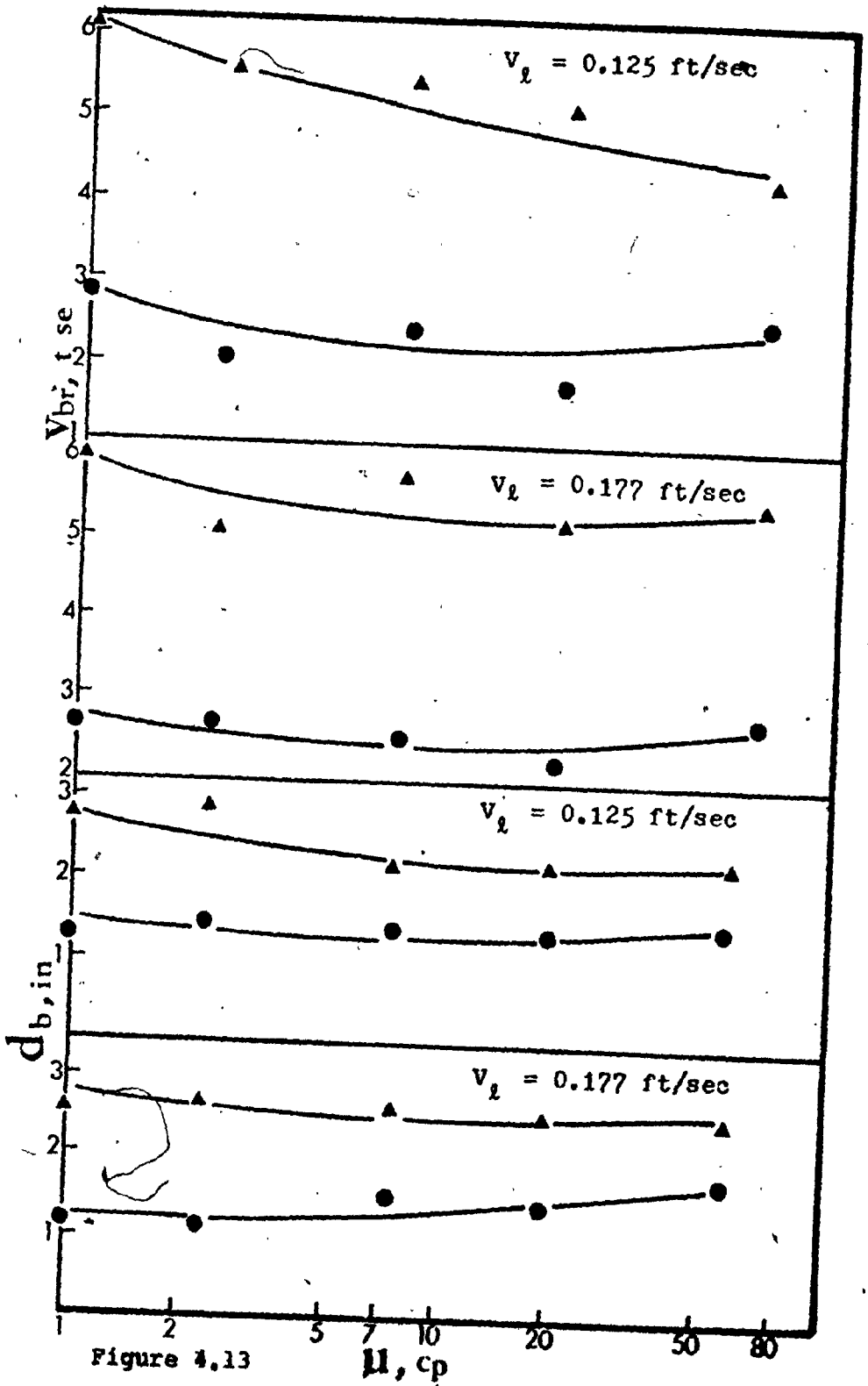

Figure 4.13

Effect of Viscosity on Bubble Size and Rising Velocity in Liquid-Gas Beds. ●: V_g=0.046 ft/sec, ▲: V_g= 0.527 ft/sec.

$$V_{br} = 5.90\ V_{\ell}^{-0.133}\ V_g^{0.341}\ \gamma^{-0.026}\ \sigma^{0.157} \quad ..(4.7)$$

$$V_{br} = 21.88\ d_b^{0.963} \quad ....(4.8)$$

where V_{ℓ} and V_g are in ft/sec, σ is in lb/sec^2 and γ (lb/ft sec^{2-n}) is defined by equation (4.2). d_b is the bubble diameter in ft and V_{br} is the relative bubble rising velocity in ft/sec. The standard errors of estimate of equations (4.7) and (4.8) are 0.513 and 0.674 respectively for 95 data points. The goodness of fit of equation (4.8) is shown in figure 4.14. As predicted by equation (4.8), the bubble rising velocity increased with bubble size in liquid-gas bubble beds. This trend has been generally observed in the published literature.

Davis and Taylor (19) showed that for a large single isolated bubble rising in an inviscid liquid:

$$V_b = 0.711\ (g\ d_b)^{0.5} \quad ....(4.9)$$

Angelino (3), who studied bubbles rising through liquids of different viscosity, obtained a similar relationship of the form:

$$V_b = k\ d_b^{m} \quad ....(4.10)$$

where k and m depended on the properties of liquid and ranged from 4.65 to 12.97 and from 0.50 to 1.14, respectively.

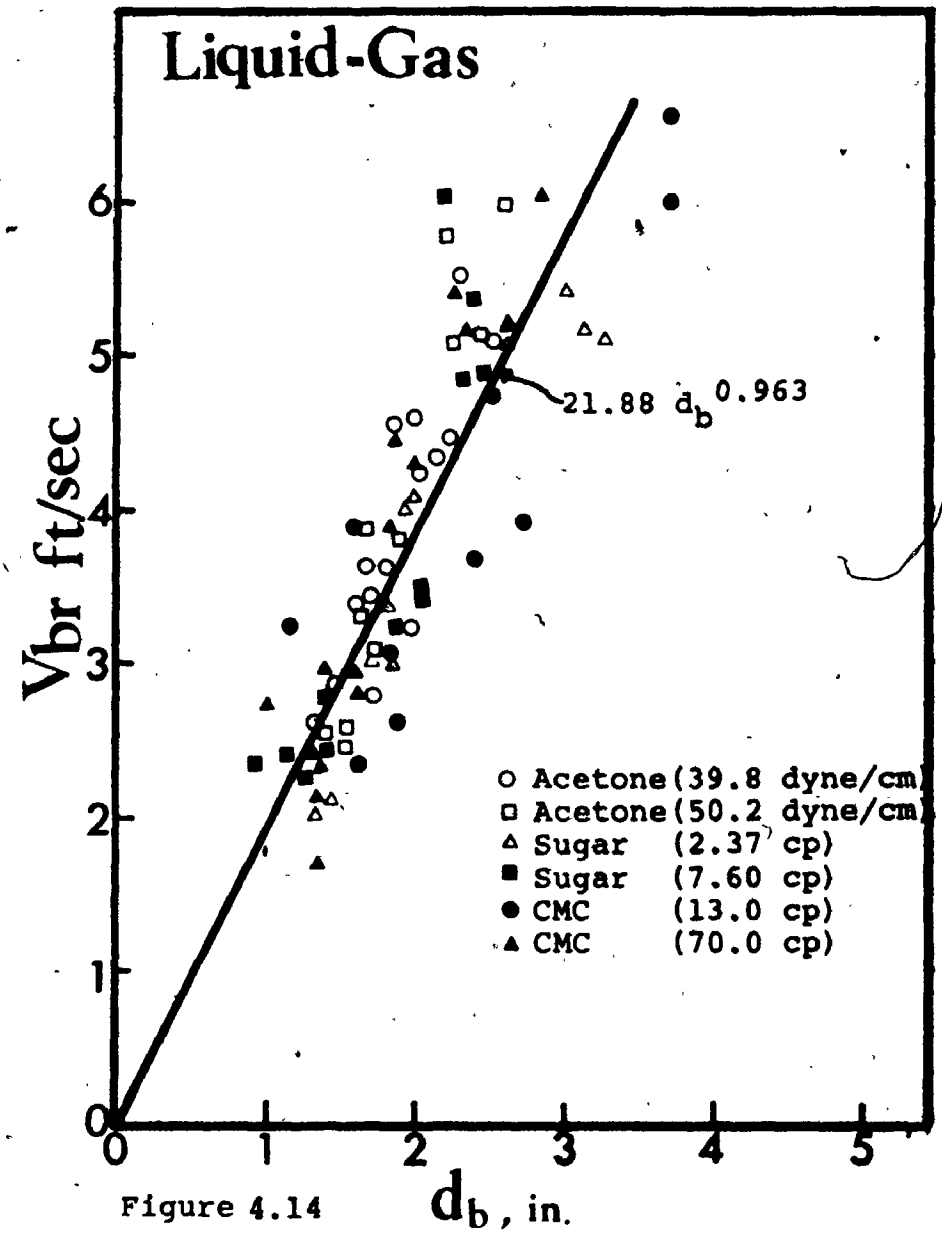

Figure 4.14

Correlation of Relative Bubble Rising Velocity with Bubble Size in Liquid-Gas Beds.

Previous experience has shown that the rising velocity of clouds of bubbles is greater than that of an isolated single bubble as predicted by equation (4.9). The present results are consistent with this finding.

4.3. LIQUID-SOLID BEDS

4.3.1. Liquid Hold-up and Bed Expansion

Since the liquid hold-up is directly proportional to the bed expansion, the liquid hold-up data only are presented in this section. The liquid flowrates were varied from 0.125 to 0.335 ft/sec. Three different particles ranging in size from 1 to 6 mm in diameter and as many as eleven different liquids were employed.

Typical plots of liquid hold-up against liquid velocity for the beds of 6 mm glass beads, 2.6 mm gravel and 1 mm glass beads are shown in figure 4.15, 4.16 and 4.17 respectively. Not unexpectedly, the liquid hold-up was found to increase with increasing liquid rate in all cases.

Variations of surface tension had no effect on the liquid hold-up as may be seen by comparing the values of ε_{ℓ_2} for beds fluidized by acetone-water (39.8 dyne/cm) and water in the above figures. However, the liquid hold-up significantly increased with viscosity in all the beds as shown in figure 4.18 as a result of the increased drag on the particles. For example, at the lowest liquid velocity, the liquid hold-up was increased 50 % by increasing the viscosity from 1 to 70 cp. The effect of particle size on the liquid hold-up is shown in figure 4.19. As may be

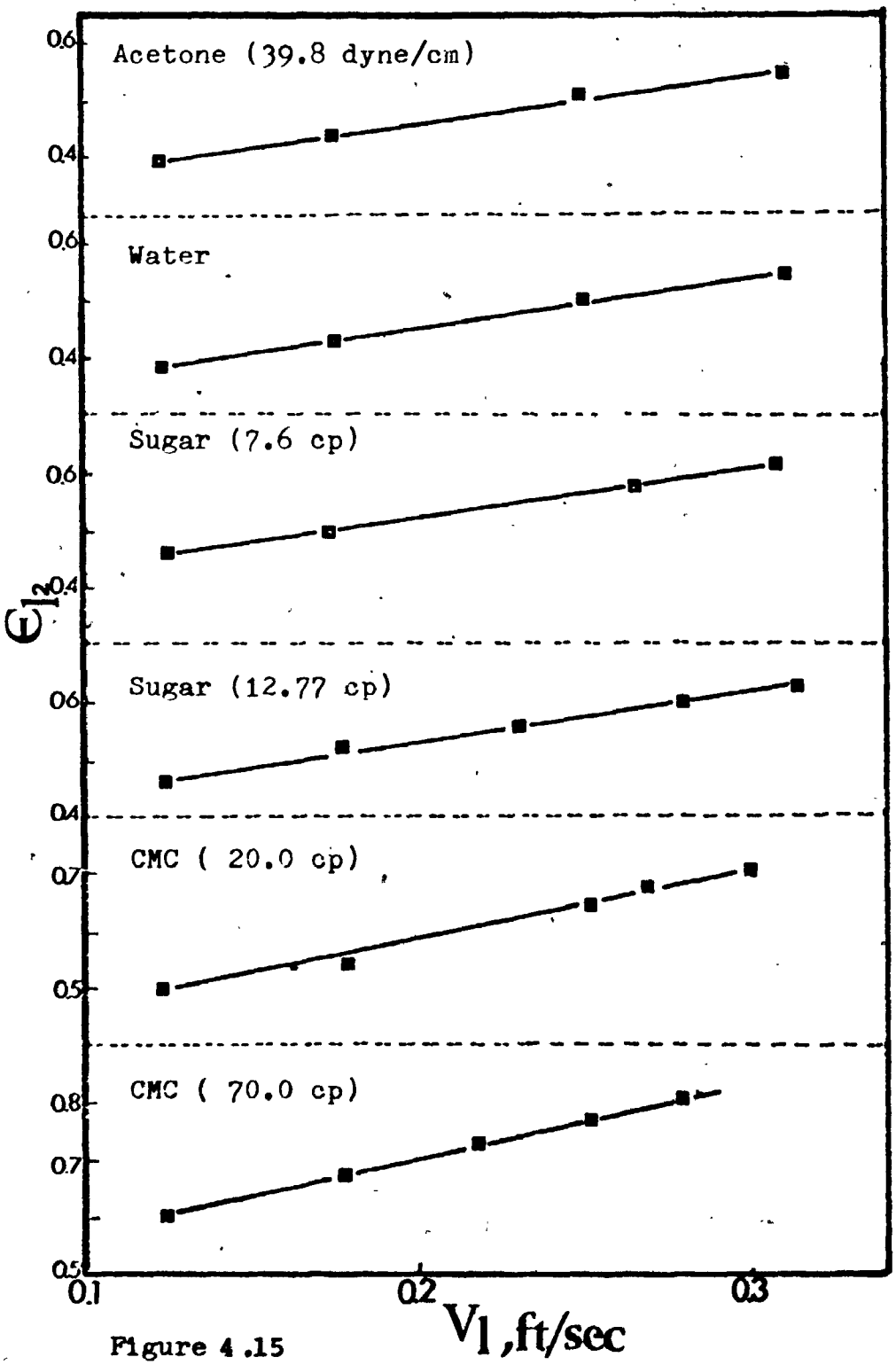

Figure 4.15

Effect of Liquid Velocity on Liquid Hold-up in Beds of 6 mm Glass beads.

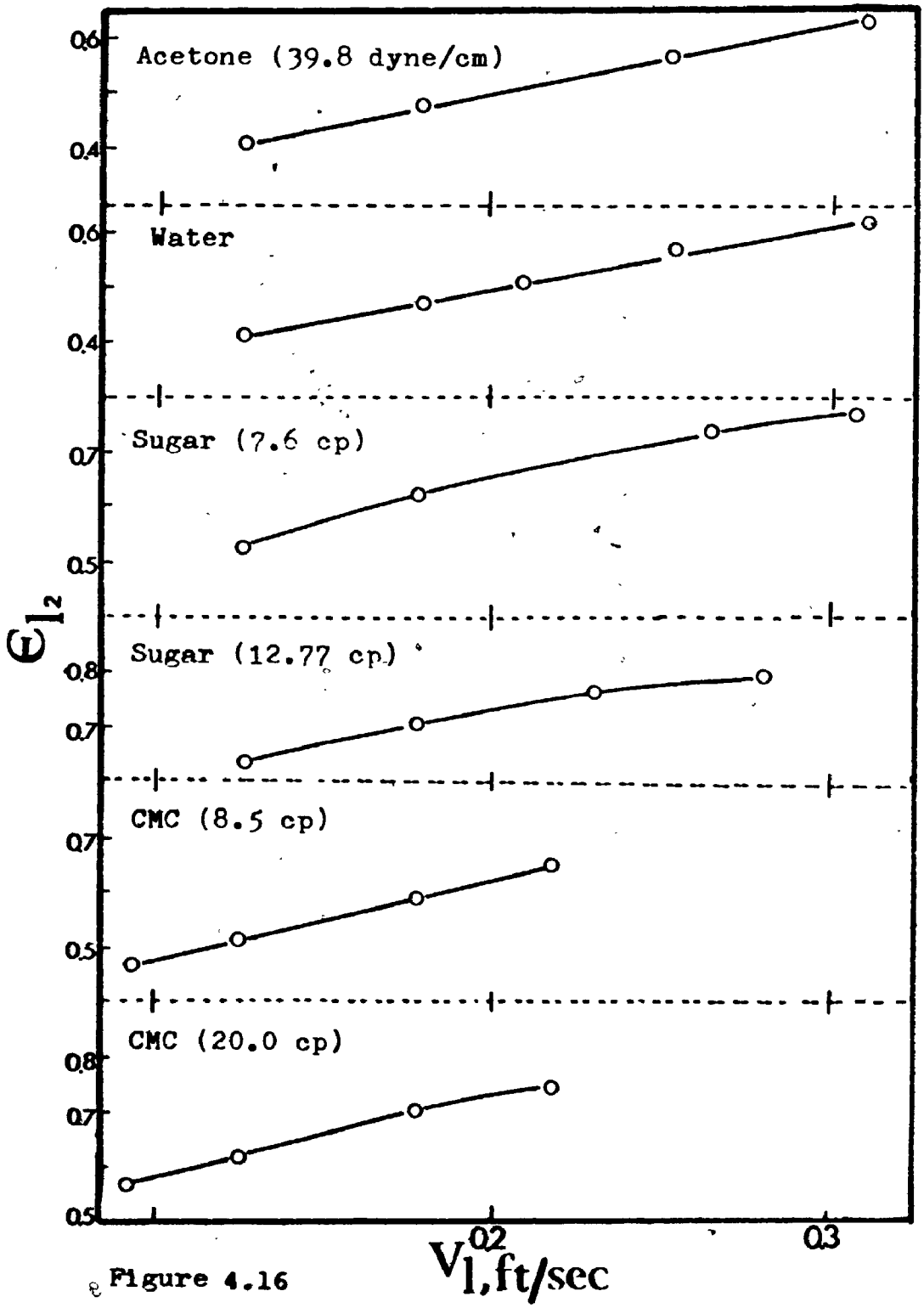

Figure 4.16

Effect of Liquid Velocity on Liquid Hold-up in Beds of 2.6 mm Gravel

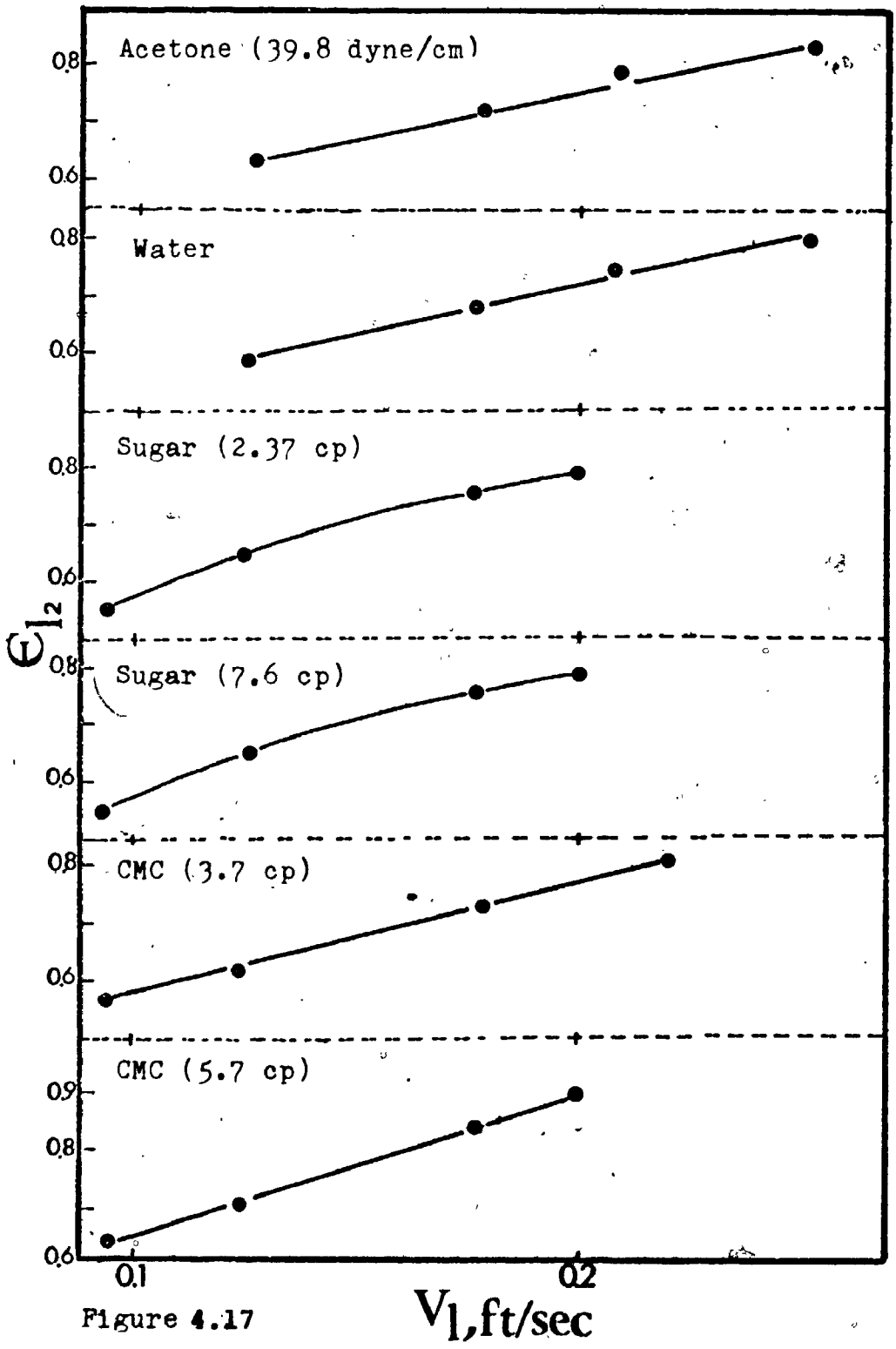

Figure 4.17

Effect of Liquid Velocity on Liquid Hold-up in Beds of 1 mm Glass beads.

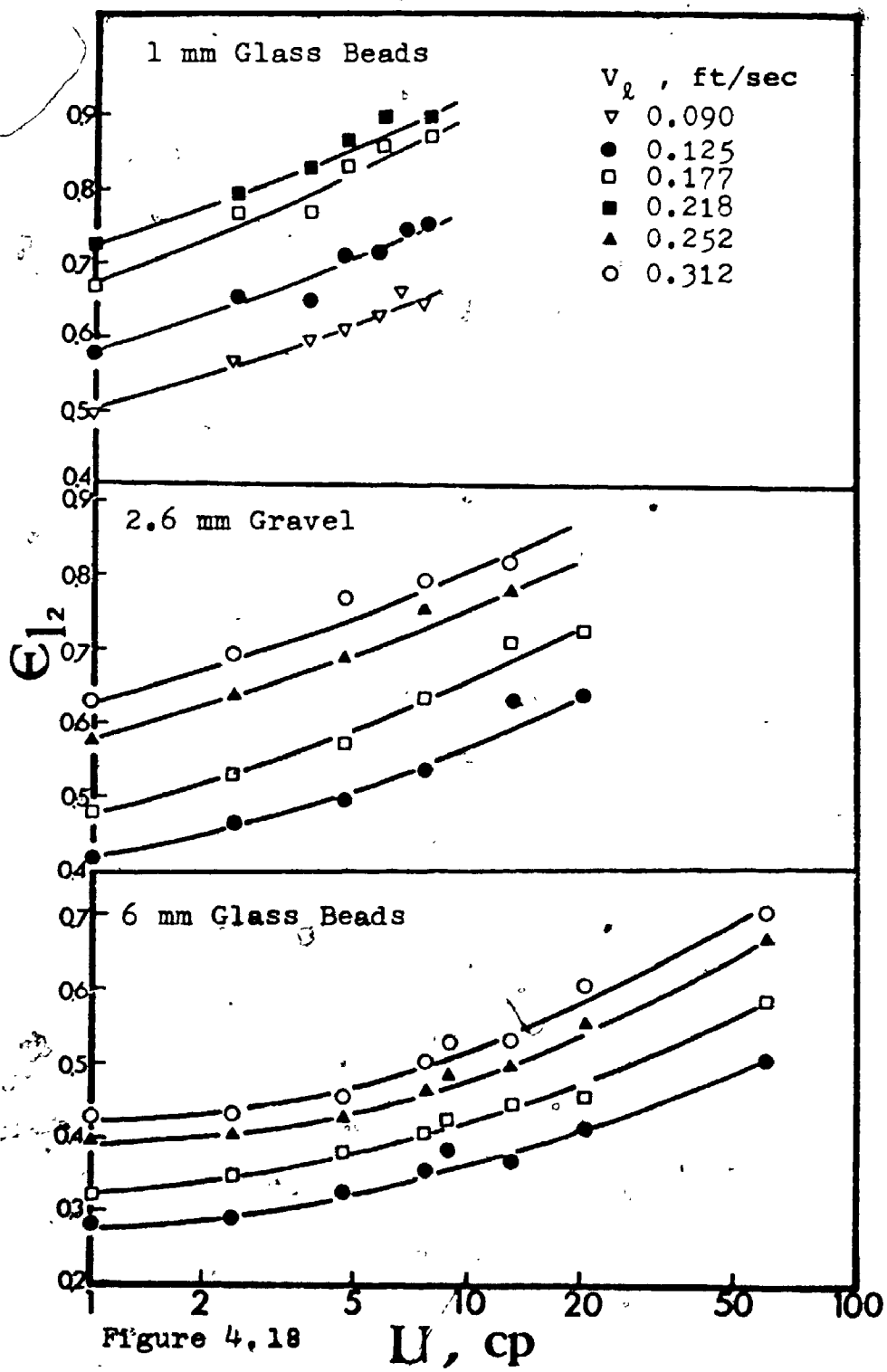

Figure 4.18

Effect of Liquid Viscosity on Liquid Hold-up in Liquid-Solid Beds.

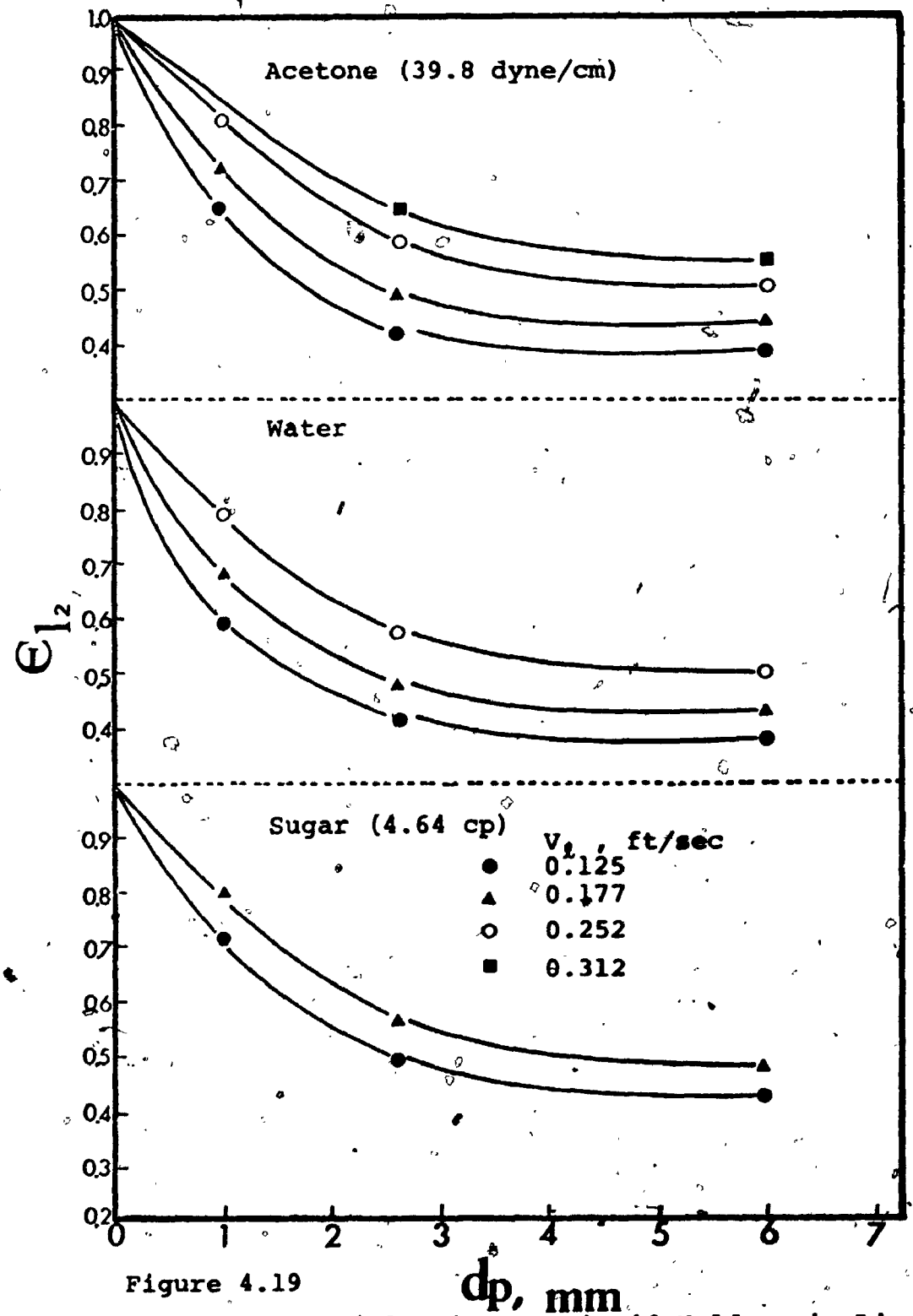

Figure 4.19

Effect of Particle Size on Liquid Hold-up in Liquid-Solid Beds.

seen, $\varepsilon_{\ell 2}$ decreased sharply with the increasing particle size up to 2.5 mm. However, above 2.5 mm, the rate of decrease was not so marked.

4.3.1.1. Correlation of the Liquid Hold-up Data

A statistical analysis was performed on the liquid hold-up data for liquid velocities V_ℓ between 0.125 and 0.335 ft/sec, viscosities μ between 1 and 70 cp, and particle diameters d_p between 1 and 6 mm. Since the effect of surface tension on ε_{ℓ_2} was found to be insignificant in the range 39.8 - 72.8 dyne/cm for all systems, it was neglected in the analysis. The following relationship resulted:

$$\varepsilon_{\ell_2} = 0.589\ V_\ell^{0.380}\ d_p^{-0.285}\ \gamma^{0.115} \qquad \ldots(4.9)$$

where V_ℓ is in ft/sec, d_p is in ft, and γ is in $lb/ftsec^{2-n}$. The standard error of estimate between the experimental and calculated values of equation (4.9) is 0.028 for 147 data points. Equation (4.9) can be expressed in dimensionless form as follows:

$$\varepsilon_{\ell 2} = 1.353\ (Fr_\ell)^{0.206}\ (Re_\ell)^{-0.100} \qquad \ldots.(4.10)$$

where Fr_ℓ is the Froude number $V_\ell^2/d_p g$, and Re_ℓ is the particle Reynolds number $V_\ell^{2-n}\ d_p^n\ \rho_\ell/\gamma$.
The standard error of estimate between experimental and the calculated values of equation (4.10) is 0.038 for 147 data points. The goodness of fit between experimental and calculated values of equation (4.10) is shown in figure 4.20.

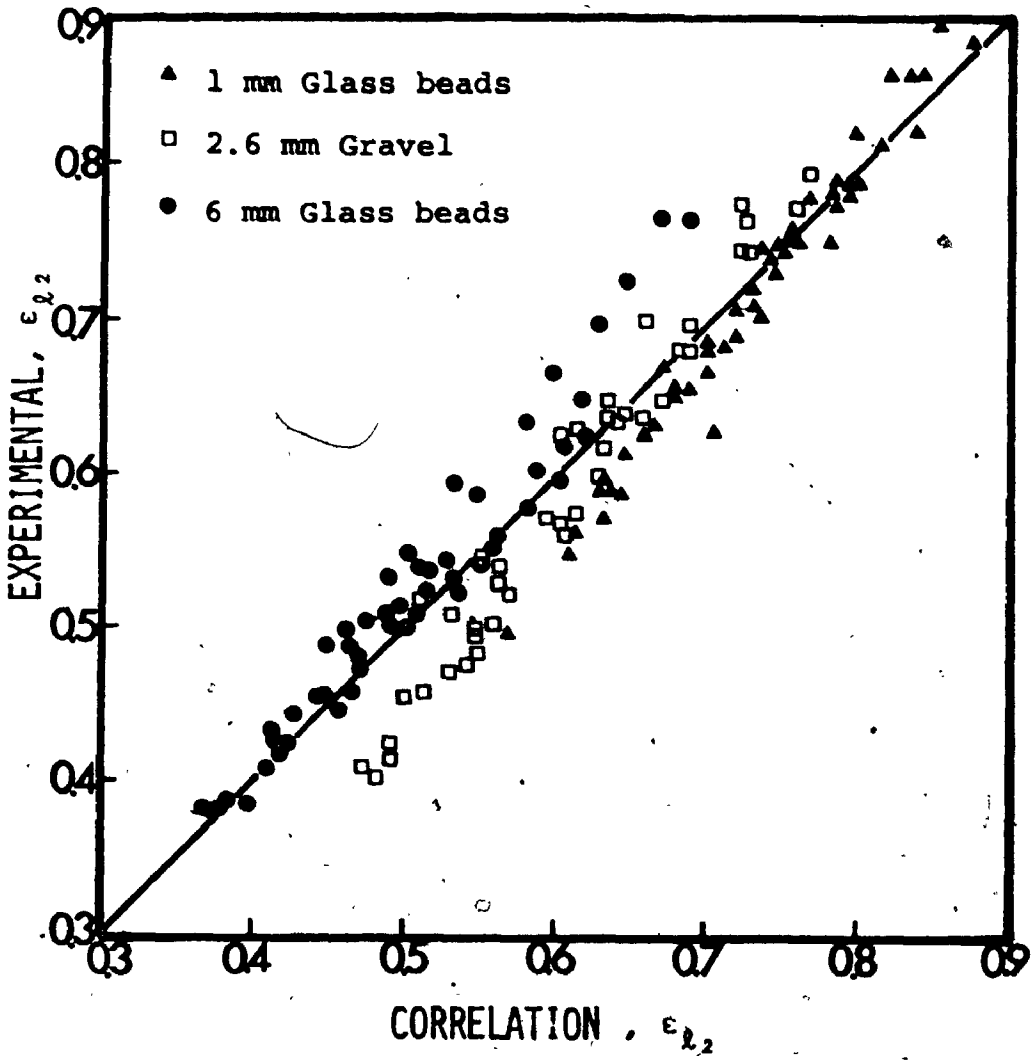

Figure 4.20. Comparison between Experimental and Calculated Values of ε_{ℓ_2} in Liquid-Solid Beds. (Equation 4.10)

The present experimental values and those predicted by Richardson and Zaki's (51) correlation were also in good agreement. The standard deviation in this case was 0.063 for 147 data points. The Reynolds numbers based on particle terminal velocity ranged between 13 and 3008 in this study.

4.3.2. Liquid Phase Axial Mixing

Axial mixing of the liquid phase in the liquid-solid fluidized beds was measured by the step and pulse tracer techniques in the beds of gravel and 6 mm glass beads. Only step injection was employed in the beds of 1 mm glass beads. Tap water was used as the liquid phase.

The initial bed height Ho was 21.5 in. for beds of gravel and 6 mm glass beads, and 10 in. for beds of 1 mm glass beads. Values of the height of the mixing unit HMU are plotted against liquid superficial velocity for three different particle sizes in figure 4.21. In general, HMU increased with increasing liquid velocity and with decreasing particle size. However, a direct comparison between the results for the 1 mm glass beads and the larger particles cannot be made due to the difference in the initial bed heights.

Significantly different values of HMU were obtained by the pulse and step tracer techniques in the beds of 6 mm glass beads. The reason for this difference is not understood, but it may be associated with experimental error due to an imperfect pulse which is significant only under conditions of extremely low axial mixing. This is supported by the much closer results obtained by the two techniques in the beds of

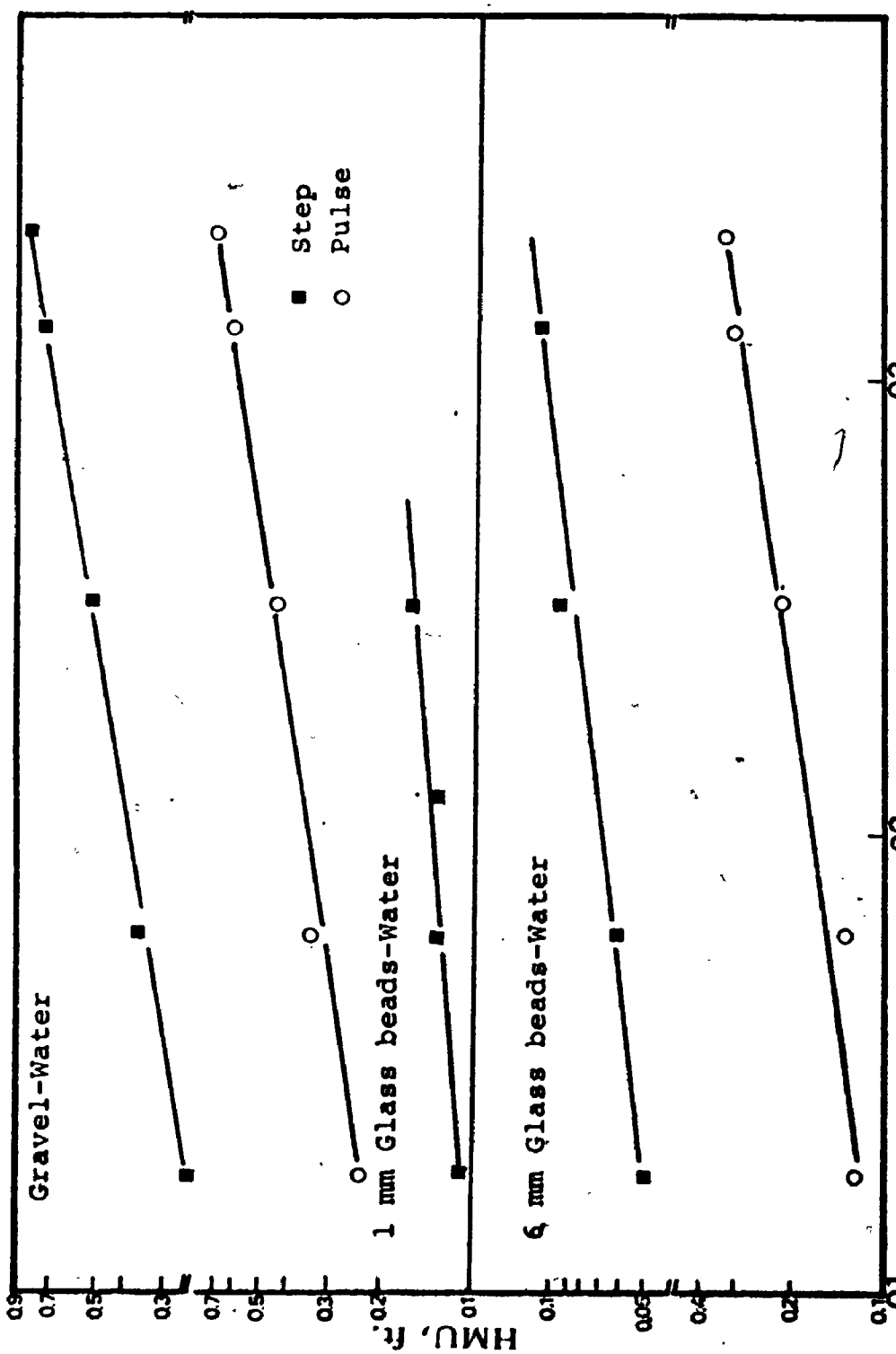

Figure 4.21
Effect of Liquid Velocity on Liquid Phase HMU in Liquid-Solids Beds.

gravel where the mixing was much better.

Examination of the axial mixing data of figures 4.7 and 4.21 shows that the HMU values are significantly larger in the liquid-gas beds than in the liquid-solid beds. It would seem therefore that, in the present case at least, the gas bubbles have considerably more influence on the liquid mixing than do the solids. It is also of interest to note that in the liquid-solid beds, HMU increased with liquid velocity in contrast to the reverse trend exhibited by the solids-free system.

The present findings are in good accord with those of Cairns and Prausnitz (10) who studied longitudinal mixing in beds of 1.3 and 3.0 mm lead shot and 3.2 mm glass beads fluidized by water. These authors found that the longitudinal mixing increased with increasing liquid hold-up and with decreasing particle size. The present observations also qualitatively agree with those of Hanratty et al. (27) and Letan and Elgin (31).

4.3.2.1. Correlation of the Liquid Phase Axial Mixing Data

A statistical analysis was performed on the liquid phase axial mixing data for liquid velocities V_ℓ from 0.125 to 0.335 ft/sec and particle diameters d_p from 1 to 6 mm. The procedure and computer program used are given in Appendix D. The following relationship resulted:

$$\frac{HMU}{Ho} = 0.049 \quad V_\ell^{1.372} \quad d_p^{-0.694} \qquad \ldots.(4.11)$$

where V_ℓ is in ft/sec, and d_p is in ft, and Ho is the initial bed height in ft. The standard error of estimate between the experimental values of HMU/Ho and those calculated by equation (4.11) is 0.08 for 22 data points. Equation (4.11) can be expressed in dimensionless form as follows:

$$\frac{HMU}{Ho} = 0.555 \ (Fr_\ell)^{0.689} \qquad \ldots.(4.12)$$

where Fr_ℓ is the Froude number $V_\ell^2/d_p g$.
The standard error of estimate between the experimental values and those calculated from equation (4.12) is 0.087 for 22 data points, the goodness of fit is illustrated in figure 4.22.

4.4. LIQUID-GAS-SOLID BEDS

The beds consisted of either 1 mm glass beads, 2.6 mm gravel or 6 mm glass beads fluidized by the cocurrent flow of air and one of a number of different liquids.
The effect of liquid and gas flowrate and the properties of the liquid and solid phases on the individual liquid and gas hold-ups, bed porosity (expanded bed height), axial mixing of the liquid phase and bubble characteristics were determined.

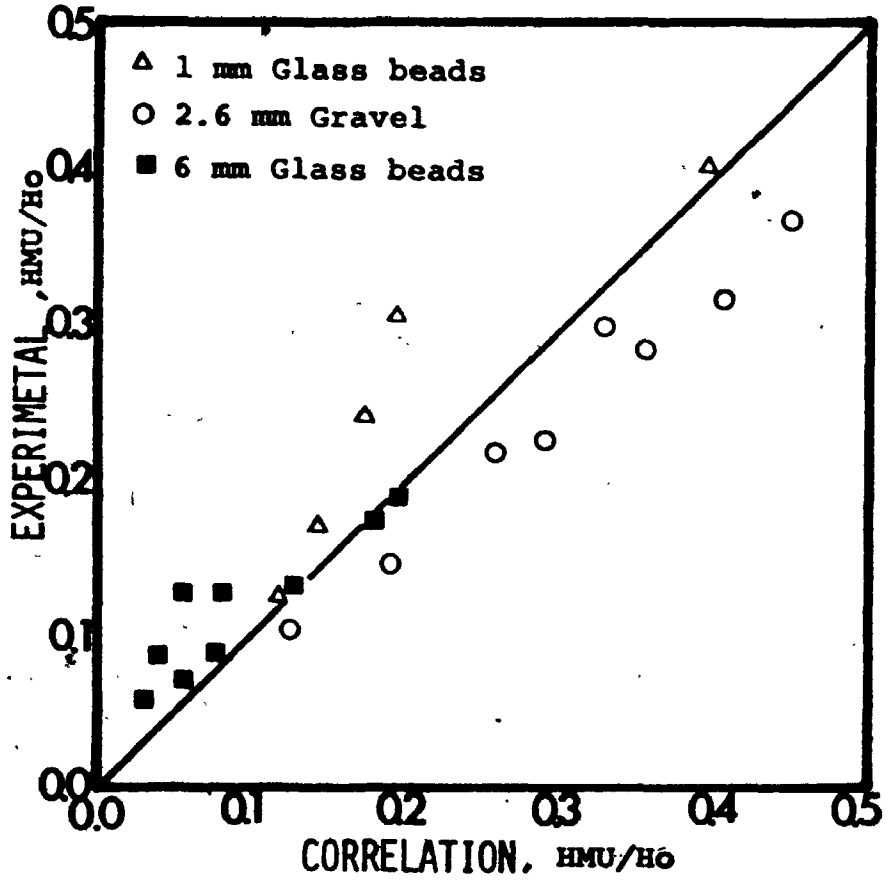

Figure 4.22 Comparison between Experimental and Calculated Values of HMU/Ho in Liquid-Solid Beds (Equation 4.12)

4.4.1. Liquid and Gas Phase Hold-ups

The liquid phase hold-up data for beds of 6 mm glass beads fluidized by air and different liquids are shown in figure 4.23. It can be noted from the figure that ε_{ls} increased with increasing liquid flowrate in all the systems studied. At given liquid and gas flowrates, the liquid hold-up also increased with increasing liquid viscosity. The same trends were observed in the beds of gravel and 1 mm glass beads as shown in figures 4.24 and 4.25. Under the same experimental conditions, the liquid hold-ups were greater in the beds of 1 mm glass beads than in the beds of larger particles. Comparison of the data in figures 4.2 and 4.23-4.25 shows that the presence of solid particles reduced the liquid hold-up. This reduction was much greater with the larger particles than with small ones.

The effect of gas flowrate on liquid hold-up in the different beds is shown in figures 4.26-4.28. Generally, ε_{ls} decreased somewhat with increasing gas flowrate. However, the rate of decrease was not very marked considering the wide range of gas velocities employed, but was noticeably more pronounced in the beds of small particles than in those of the larger particles.

As may be anticipated, the gas hold-up increased markedly with increasing gas flowrate in all the systems

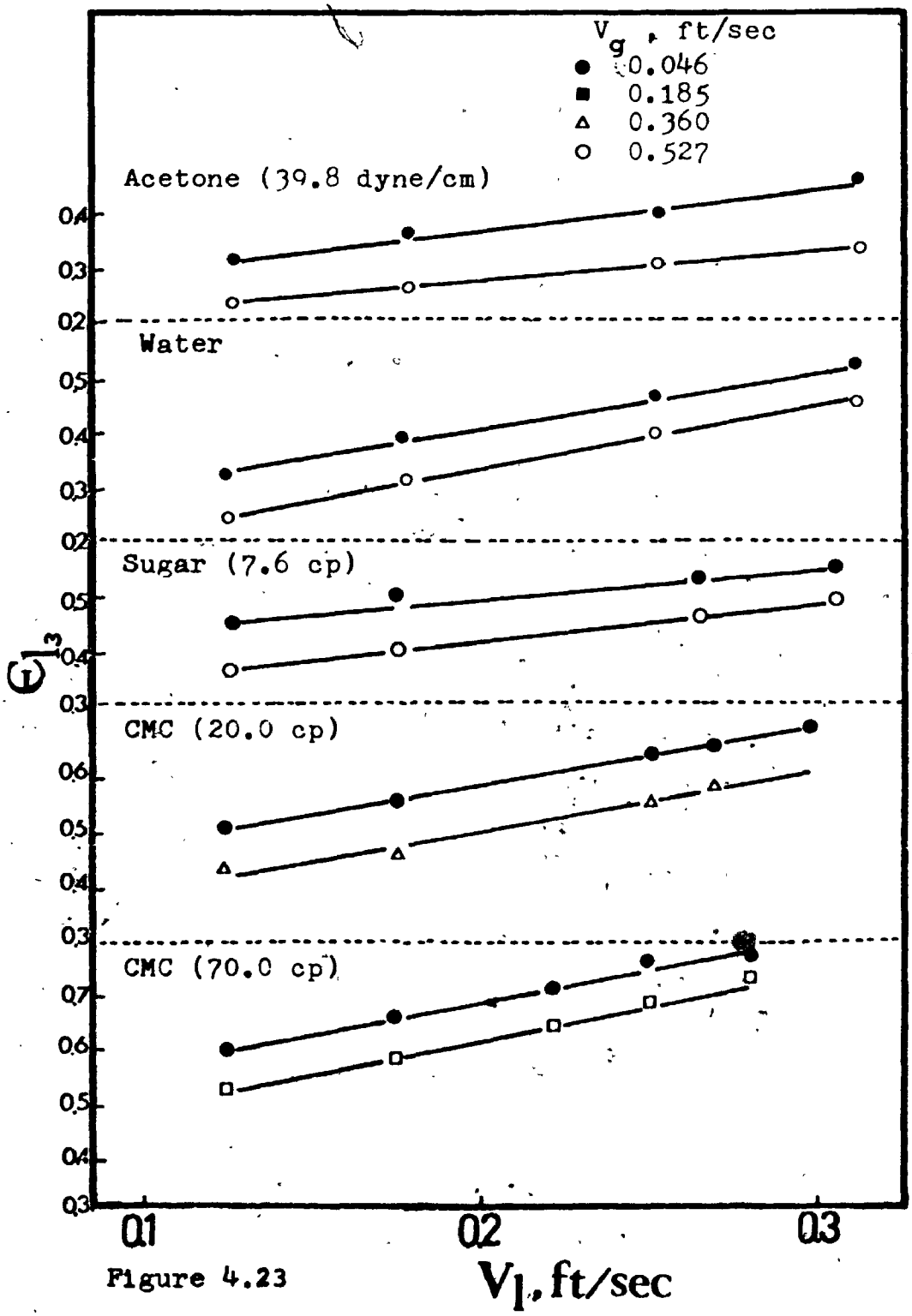

Figure 4.23

Effect of Liquid Velocity on Liquid Hold-up in Three Phase Beds of 6 mm Glass Beads.

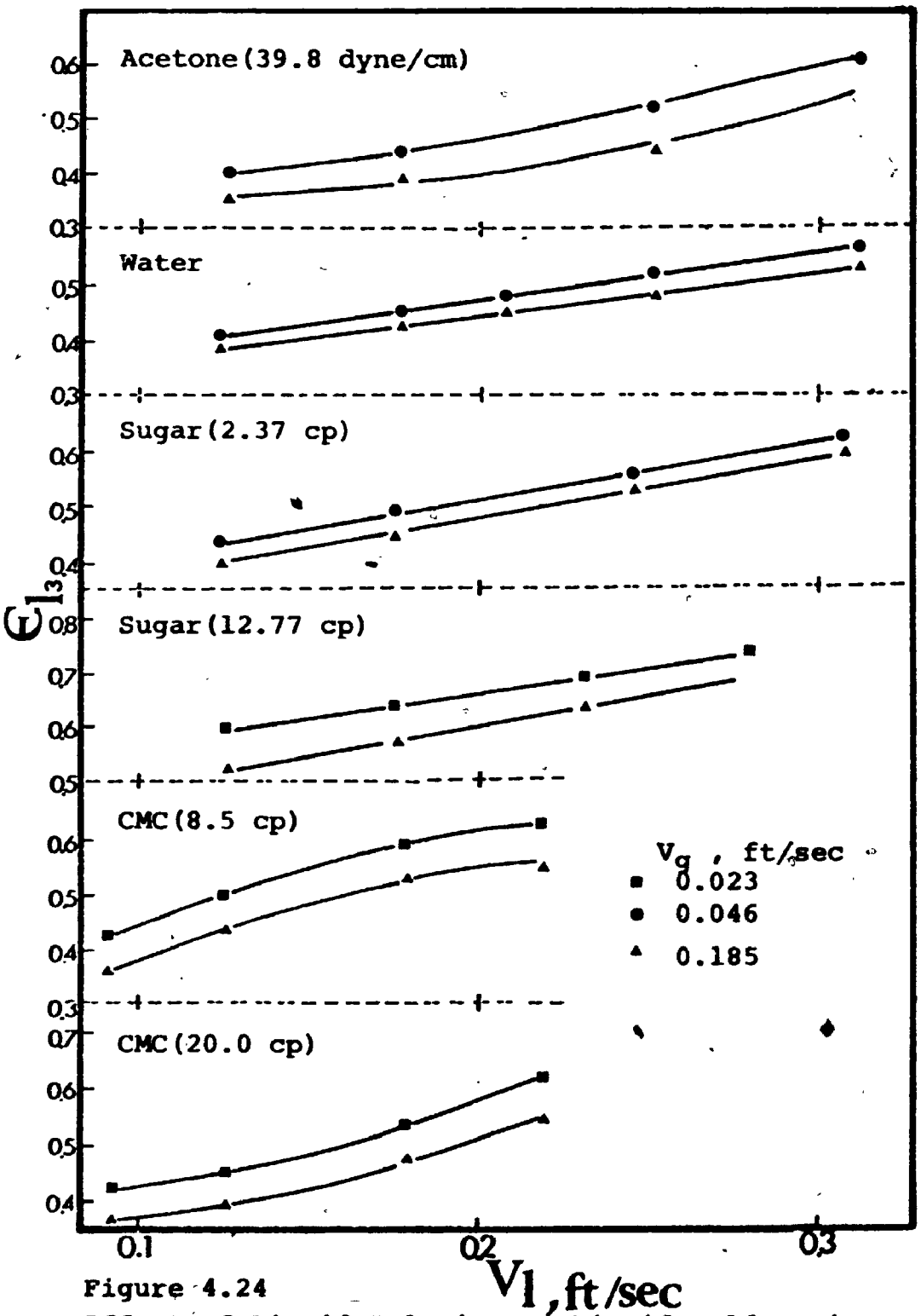

Figure 4.24
Effect of Liquid Velocity on Liquid Hold-up in Three Phase Beds of Gravel.

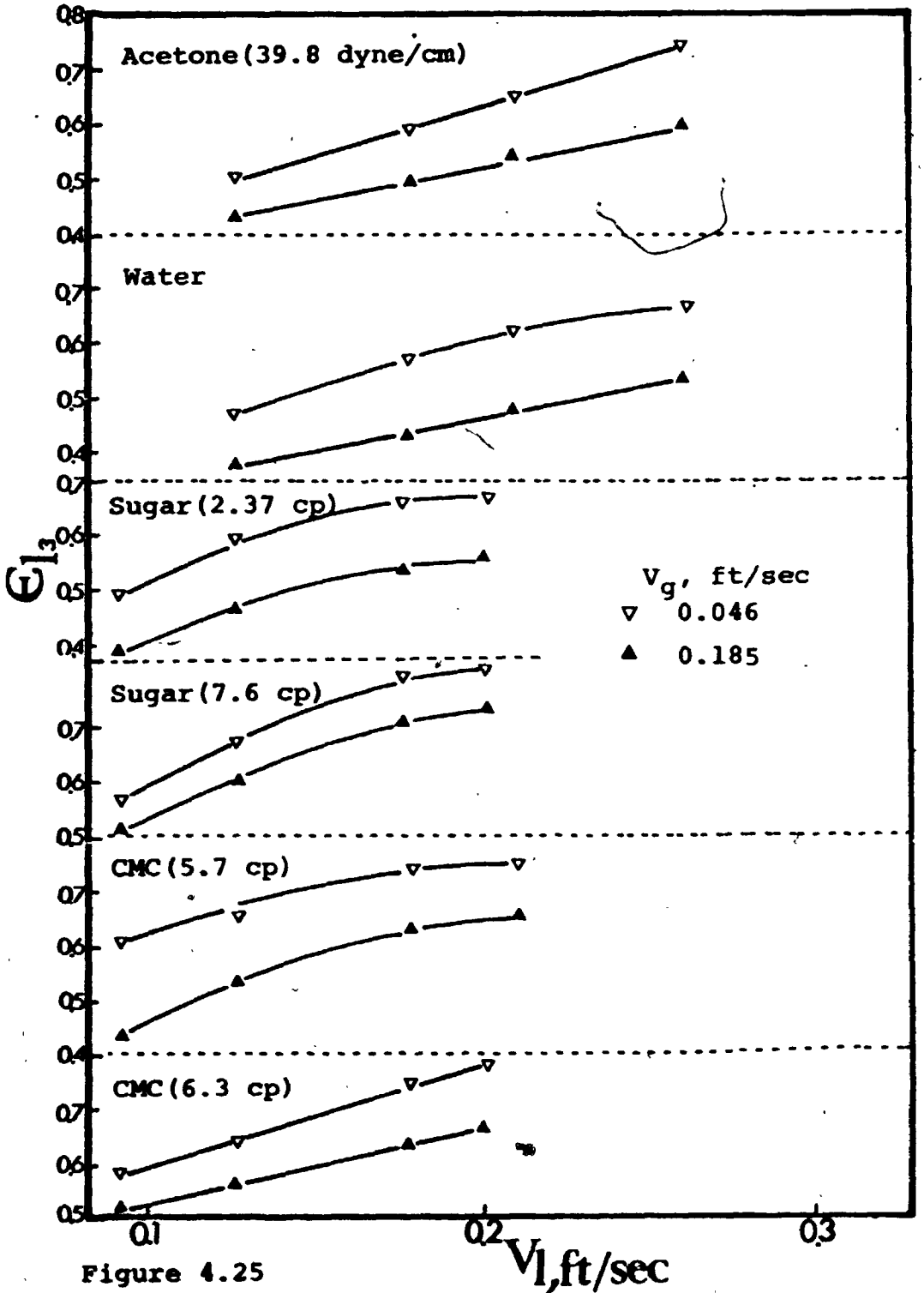

Figure 4.25

Effect of Liquid Velocity on Liquid Hold-up in Three Phase Beds of 1 mm Glass beads.

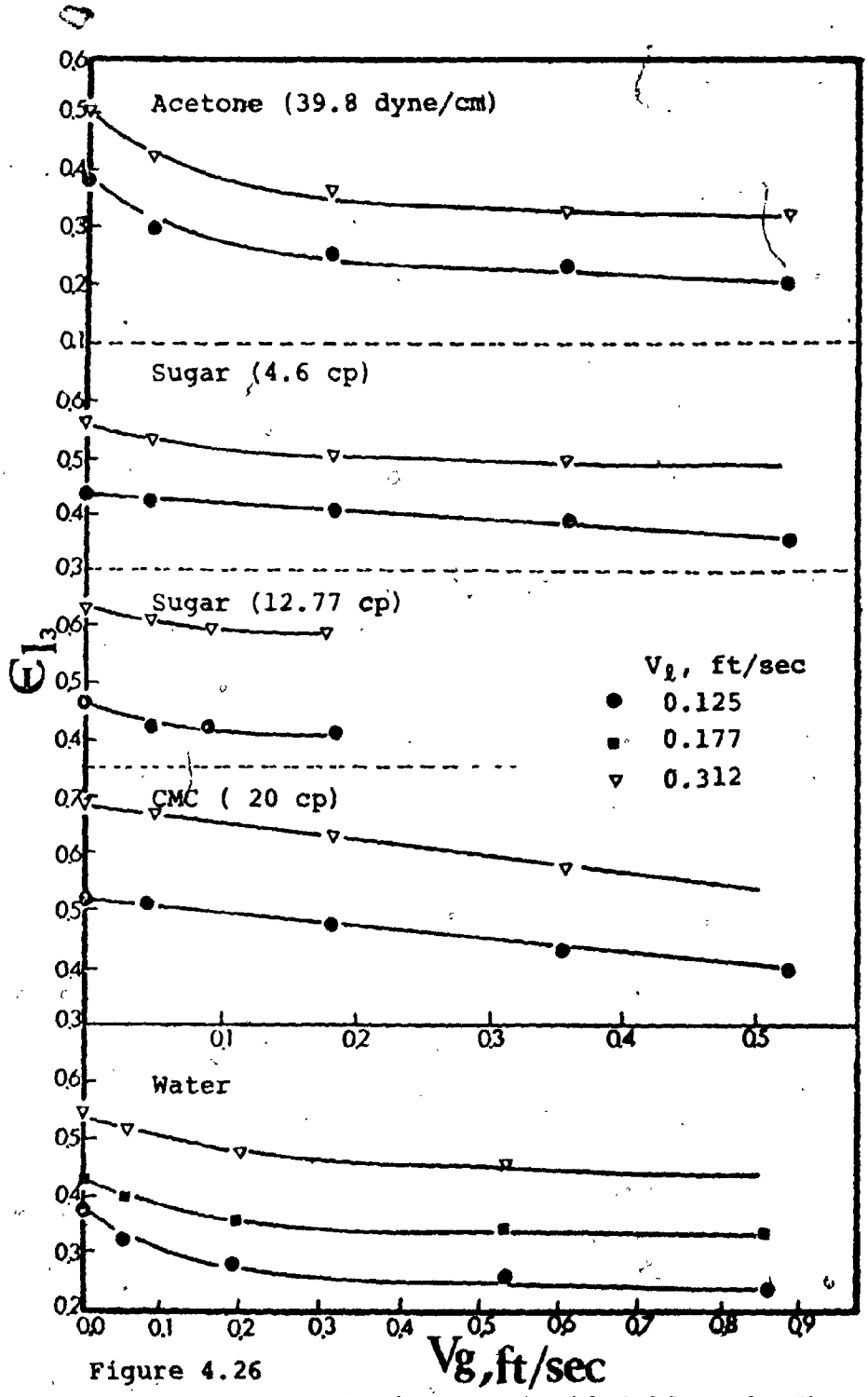

Figure 4.26
Effect of Gas Velocity on Liquid Hold-up in Three Phase Beds of 6 mm Glass beads.

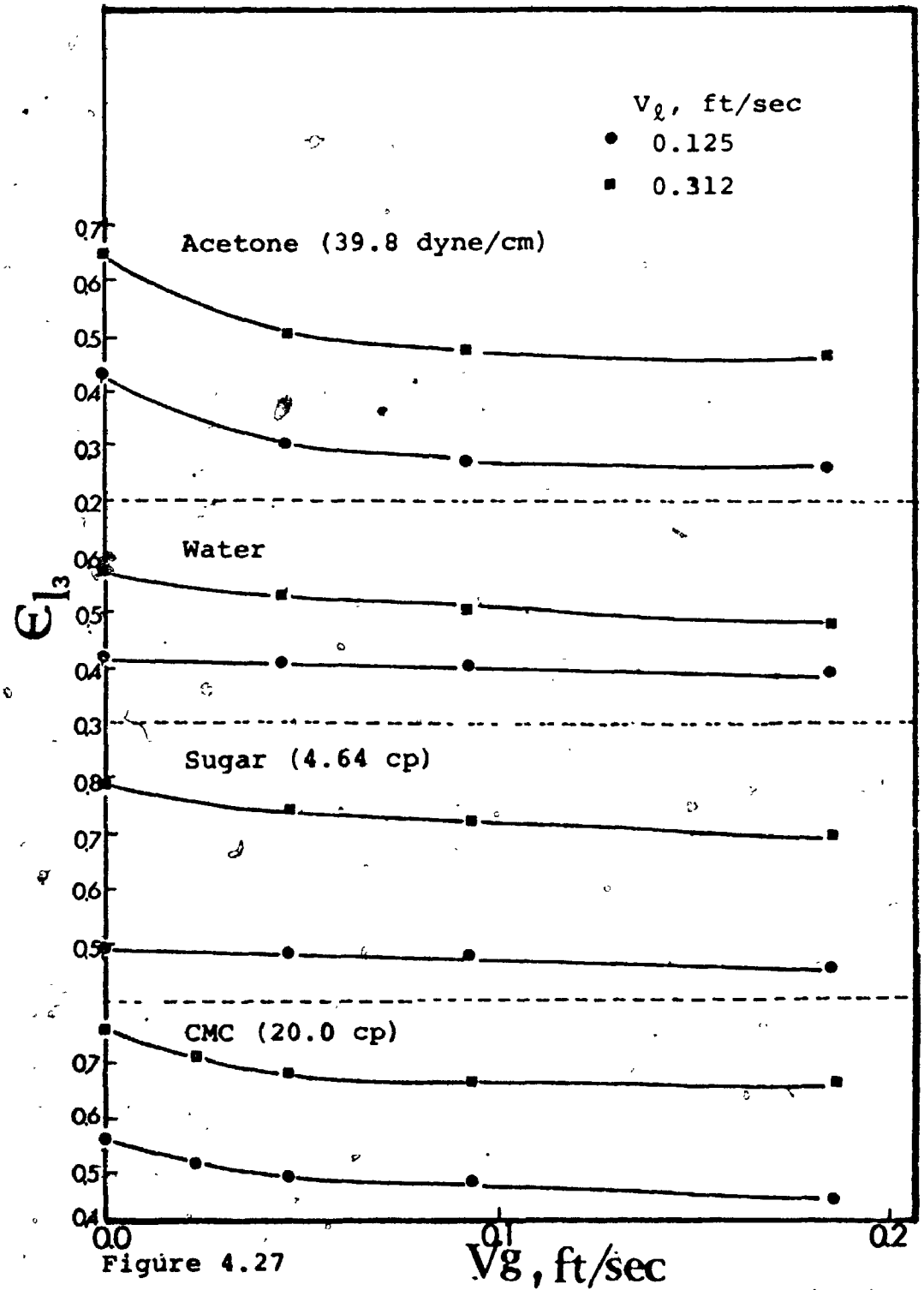

Figure 4.27 Effect of Gas Velocity on Liquid Hold-up in Three Phase Beds of Gravel

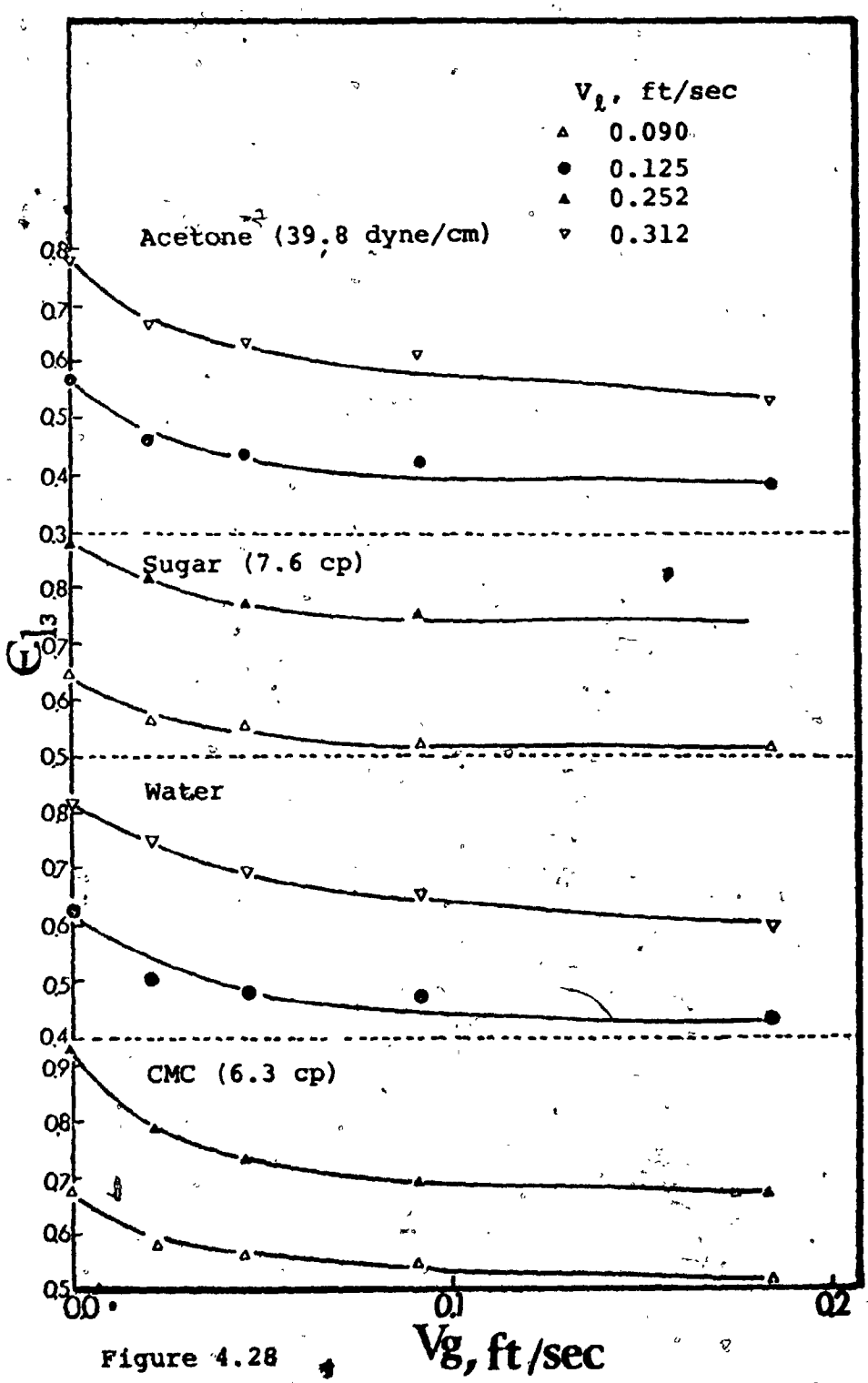

Figure 4.28

Effect of Gas Velocity on Liquid Hold-up in Three Phase Beds of 1 mm Glass beads.

studied (figures 4.29-4.31). In many cases it was not possible to determine a reliable trend of ε_g with V_ℓ because of the comparatively small magnitude of the former in comparison to the experimental error. However, at least at higher gas rates, it does appear that the gas hold-up decreased with increasing liquid flowrate.

Comparison of the different systems shows that the rate of increased ε_g with increasing gas velocity was more pronounced in the beds of small particles than those of large particles.

The effect of surface tension on the liquid hold-up in the different beds at given liquid and gas velocities is shown in figure 4.32. It can be observed that $\varepsilon_{\ell,}$ decreased with increasing surface tension throughout the range of liquid and gas velocities studied in the beds of 1 mm glass beads. However, the reverse trend was observed in the beds of gravel and 6 mm glass beads.

Comparison with the data of figure 4.4 shows that the same trends were observed in the liquid-gas beds as in the beds of gravel and 6 mm glass beads.

With one exception, the gas hold-up decreased with increasing surface tension in the all cases studied (figure 4.33). In the beds of 6 mm glass beads at the highest gas rate and lowest liquid rate, $\varepsilon_{g,}$ appeared to increase slightly with V_g. However, in this case, the liquid velocity was below the minimum fluidizing velocity and consequently the particles were fluidized by both gas and liquid rather than by the liquid flow alone.

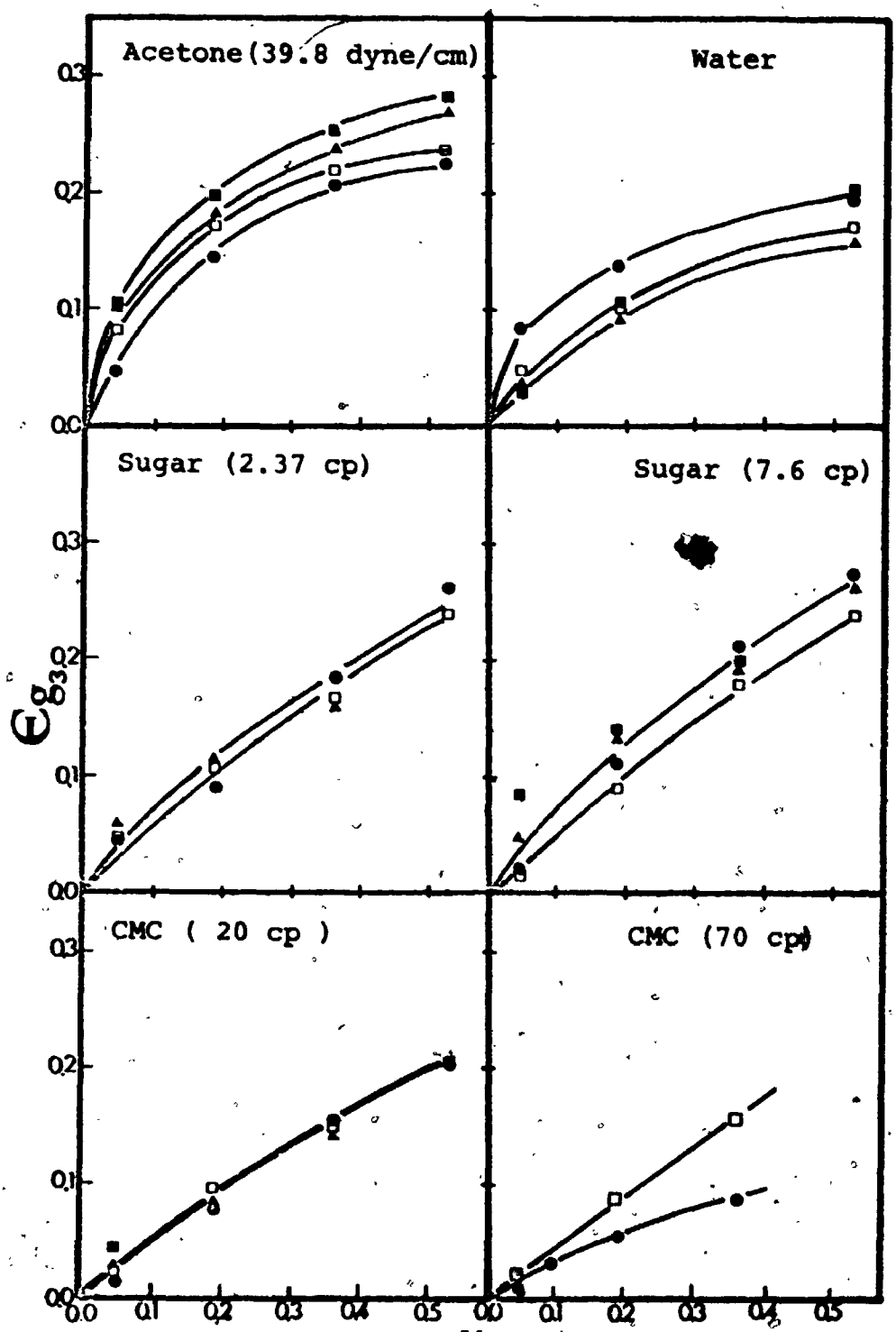

Figure 4.29.
Effect of Gas Velocity on Gas Hold-up in Three Phase Beds of 6 mm Glass beads., ●: V_ℓ = 0.125 ft/sec, □: V_ℓ = 0.177 ft/sec, ▲: V_ℓ = 0.252 ft/sec, ■: V_ℓ = 0.312 ft/sec.

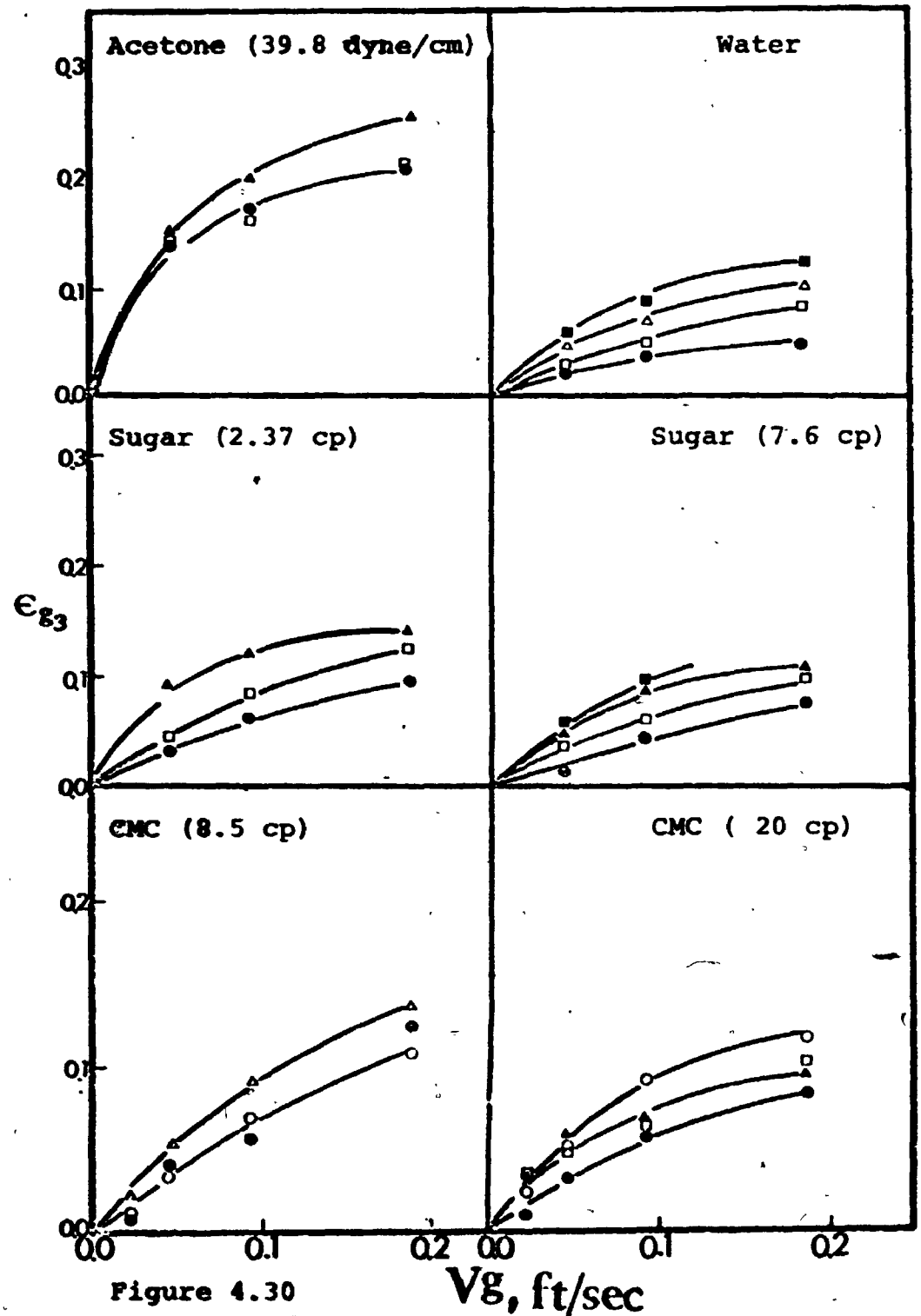

Figure 4.30

Effect of Gas Velocity on Gas Hold-up in Three Phase Beds of Gravel. ●: V_ℓ = 0.125 ft/sec, □: V_ℓ = 0.177 ft/sec, ▲: V_ℓ = Q.252 ft/sec, ■: V_ℓ = 0.312 ft/sec.

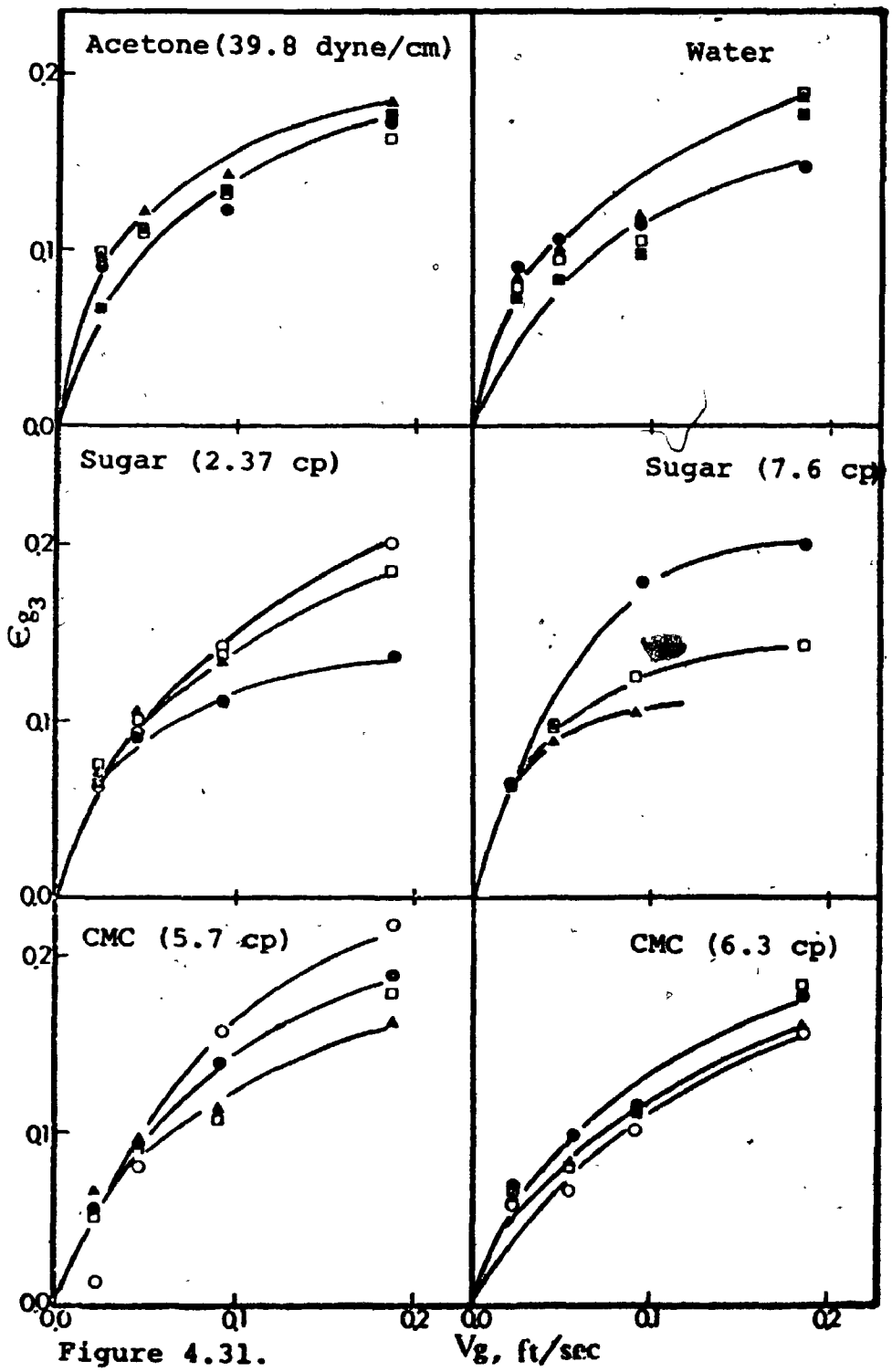

Figure 4.31.
Effect of Gas Velocity on Gas Hold-up in Three Phase Beds of 1 mm Glass Beads. ○:V_ℓ=0.090 ft/sec, ●:V_ℓ = 0.125 ft/sec, □: V_ℓ = 0.177 ft/sec, ▲: V_ℓ = 0.200 ft/sec.

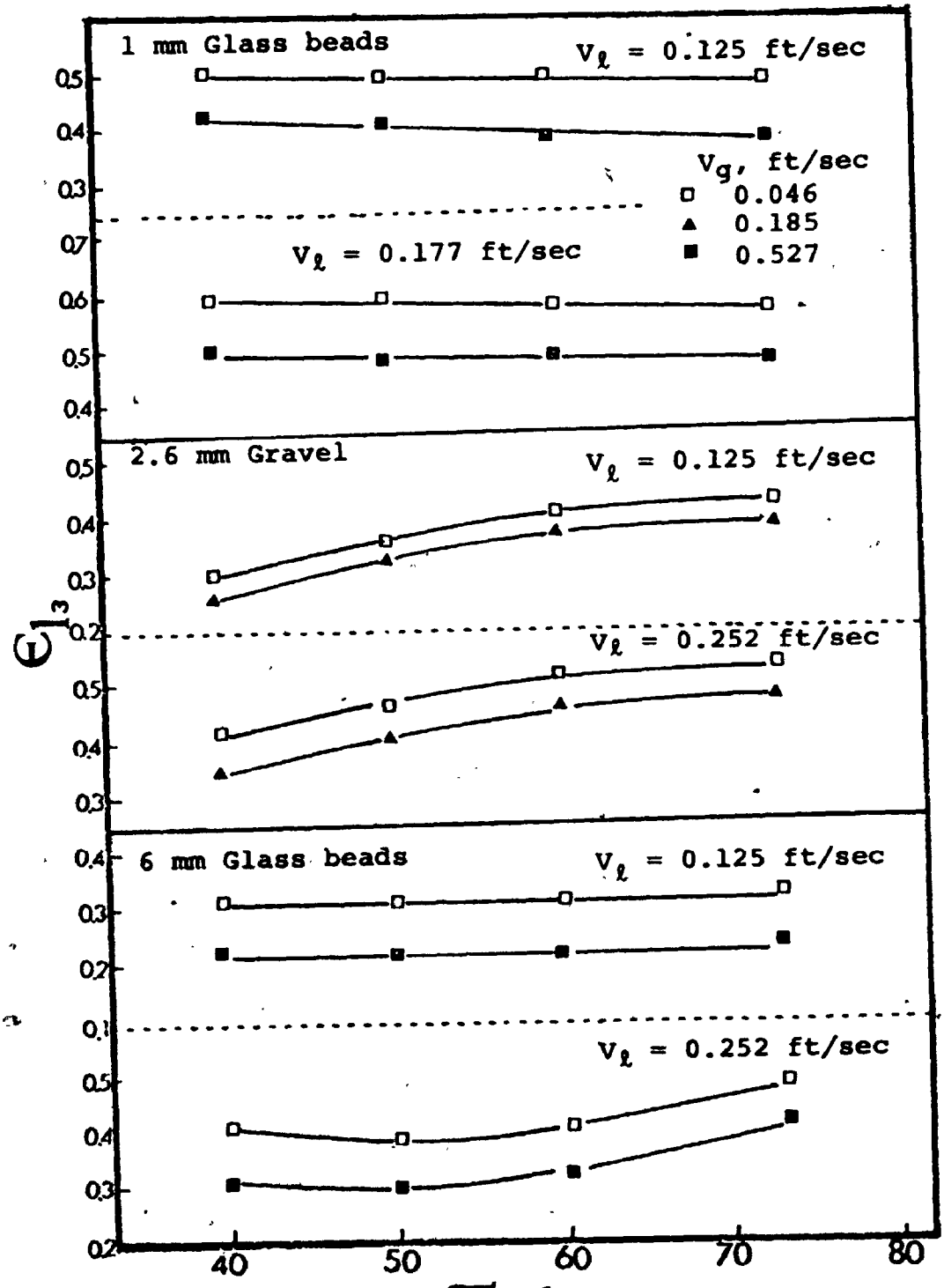

Figure 4.32 Effect of Surface Tension on Liquid Hold-up in Three Phase Beds.

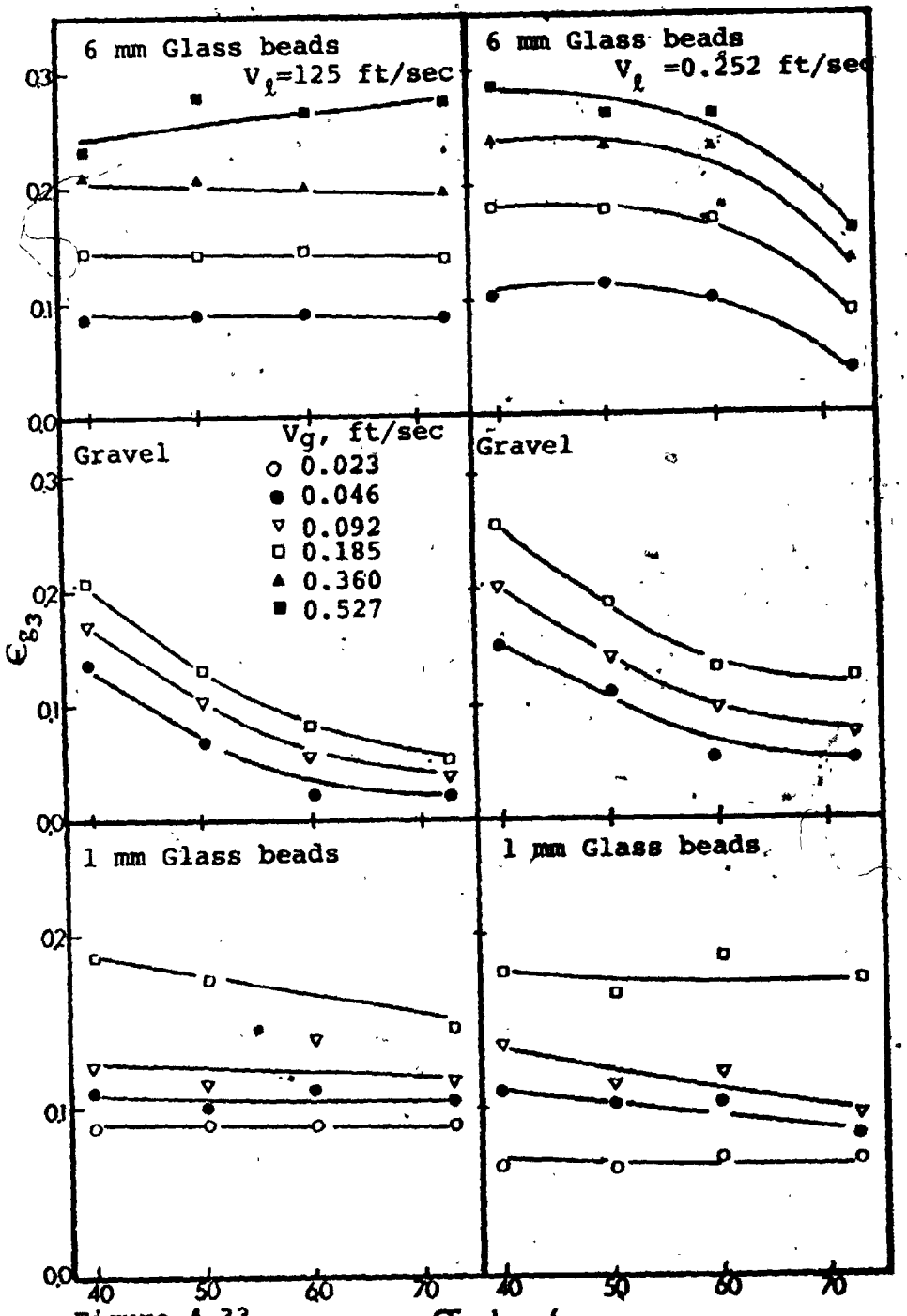

Figure 4.33 Effect of Surface Tension on Gas Hold-up in Three Phase Beds.

Comparison of the data with that for the solids-free systems shows that the same trend was observed in both systems, namely that the gas hold-up decreased with increasing surface tension.

As may be seen in figure 4.34, ε_{ℓ_3} increased proportionally with viscosity in the beds of 1 mm glass beads. In the beds of gravel, the increase in ε_{ℓ_3} was somewhat more slow. The rate of increase in the beds of 6 mm glass beads was small up to about 10 cp but thereafter, it increased sharply with increases in the liquid viscosity. In contrast to these results it will be recalled that the effect of liquid viscosity on ε_{ℓ} was not significant in solids-free systems.

The effect of liquid viscosity on the gas hold-up is shown in figure 4.35. In the beds of 1 mm glass beads, ε_g decreased with increasing liquid viscosity throughout the range of gas and liquid velocities studied. The effect of viscosity was small in the beds of gravel and 6 mm glass beads. However, in the latter case, ε_g appeared to decrease slightly with increasing liquid viscosity.
In comparison, the gas hold-up in liquid-gas beds (figure 4.5) was essentially independent of liquid viscosity.

The liquid hold-up decreased with particle size in three phase fluidized beds as shown in figure 4.36. This decrease was most marked between particle sizes of zero (liquid-gas beds) and 1 mm. Thereafter, the rate of decrease was much slower.

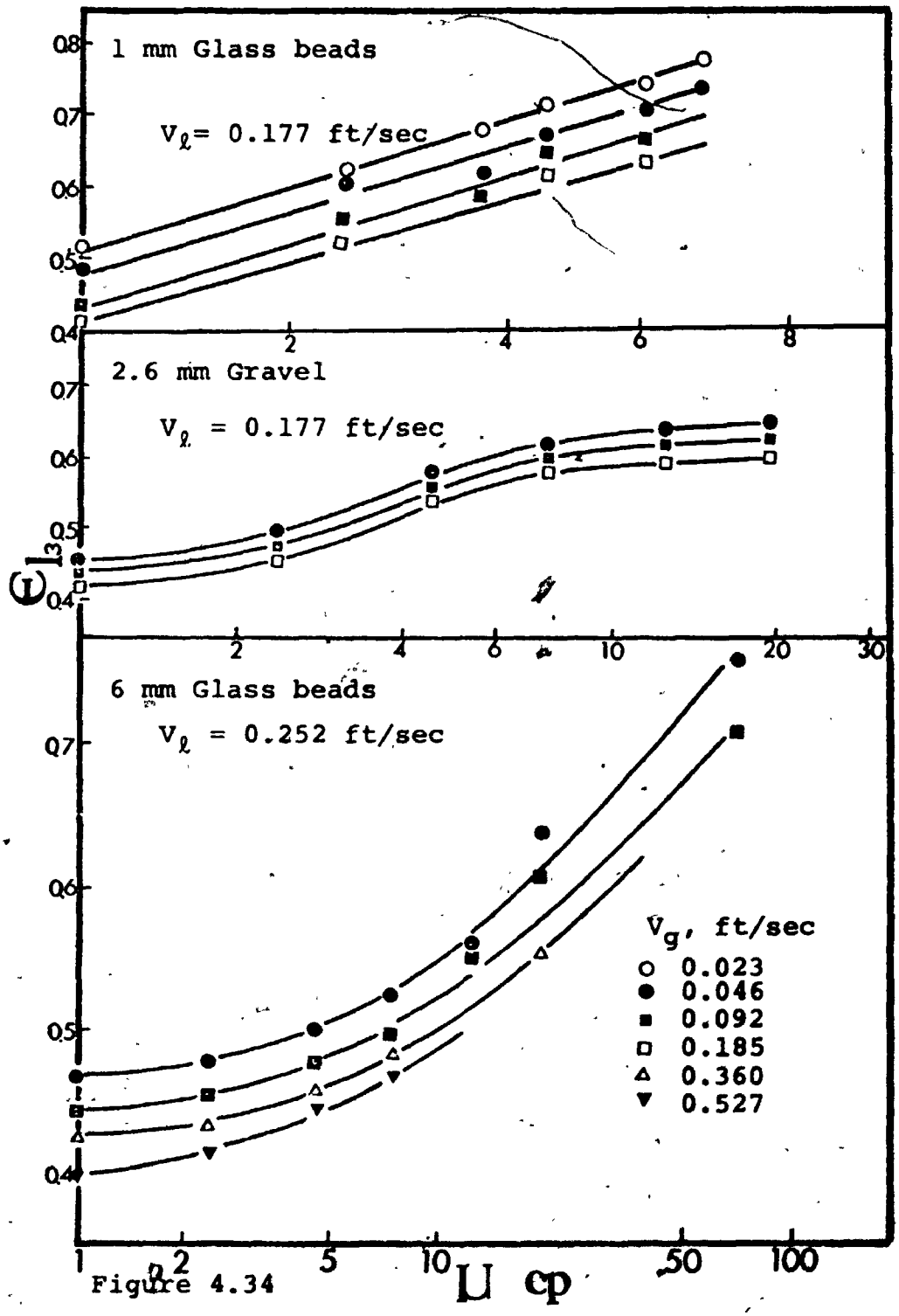

Figure 4.34

Effect of Viscosity on Liquid Hold-up in Three Phase Beds.

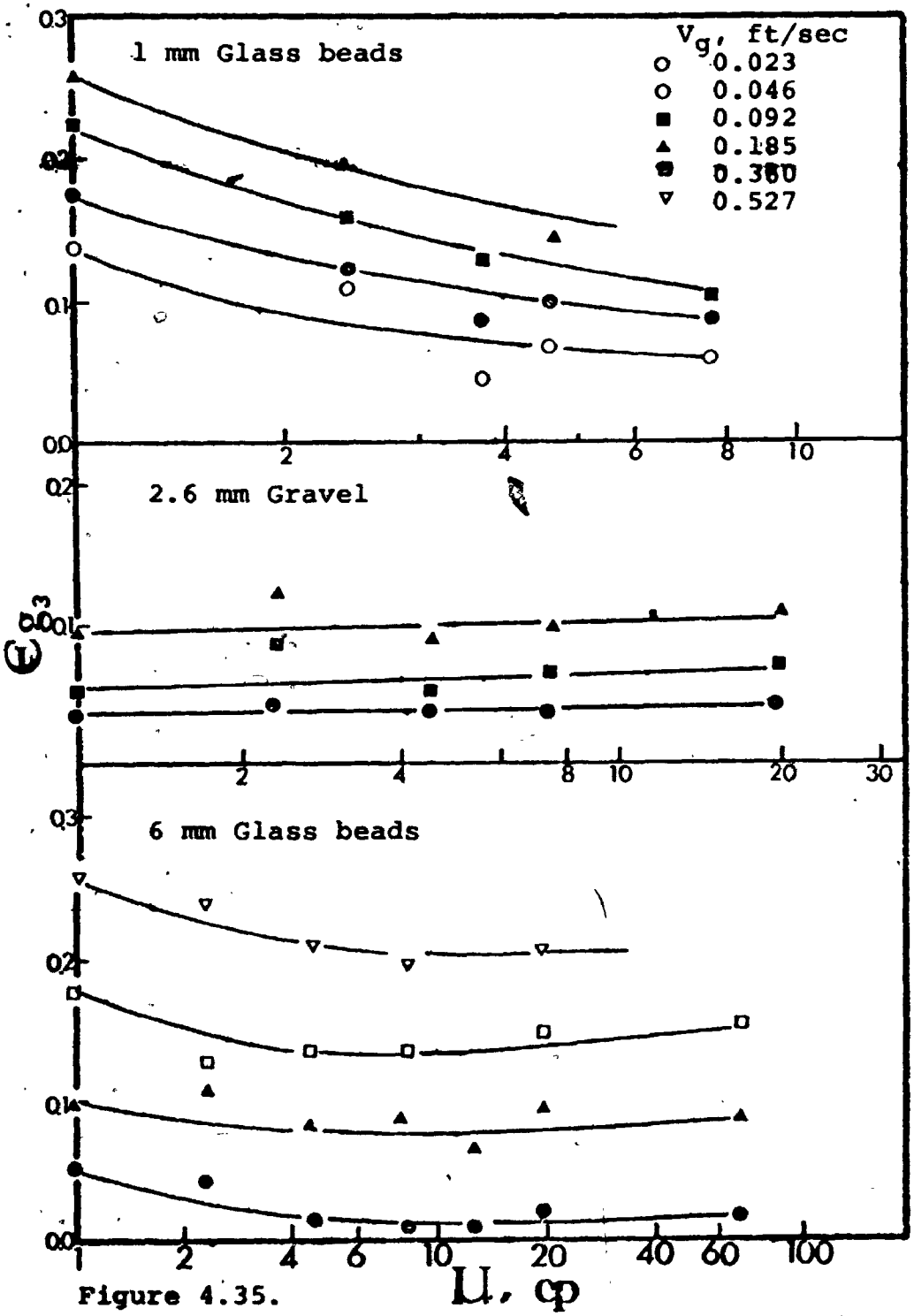

Figure 4.35.
Effect of Viscosity on Gas Hold-up in Three Phase Beds., V_ℓ = 0.177 ft/sec.

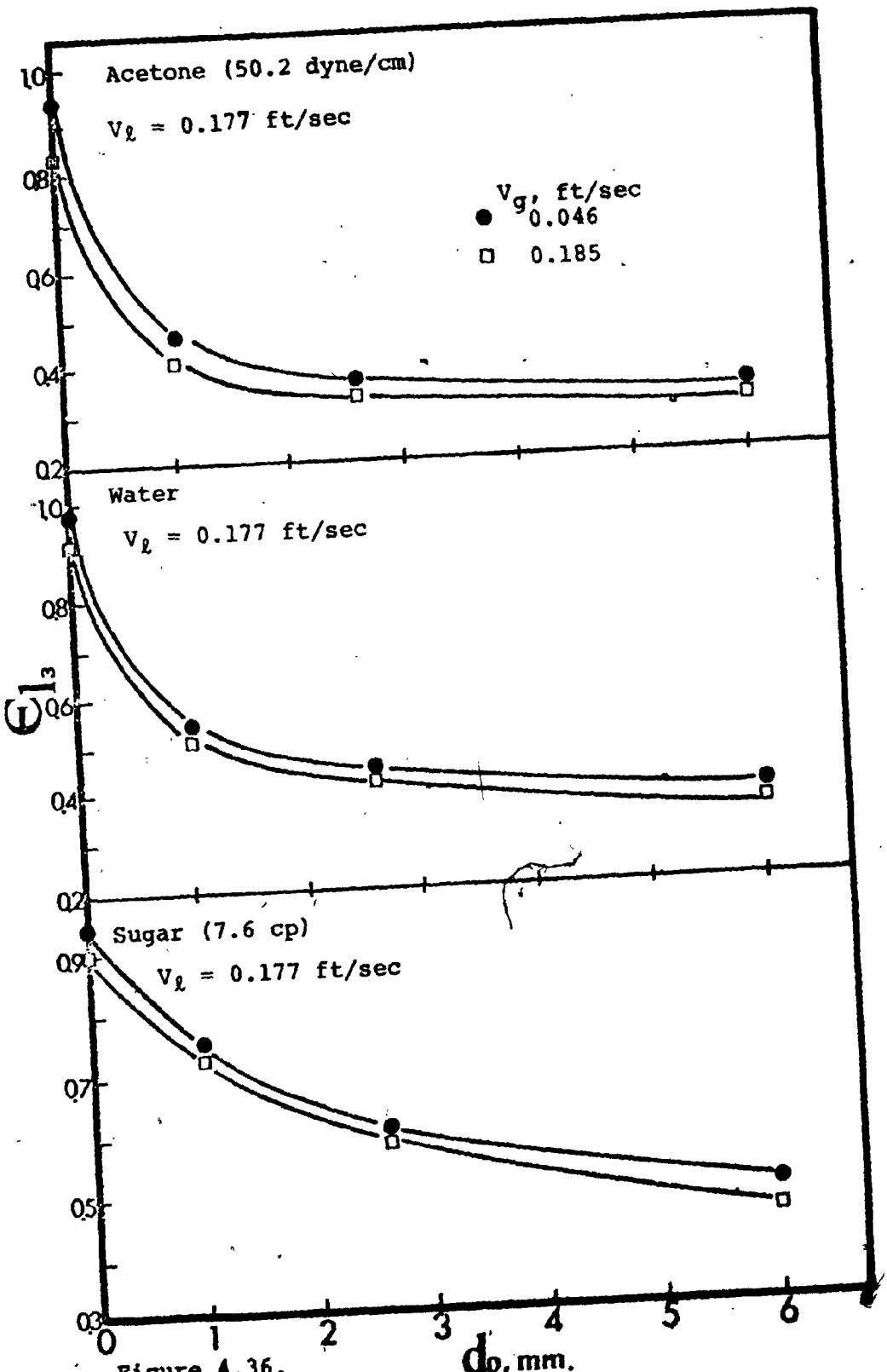

Figure 4.36.
Effect of Particle Size on Liquid Hold-up in Three Phase Beds.

On the basis of present findings and those of others, it can be concluded that the liquid hold-up increased with increasing liquid velocity and the gas hold-up increased with increasing gas flowrate in three phase fluidized beds. The gas hold-up was found to be independent of liquid velocity in the beds of small particles. However, in the beds of larger particles, the gas hold-up decreased with increasing liquid velocity (36,37,57*). Since the effects of liquid viscosity and surface tension on liquid and gas hold-ups in three phase fluidized beds have not been reported in the literature, the present data cannot be compared with those of others.

4.4.1.1. Correlation of the Liquid Phase Hold-up Data

A statistical analysis was performed on the liquid phase hold-up data for liquid velocities V_ℓ between 0.090 and 0.335 ft/sec, gas velocities V_g between 0.023 and 0.854 ft/sec, liquid surface tensions σ between 39.8 and 72.8 dyne/cm, viscosities μ between 1 and 70 cp, and particle diameters d_p between 1 and 6 mm. The detailed data can be found in Appendix D. The following relationship resulted:

$$\varepsilon_{\ell,} = 1.036\ V_\ell^{0.411}\ V_g^{-0.078}\ d_p^{-0.220}\ \gamma^{0.147}\ \sigma^{0.198} \qquad .....(4.13)$$

In this equation, V_ℓ and V_g are in ft/sec, d_p is in ft, γ as defined by equation (4.2), is in lb/ft sec^{2-n}, and σ is in lb/sec^2. The standard error of estimate between experimental values of $\varepsilon_{\ell,}$ and those calculated by equation (4.13)

is 0.035 for 527 data points. Equation (4.13) can be expressed in dimensionless form as follows:

$$\varepsilon_{\ell_3} = 1.504\ (Fr_\ell)^{0.234}\ (Fr_g)^{-0.086}\ (Re_\ell)^{-0.082}\ (We)^{0.092} \quad \ldots.(4.14)$$

where Fr_ℓ is the liquid phase Froude number $V_\ell^2/d_p g$, Fr_g is the gas phase Froude number $V_g^2/d_p g$, Re_ℓ is the Reynolds number based on particle diameter $d_p^n\ V_\ell^{2-n}\ \rho_\ell/\gamma$, and We is the Weber number $V_g \gamma/\sigma$.

The standard error of estimate between the experimental and calculated values of equation (4.14) is 0.039 for 527 data points. Figure 4.37 shows the goodness of fit between the experimental and calculated values.

For three phase beds of 1 mm glass beads, Michelson and Østergaard's correlation (36) predicted generally higher liquid hold-ups than found in the present work. In the case of 6 mm glass beads, their correlation predicted higher values of ε_{ℓ_3} for the lower viscosity solutions. However, the reverse trend was observed at higher viscosities. The correlation of Rhzumov et al.(50), equation (2.21), predicted the liquid hold-ups in three phase fluidized beds to be somewhat lower than the present values. Since both of these correlations were derived from experiments using only water as the liquid phase and air as the gas phase, they cannot be expected to accurately describe the variation of

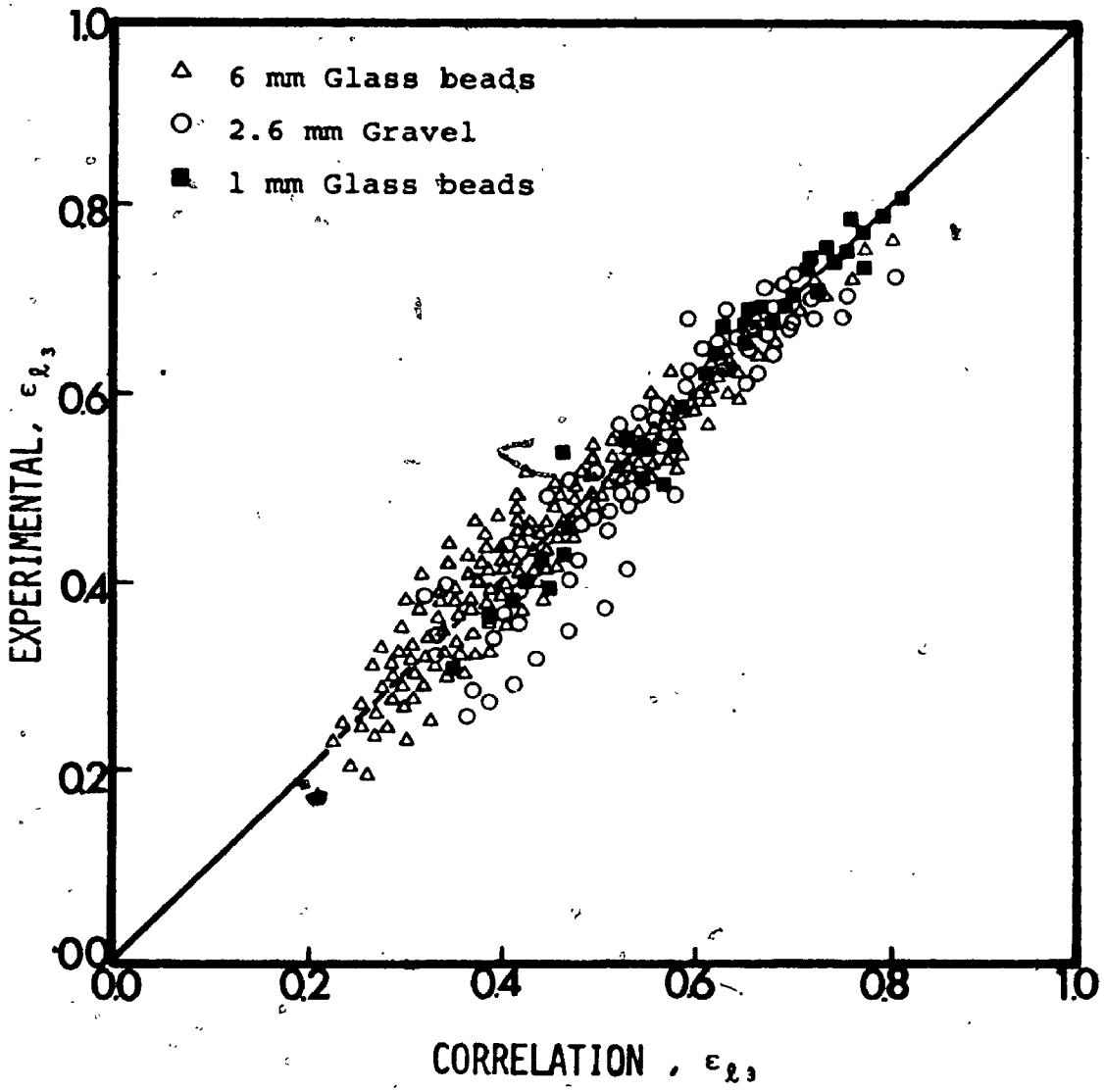

Figure 4.37 Comparison between Experimental and Calculated Values of Liquid Hold-up in Three Phase Fluidized Beds. (Equation 4.14)

ε_{ℓ_3} with wide variations of liquid viscosity and surface tension.

4.4.2. Bed Porosity (Expanded Bed Height)

The bed porosity is defined as the fraction of the bed volume occupied by both the gas and liquid phases and, as such, is directly related to the expanded bed height. Consequently these two parameters are discussed together in this section.

The effect of liquid flowrate on the bed porosity in the beds of 6 mm glass beads is shown in figure 4.38 for six different liquids. As may be seen, $(\varepsilon_\ell + \varepsilon_g)$ increased with increasing liquid velocity in all cases. The rate of increase in bed porosity with increasing liquid velocity was larger with the liquids of higher viscosity.

Figures 4.39 and 4.40 show similar plots for the three phase beds of gravel and 1 mm glass beads. The trend of increasing $(\varepsilon_\ell + \varepsilon_g)$, and hence bed expansion, with increasing liquid rate is again evident in these systems. However, the rates of increase do not appear to be particularly dependent on viscosity as in the beds of 6 mm glass beads. Comparison of the magnitudes of $(\varepsilon_\ell + \varepsilon_g)$ in the beds of different size particles shows that the increase in the bed porosity with liquid velocity was more pronounced in the beds of smaller particles than in those of the larger particles.

The bed expansion and contraction characteristics of

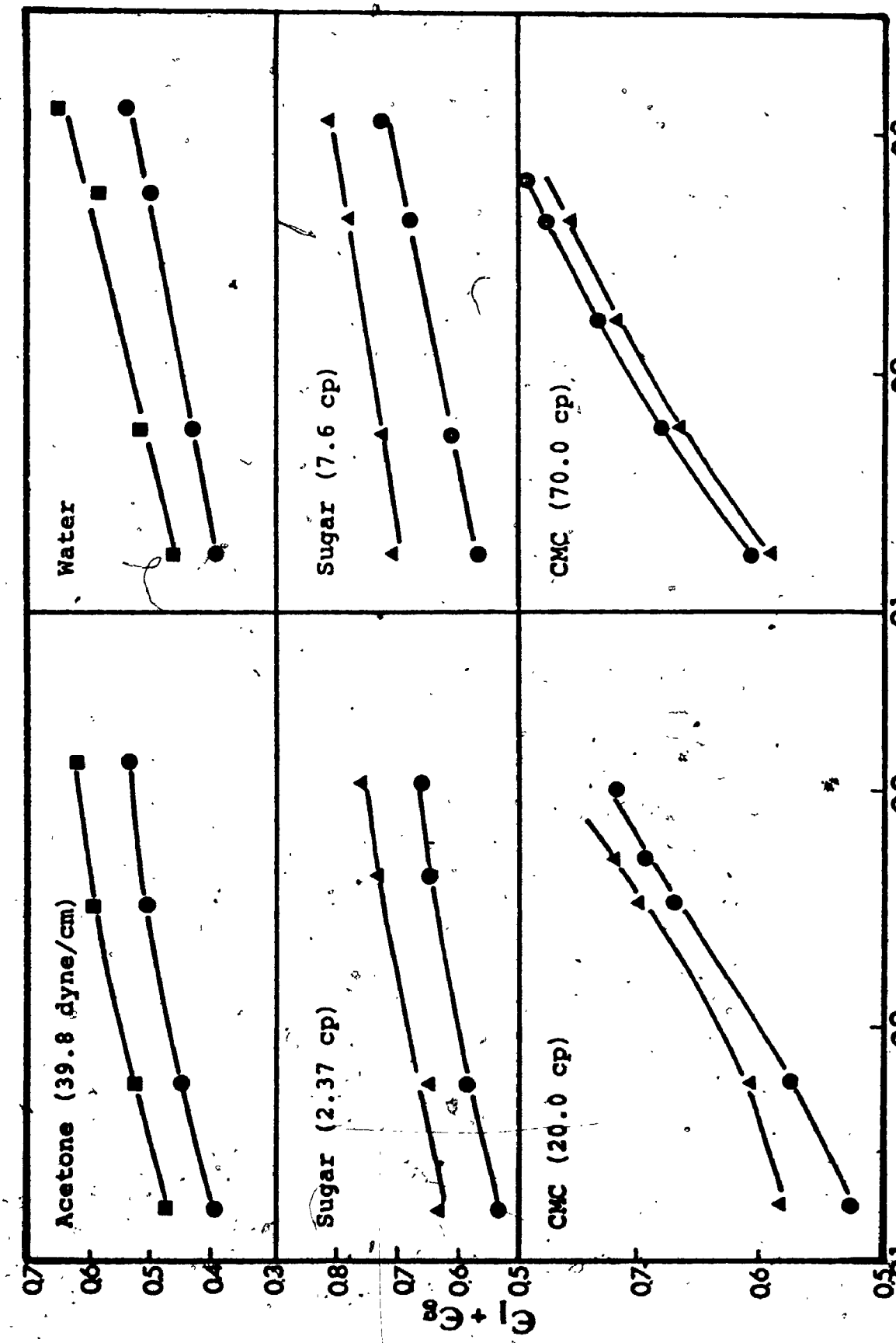

Figure 4.38

Effect of Liquid Velocity on Bed Porosity in Three Phase Beds of 6 mm Glass Beads.
●: V_g = 0.046 ft/sec, ▲: V_g = 0.360 ft/sec, ■: V_g = 0.527 ft/sec.

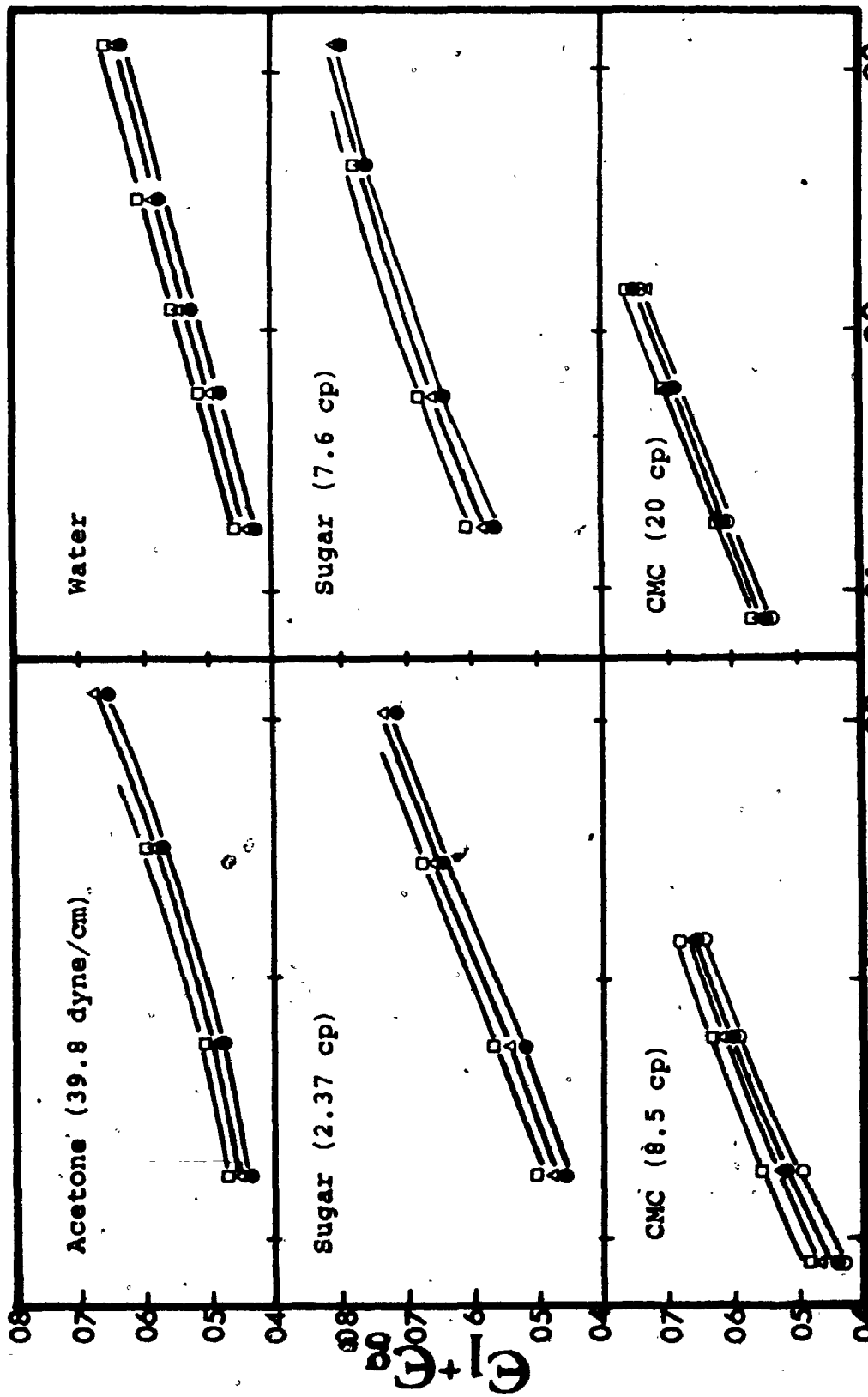

Figure 4.39 Effect of Liquid Velocity on Bed Porosity in Three Phase Beds of Gravel.
o: V_g = 0.023 ft/sec, ●: V_g = 0.046 ft/sec, △: V_g = 0.092 ft/sec,
□: V_g = 0.185 ft/sec.

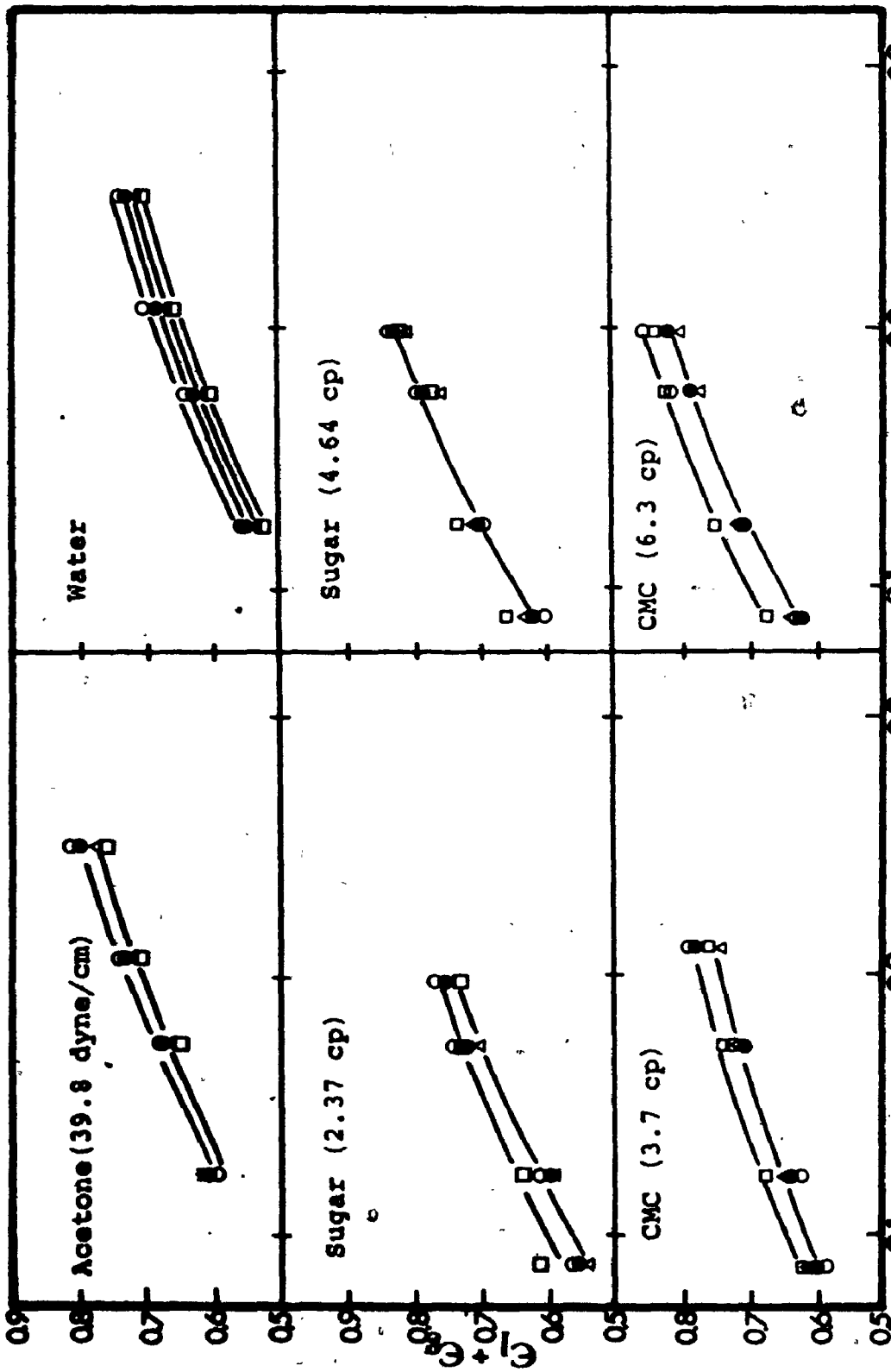

Figure 4.40
Effect of Liquid Velocity on Bed Porosity in Three Phase Beds of 1 mm Glass Beads., ○: V_g=0.023 ft/sec, ●:V_g=0.046 ft/sec, □:V_g = 0.092 ft/sec. △: V_g=0.185 ft/sec.

three phase fluidized beds can easily be observed by plotting the bed porosity against gas flowrate.

Such plots, for beds of 6 mm glass beads, are shown in figure 4.41. In general, the bed porosity increased with gas as well as the liquid velocity. However, one exception was observed for the bed of 6 mm glass beads fluidized by air and CMC solution (70 cp) in which the bed porosity decreased slightly with increasing gas velocity. To our knowledge, this is the first time that this behaviour has been observed in beds of such large particles. This behaviour is typical of beds containing much smaller particles fluidized by air and water which exhibit a contraction at low gas rates.

An example of this is given below for the beds of 1 mm glass beads.

Visual observation of the transparent column showed that the bubble size was relatively larger than that in the solutions of lower viscosity at almost all the gas and liquid flowrates studied. The contraction was more pronounced at higher liquid rates and consequently in beds of higher initial height. In such beds, injection of a small amount of gas caused the bed to progressively collapse with increasing gas flowrate up to around 0.2 ft/sec. Thereafter, the bed height again increased with increasing gas rate as in the beds of smaller particles. The quantity of solid particles in the dilute phase increased with increasing gas rate. However, the solids hold-up in the dilute phase was negligible compared to that in the main fluidized bed.

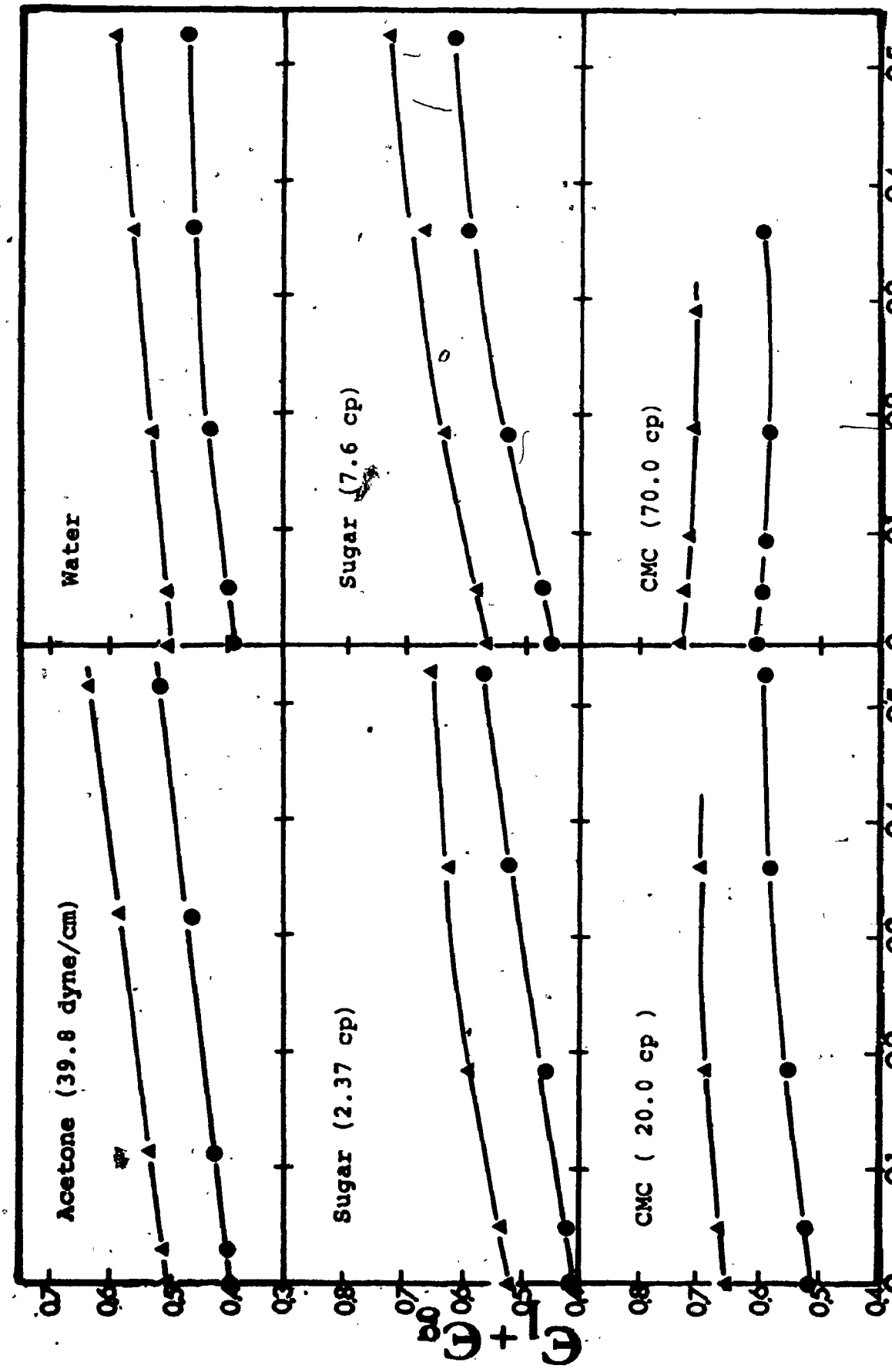

Figure 4.41

Effect of Gas Velocity on Bed Porosity in Three Phase Beds of 6 mm Glass Beads.
●: V_l = 0.125 ft/sec, ▲: V_l = 0.252 ft/sec

The variation of bed porosity with gas flowrate in the beds of gravel particlesis shown in figure 4.42. As may be seen, $(\varepsilon_\ell+\varepsilon_g)$ increased with increasing gas velocity in the beds fluidized by all the liquids except the higher viscosity solutions (8.5, 12.77 and 20 cp). With these liquids, the beds again contracted on injecting gas resulting in a decrease in bed porosity. However, the latter increased with further increases in the gas flowrate. Visual observation showed that the bubble size was again larger in these beds than in those fluidized by lower viscosity solutions. The contractions were more pronounced at higher liquid rates and consequently in beds with higher initial height. The rate of contractions was more pronounced in higher viscosity solutions than that in lower viscosity solutions. As in the case of the beds of 6 mm glass beads, the quantity of solid particles in the dilute phase increased with increasing gas flowrate. However, the solids hold-up in the dilute phase was negligible compared to that in the main fluidized bed and could not have accounted for the contraction.

The effect of gas flowrate on $(\varepsilon_\ell+\varepsilon_g)$ in the beds of 1 mm glass beads fluidized by air and different liquids are shown in figure 4.45. The bed porosity initially decreased with increasing gas flowrate in all the systems studied. The initial rate of decrease in $(\varepsilon_\ell+\varepsilon_g)$ at lower velocities was more pronounced at higher liquid velocities as well as at higher liquid viscosities. For the same fluidizing conditions, a comparison of the data of figures 4.41-4.43

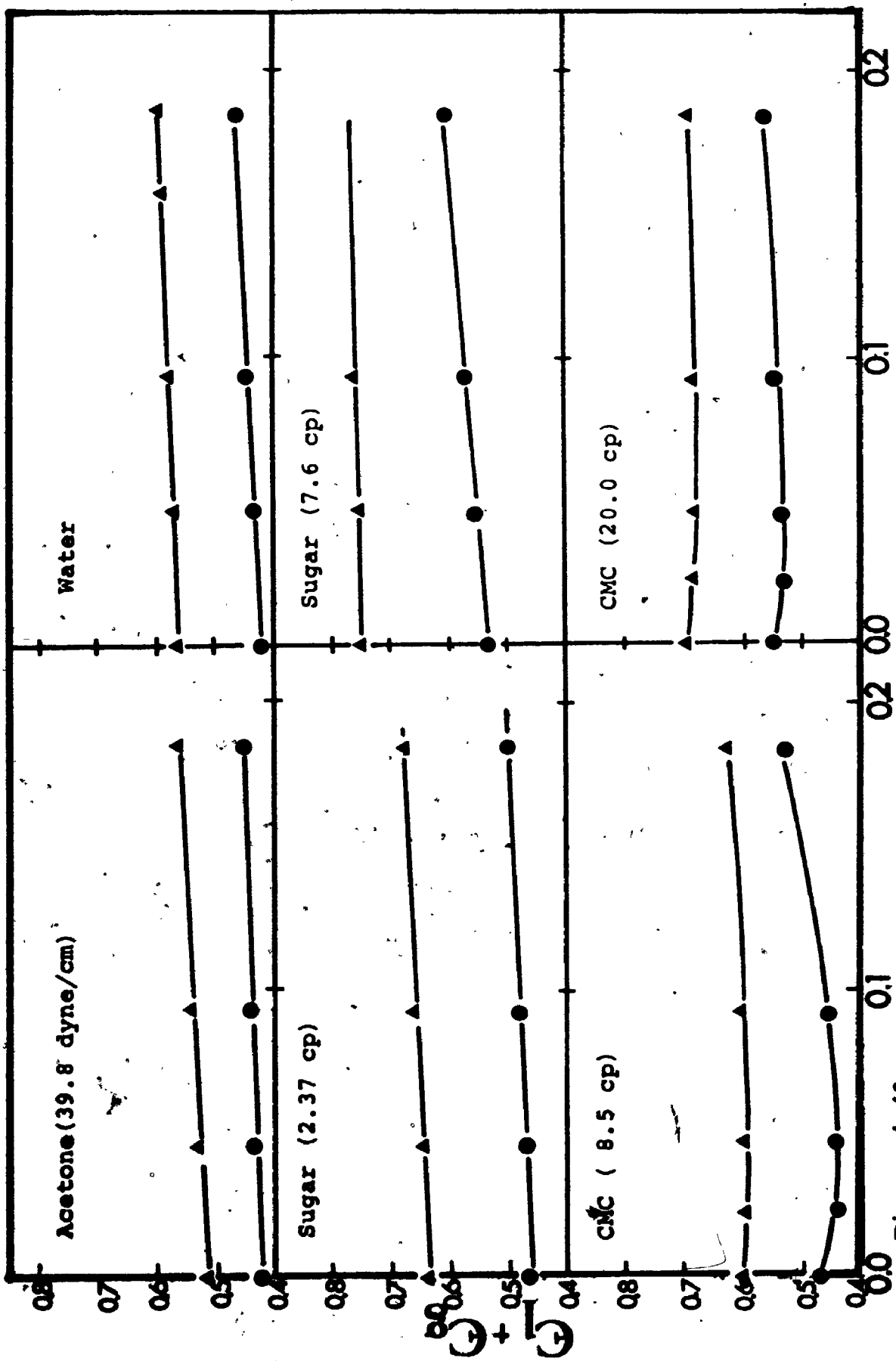

Figure 4.42

Effect of Gas Velocity on Bed Porosity in Three Phase Beds of 2.6 mm Gravel.
●: V_l = 0.125 ft/sec, ▲: V_l = 0.252 ft/sec

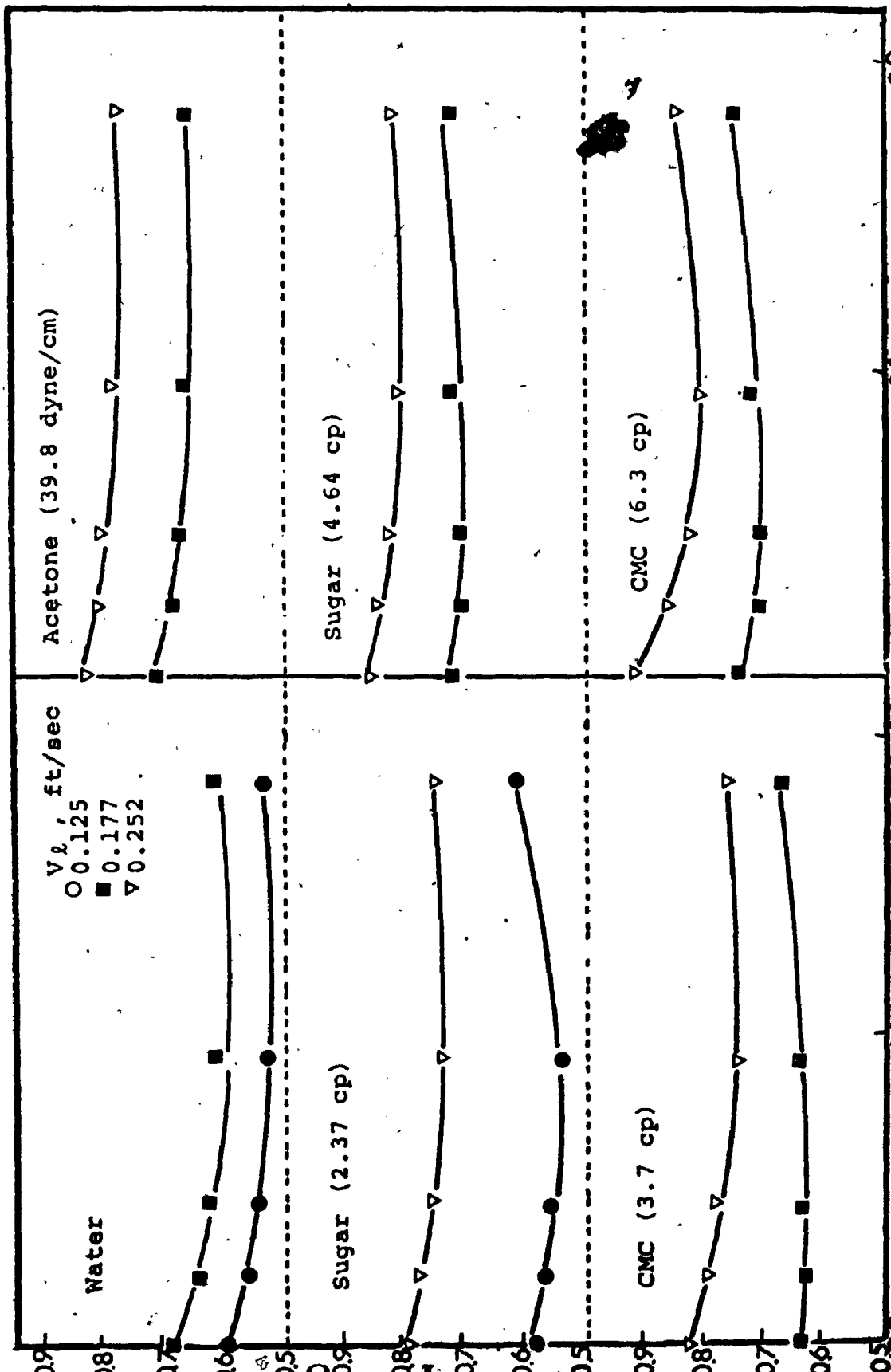

Figure 4.43 Effect of Gas Velocity on Bed Porosity in Three Phase Beds of 1 mm Glass Beads.

shows that the bed porosity decreased with increasing particle size.

The liquid viscosity was varied from 1 to 70 cp in this study. The effect of this variation on $(\varepsilon_\ell + \varepsilon_g)$ in beds of 1 mm glass beads, gravel and 6 mm glass beads is shown in figure 4.44. The bed porosity increased with increasing liquid viscosity in all the beds as a result of the increased drag force on the particles. The rate of bed expansion of liquid-solid beds was less than that of the three phase fluidized beds.

Variations in surface tension of the liquid in the range 39.8-72.8 dyne/cm had a relatively minor influence on the bed porosity (figure 4.45). The effect was extremely small in the beds of gravel and 6 mm glass beads. For the latter, $(\varepsilon_\ell + \varepsilon_g)$ does appear to go through a shallow minimum at higher liquid and gas flowrates. However, the differences involved are of the same magnitude as the experimental error and are hardly statistically significant.

In the beds of 1 mm glass beads, the bed porosity decreased with increasing surface tension throughout the ranges of gas and liquid velocity studied.

The effect of particle size on the bed porosity for a variety of conditions is shown in figure 4.46. In general, the bed porosity decreased with increasing particle size. The rate of decrease was most marked in the particle size range zero to 1 mm; thereafter the decrease was small.

Based on the present findings and those of other workers, it can be concluded that the bed porosity increased with

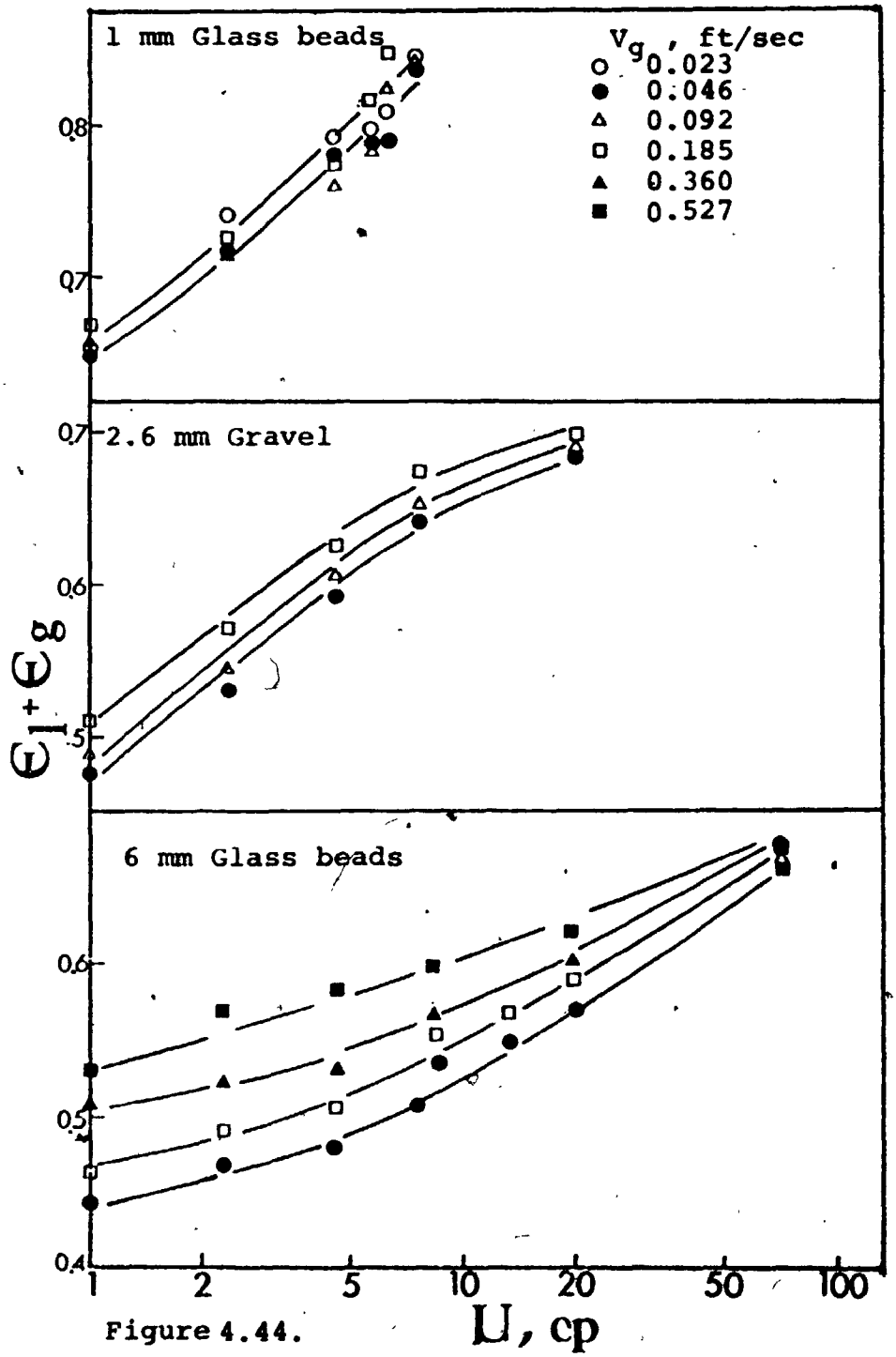

Figure 4.44.

Effect of Liquid Viscosity on Bed Porosity in Three Phase Beds. V_ℓ = 0.177 ft/sec.

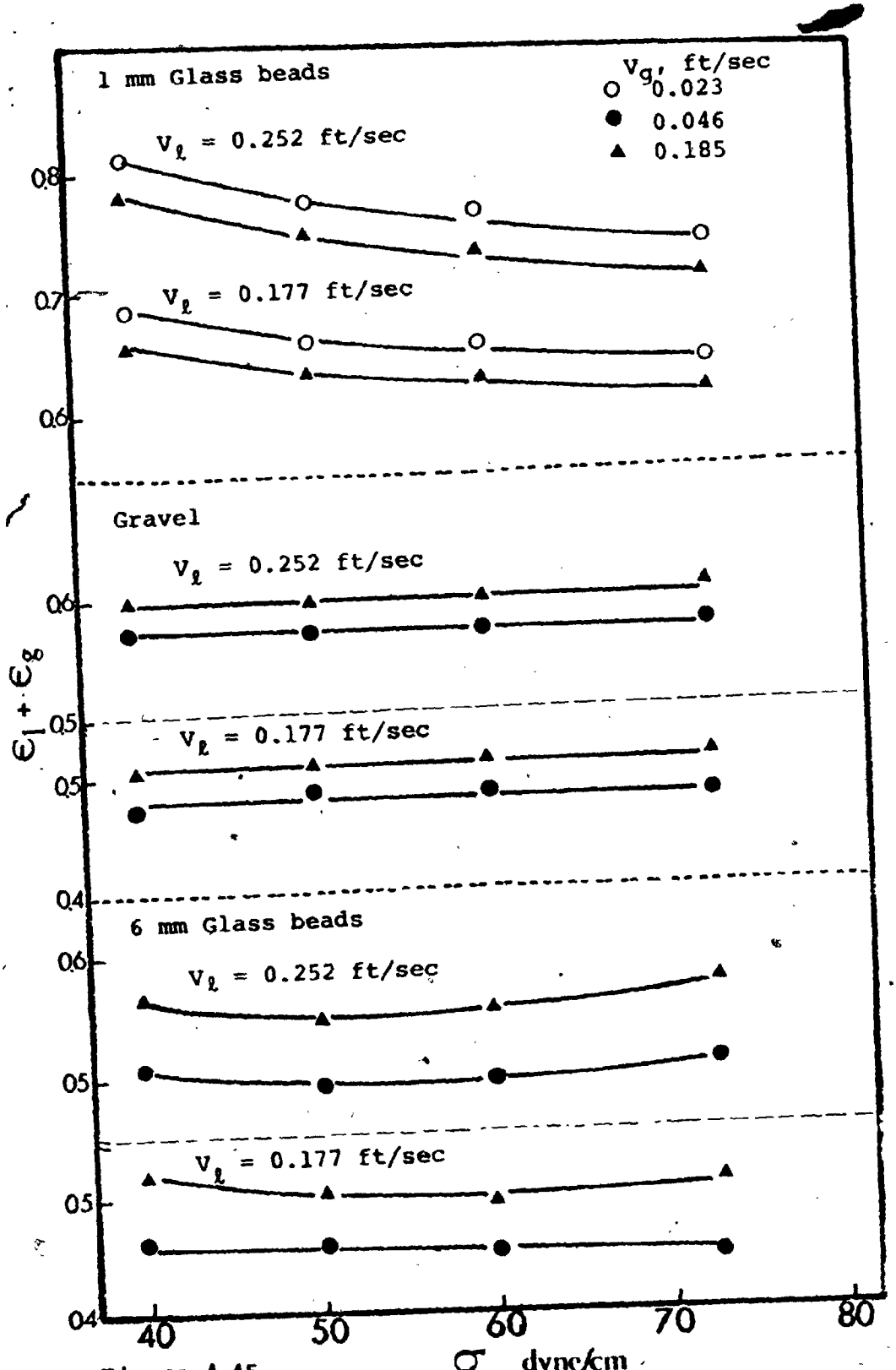

Figure 4.45
Effect of Surface Tension on Bed Porosity in three Phase Beds.

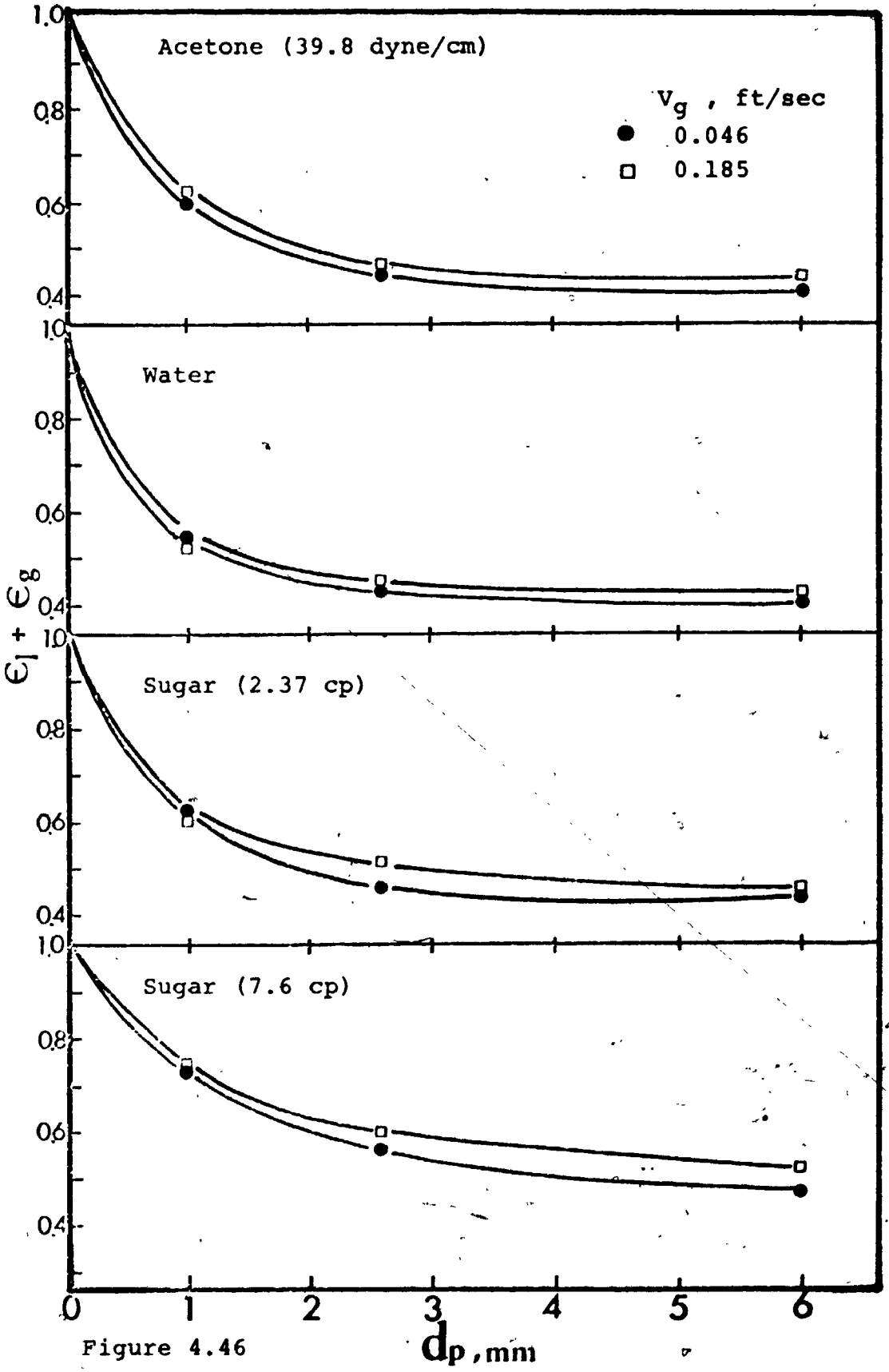

Figure 4.46

Effect of Particle Size on Bed Porosity in Three Phase Beds. V_ℓ = 0.125 ft/sec

increasing liquid flowrate and decreased with increasing particle size in three phase fluidized beds. In general, the bed porosity increased with gas rate in the beds of larger particles ($d_p > 2.5$ mm). However, in the beds of smaller particles ($d_p < 2.5$ mm), $(\varepsilon_\ell + \varepsilon_g)$ decreased with increasing gas flowrate up to a value of the latter approximately equal to the liquid velocity. Thereafter the bed porosity again increased with increasing gas flowrate. The rate of decrease in bed porosity was more pronounced with decreasing particle size and increasing liquid-solid bed height. Previous studies (7, 15) have shown that the initial contraction on injecting gas did not occur in the beds of high density or non-wettable particles, or in beds fluidized by liquids of low surface tension. Consequently the above finidings cannot be considered to apply to all three phase fluidized beds.

4.4.2.1. Correlation of the Bed Porosity Data

A statistical analysis was performed on the bed porosity data for all the beds studied. For the beds which expanded on introducing gas, the following relationship resulted:

$$(\varepsilon_\ell + \varepsilon_g) = 0.953\ V_\ell^{0.330}\ V_g^{0.059}\ d_p^{-0.182}\ \gamma^{0.088}\ \sigma^{0.053} \qquad \ldots\ldots(4.15)$$

where V_ℓ and V_g are in ft/sec, and d_p, γ and σ are in ft, lb/ft sec^{2-n}, lb/sec^2, respectively. The standard error of estimate between the experimental values and those calculated from equation (4.15) is 0.032 for 307 data points.

Equation (4.15) can be also expressed in dimensionless form as follows:

$$(\varepsilon_\ell + \varepsilon_g) = 1.40\ (Fr_\ell)^{0.170}\ (We)^{0.078} \qquad \ldots.(4.16)$$

where Fr_ℓ and We are the Froude number $V_\ell^2/d_p g$, and the Weber number $V_g \gamma / \sigma$, respectively. The standard error of estimate between the experimental and calculated values of equation (4.16) is 0.040 for 307 data points.

For the beds which initially contracted on the injection of gas, the following relationship resulted:

$$(\varepsilon_\ell + \varepsilon_g) = 0.612\ V_\ell^{0.347}\ V_g^{0.003}\ d_p^{-0.270}\ \gamma^{0.138}\ \sigma^{-0.038} \qquad \ldots..(4.17)$$

The standard error of estimate for equation (4.17) is 0.021 for 221 data points. On the basis of the present findings and those of other workers, it can be concluded that the fractional bed contraction is a function of the ratio of the liquid and gas velocities and the liquid hold-up in the liquid-solid fluidized beds. The following dimensionless equation was found to predict a bed contraction at lower gas rates and bed expansion at higher gas velocities:

$$(\varepsilon_\ell + \varepsilon_g) = 1.301\ (Fr_\ell)^{0.128}\ (We)^{0.073}\ e^{0.031(V_\ell/V_g)\varepsilon_{\ell_2}} \qquad \ldots.(4.18)$$

In this equation, Fr_ℓ and We are the Froude and Weber numbers, and V_ℓ, V_g, ε_{ℓ_2} are the superficial velocities of the liquid and gas phases and the liquid hold-up in the liquid-solid bed, respectively. The standard error of estimate between the experimental values and those calculated from equation (4.18) is

0.035 for 221 data points. The goodness of fit between experimental and the calculated values of equations (4.16) and (4.18) are shown in figures 4.47 and 4.48.

A comparison was made between the correlations of Dakshinamurty et al. (15), equations (2.15) and (2.16), Razumov et al. (50), equation (2.20), and the present experimental data. The standard deviation between the present values and those predicted by Dakshinamurty et al. is reasonable, 0.167. However, their correlation did not indicate a bed contraction at lower gas flowrate and also predicted generally higher bed porosities than those obtained in this study. The present experimental values and those predicted by the correlation of Razumov et al. were also in reasonable agreement. The standard deviation in this case was 0.111 for 527 data points. Their correlation predicts, in general, somewhat lower values of $(\varepsilon_l+\varepsilon_g)$ than those obtained in this study. Again, their correlation failed to predict a bed contraction in the beds of small particles at lower gas flowrates. Since the correlations of Østergaard (44) and of Bhatia (9) are trial and error in nature, a direct comparison with the present data was not attempted. Furthermore, the experimental data given in a more recent paper by Østergaard (43) shows that his own correlation, equations (2.6)-(2.10), only for the given particle size over a limited range of bed heights.

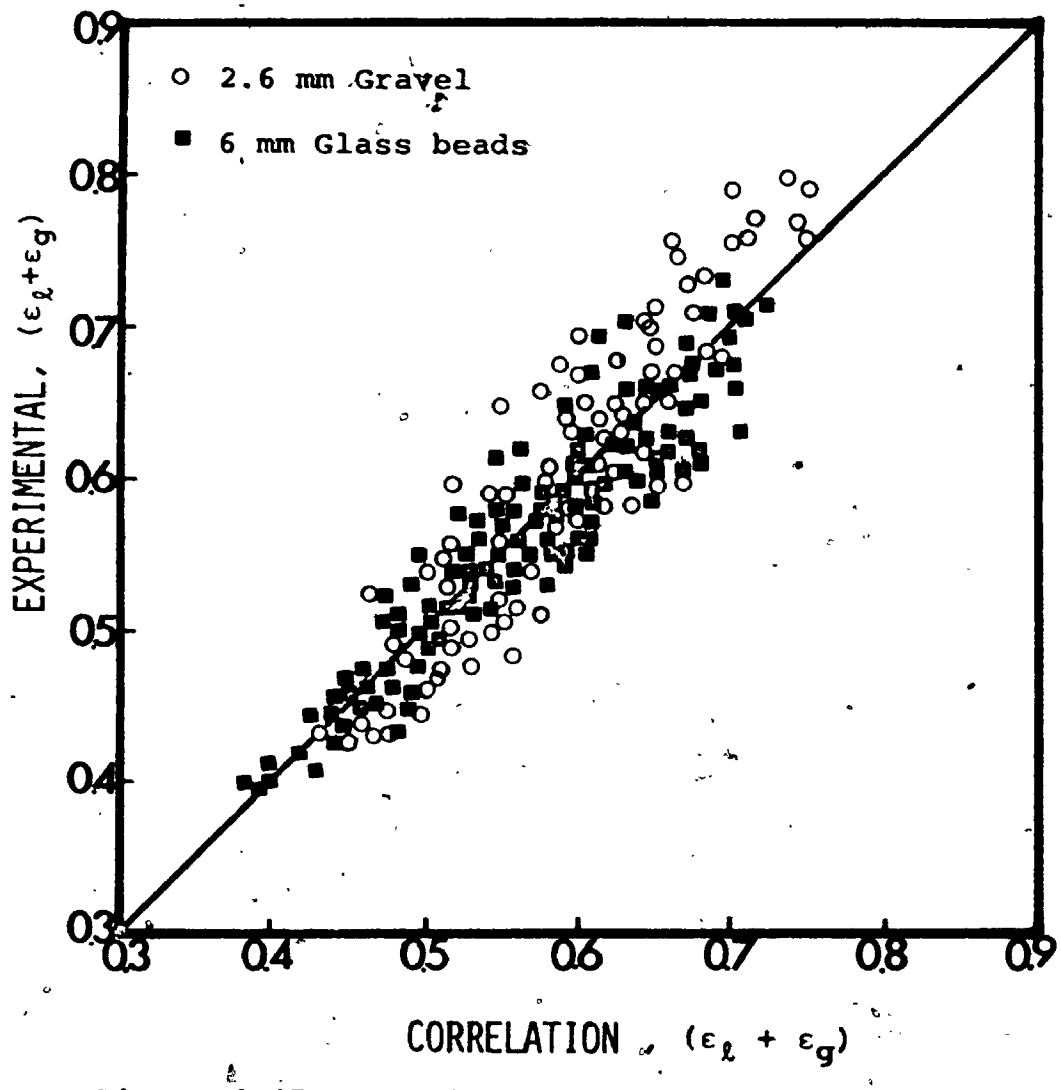

Figure 4.47 Comparison between Experimental and Calculated Values of Bed Porosity in Expanded Three Phase Beds. (Equation 4.16)

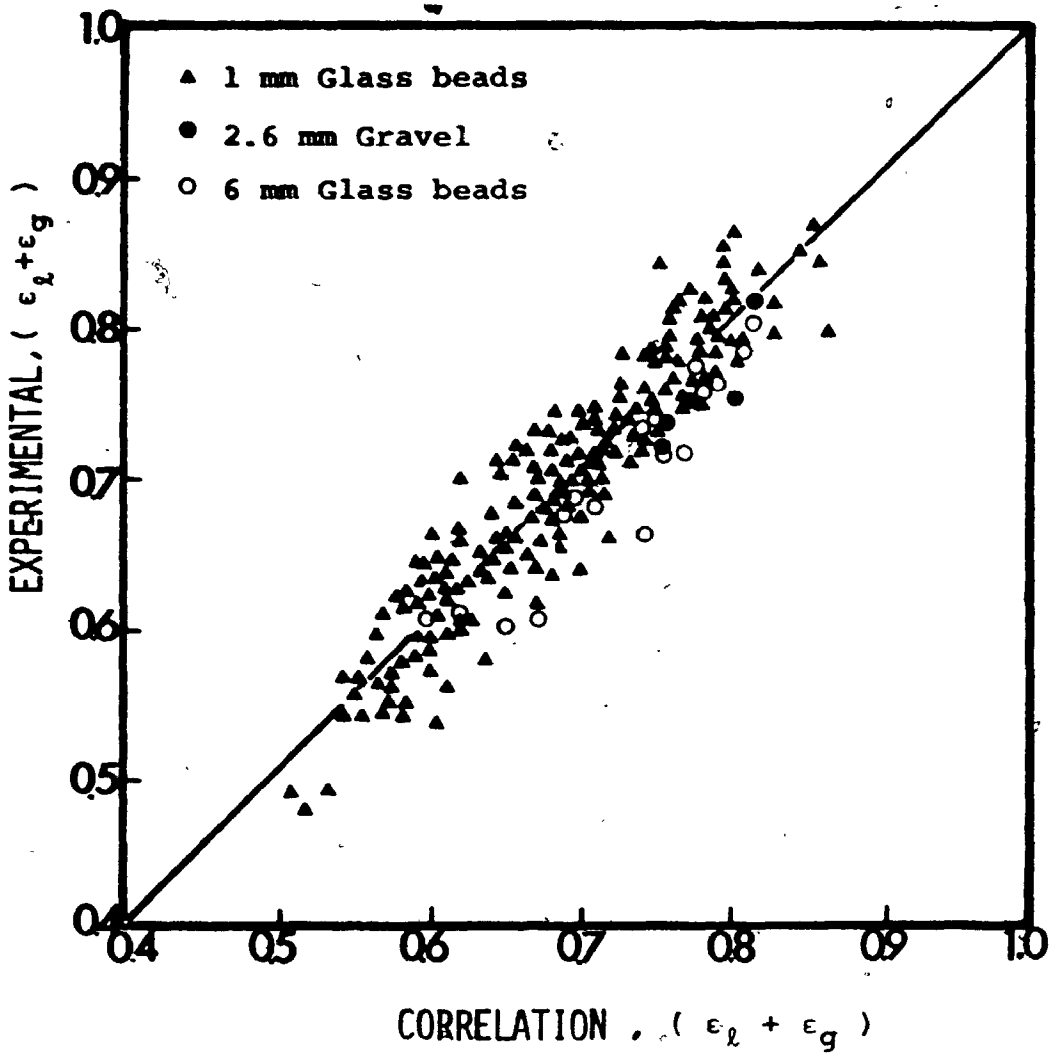

Figure 4.48 Comparison between Experimental and Calculated Values of Bed Porosity in Contracted Three Phase Beds. (Equation 4.18)

4.4.3. Liquid Phase Axial Mixing

Axial mixing of the liquid phase in three phase fluidized beds was measured by two tracer techniques, namely pulse and step injection, in the beds of gravel and 6 mm glass beds. Only step injection was employed in the beds of 1 mm glass beads. The particles were fluidized by the cocurrent flow of air and water throughout the studies. The initial bed height Ho, was 21.5 in. for the gravel and 6 mm glass beads and 10 in. for the 1.0 mm glass beads.

Liquid Phase mixing increased with increasing liquid velocity in all beds as shown in figures 4.49 and 4.50. As may be seen in these figures, the agreement between the results obtained by the two techniques was reasonably good. The rates of increase in HMU with increasing liquid velocity, which were essentially independent of gas flowrate, were somewhat lower in the beds of 1 mm glass beads than those in the beds of gravel and 6 mm glass beads and were, in general, larger in the liquid-solids beds than that in the three phase fluidized beds.

Because of the difference in initial bed height, a direct comparison between the HMU values for the beds of 1 mm glass beads and the other beds cannot be made. However, for the beds of gravel and 6 mm glass beads, the liquid phase HMU increased with decreasing particle size. It should be noted that the effect of liquid flowrate on HMU in three phase fluidized beds was the reverse of that exhibited by the solids-free systems.

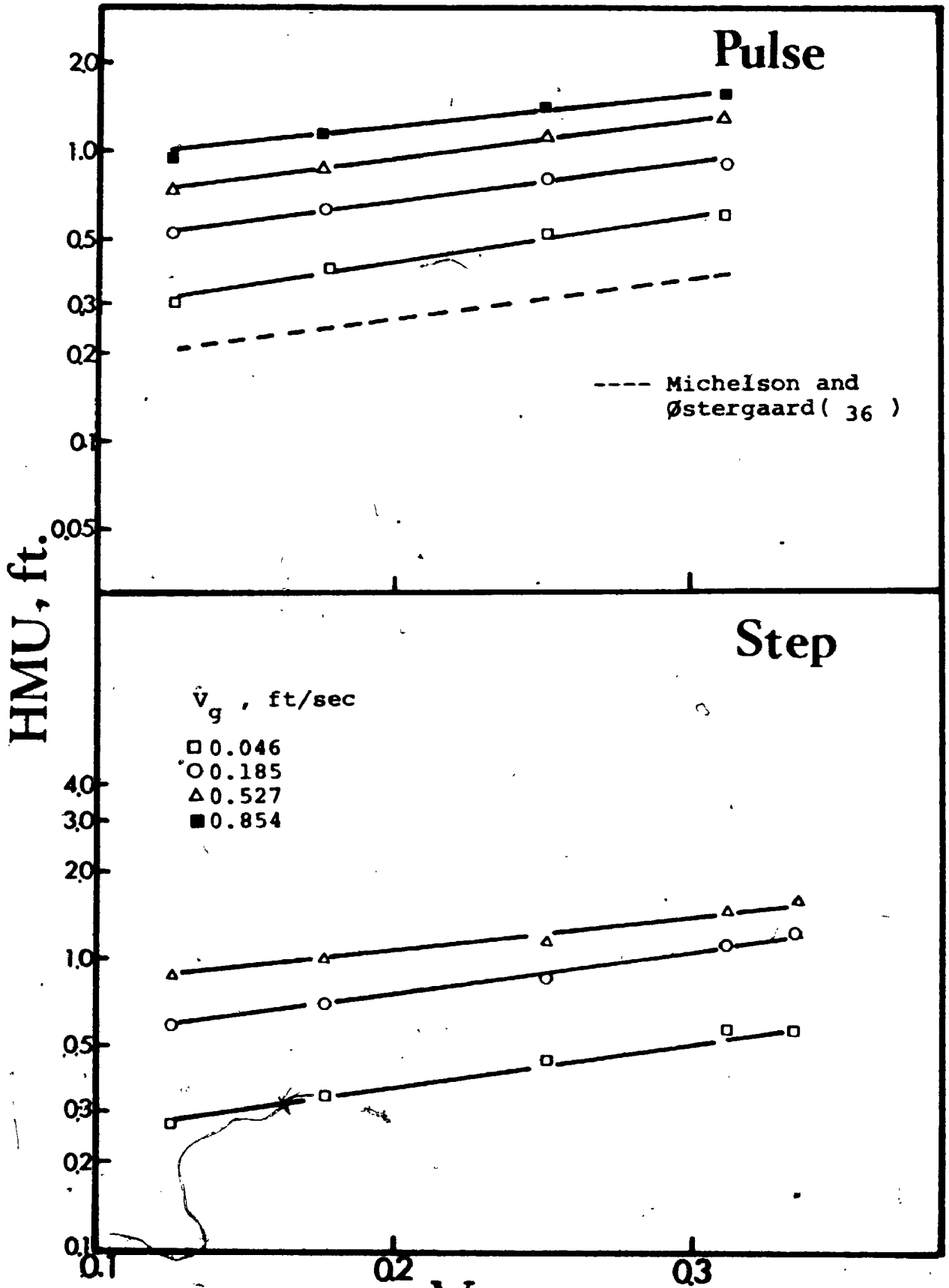

Figure 4.49.
Effect of Liquid Velocity on Liquid Phase HMU in Three Phase Beds of 6 mm Glass beads.

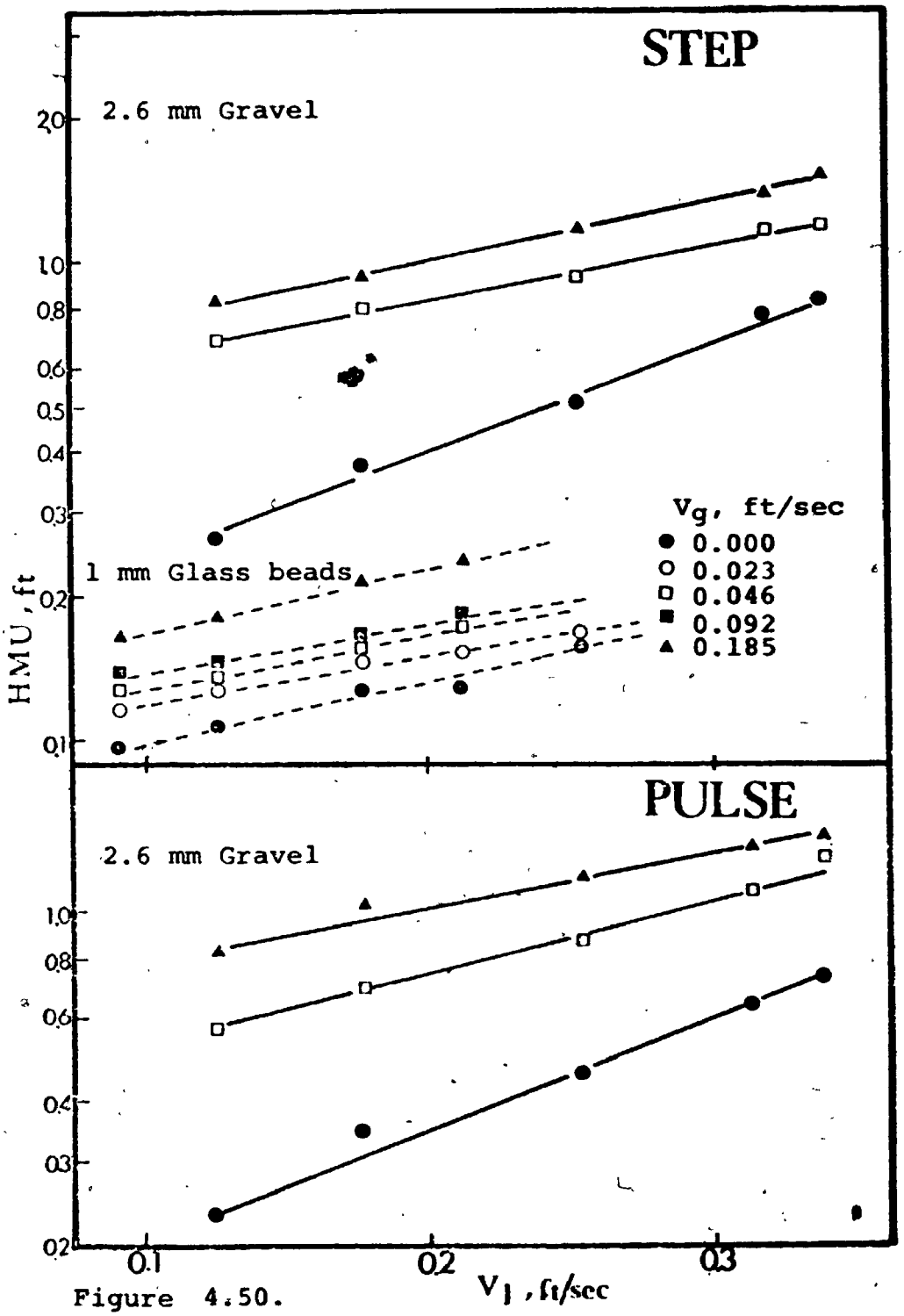

Figure 4.50.
Effect of Liquid Velocity on Liquid Phase HMU in Three Phase Beds of Gravel and 1 mm Glass beads.

The effect of gas flowrate on liquid phase axial mixing in the different beds is shown in figure 4.51 and 4.52. As noted above, the values obtained by the two tracer techniques were nearly identical. The figures show that HMU increased with increasing gas velocity in all the beds. This finding is qualitatively in accord with those of Vail et al. (62), Schügerl (55) and Michelson and Østergaard (36). The HMU was sharply increased by introducing small amounts of gas. However, the initial rate of increase was not maintained with further increases in the gas flowrate in the beds of gravel and 6 mm glass beads. On the other hand, in the beds of 1 mm glass beads, as in the liquid-gas beds, HMU increased proportionally with gas flowrate over the entire range. Comparison of the data of figures 4.7 and 4.52 indicates that the rate of increase of HMU with gas flowrate was greater in the three phase fluidized beds than in the air-water systems.

From the above findings and those of other workers, it can be concluded that liquid phase axial mixing increased with increasing gas flowrate. However, the effect of liquid velocity is not well defined. The present data qualitatively agree with those of Schügerl (55) and of Michelson and Østergaard (36) for the beds of larger particles. However, Vail et al. (62) and Michelson and Østergaard (36) found that liquid phase axial mixing decreased with increasing liquid velocity in beds of smaller particles fluidized by water and air.

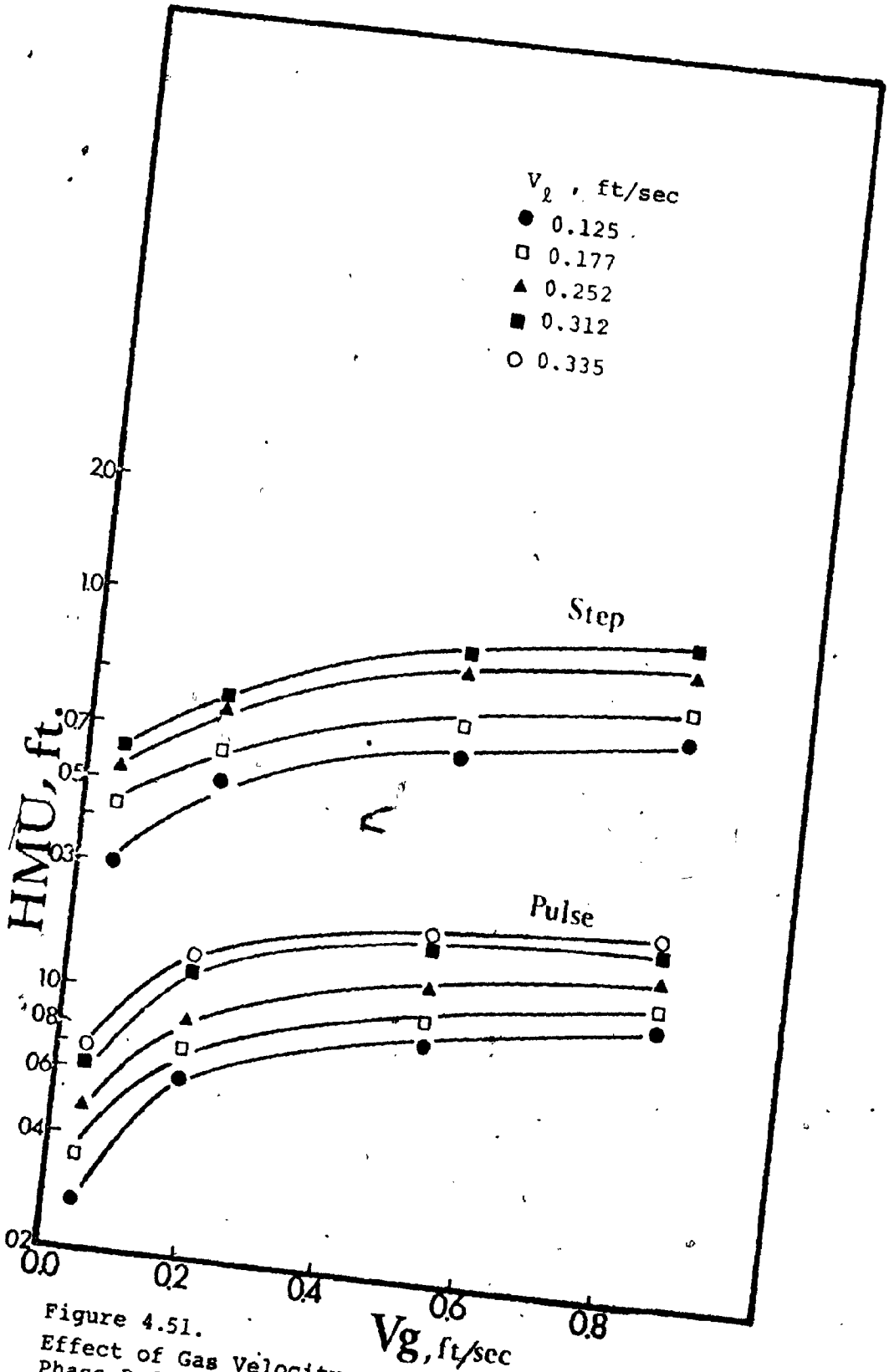

Figure 4.51.
Effect of Gas Velocity on Liquid Phase HMU in Three Phase Beds of 6 mm Glass beads.

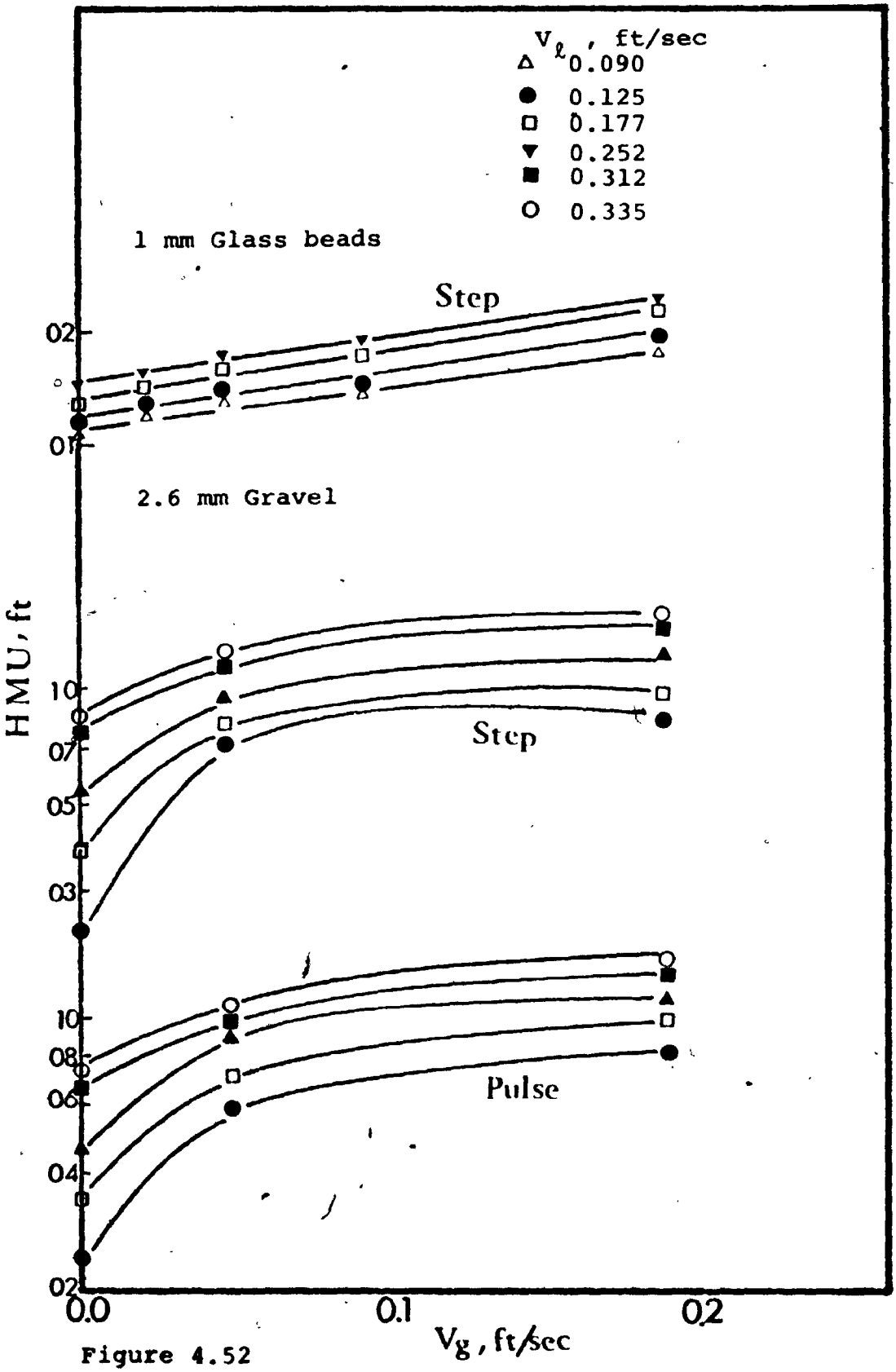

Figure 4.52

Effect of Gas Velocity on Liquid Phase HMU in Three Phase Beds of Gravel and 1 mm Glass beads.

4.4.3.1. Correlation of the Liquid Phase Axial Mixing Data

A statistical analysis was performed on the liquid phase HMU data for liquid velocities V_ℓ between 0.090 and 0.335 ft/sec, gas velocities V_g between 0.023 and 0.854 ft/sec, and particle sizes d_p between 1 and 6 mm. The liquid phase mixing data can be found in the Appendix H .
The following relationship resulted:

$$\frac{HMU}{Ho} = 2.82 \; V_\ell^{0.815} \; V_g^{0.309} \qquad \ldots.(4.20)$$

In this equation, V_ℓ, V_g are the liquid and gas superficial velocities in ft/sec, and Ho is the initial bed height in ft. The particle size term was excluded due to its small exponent (0.083) compared to those of the V_ℓ and V_g terms. The standard error of estimate between the experimental values and those calculated by equation (4.20) is 0.102 for 73 data points. Since the liquid phase HMU is mainly function of V_ℓ and V_g, it was not considered meaningful to express this equation in dimensionless form. The goodness of fit between the experimental and calculated values is shown in figure 4.53.

A comparison was made between the correlations of Michelson and Østergaard (36) and the present experimental data. For three phase beds of 1 mm glass beads, Michelson and Østergaad's correlation predicts generally higher liquid axial mixing than found in the present study. For 6 mm glass beads, their correlation predicted values of HMU which were both considerably

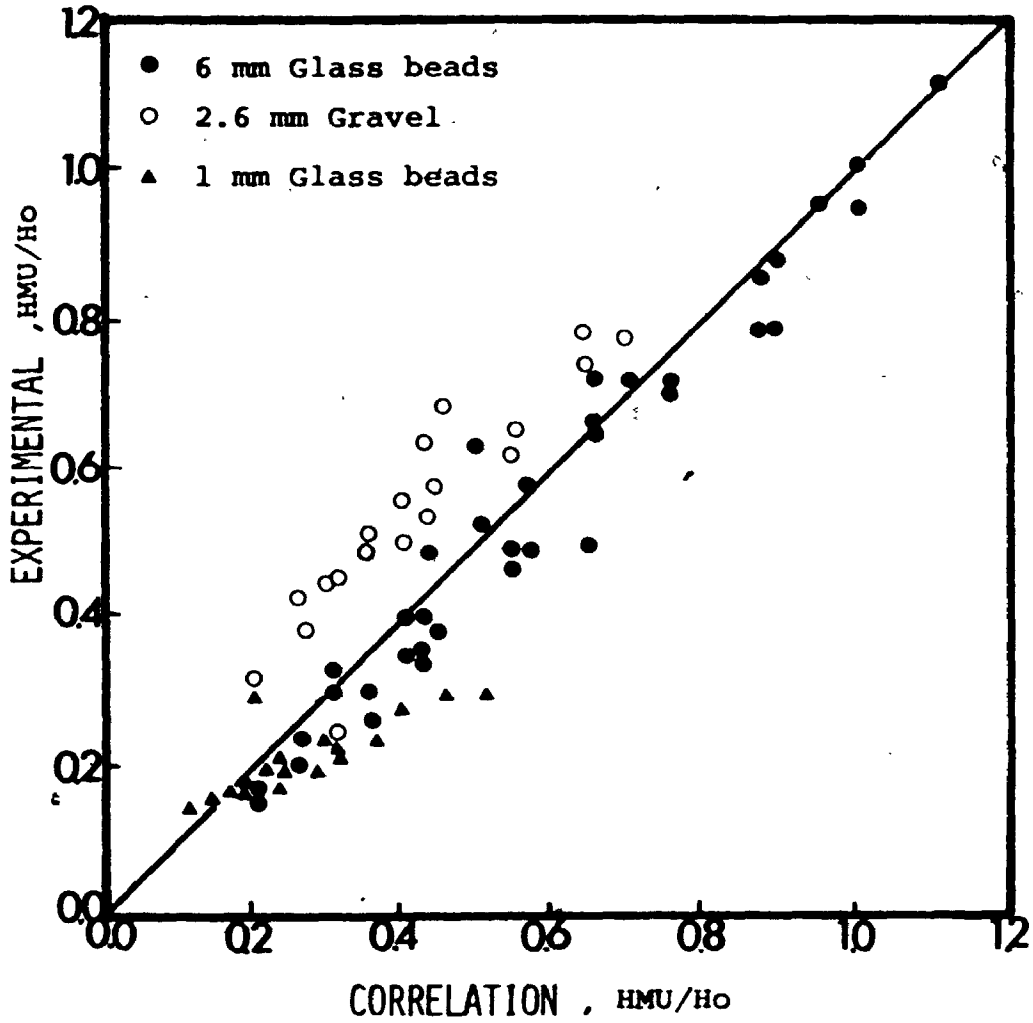

Figure 4.53 Comparison between Experimental and Calculated Values of HMU/Ho in Three Phase Fluidized Beds. (Equation 4.20)

lower than those found in the present study and also independent of gas rate. Michelson and Østergaard's (36) correlation for the beds of 6 mm glass beads is depicted as a dotted line in figure 4.49.

4.4.4. Bubble Characteristics

To complement the hold-up and axial mixing studies, the effect of liquid and gas velocity and liquid surface tension and viscosity on the bubble size, size distribution and rising velocity were studied. The detailed data are given in Appendix I.

4.4.4.1. Mean Bubble Size, Size Distribution and Rising Velocity

Liquid flowrates were varied from 0.090 to 0.335 ft/sec. As can be seen in figure 4.54 the effect of liquid velocity on bubble size depends upon the characteristics of both the liquid and solid phases. With acetone solution (50.2 dyne/cm) as the liquid fluidizing medium, the bubble size decreased with increasing liquid velocity in the beds of 1 mm glass beads and gravel. However, the reverse was true in the beds of 6 mm glass beads. With water as the liquid phase, the bubble size increased slightly with increasing liquid rate in all beds. In the beds fluidized by higher viscosity solutions (7.6, 20 and 70 cp), the bubble size increased somewhat with increasing liquid flowrate in the beds of 1 mm glass beads and gravel.

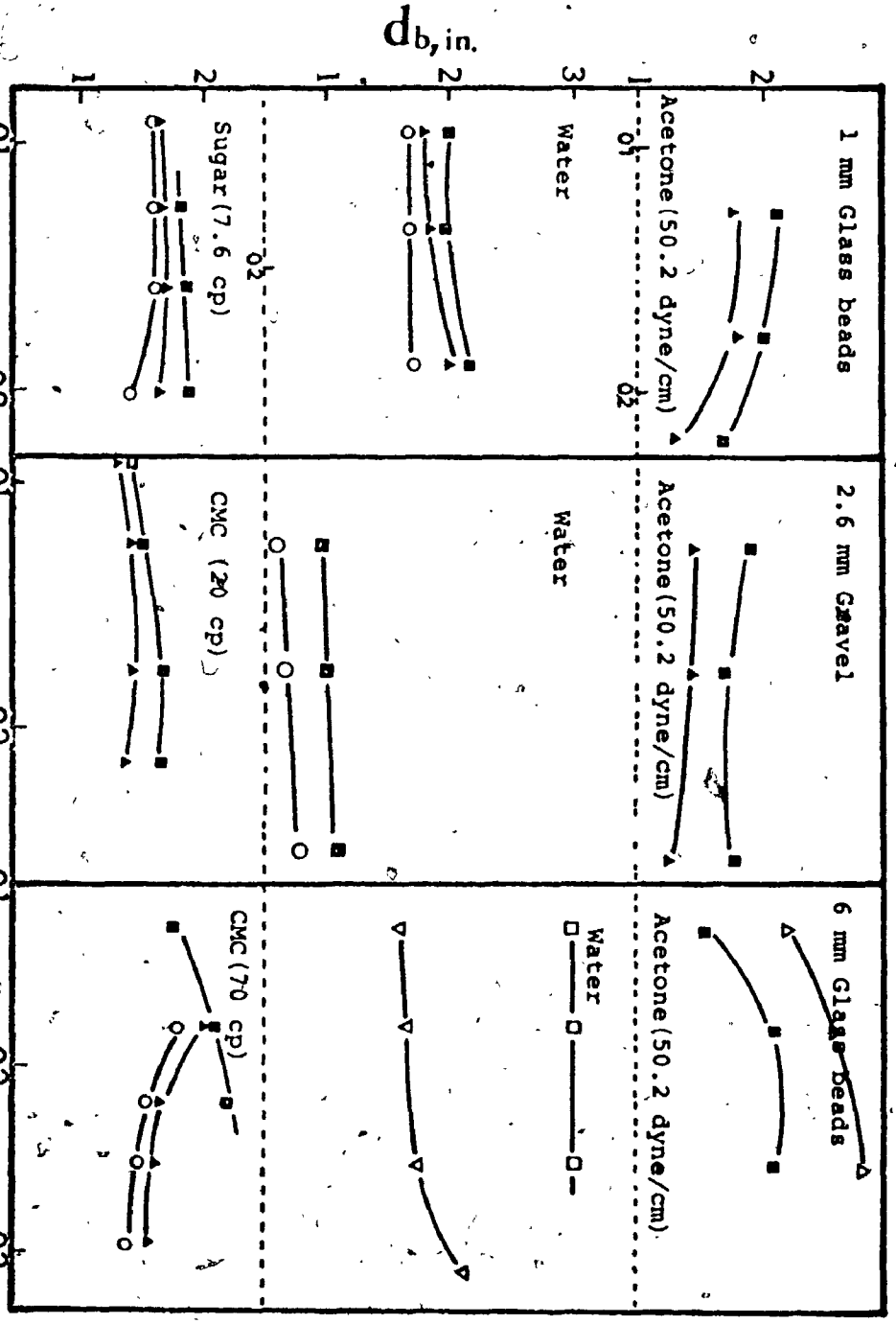

Figure 4.54

Effect of Liquid Velocity on Bubble Size in Three Phase Fluidized Beds.
o: V_g = 0.046 ft/sec, Δ: V_g = 0.092 ft/sec, ■: V_g = 0.185 ft/sec,
▽: V_g = 0.527 ft/sec, □: V_g = 0.854 ft/sec.

However, in the beds of 6 mm glass beads, the bubble size decreased with increasing liquid velocity at lower gas rates and increased at higher gas rates. At the lower gas rates the bed was contracted whereas it was expanded at the higher gas velocities. It would therefore appear that the bed expansion characteristics are related to the change of bubble size with liquid velocity.

The effect of liquid velocity on bubble rising velocity in different beds is shown in the figure 4.55. It can be observed that V_{br} decreased slightly with increasing liquid velocity in the beds fluidized by air and acetone (50.2 dyne/cm) solution. With water as fluidizing medium V_{br} increased slightly with increasing liquid rate in the beds of 1 mm glass beads, and was independent of V_ℓ in the beds of gravel. However, in the beds of 6 mm glass beads, V_{br} increased with increasing liquid rate at higher gas rates whereas it decreased at lower gas rates.

In the higher viscosity solutions, V_{br} was nearly independent of liquid flowrate in all cases.

Typical bubble size distributions in the three phase beds are shown in figure 4.56. As may be seen, the size distribution widened somewhat with increasing liquid rate in the beds of 6 mm glass beads and gravel. In contrast, the reverse trend was observed in the beds of 1 mm glass beads which is qualitatively in accord with previous findings of Page and Harrison (48), and of Rigby et al. (52).

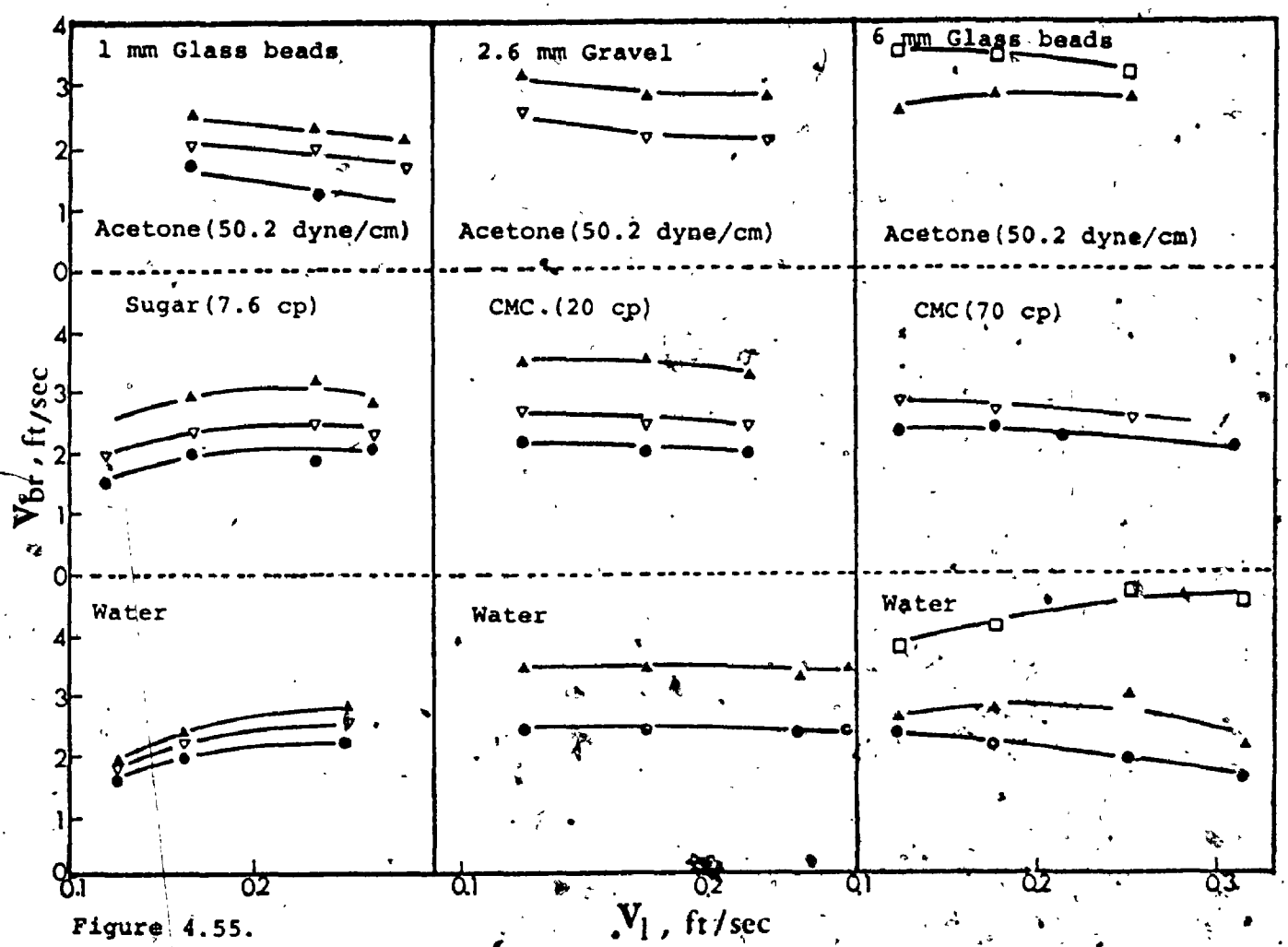

Figure 4.55.

Effect of Liquid Velocity on Relative Bubble Rising Velocity in Three Phase Fluidized Beds., ●: V_g = 0.043 ft/sec, ★: V_g = 0.092 ft/sec, ▲: V_g = 0.185 ft/sec, □: V_g = 0.527 ft/sec.

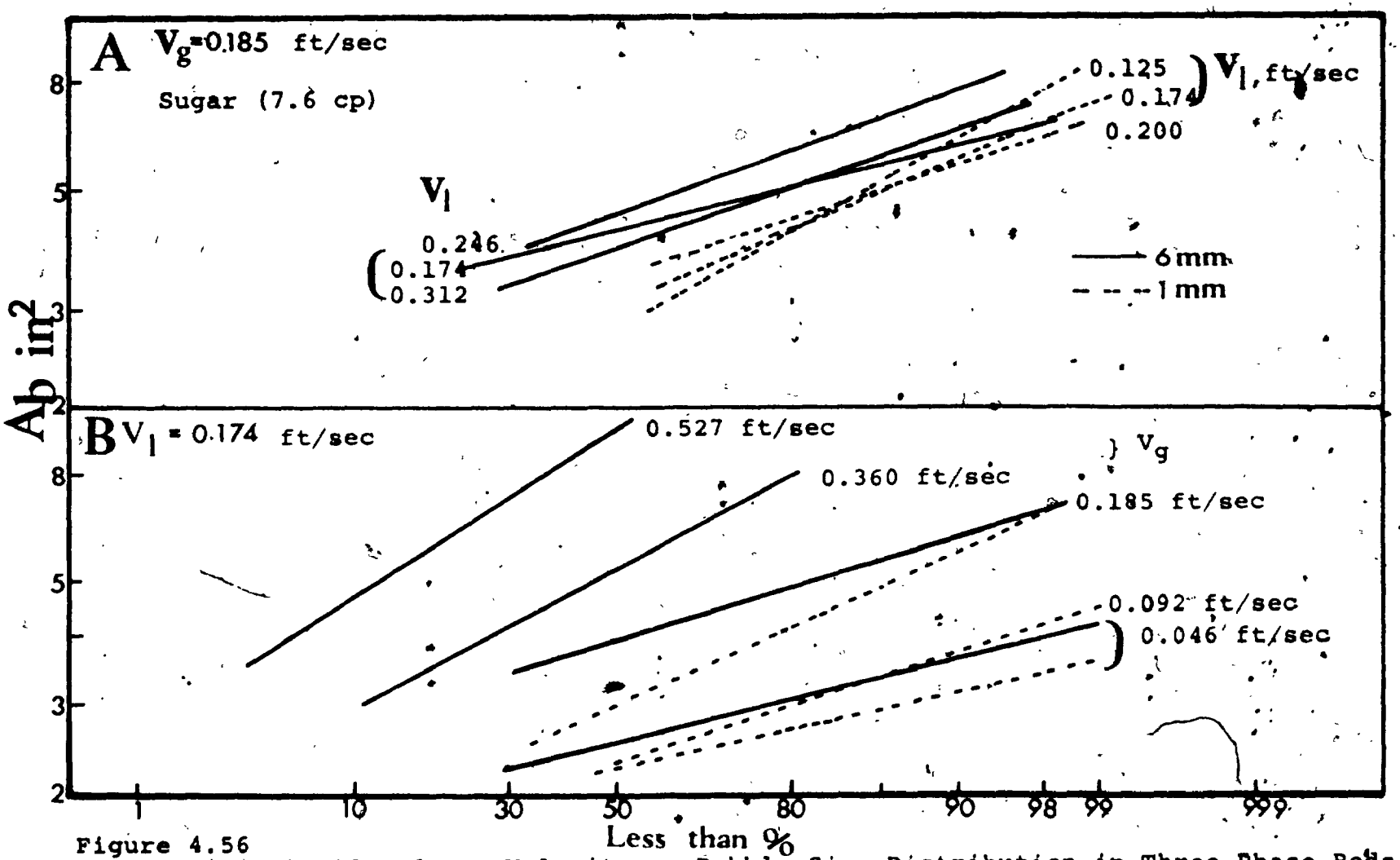

Figure 4.56
Effect of Liquid and Gas Velocity on Bubble Size Distribution in Three Phase Beds.
(log Probability Paper)

The effect of gas velocity on bubble size and rising velocity is shown in figures 4.57-4.59. Regardless of liquid flowrate, d_b and V_{br} increased with increasing gas flowrate in all the beds.

It may be noted from figure 4.56B that the size distribution generally widened with increasing gas velocity.

The effect of surface tension on bubble size and rising velocity are shown in figures 4.60-4.62. As in the liquid-gas beds, these parameters decreased with increasing surface tension in all three phase beds.

The effect of liquid viscosity on d_b and V_{br} are shown in figure 4.63. The mean bubble size increased with increasing viscosity in the beds of gravel and 6 mm glass beads. However, the bubble size was nearly independent of viscosity in the beds of 1 mm glass beads and at higher gas flowrates in the beds of gravel. In the beds of gravel and 6 mm glass beads at lower gas rates, the bubble rising velocity was nearly independent of liquid viscosity. With higher gas rates in the beds of 6 mm glass beads, the bubble rising velocity was independent of viscosity in the range 1 to 10 cp. However, the bubble velocity decreased at higher viscosities.

From the present findings and those of others, it can be concluded that the bubble size and rising velocity increased with increasing gas flowrate in three phase fluidized beds. However, the bubble size either decreased (42,52,57) with or was independent of liquid flowrate (48).

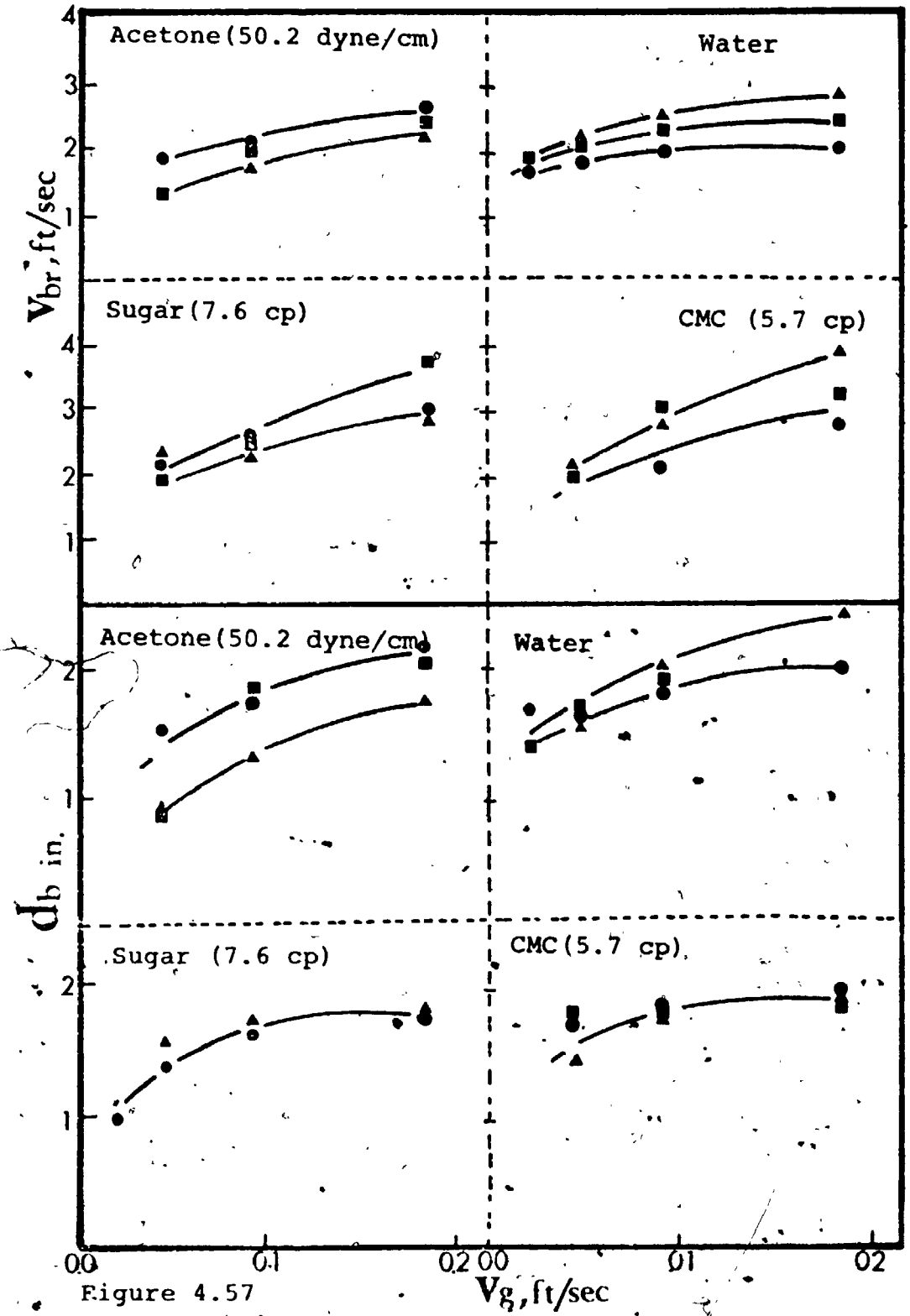

Figure 4.57

Effect of Gas Velocity on Bubble Size and Rising Velocity in Three Phase Beds of 1 mm Glass beads. ●: V_ℓ = 0.125 ft/sec, ■: V_ℓ = 0.177 ft/sec, ▲: V_ℓ = 0.20 ft/sec.

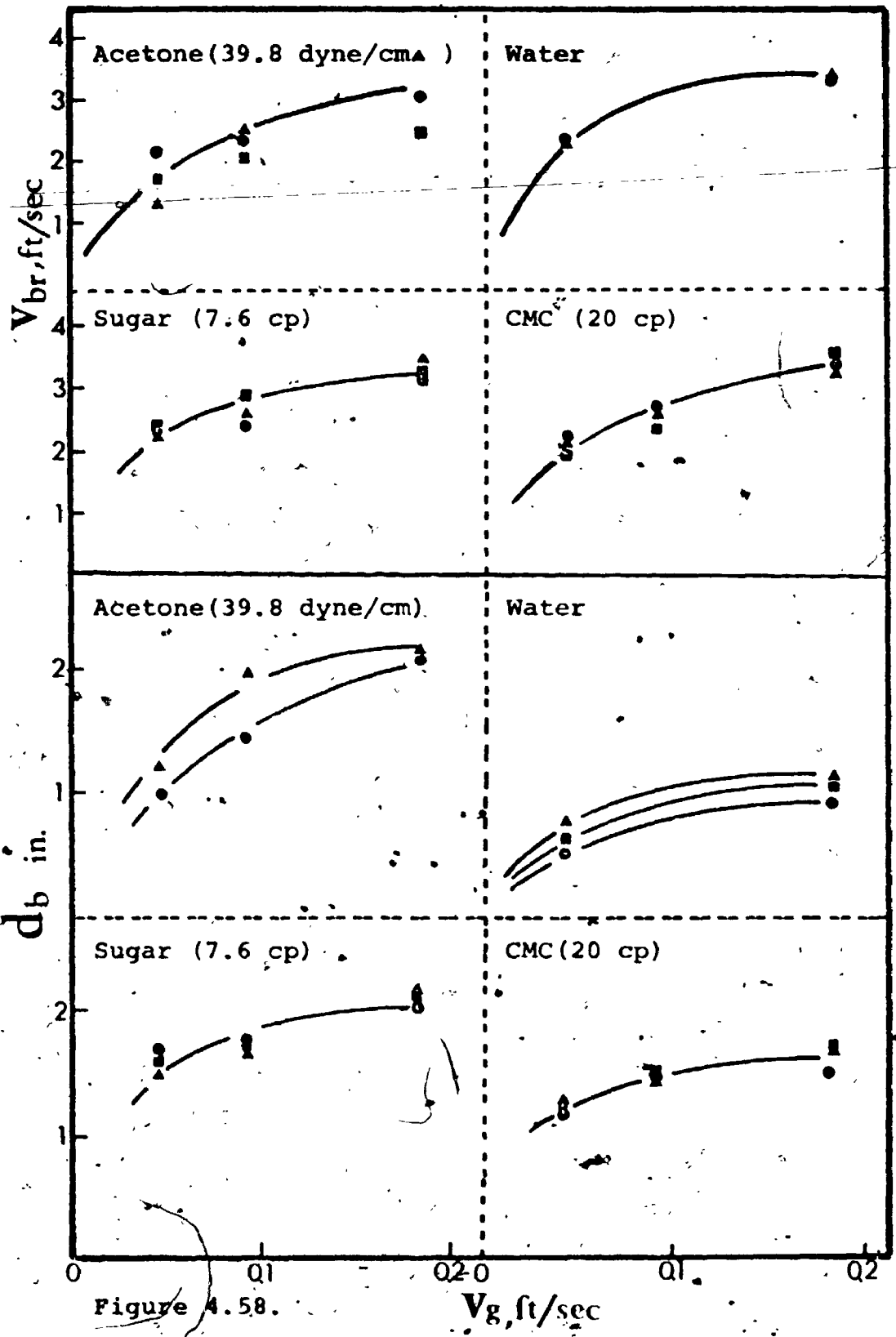

Figure 4.58.

Effect of Gas Velocity on Bubble Size and Rising Velocity in Three Phase Beds of Gravel.,
●: V_ℓ = 0.125 ft/sec, ■: V_ℓ = 0.177 ft/sec,
▲: V_ℓ = 0.252 ft/sec.

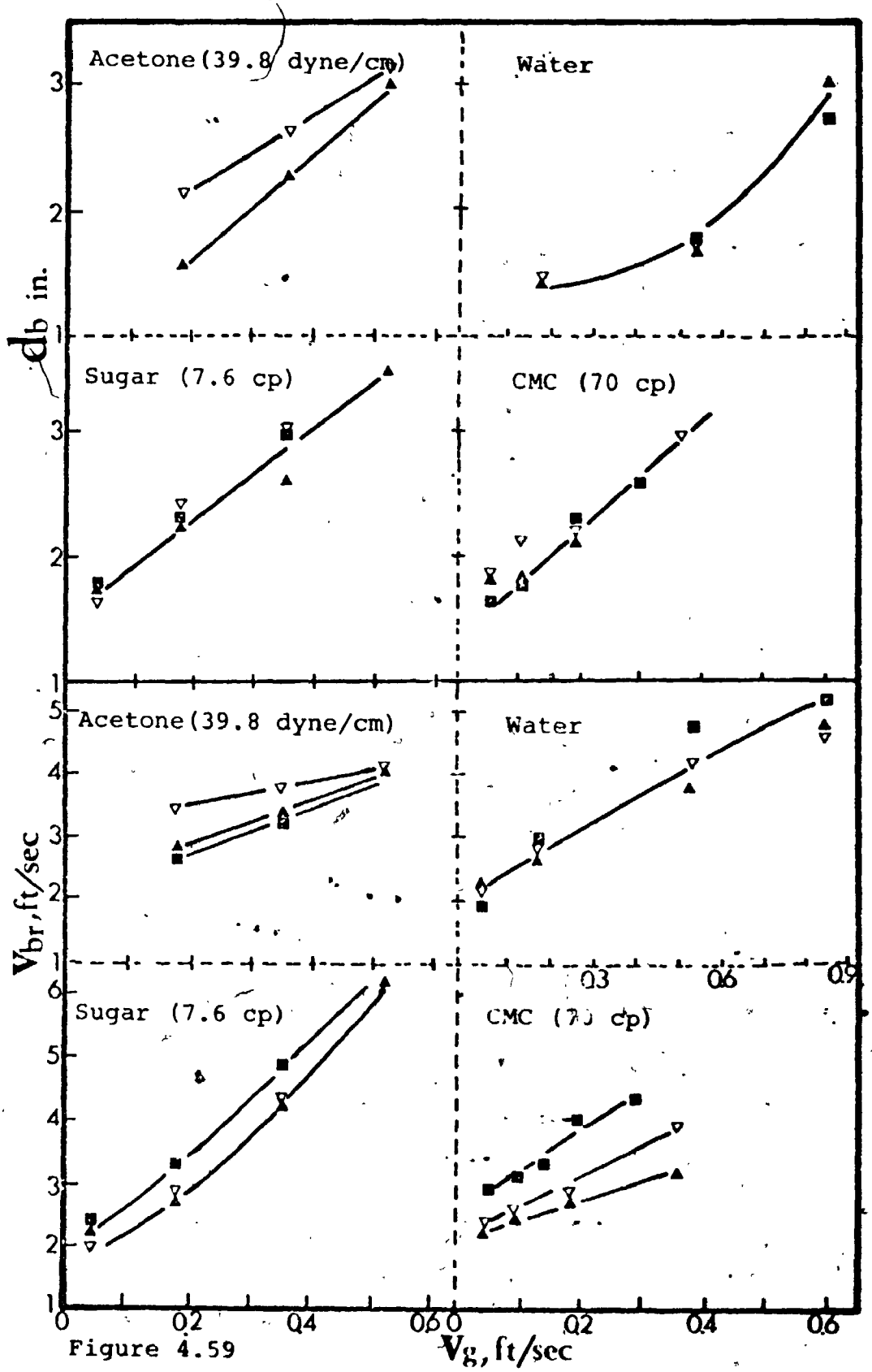

Figure 4.59

Effect of Gas Velocity on Bubble Size and Rising Velocity in Three Phase Beds of 6 mm Glass beads.
▲: V_ℓ = 0.125 ft/sec, ▽: V_ℓ = 0.177 ft/sec,
■: V_ℓ = 0.252 ft/sec.

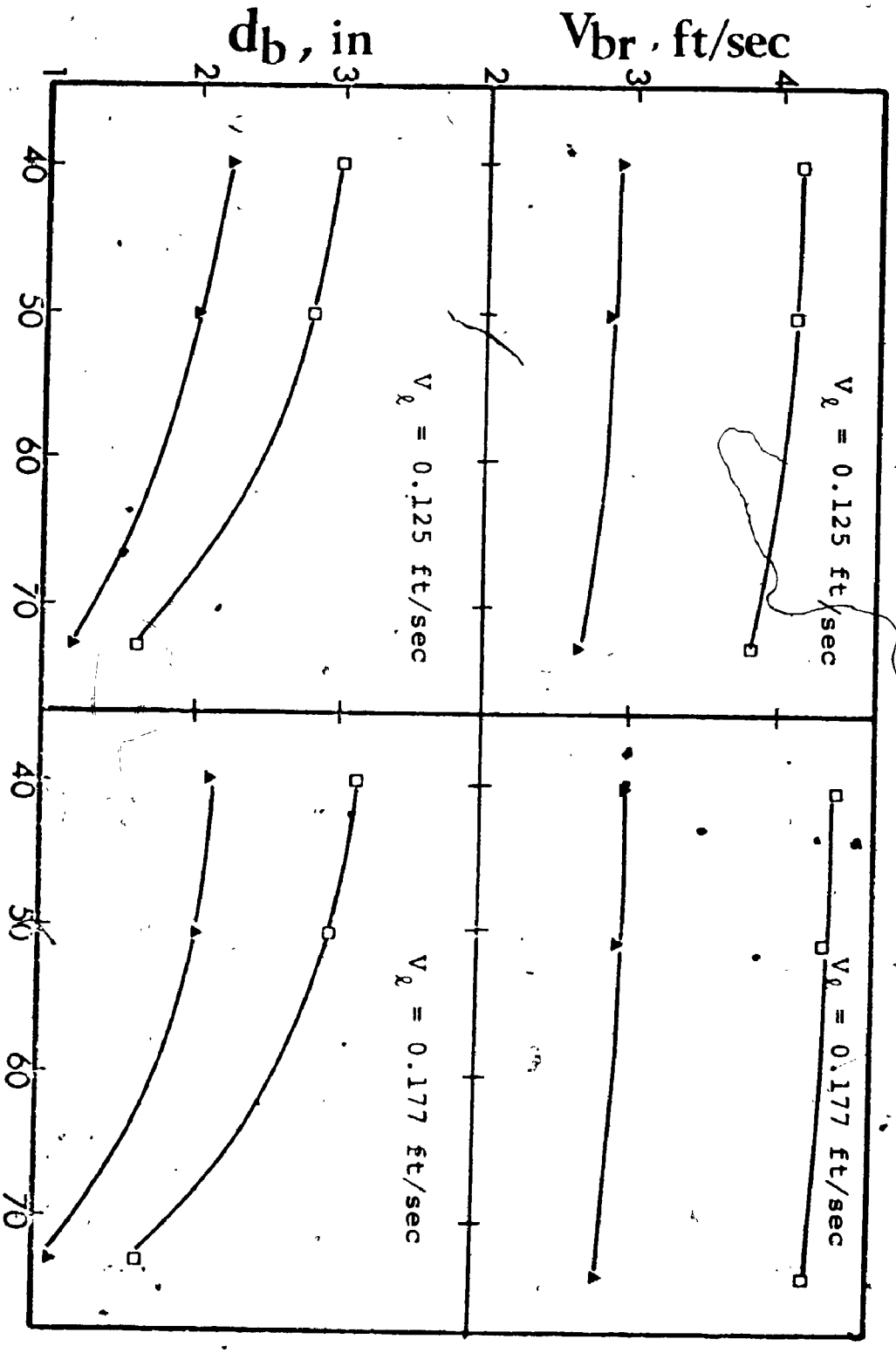

Figure 4.60
Effect of Surface Tension on Bubble Size and Rising Velocity in Three Phase Beds of 6 mm Glass beads., ▲: V_g=0.046 ft/sec, □: V_g = 0.527 ft/sec

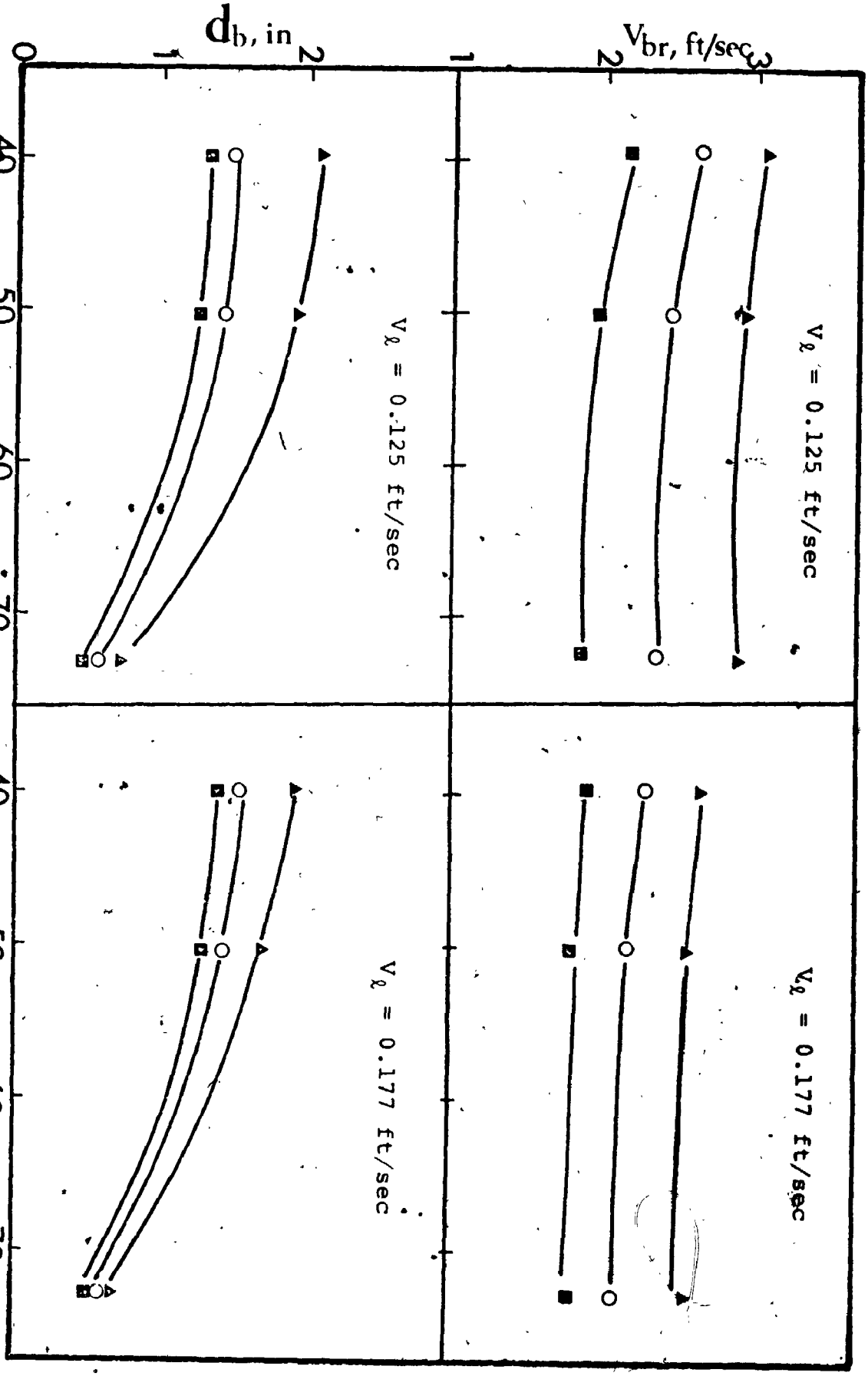

Figure 4.61

Effect of Surface Tension on Bubble Size and Rising Velocity in Three Phase Beds of 2.6 mm Gravel., □, V_g = 0.046 ft/sec, ○:V_g = 0.092 ft/sec, ▲:V_g = 0.185 ft/sec.

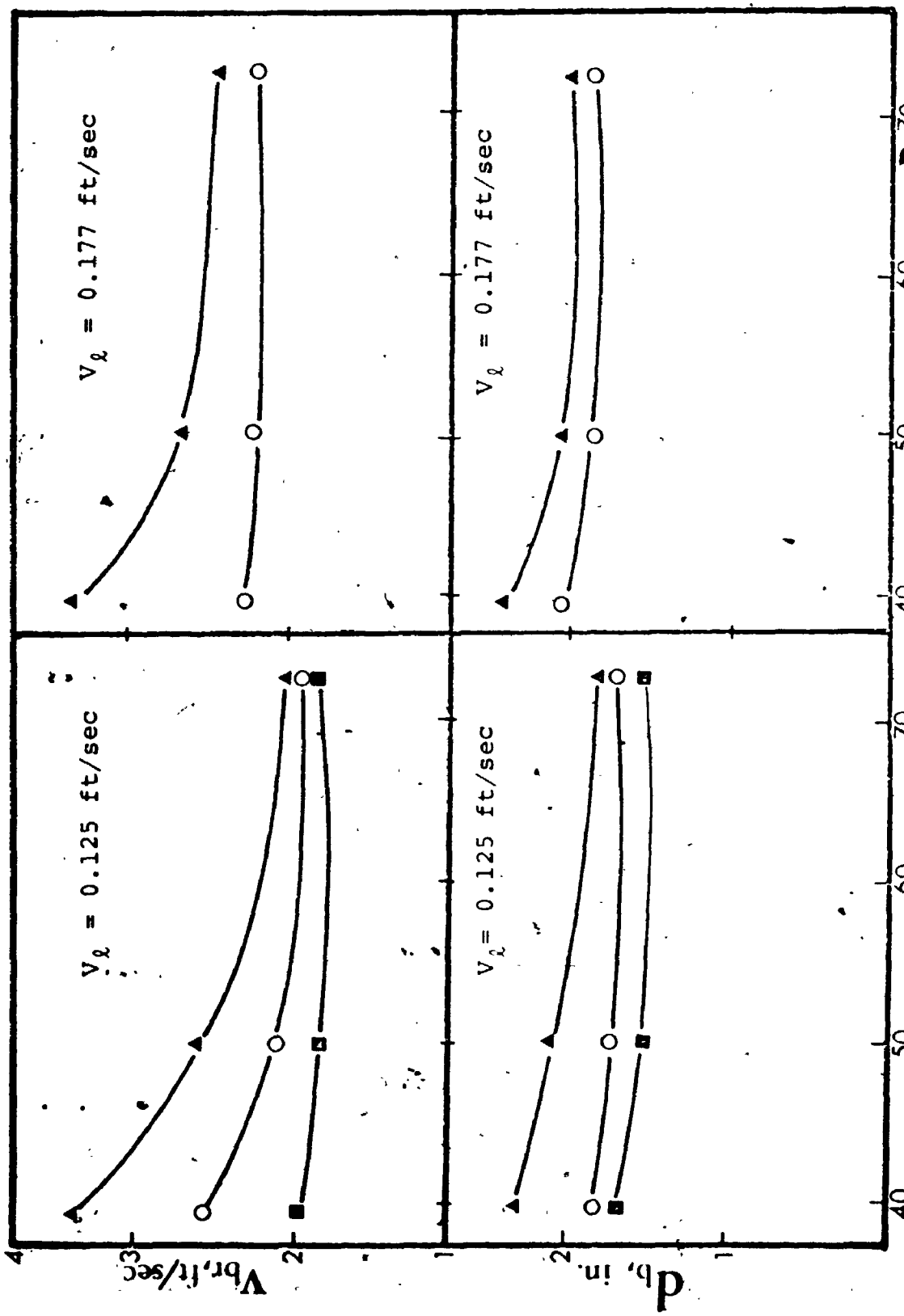

Figure 4.62

Effect of Surface Tension on Bubble Size and Rising Velocity in Three Phase Beds of 1 mm Glass beads. ■: V_g = 0.046 ft/sec, O:V_g = 0.092 ft/sec, ▲: V_g = 0.185 ft/sec

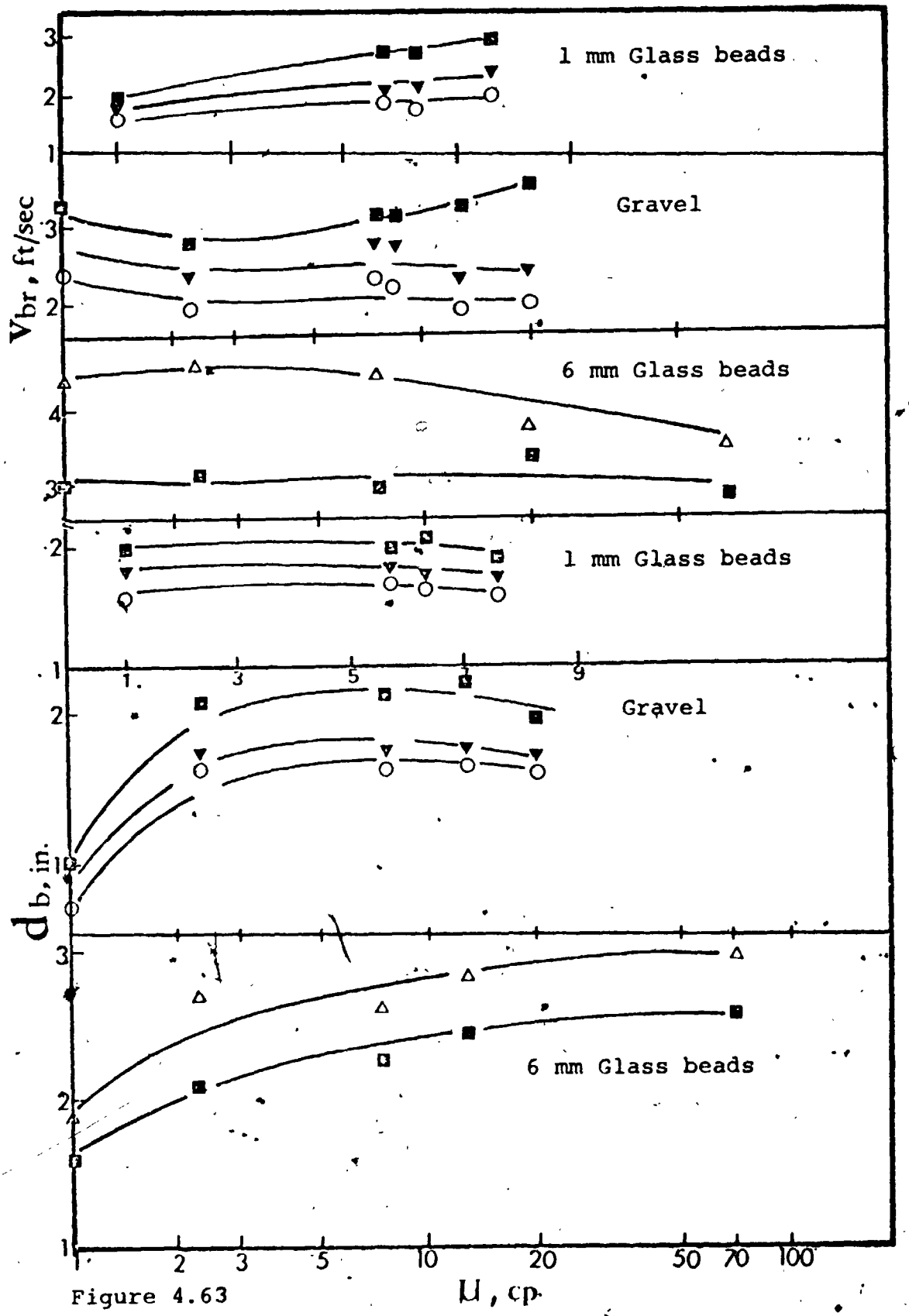

Figure 4.63

Effect of Viscosity on Bubble Size and Rising Velocity in Three Phase Beds., ○: V_g=0.046 ft/sec, ▼:V_g=0.092 ft/sec, ■: V_g=0.185 ft/sec, △: V_g=0.360 ft/sec, at V_l=0.177 ft/sec.

Rigby et al. (52) found that the bubble rising velocity increased with increasing water velocity which is in agreement with the results of the present study. No data has been published in the literature on the influence of viscosity and surface tension on bubble properties in three phase fluidized beds. Consequently, no comparison can be made with the present data.

4.4.4.2. Correlation of Bubble Size and Rising Velocity Data

A statistical analysis was performed on the bubble size and rising velocity for liquid velocities V_ℓ between 0.090 and 0.335 ft/sec, gas velocities V_g between 0.023 and 0.854 ft/sec, particle diameters d_p between 1 and 6 mm, liquid surface tensions σ between 39.8 and 72.8 dyne/cm and viscosities μ between 1 and 70 cp. The following relationship resulted:

$$V_{br} = 9.858\ V_\ell^{0.065}\ V_g^{0.339}\ \gamma^{0.025}\ \sigma^{0.179} \quad \ldots(4.22)$$

in which V_ℓ and V_g are the liquid and gas superficial velocities in ft/sec, σ is the surface tension in lb/sec^2 and γ is the viscosity defined as equation (4.2) in $lb/ft\ sec^{2-n}$. The bubble rising velocity was also correlated with bubble size as follows:

$$V_{br} = 16.93\ d_b^{0.989} \quad \ldots.(4.23)$$

where d_b is in ft.

The standard errors of estimate between the experimental values and those of calculated from equations (4.22) and (4.23) are 0.538 and 0.585 respectively for 181 data points. The goodness of fit of equation (4.23) is shown in figure 4.64. Elimination of V_{br} between equations (4.22) and (4.23) yields the following relationship:

$$d_b = 0.319\ V_\ell^{0.052}\ V_g^{0.248}\ \gamma^{0.008}\ \sigma^{0.034} \quad \ldots(4.24)$$

There was good agreement between the present data and the correlation of Rigby et al. (52), equation (2.26), at low liquid and gas velocities. However, the agreement became poor at higher flowrates which were outside the range of those studied by these authors.

4.4.5. Wake Characteristics in Three Phase Fluidized Beds

It has been shown in both the present and previous studies that the addition of small amounts of gas to a liquid fluidized bed may result in a reduction of its expanded bed height. An explanation of this has been given by Stewart and Davidson (59) and also by Østergaard (44) based on the assumption that the bed consists of three fluid phases, namely a gas bubble phase, a bubble wake phase, and a continuous liquid phase. It has been further assumed that the wake phase moves at the bubble velocity which is greater than the average liquid velocity. The velocity in the continuous liquid phase is thereby reduced and the hold-up of this

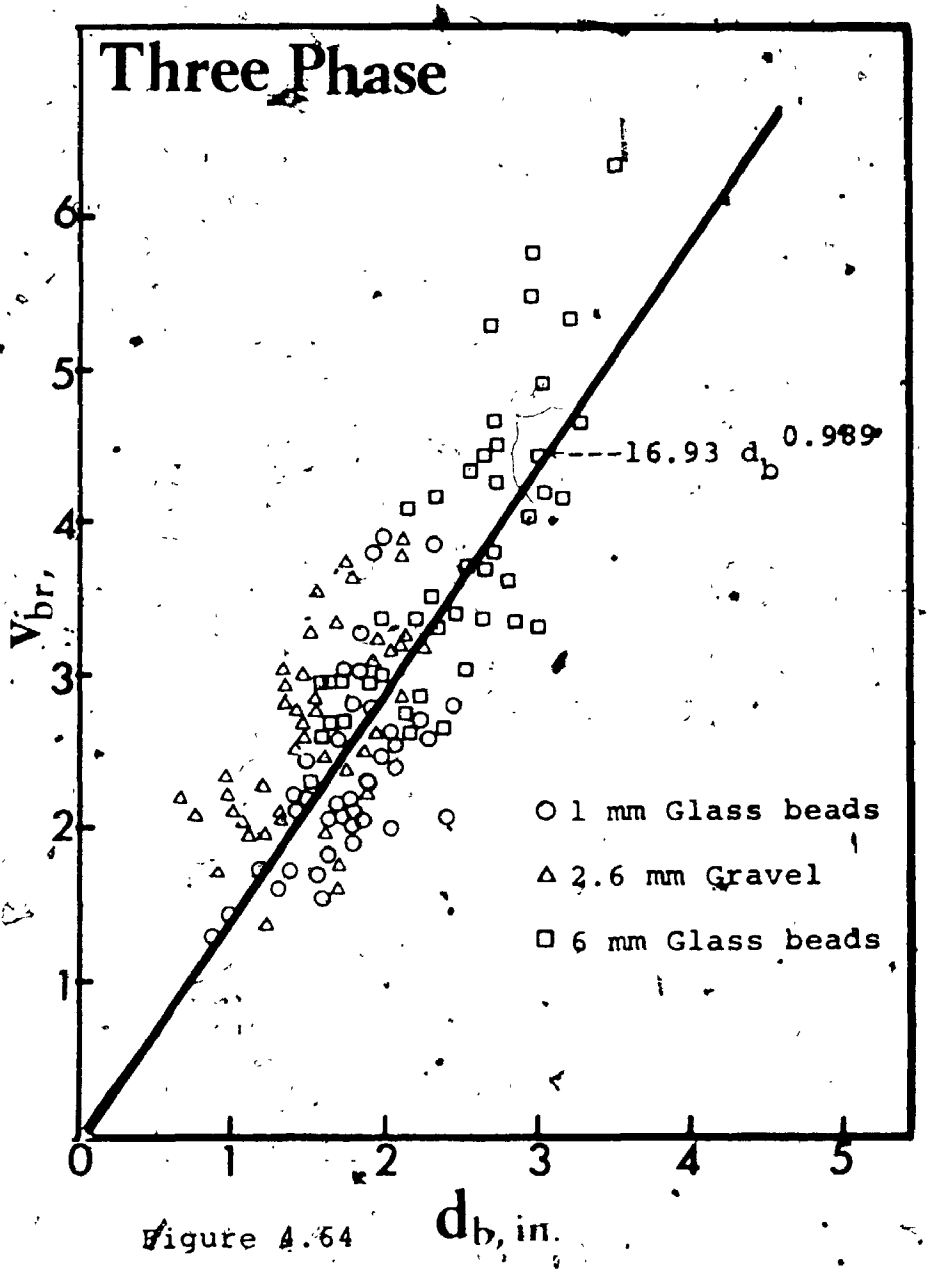

Figure 4.64

Correlation of Bubble Rising Velocity in Three Phase Beds. (Equation 4.23)

3 4

OF/DE

phase is reduced correspondingly.

Østergaard assumed that the hold-up of solids in the bubble wake is identical to that of the continuous liquid phase, in contrast, Stewart and Davidson claimed that the liquid wake is almost free of particles. In the present study, clear bubble wakes behind the swarm of gas bubbles were not observed. Therefore, it may be assumed that the bubble wakes contain solid particles.

4.4.6.1. Calculation of Wake Hold-up

It is assumed that the bubble wakes move at the same velocity as the bubbles and that their solids hold-up is identical to that in the continuous liquid phase.

The liquid hold-up in a three phase fluidized bed ε_{ℓ_3} is related to the liquid hold-up in the continuous phase $\varepsilon_{\ell c}$ and the gas hold-up ε_g by the following relationship (44):

$$\varepsilon_{\ell_3} = \varepsilon_{\ell c} (1 - \varepsilon_g) \qquad \ldots.(4.24)$$

in which ε_{ℓ_3} can be calculated from equation (4.14), ε_g from equations (4.14) and (4.17). It is assumed that $\varepsilon_{\ell c}$ may be calculated from equation (4.10).

The superficial liquid velocity in the continuous liquid phase V'_ℓ can be calculated from a material balance:

$$V_\ell = V'_\ell (1 - \varepsilon_g - \varepsilon_w) + V_b \varepsilon_w \varepsilon_{\ell c} \qquad \ldots(4.25)$$

where V_ℓ is the average superficial liquid velocity, V_b is the

bubble rising velocity, and ε_w is the fractional bed volume occupied by the bubble wakes.

Rearranging equation (4.25) gives,

$$\varepsilon_w = \frac{V'_\ell\ (1 - \varepsilon_g) - V_\ell}{V'_\ell - V_b \varepsilon_{\ell c}} \qquad .....(4.26)$$

in which V'_ℓ and V_b can be calculated from equations (4.14) and (4.22).

The results obtained from equation (4.26) are expressed in terms of $\varepsilon_w/\varepsilon_g$, that is the ratio of the wake to gas volume.

The effect of gas velocity on $\varepsilon_w/\varepsilon_g$ in the beds of 1 mm glass beads is shown in figure 4.65 for different liquids. As may be seen in this figure, $\varepsilon_w/\varepsilon_g$ decreased with increasing gas velocity for all the liquids studied. The same trends were observed in the beds of gravel and 6 mm glass beads as shown in figures 4.66 and 4.67. Because of the difference in initial bed heights, a direct comparison between the values of $\varepsilon_w/\varepsilon_g$ for the beds of 1 mm glass beads and the other beds cannot be made. However, a comparison of the data for the beds of gravel and 6 mm glass beads shows that $\varepsilon_w/\varepsilon_g$ increased with decreasing particle size. This is in qualitative agreement with the findings of Rigby and Capes (53).

As may be seen in figure 4.68, at the lower gas rates, $\varepsilon_w/\varepsilon_g$ went through a maximum at a liquid velocity of about 0.125 ft/sec in the beds of 1 mm glass beads. At higher gas rates, $\varepsilon_w/\varepsilon_g$ increased somewhat with increasing liquid velocity over the entire range studied. The same maxima were also exhibited

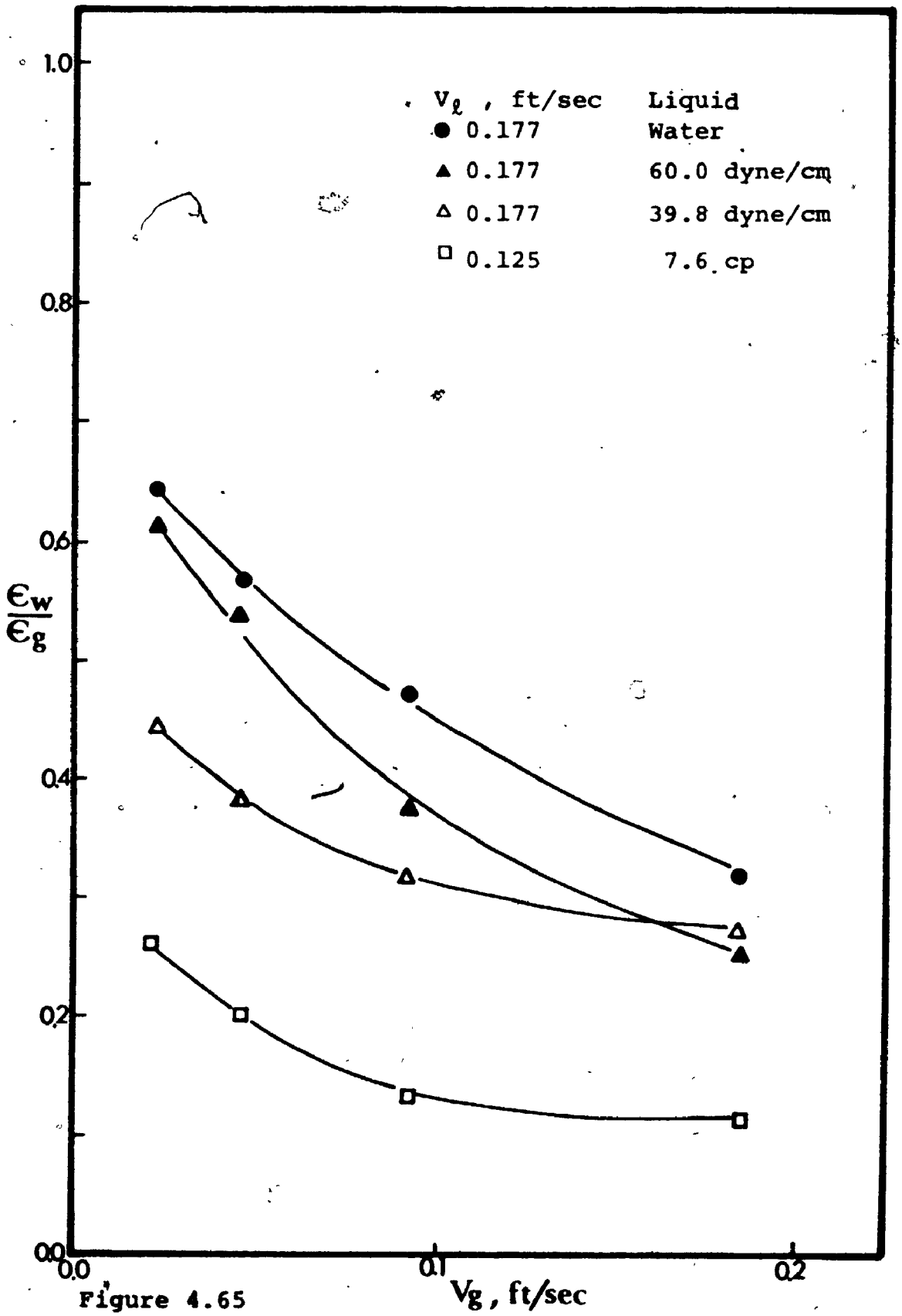

Figure 4.65

Effect of Gas Velocity on the Ratio of Wake to Gas Volume in Three Phase Beds of 1 mm Glass beads.

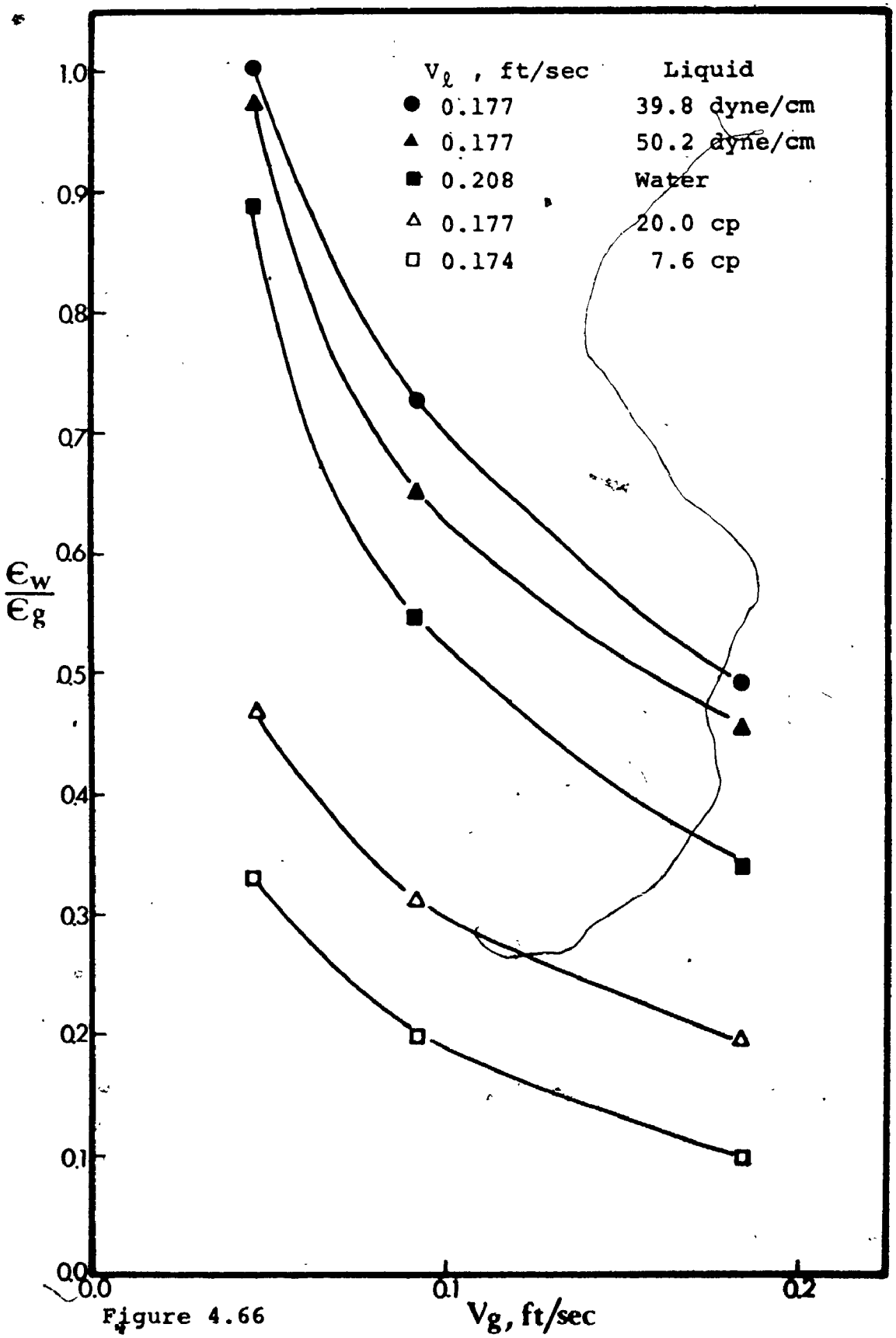

Figure 4.66

Effect of Gas Velocity on the Ratio of Wake to Gas Volume in Three Phase Beds of Gravel.

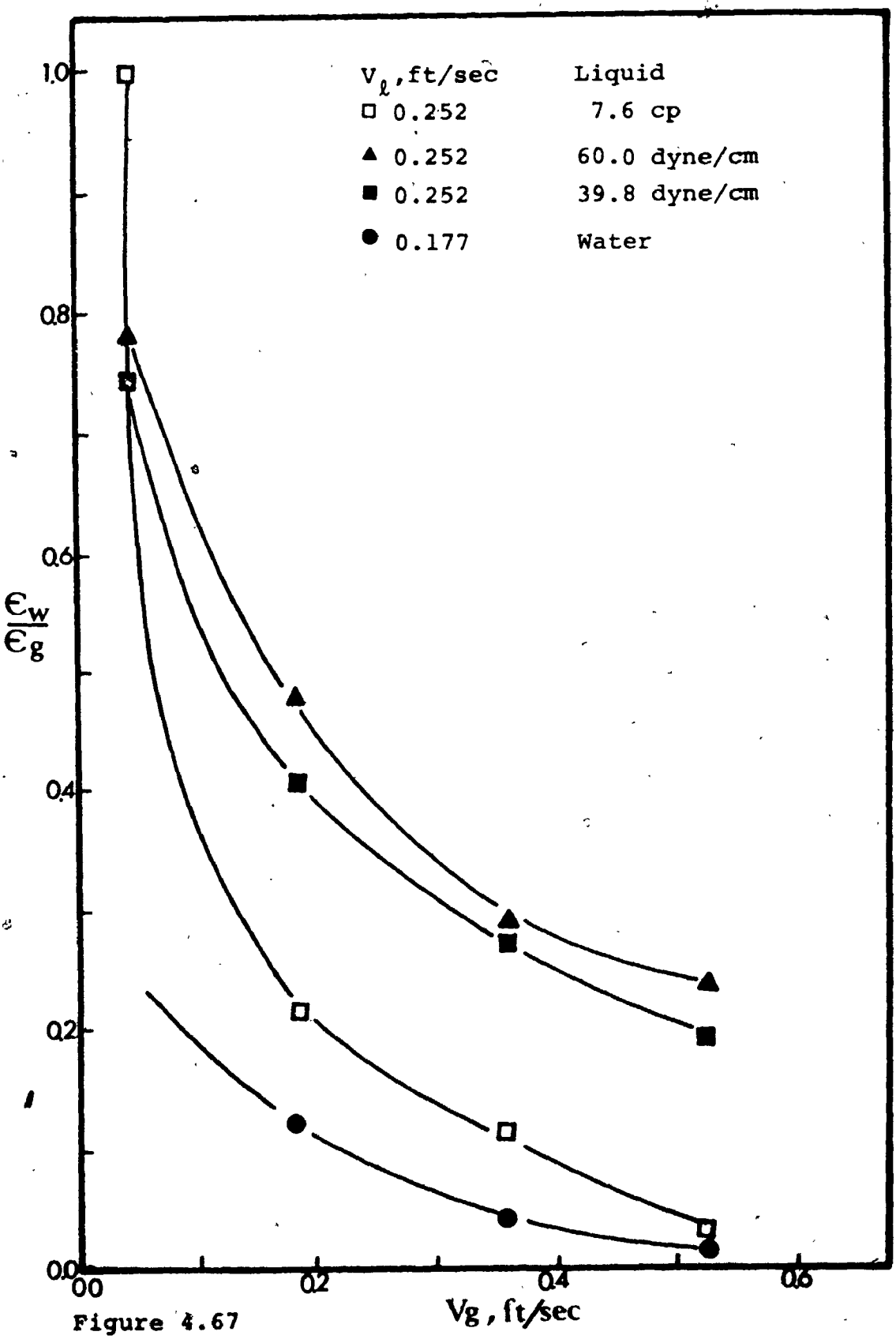

Figure 4.67

Effect of Gas Velocity on the Ratio of Wake to Gas Volume in Three Phase Beds of 6 mm Glass beads.

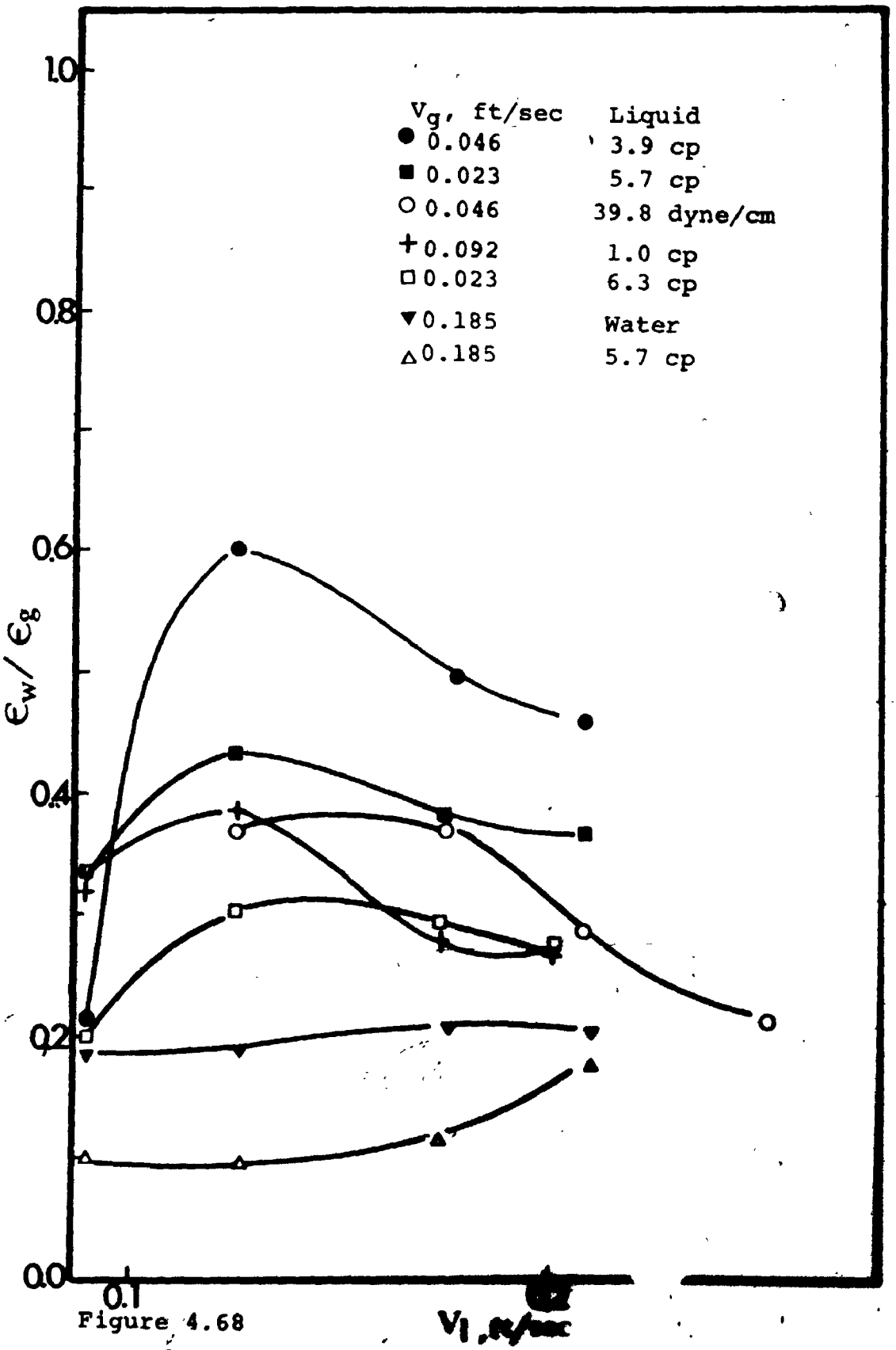

Figure 4.68

Effect of Liquid Velocity on the ratio of Water to Gas Volume in Three Phase Beds of 1 mm Glass Beads.

in the beds of gravel and 6 mm glass beads as shown in figures 4.69 and 4.70. However, in these cases, the maxima occured at liquid velocities of about 0.18 and 0.25 ft/sec respectively all the gas velocities.

Since bubble size increased with gas velocity, equation 4.23, in three phase fluidized beds, the ratio of the wake to gas volume decreased with bubble size in all the cases as shown in figure 4.71.

All the values of $\varepsilon_w/\varepsilon_g$ calculated from equation (4.26) can be found in Appendix G.

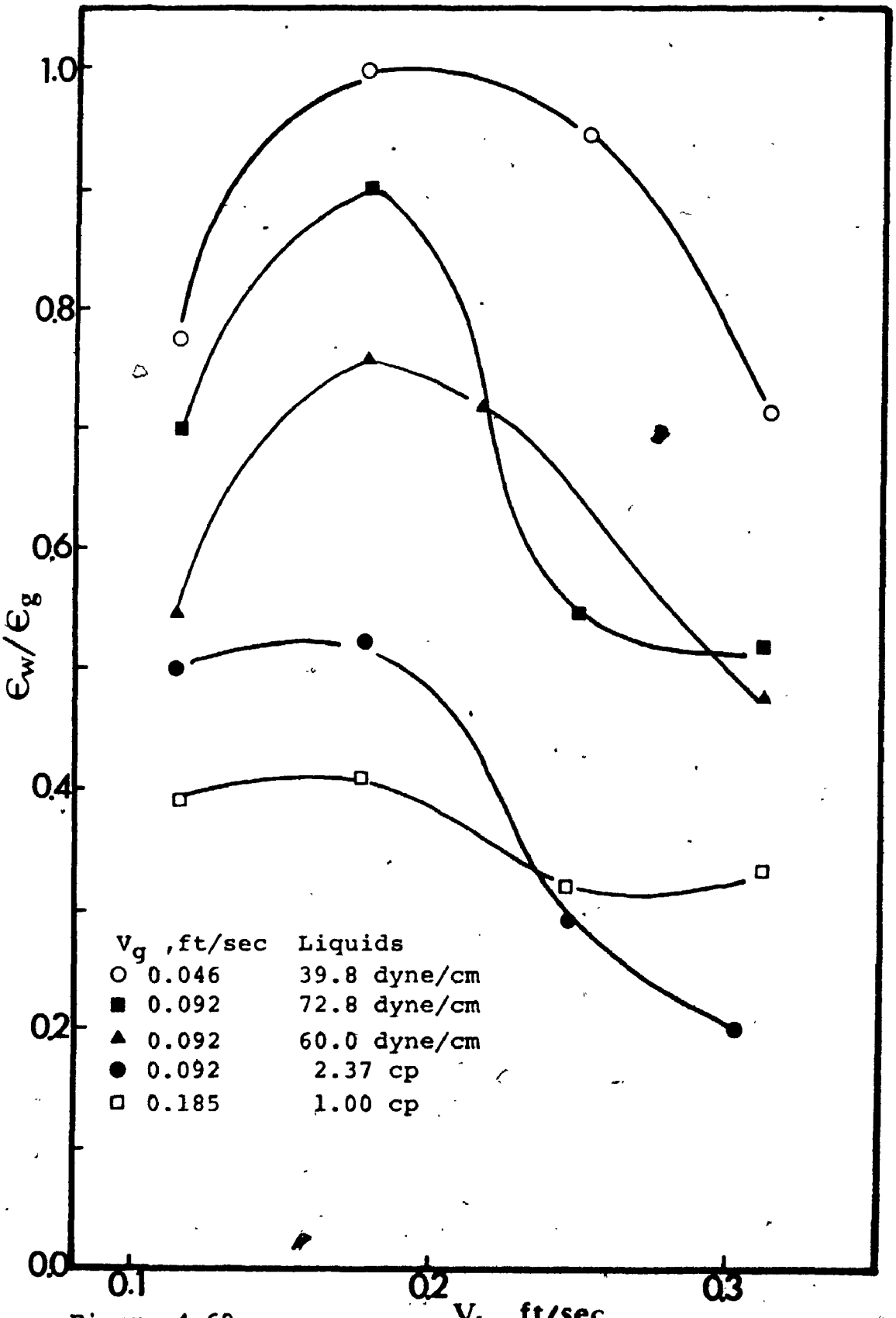

Figure 4.69
Effect of Liquid Velocity on the ratio of wake to gas Volume in Three Phase Beds of Gravel

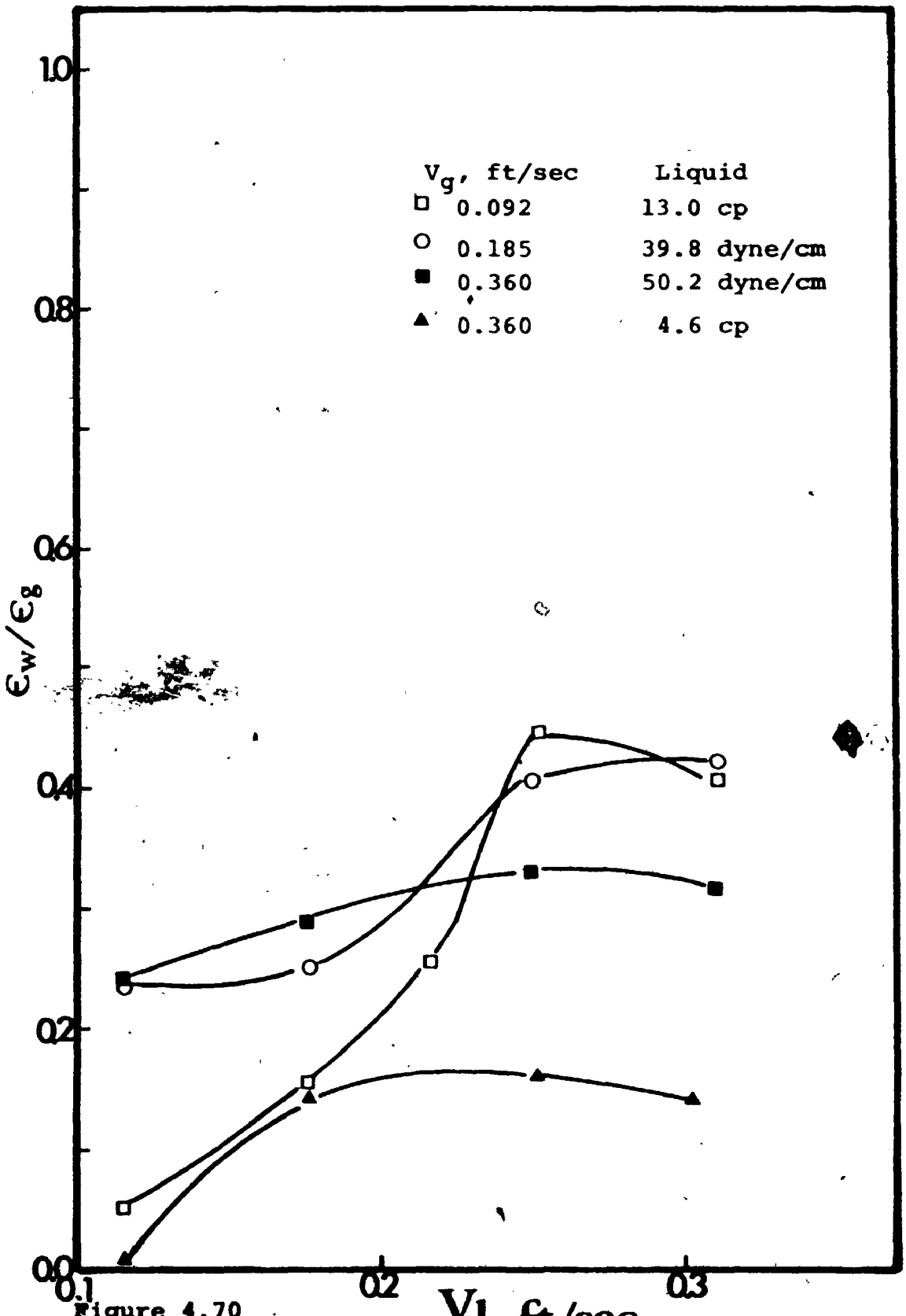

Figure 4.70

Effect of Liquid Velocity on the Ratio of Wake to Gas Volume in Three Phase Beds of 6 mm Glass Beads.

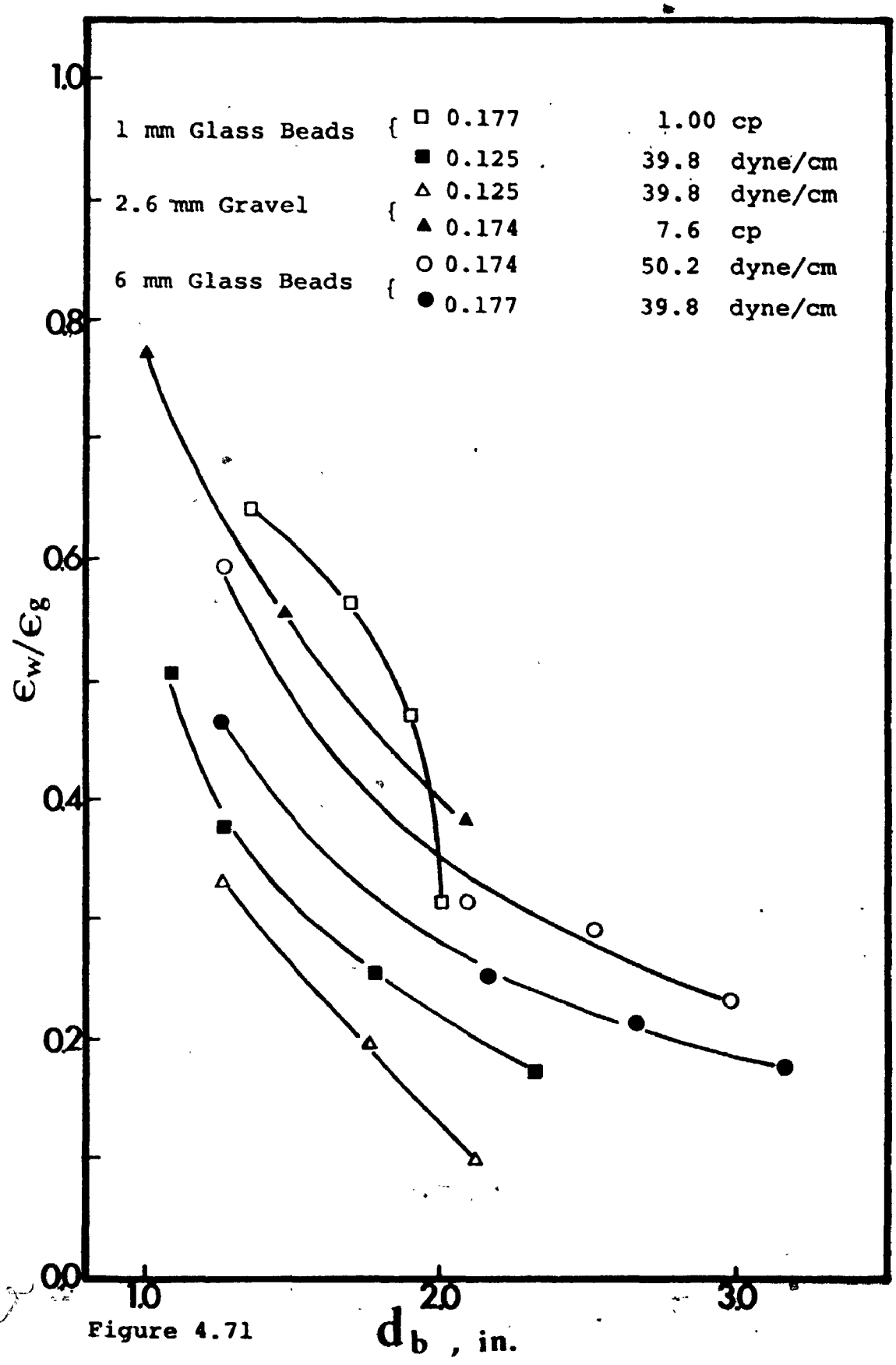

Figure 4.71

Effect of Bubble Size on the Ratio of Wake to Gas Volume in Three Phase Beds.

CHAPTER 5

DISCUSSION

Theoretical one dimensional models of two and three phase flow have been limited to the bubbly and slug flow regimes. In the former, the gas bubbles rise as independent entities with uniform size and no bubble coalescence occurs; in the latter there is complete coalescence and the bubbles occupy virtually the whole cross section of the column. Since the one dimensional flow models neglect effects such as inter-particle forces and buoyancy, they cannot adequately describe the behaviour of industrial chemical reactors.

In the present study, as in most cases of practical importance, the characteristics of the beds were intermediate between those of the bubble and slug flow regimes. In all cases, considerable, though not complete, coalescence occured. No model of this intermediate flow regime has been proposed due to the complexity of the hydrodynamics. Moreover, attempts to fit the present data to the existing model for bubble (6,70) and slug (25) flow proved quite unsatisfactory. Under these circumstances, the present correlations provide an extremely useful method of computing the individual phase hold-ups, the bed expansion, the degree of axial mixing of the liquid phase and the bubble characteristics in two and three phase fluidized beds.

In this work, bed characteristics have been studied at considerably higher gas velocities and over much wider ranges of liquid surface tension and viscosity than have been reported previously. Consequently, the correlations published here can be expected to be of more practical use for design purposes. As shown on page 128, considerable error can be introduced in the calculatated values of the individual hold-ups by employing Michelson and Østergaard's correlation ouside the range of gas velocities employed in that study. Moreover, the present correlations are unique in that they include the effect of particle size. Published correlations for predicting the bed porosity in three phase fluidized beds are somewhat complex in nature, normally require a trial and error solution (8,44) and do not indicates the bed contraction trend (15,16, 50). Moreover, the reasonable agreement between the present and published correlations indicate that the present data also apply to three dimensional beds.

In liquid-gas cocurrent flow, several different flow regimes are known to exist. These were characterized by Griffith and Wallis (25) who obtained a flow regime map by plotting $V_g/(V_\ell+V_g)$ against the Froude number $(V_\ell+V_g)^2/d_c g$. Such a map is shown in figure 5.1, in which the present liquid-gas data are plotted and may be seen to lie in both the bubble and slug flow regimes. In a circular bed, slugging occurs when the diameter of the bubbles approach that of the column. However, in a two dimensional bed, such as was employed in the present work, the bed may be said to be slugging when the

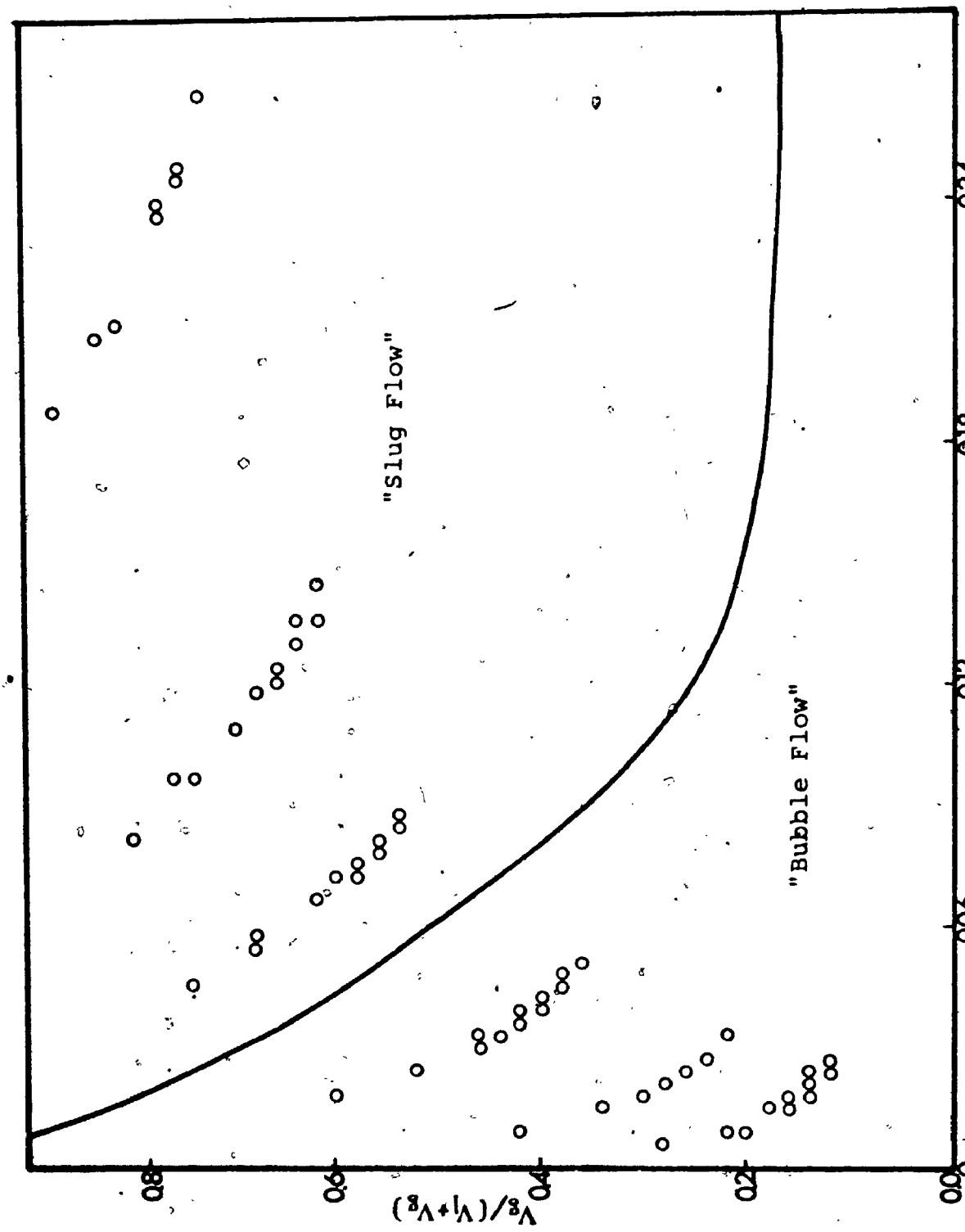

Figure 5.1 Flow Regime Map in Liquid-Gas Beds

bubble size approximates the hydraulic diameter of the bed.

A similar flow regime map for those three phase beds which initially contracted upon the injection of gas is presented in figure 5.2. In this case the linear dimension in the Froude number is particle diameter. The points above the solid line in this figure represent expanded beds and, conversely, those points below the solid line represents contracted beds. By analogy with liquid-gas beds, it may be concluded that contracted three phase beds lie in the bubble flow regime while the expanded beds lie in the slugging regime. This conclusion, it must be stressed, applied only for beds which contract on the addition of small amounts of gas and expand at higher gas rates.

From a comparison of the gas hold-ups in the liquid-gas and three phase beds, it can be observed that the presence of solid particles tends to increase the gas hold-up. This is in accordance with the observations reported by Massimilla et al. (33) on the rate of rise of air bubbles in three phase fluidized beds. These authors reported that the rising velocity of an air bubble is retarded by the presence of solid particles and hence that the gas hold-up increases. This was also found to be true in the present work on three phase fluidized beds as shown by equations 4.8 and 4.22. It may be seen from equation 4.22 that the bubble rising velocity depends mainly on its size regardless of particle size.

In a recent publication, Kim et al. (29) concluded

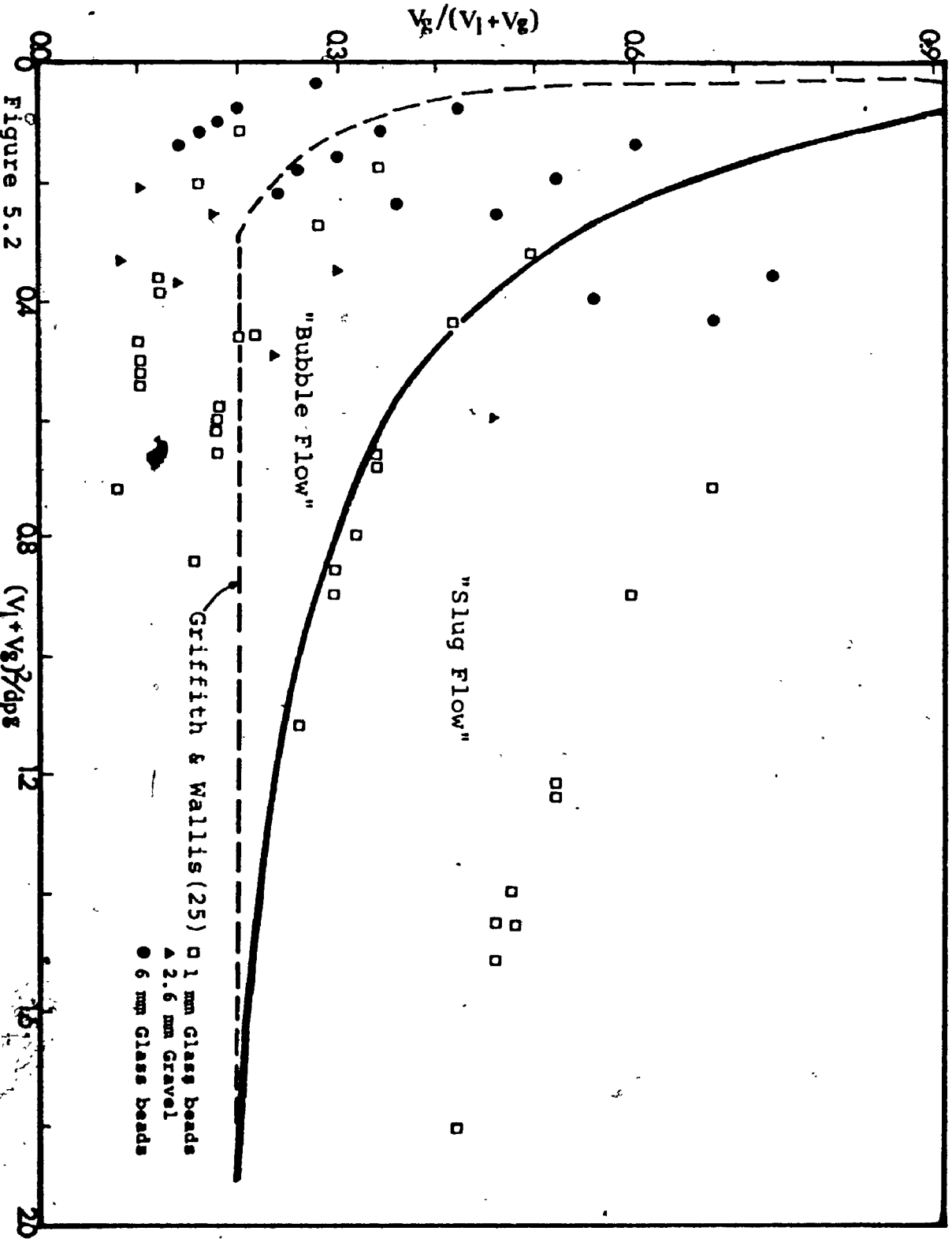

Figure 5.2 Flow Regime Map in Three Phase Fluidized Beds

from an examination of their results and those of other workers that there exist two distinct types of three phase fluidization These may be termed bubble coalescing and bubble disintegrating. The former occurs when the particles are smaller than some critical size and the latter when they are larger.

The addition of particles smaller than the critical size to a liquid-gas bed results in an increase in the mean bubble size as found in the beds of 1 mm glass beads. This bed is said to be of the bubble coalescing type. Bubble coalescence becomes more marked as the particle size is increased within a certain range and as the liquid velocity is reduced (33,42). The bubble size distribution is narrowed by increasing the liquid flowrate (48,53).

The major distinguishing feature of bubble coalescing beds is that the injection of small quantities of gas into a liquid fluidized bed results in a lowering of the bed height. This was first attributed by Stewart and Davidson (59) to predominately liquid wakes which are dragged through the bed behind the fast moving bubbles. This results in a reduction in the continuous liquid phase velocity and a consequent bed contraction. Rigby and Capes (52) also found that vortex shedding contributed significantly to the reduction in bed height even when the wake volume was small.

The major distinguishing feature of bubble-disintegrating beds is that the addition of solids larger than the critical size results in a reduction in bubble size and a corresponding

increase in gas hold-up (35,66).

In contrast to bubble coalescing beds, larger bubbles are favoured by small particle sizes and high liquid velocities.

The two types of bed do however display some common characteristics. In both cases, increasing the gas rates results in corresponding increases in bubble size, frequency and gas hold-up. The bubble size distribution widened with increasing gas velocity in both beds.

As mentioned above, particle size is an important criterion in determining which type of three phase fluidization is observed. This is supported by the results of other workers (8,9,15,29,36,37,43,57,66) who noted that the bed contraction on injecting gas diminished as the particle size was increased. From their data and the present findings, it would appear that the critical size for particles having a density similar to that of glass is about 2.5 mm for beds fluidized by air and comparatively low viscosity liquids. In the present studies, it was found that liquid viscosity also plays an important role in determining which type of fluidized bed behaviour is observed. It is evident from the experimental findings that the beds of gravel and 6 mm glass beads fluidized by air and low viscosity solutions exhibit bubble disintegrating behaviour. However, a trend towards bubble coalescing behaviour is observed by increasing the viscosity of the liquid fluidizing medium. This finding is supported by the work of Calderbank et al. (11) who observed that bubble coalescence was very much more pronounced in bubble beds containing liquids of higher viscosity.

On the basis of the present and published data, it can be concluded that the bed expansion characteristics are dependent on liquid viscosity, particle size and the ratio of liquid and gas flowrates. Since the minimum fluidization velocity of the particles fluidized by the liquid is also a function of liquid viscosity and particle size, it is likely that this parameter is of importance in determining the bed characteristics. From an analysis of the present and literature data (15,29,36,37,52,53,59,66), it was found that solids having a minimum fluidizing velocity in the liquid phase of less than around 0.042 ft/sec exhibited bed contraction upon injection of gas into the system. In contrast, beds of solids having a minimum fluidizing velocity exceeding 0.042 ft/sec, expanded upon introducing gas. This finding is also supported by the results of Dakshinamurty et al.(15) and Bhatia (9) which indicated that the particle density, which also influences the minimum fluidizing velocity, may also play an important role in determining the critical size of particles.

As found in this study and that of Rigby and Capes (53), the ratio of the wake to gas volume increased with decreasing gas velocity and particle size. The bed contraction resulting from the presence of wakes is dependent not only on the volume of the wakes but also on the velocity difference between the bubbles and the liquid. The latter can be expected to be small as a result of the small bubble size. However, in the bubble coalescing beds, the bubble size is comparatively larger than that in bubble disintegrating beds. Therefore, both the velocity difference between the bubbles and the liquid and

the wake volume are large.

In bubble coalescing beds, the ratio of the wake to gas volume was found to increase with decreasing gas velocity. Therefore, the wake volume is large at the lower gas rates and consequently results in a reduction in the bed height in the bubble flow regime. In contrast, at higher gas rates, the wake volume is comparatively small and consequently the bed height increases at higher gas rates in the slug flow regime.

In bubble disintegrating beds, the ratio of the wake to gas volume and the velocity difference between the bubble and the liquid are small due to the small bubble size and large particle size. It may therefore be concluded that the presence of wakes does not result in bed contraction.

In addition, the initial expanded bed height of the liquid fluidized bed was found to govern the degree of contraction in three phase fluidized beds. Since the bubble size was found to increase with expanded bed height (33,52), the contraction in the beds of greater initial height can be attributed to the large velocity difference between the bubbles and liquid.

Assuming that the number of bubbles per unit volume of bed is constant, that they are uniformly spaced, and have equal volumes and rising velocities, the following relationship can be derived from a material balance for liquid-gas and three phase fluidized beds.

$$\epsilon_g = V_g/V_b \qquad \ldots.(5.1)$$

where ϵ_g and V_g are the gas hold-up and gas superficial

velocity and V_b is the absolute bubble rising velocity which can be calculated from equations (4.7) and (4.1) for liquid-gas beds and from equations (4.22) and (4.14) for three phase fluidized beds.

Since the assumptions made in deriving equation (5.1) only apply in the ideal bubble flow regime, the agreement between the experimental values of ε_g and those calculated from equation (5.1) were in reasonable agreement only at lowest gas flowrate. However, the agreement became poorer with increasing gas velocity. The percentage deviations from the experimental values of ε_g and those calculated from equation (5.1) were 65 % for the liquid-gas beds, 68 % for the three phase beds of 6 mm glass beads, 34 % for the three phase beds of gravel and 46 % for the three phase beds of 1 mm glass beads. Since the maximum gas flowrate employed in the liquid-gas and the three phase beds of 6 mm glass beads was much higher (0.854 ft/sec) than that in the beds of gravel and 1 mm glass beads (0.185 ft/sec), it is not surprising that the deviations were greater in the liquid-gas and 6 mm glass beads beds. It can therefore be concluded that the equation (5.1) cannot be applied quantitatively outside the bubble flow regime.

As may be seen in equation (4.7) for the liquid-gas beds, increasing the liquid velocity resulted in a decrease in the bubble velocity and consequently an increased gas hold-up (figure 4.2). In the same manner, an increase in V_g also

resulted in an increased gas hold-up (figure 4.3) and an increase in viscosity a slight increase in ε_g (figure 4.5). In contrast, the gas hold-up decreased with increasing surface tension (figure 4.4).

As may be expected, liquid phase axial mixing in two and three phase beds, was governed mainly by the bubble size and rising velocity. Momentum transfer from the gas bubbles to the liquid phase presumably increases with bubble size and velocity and leads to more vigorous mixing in the liquid phase. Since the bubble size and rising velocity decreased with increasing liquid flowrate, it is logical that liquid phase axial mixing decreased with increasing liquid flowrate (figure 4.10). In contrast, the bubble size and rising velocity and consequently HMU increased with increasing gas flowrate (figure 4.10).

Since an increasing liquid velocity resulted in a greater bed expansion, the liquid hold-up in liquid-solid beds increased with increasing liquid flowrate in all cases studied (figures 4.15-4.17). The expanded bed height increased with increasing liquid viscosity due to the higher drag force on the particles (figure 4.18). Since the momentum transfer from the liquid to the solid phases increased with increasing liquid flowrate, liquid phase mixing can also be expected to increase with increasing liquid velocity (figure 4.21).

In all the three phase fluidized beds, the liquid hold-up increased with the velocity of the liquid since the latter is the main fluidizing medium. The effect of liquid and gas

flowrate, surface tension and viscosity on the gas hold-up can be seen in equations (5.1) and (4.22). In general, the gas hold-up decreased with increasing liquid velocity, viscosity and surface tension at a given gas flowrate. However, ε_g increased with gas flowrate in all the three phase beds due to increases in the bubble size and frequency.
The effect of the experimental parameters on bubble size and rising velocity can be seen from equations (4.22) and (4.23) in three phase fluidized beds.

The initial contraction in beds of 1 mm glass beads has been observed frequently by previous workers. However, the contraction in the higher viscosity beds of gravel and 6 mm glass beads is surprising since there has been no report of this in the literature. The reason for this contraction is not well understood, but it may be associated with the bubble characteristics in these beds. Visual observation indicated that the bubble size was larger in these beds which consequently led to an increased bubble velocity. Therefore, the liquid moving in the form of wakes behind the gas bubbles also moves more rapidly than the liquid in the interstices between the particles as explained previously. However, the wake volume associated with such gas bubbles may be seen from equation (4.26) to be relatively small due to the large bubble size. The findings of Rigby and Capes (53) that vortex shedding also contributes significantly to the reduction in bed height even when there is minimal wake formation may thus be of importance for beds of larger particles fluidized by

air and higher viscosity liquids. Furthermore, the initial bed height of the liquid fluidized bed has been found to be a prime factor governing the degree of bed contraction. Since the initial expanded bed height in the beds of 6 mm glass beads fluidized by CMC (70 cp) solution at the higher liquid rates was over twice that of beds fluidized by water, this may also be an additional factor which the causes the contraction in these beds. However, much more work is needed to define the precise reason for this anomalous behaviour.

As may be seen in figures 4.68-4.70, the effect of liquid velocity on the ratio of the wake to gas volume depends mainly on the particle size. This ratio increased with liquid velocity at lower liquid flowrates, went through a maximum, and decreased with further increases in the liquid rate. The liquid velocity at which the maximum values of this ratio occured increased with increasing particle size. It may be implied that the bubble size decreased with increasing liquid velocity in the lower bed fluidity. Since the beds of larger particles required a higher liquid flowrate to maintain the same expanded bed height (fluidity), it may be anticipated that the liquid velocity corresponding to the maximum value of the wake to gas volume increased with increasing particle size.

CHAPTER 6

CONCLUSIONS AND RECOMMENDATIONS

6.1. Conclusions

The major findings of the present experimental studies on liquid and gas phase hold-ups; liquid phase axial mixing, bed expansion and bubble characteristics in two and three phase fluidized beds can be summarized as follows:

A) Liquid-Gas Beds

1) The liquid hold-up decreased with increasing liquid and gas velocity. The variation of liquid and gas hold-up with height in the bed was not significant. The effect of liquid viscosity and surface tension on the individual phase hold-ups was found to be insignificant. The liquid hold-up data were found to fit the following equation:

$$\varepsilon_{\ell_1} = 0.90 \left(We_m \right)^{-0.043}$$

where We_m is the modified Weber number.

2) The liquid phase HMU increased with increasing gas velocity and decreased with increasing liquid flowrate. The HMU data were correlated by the following equation:

$$HMU = 1.385\ V_\ell^{-0.543}\ V_g^{0.185}$$

where V_ℓ and V_g are the liquid and gas superficial velocities.

3) The bubble size and rising velocity increased with increasing gas velocity and decreased with increasing liquid velocity. The bubble size distribution narrowed with increasing liquid velocity; the reverse trend was observed with increasing gas velocity. The effect of liquid viscosity on bubble size and rising velocity was minimal. However, decreasing surface tension was found to increase the bubble size and rising velocity.

The relative bubble rising velocity data were found to fit the following equation:

$$V_{br} = 21.88 \; d_b^{0.968}$$

where d_b is the bubble diameter.

The bubble size data were found to fit the following equation:

$$d_b = 0.119 \; V_\ell^{-0.237} \; V_g^{0.276} \; \gamma^{0.008} \; \sigma^{-0.182}$$

where V_ℓ and V_g are the liquid and gas superficial velocities, γ and σ are the liquid viscosity and surface tension, respectively.

B) <u>Liquid-Solid Fluidized Beds</u>

1) The liquid hold-up increased with increasing liquid velocity, viscosity and with decreasing particle size and was independent of liquid surface tension. The liquid hold-up data were correlated by the following equation:

$$\varepsilon_{\ell 2} = 1.354 \; (Fr_\ell)^{0.206} \; (Re_\ell)^{-0.100}$$

where Fr_ℓ and Re_ℓ are the liquid phase Froude and Reynolds

numbers.

2) Liquid Phase axial mixing increased with increasing liquid velocity and decreasing particle size. The liquid phase axial mixing data were found to fit the equation:

$$\frac{HMU}{Ho} = 0.520 \left(Fr_\ell \right)^{0.580}$$

where Fr_ℓ and Ho are the Froude number and the initial bed height.

C) Liquid-Gas-Solid Fluidized Beds

1) The liquid phase hold-up increased with increasing liquid velocity, viscosity and surface tension and with decreasing particle size, whereas it decreased with increasing gas velocity. The liquid hold-up data were found to fit the following equation:

$$\varepsilon_{\ell_3} = 1.504 \, (Fr_\ell)^{0.234} \, (Fr_g)^{-0.086} \, (Re_\ell)^{-0.082} \, (We)^{0.092}$$

where Fr_ℓ, Fr_g are the liquid and gas phase Froude numbers and Re_ℓ, and We are the Reynolds and Weber numbers respectively.

2) The gas hold-up increased with gas velocity and decreased with liquid surface tension. However, in general, the gas hold-up was nearly independent of liquid velocity and viscosity.

3) The liquid phase axial mixing increased with increasing liquid and gas velocity and with decreasing particle size. The liquid phase axial mixing data were correlated by the

following equation:

$$\frac{HMU}{Ho} = 2.82 \quad V_\ell^{0.815} \quad V_g^{0.309}$$

where V_ℓ, V_g, Ho are the superficial velocities of the liquid and gas and the initial bed height, respectively.

4) The bed porosity increased with increasing liquid velocity, viscosity and decreased with increasing particle size. For solids having a minimum fluidizing velocity below around 0.042 ft/sec in the liquid, the bed contracted upon injection of small amounts of gas. However, the reverse trend was found for beds of solids having a minimum fluidizing velocity above 0.042 ft/sec. Based on this criterion, the bed porosity data for the beds which exhibited initial expansion were found to fit the following equation:

$$(\varepsilon_\ell + \varepsilon_g) = 1.40 \ (Fr_\ell)^{0.170} \ (We)^{0.078}$$

where Fr_ℓ and We are the Froude and Weber numbers.

For beds exhibiting an initial bed contraction, the bed porosity data were found to fit the following equation:

$$(\varepsilon_\ell + \varepsilon_g) = 1.30 \ (Fr_\ell)^{0.128} \ (We)^{0.073} \ e^{0.031(V_\ell/V_g)\varepsilon_{\ell 2}}$$

where Fr_ℓ, We, V_ℓ, V_g and ε_{ℓ_2} are the Froude and Weber numbers, the superficial velocities of the liquid and gas, and the liquid hold-up in the corresponding liquid-solid fluidized bed, respectively.

5) The bubble size and rising velocity increased with increasing gas velocity and decreasing surface tension. The bubble size increased somewhat with increasing liquid viscosity in the beds of 6 mm glass beads and gravel. However, it was nearly independent of viscosity in the beds of 1 mm glass beads. The bubble size and rising velocity were nearly independent of liquid velocity. The bubble rising velocity and bubble size data were found to fit the following equations:

$$V_{br} = 16.93 \; d_b^{0.989}$$

where d_b is the bubble diameter.

$$d_b = 0.319 \; V_\ell^{0.052} \; V_g^{0.248} \; \gamma^{0.008} \; \sigma^{0.034}$$

where V_ℓ and V_g are the liquid and gas superficial velocities, γ and σ are the liquid viscosity and surface tension, respectively.

The bubble size distribution widened somewhat with increasing liquid velocity in the beds of gravel and 6 mm glass beads. In contrast, the reverse trend was observed in the beds of 1 mm glass beads. Bubble size decreased with increasing particle size in three phase fluidized beds.

6) The wake volume increases with decreasing bubble size, gas velocity and particle size. The ratio of the wake to gas volume increased with liquid velocity at lower liquid flowrates, went through a maximum, and decreased with further increases in the liquid rate. The liquid velocity

at which the maximum values of this ratio occured increased with increasing particle size.

6.2. Recommendations

The bed contraction and expansion characteristics were found to be a function of the initial bed height of the liquid fluidized bed, the liquid viscosity, the particle diameter, and the ratio of the liquid and gas flowrates. A more detailed study is needed to determine the contribution of each of the above parameters.

Since the proposed equations for liquid hold-up, liquid phase axial mixing, bed height (bed porosity), and bubble characteristics were obtained in a two dimensional column, it may be necessary to undertake further work to validate the equations for use in three dimensional columns.

Further study, outside the scope of this work, on liquid and gas phase mixing is needed to cover the wide variation of liquid and gas properties used in industry.

Hydrodynamic studies using particles having a wide range of sizes would be of industrial interest.

More systematic studies are needed to establish a flow regime map for three phase fluidized beds.

APPENDIX A.

MINIMUM FLUIDIZING VELOCITY MEASUREMENTS

MINIMUM FLUIDIZING VELOCITY MEASUREMENTS

In order to determine the minimum fluidizing velocities of the different solids with each of the liquids, pressure drop measurements were made in both the fixed and fluidized bed regions. The liquid flowrates were measured with the venturi-meter which for this purpose was connected to a manometer containing carbon tetrachloride instead of mercury.

A weighed amount of solids was loaded onto the grid inside the column to give the required initial bed height. Liquid was introduced into the column at the desired superficial velocity. When steady-state was reached, the pressure profile up the entire height of the column was measured using the manometers containing the same liquid as in the column. The pressure profiles were determined at several different velocities with both increasing and decreasing flows to check whether there was any hysteresis. Values of the difference between pressure drop across the bed measured at a given liquid flowrate and that measured at zero liquid flow are given in Table 3.3.

The minimum fluidizing velocities were taken as the highest velocity at wh ich the slope of the fixed bed deviated from linearity. The plots of these are shown in figures A.1 - A.4.

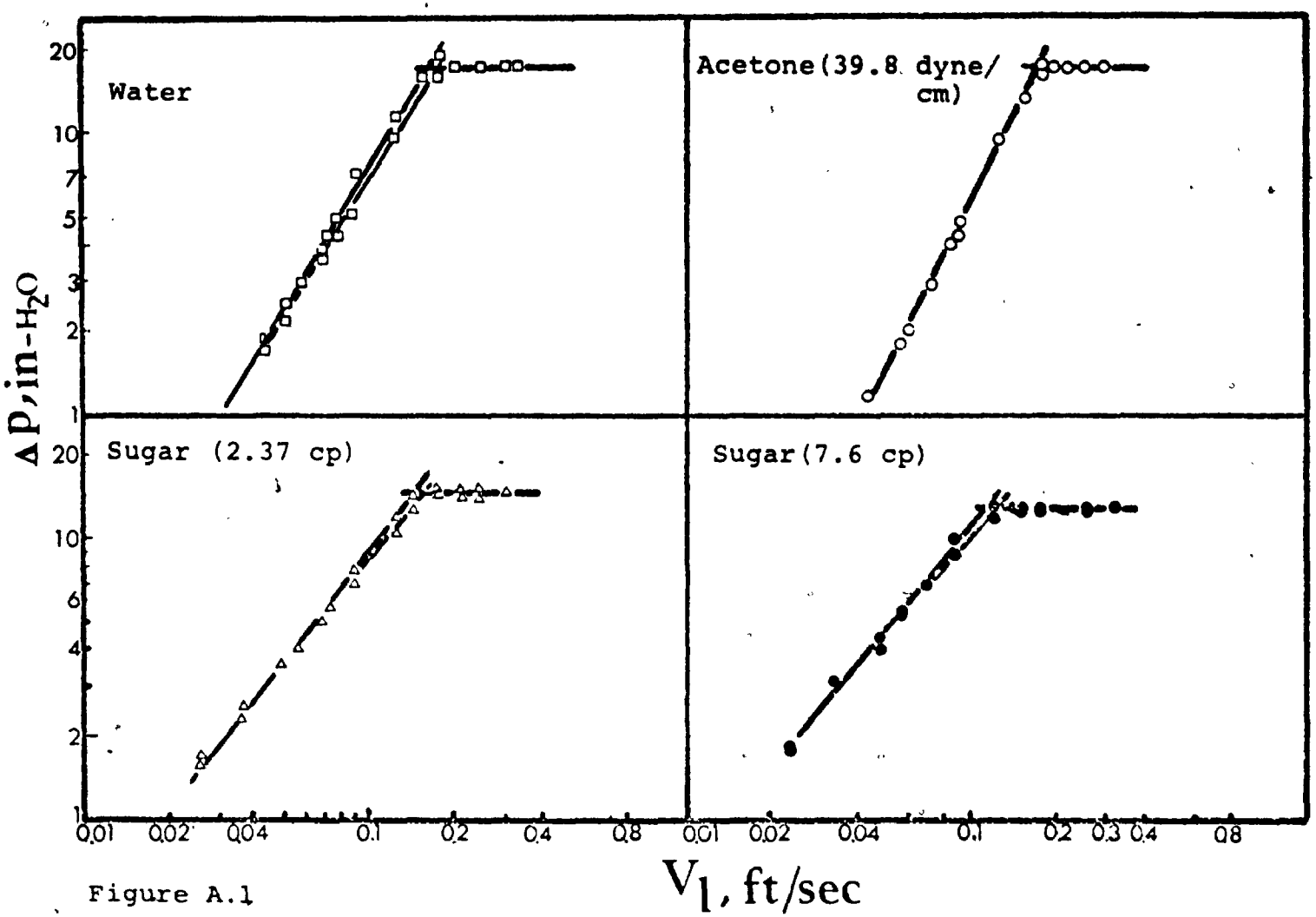

Figure A.1

Pressure Drop versus Liquid Velocity in the Beds of 6 mm Glass beads.

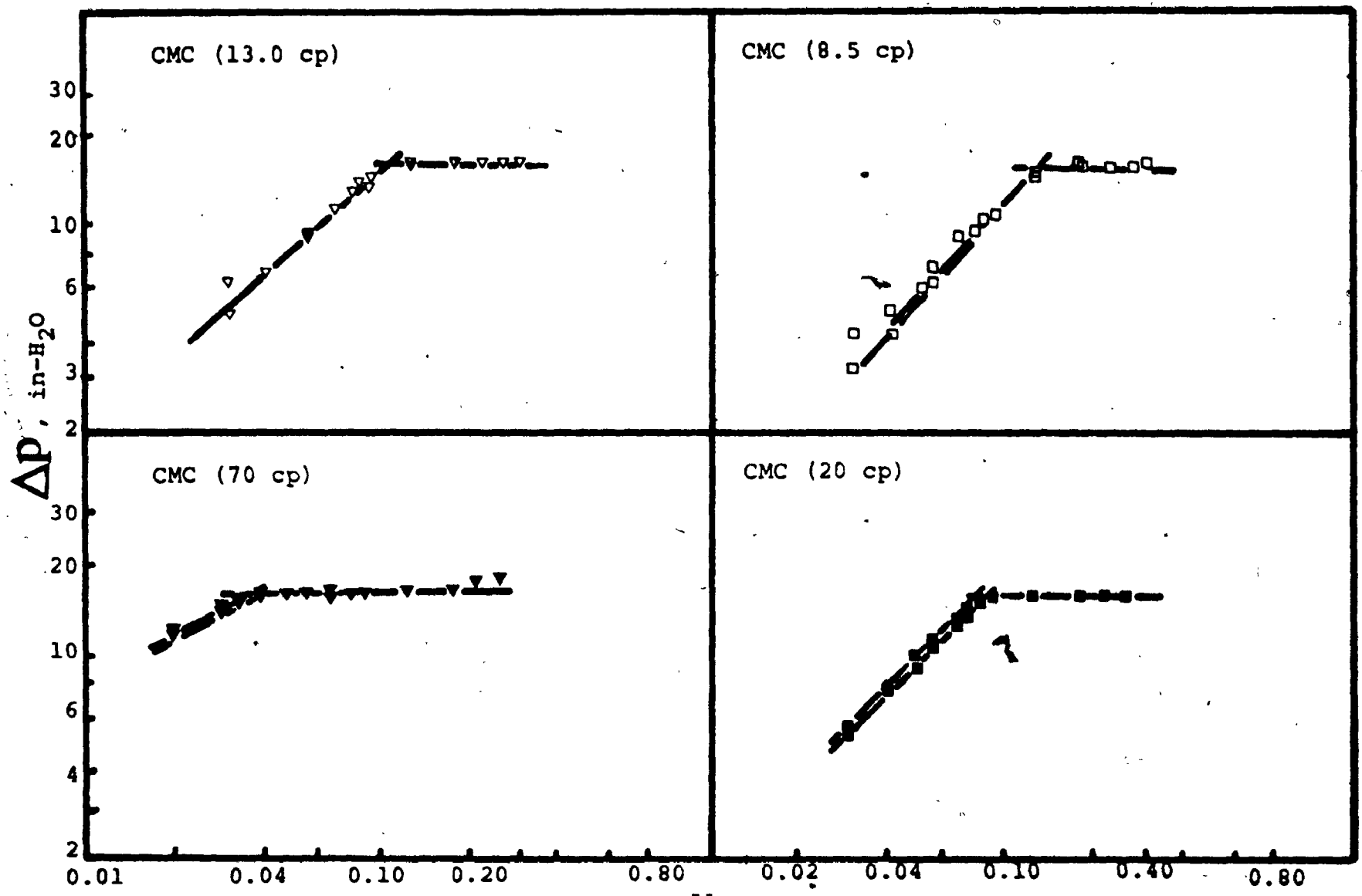

Figure A.2
Pressure Drop versus Liquid Velocity in the Beds of 6 mm Glass beads.

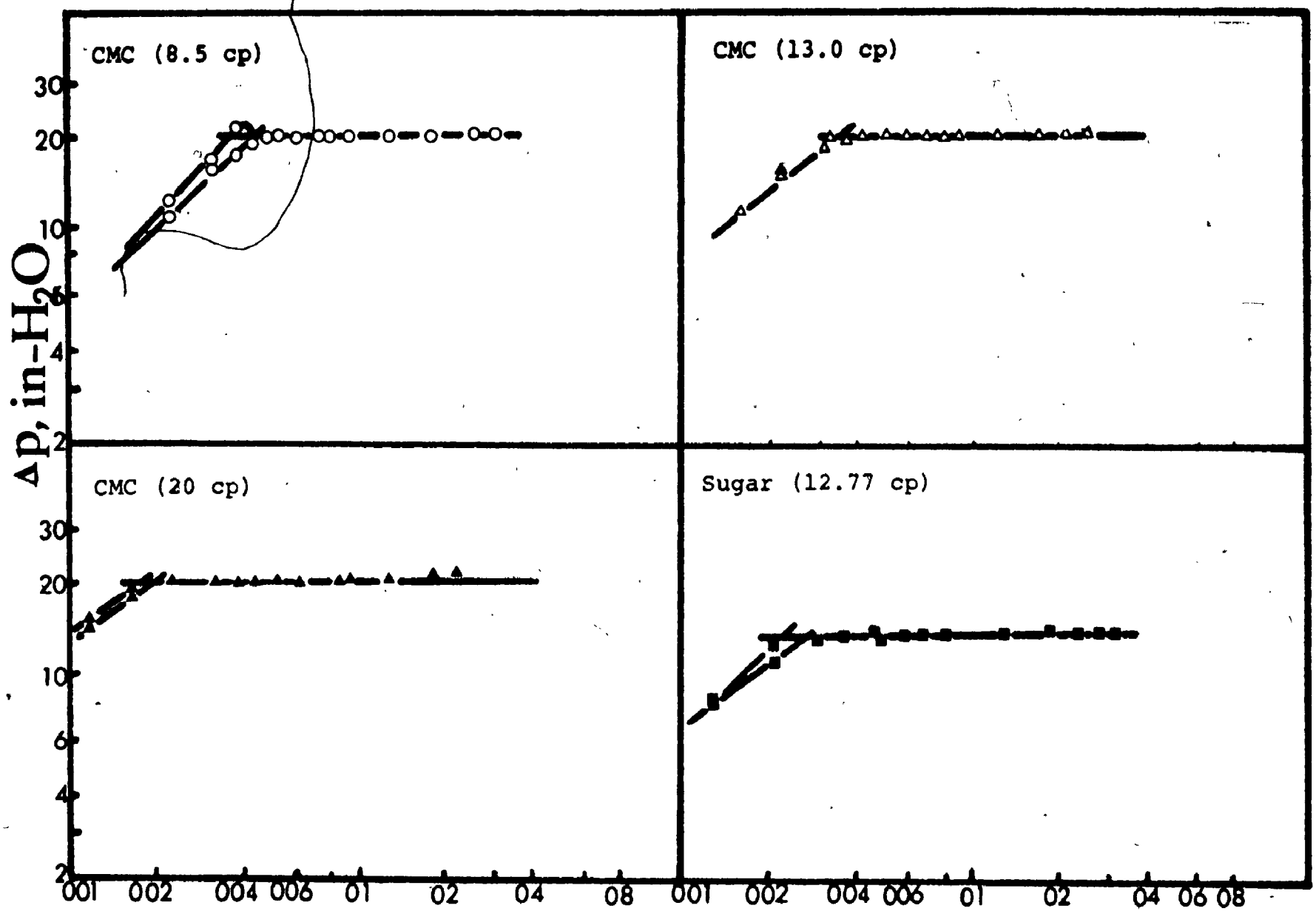

Figure A.3

Pressure Drop Versus Liquid Velocity in the Beds of Gravel.

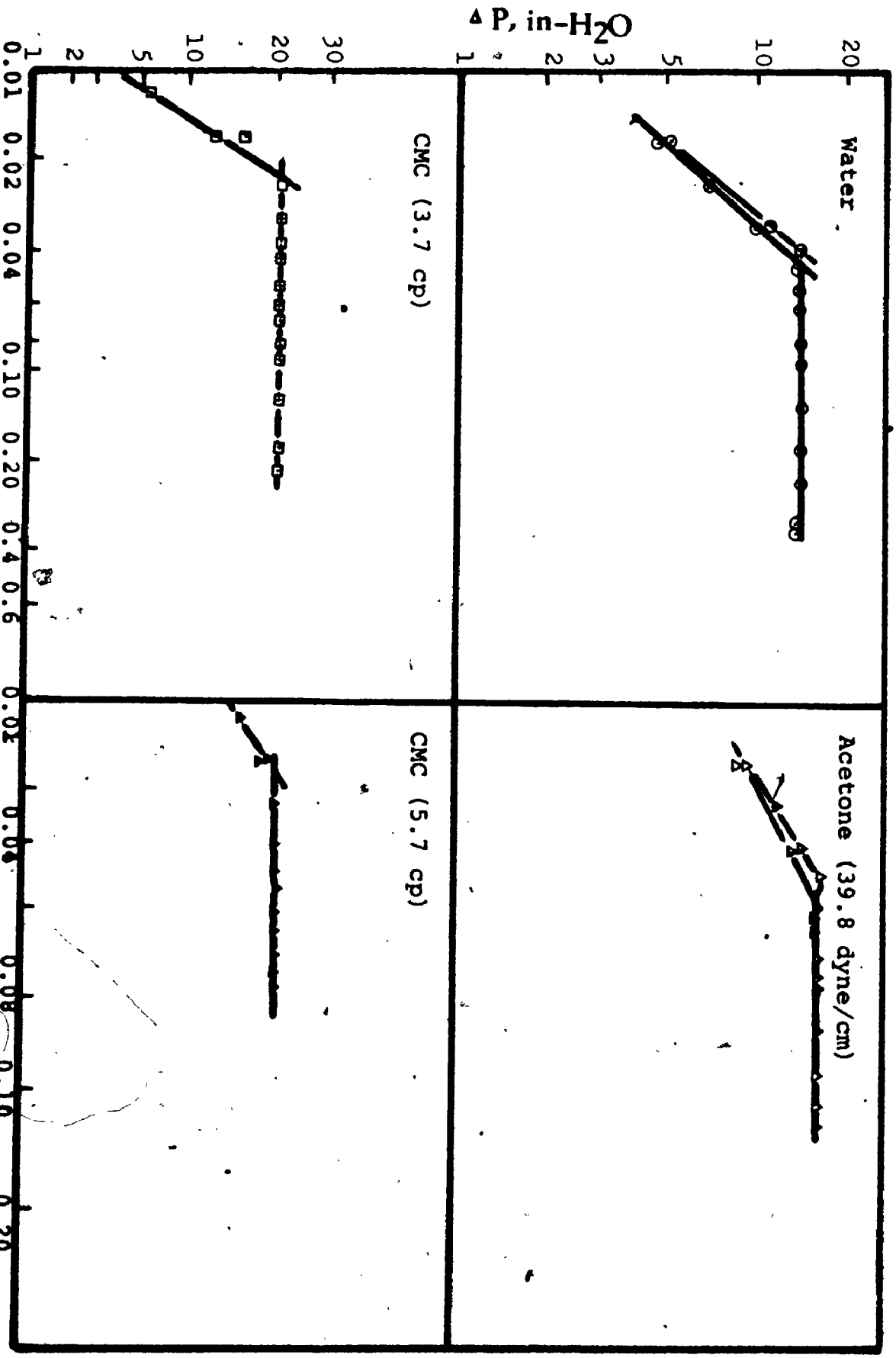

Figure A. 4
Pressure Drop Versus Liquid Velocity in the Beds of 1 mm Glass Beads.

APPENDIX B.1

CALIBRATION OF VENTURI METER

The venturi-meter was calibrated by recording the time taken to collect 40-100 lbs of each liquid. Special care was taken to keep the liquid temperature nearly constant when calibrating the flowmeter for the viscous solutions. The calibration curves for the various liquids are shown in figures B.1.1 - B.1.3.

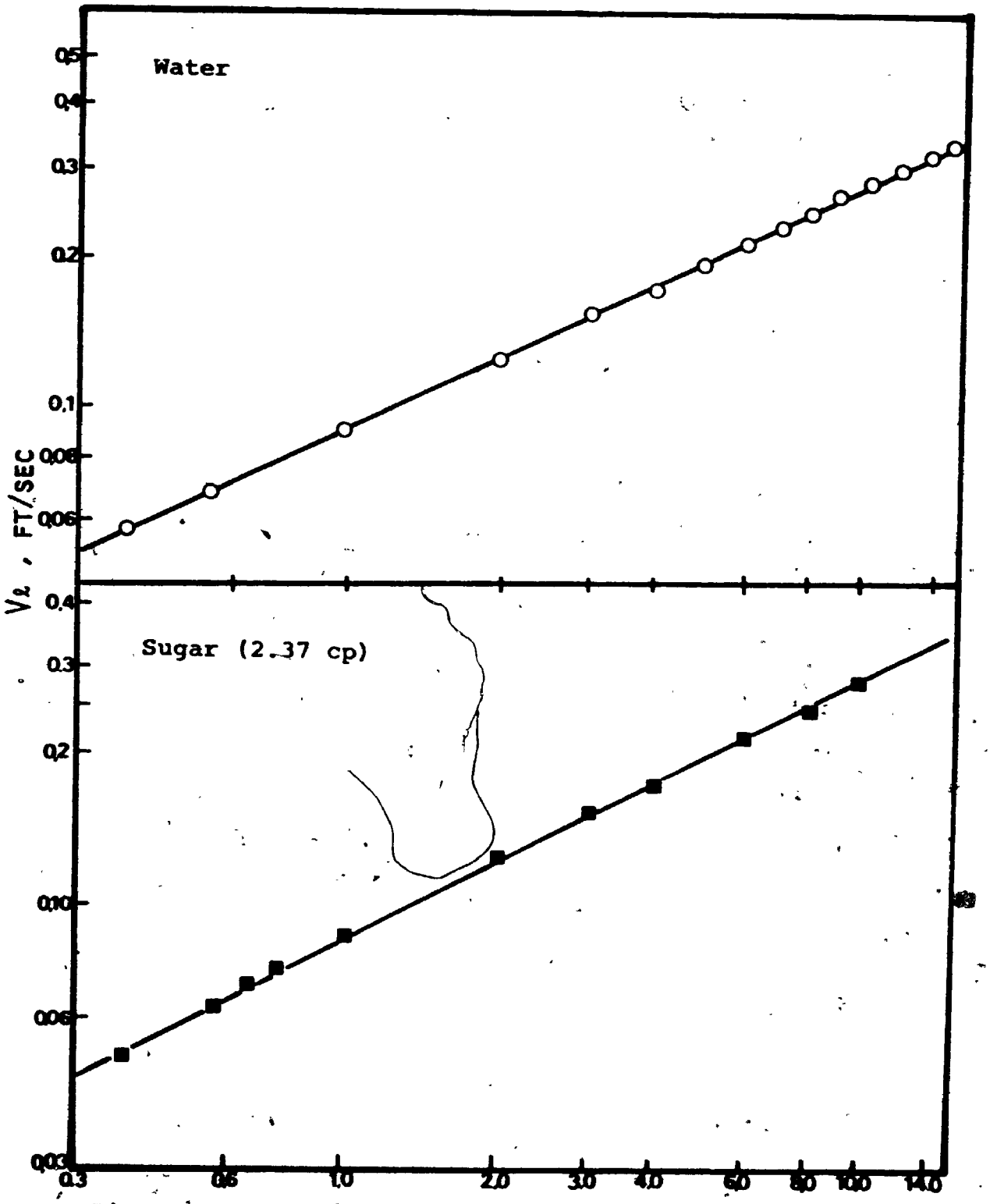

Figure B.1.1
Calibration Curves of Venturi-meter for water and Sugar(2.37 cp) solution.

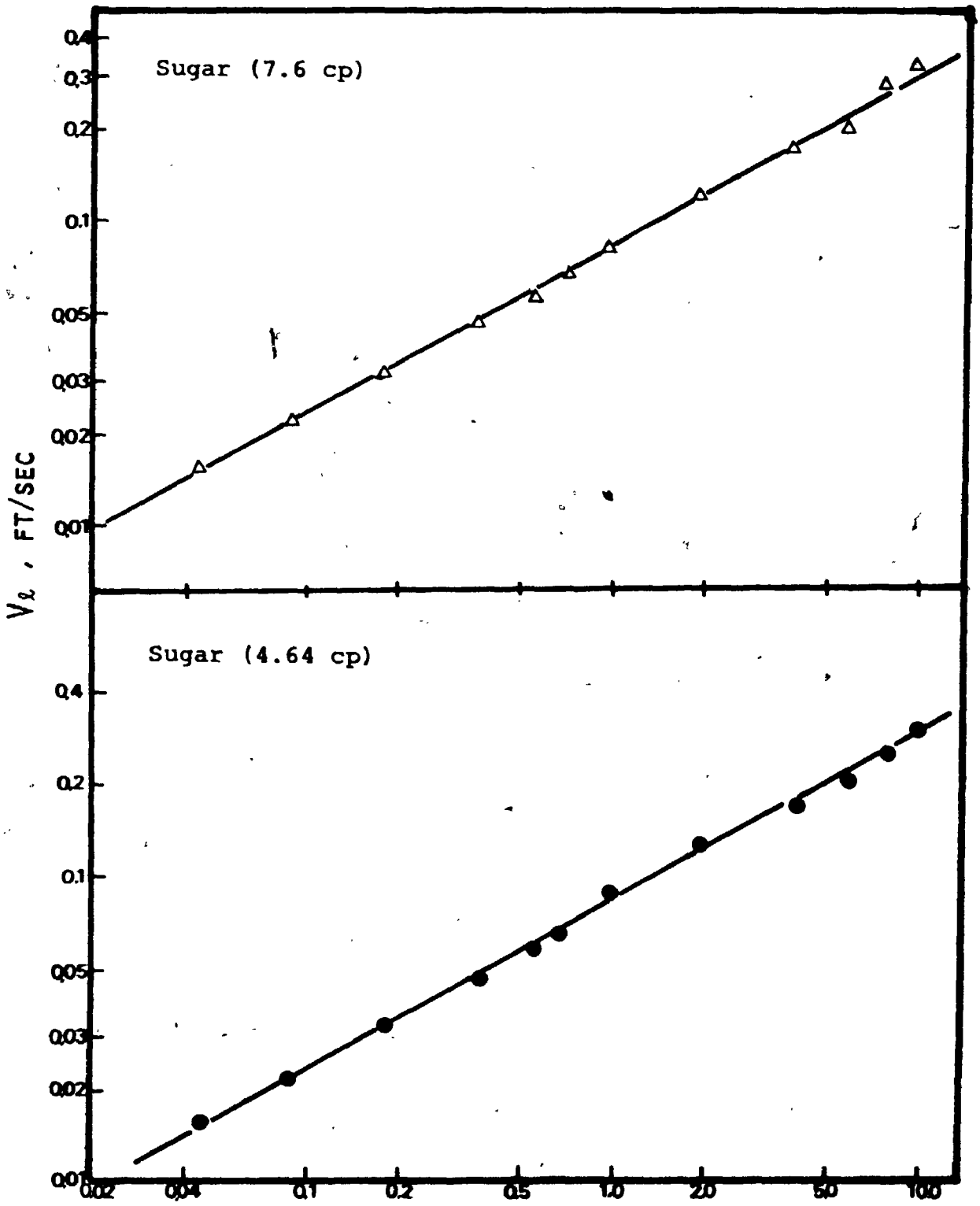

Figure B.1.2. Calibration Curves of Venturi-meter for Sugar Solutions.

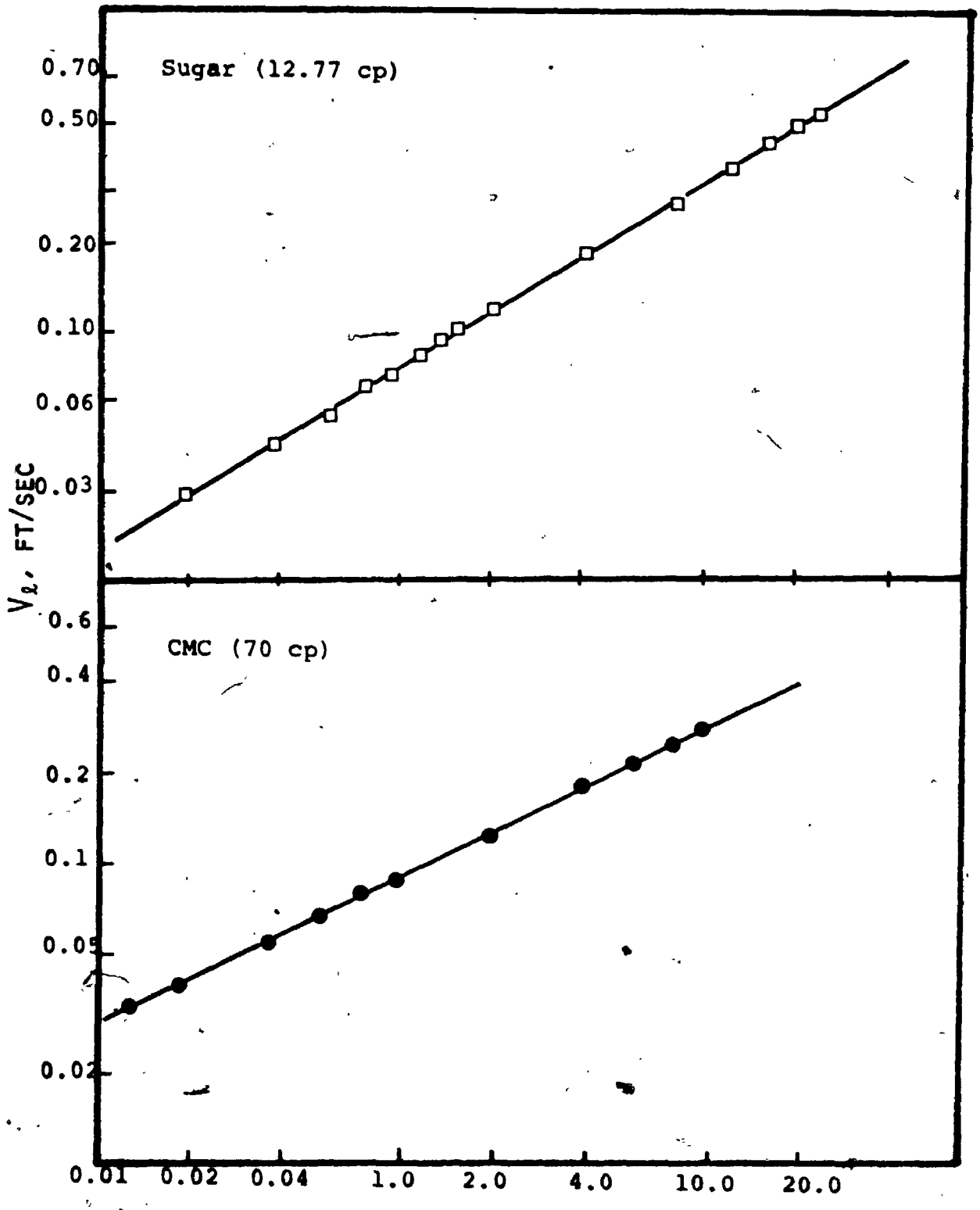

Figure B.1.3. Calibration Curves of Venturi-meter for Sugar and CMC Solutions.

APPENDIX B.2

CALIBRATION OF ROTAMETERS

Two rotameters (Brook's Sho-Rate) were used to measure the air flowrates. For calibrating these rotameters, the air line was pressurized by compressor air at 40 psi. Air was then metered with a wet-test gas meter for a period of 2-5 minutes. The calibration curves so obtained are shown in figures B.2.1 and B.2.2.

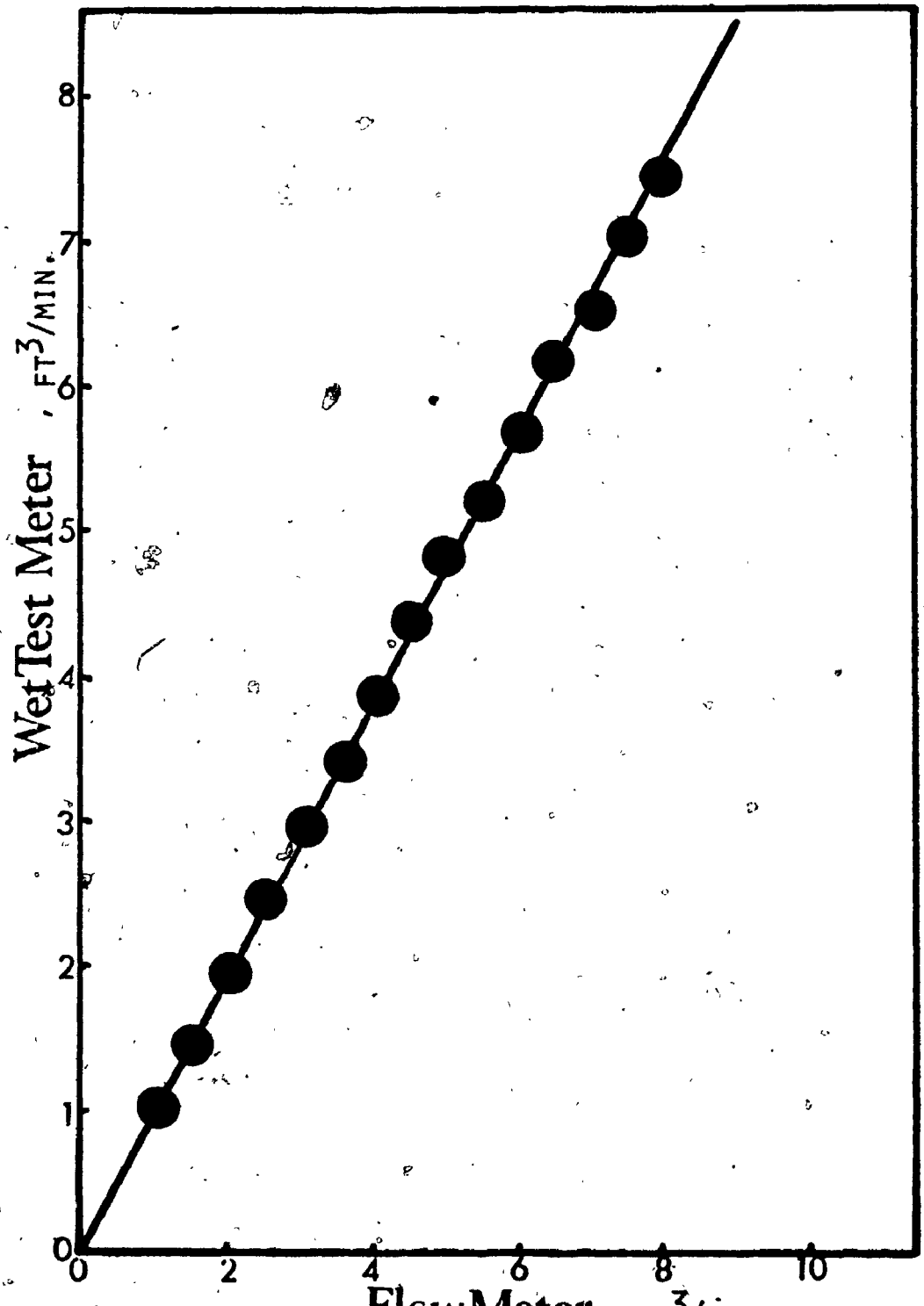

Figure B.2.1. Calibration Curve for Air Flow Meter.

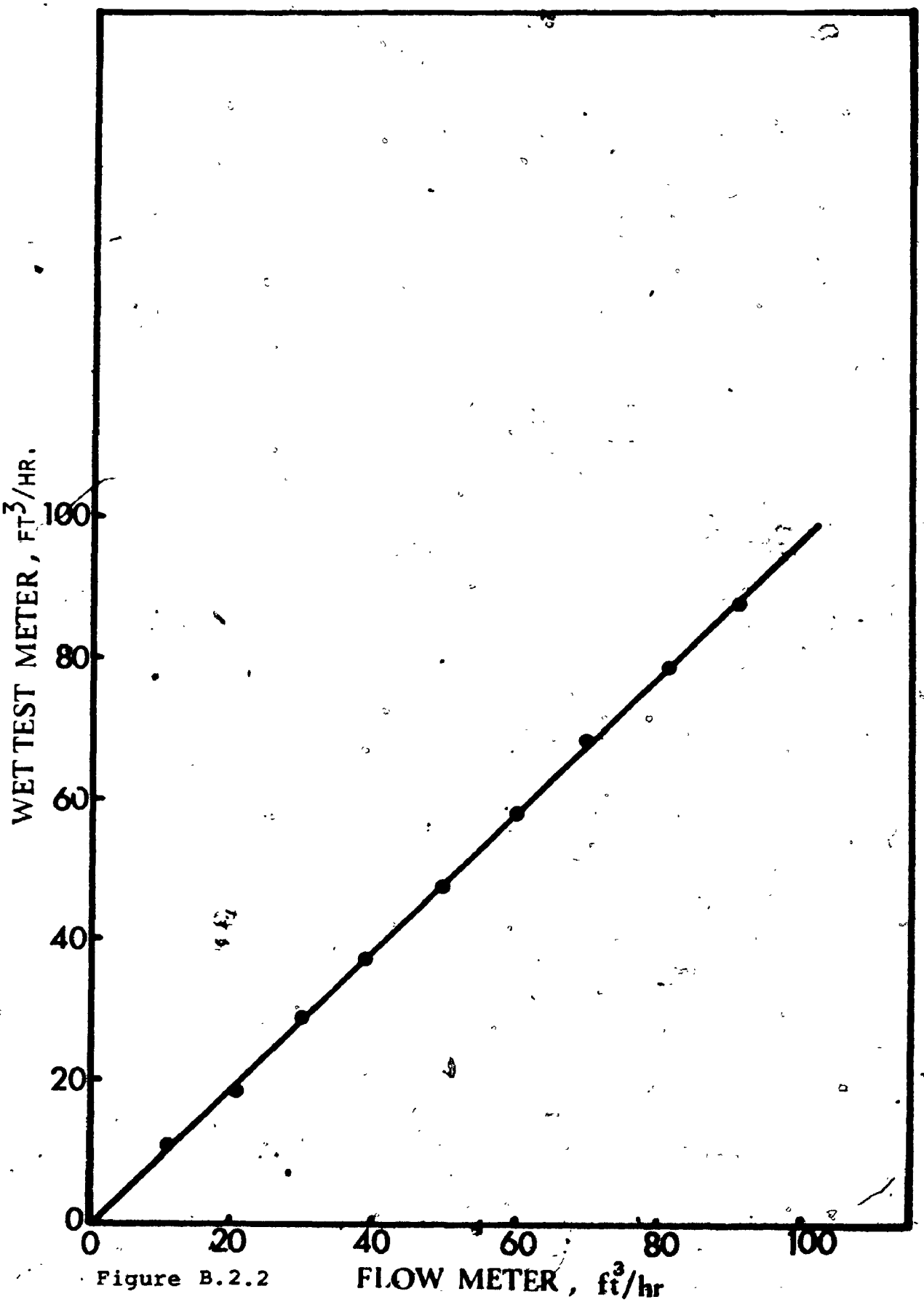

Figure B.2.2 Calibration Curve for Air Flow Meter

APPENDIX B.3

CALIBRATION OF SPECTROPHOTOMETER

The wavelength was adjusted to 525 millimicron, which corresponded to the absorption peak for potassium permanganate solution. The transmittance and absorbance were then measured using potassium permaganate solutions of known concentration at this wavelength. The relationship between transmittance and concentration are shown in figure B.3.1.

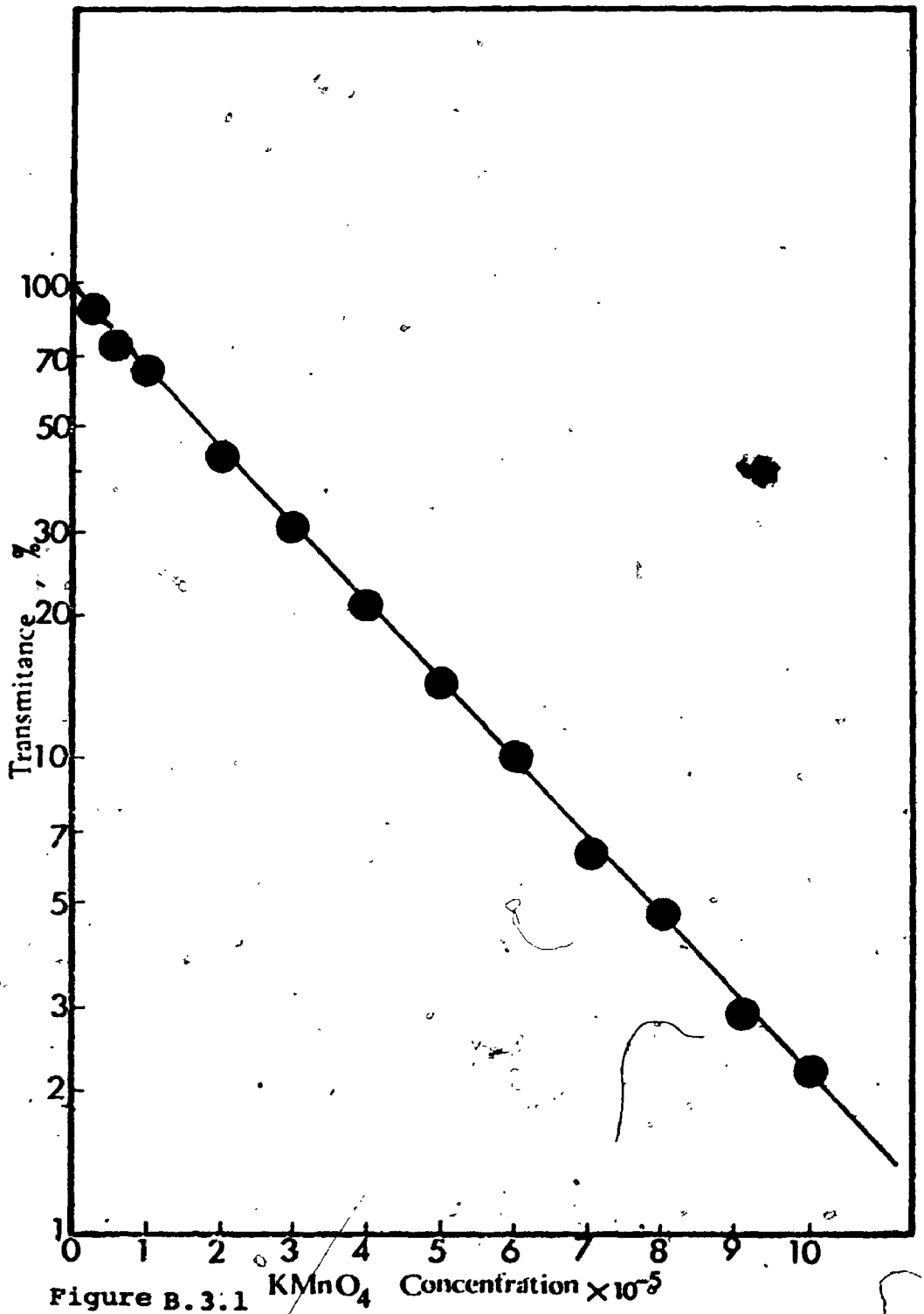

Figure B.3.1 Calibration curve for spectrophotometer at wave length 525 mμ.

APPENDIX C

BED PRESSURE DATA IN LIQUID-GAS BEDS

BED PRESSURE AT DIFFERENT LIQUID FLOWRATES IN LIQUID-GAS BEDS

LIQUID	LIQUID VELOCITY (ft/sec)	BED PRESSURE (in.)
Water	0.000	68.0
	0.252	68.0
	0.335	68.0
Acetone	0.000	68.0
(39.8 dyne/cm)	0.252	67.9
	0.312	67.8
Acetone (50.2 dyne/ cm)	0.000	68.0
	0.252	68.0
	0.312	68.0
Sugar	0.000	68.0
(2.37 cp)	0.252	67.7
	0.312	67.4
CMC	0.000	68.0
(13 cp)	0.252	67.9
	0.312	67.7
CMC	0.000	68.0
(70 cp)	0.252	67.8
	0.290	67.8

APPENDIX D

STATISTICAL ANALYSIS FOR EXPERIMENTAL RESULTS

D.1 MULTIPLE REGRESSION ANALYSIS OF DATA

An analysis of the data for liquid phase hold-up, bed porosity, liquid phase axial mixing and bubble characteristics in two and three phase fluidized beds was carried out in which the following functional form was assumed:

$$f(V_\ell, V_g, \sigma, \gamma; k, x, y, z, w) = k\, V_\ell^{x}\, V_g^{y}\, \sigma^{z}\, \gamma^{w} \qquad \ldots(D.1)$$

where k,x,y,z and w are unknown parameters.
This nonlinear form was decided upon inspection of the data plots.

Taking the natural logarithms of both sides of equation (D.1) gives:

$$\ln[f(V_\ell, V_g, \sigma, \gamma; k, x, y, z, w)] = \ln k + x \ln V_\ell + y \ln V_g + z \ln \sigma + w \ln \gamma \qquad \ldots(D.2)$$

Equation (D.2) can be solved for ln k, x,y,z and w by using a multiple linear least squares technique.
For this analysis, the IBM scientific subroutine REGRE was used in which the means and standard deviations of the experimental parameters, the regression coefficient, the multiple correlation coefficient, the F-value for the analysis of variance, the standard error of estimate, and the t-value were calculated. The detailed calculated values of above statistical parameters are shown in Tables D.1-D.20.

D.2 Computer Program Used

The following is a replica of the computer program used in the analysis:

```
C      MAIN PROGRAM FOR MULTIPLE REGRESSION-REGRE
C      THE FOLLOWING DIMENSIONS MUST BE GREATER THAN TO THE NUMBER OF VARIABLES
       DIMENSION XBAR(7),STD(7),D(7),RY(7),ISAVE(7),B(7),SB(7),T(7),W(7)
C      THE FOLLOWING DIMENSION MUST BE GREATER THAN TO THE PRODUCT OF M*M
       DIMENSION RX(50)
C      THE FOLLOWING DIMENSION MUST BE GREATER THAN (M+1)*M/2.
       DIMENSION R(30)
C      THE FOLLOWING DIMENSION MUST BE GREATER THAN 10.
       DIMENSION ANS(10)
       COMMON MX,MY
       READ(MY,15) MX,MY
     1 FORMAT(A4,A2,I5,2I2)
     2 FORMAT(////25H MULTIPLE REGRESSION.....A4,A2//6X,14HSELECTION.....
      1I2//)
     3 FORMAT(//9H VARIABLE,5X,4HMEAN,6X,8HSTANDARD,6X,11HCORRELATION,4X,
      110HREGRESSION,4X,10HSTD. ERROR,5X,8HCOMPUTED/6H   NO.,18X,9HDEVIAT
      2ION,7X,6HX VS Y,7X,11HCOEFFICIENT,3X,12HOF REG.COEF.,3X,7HT VALUE)
     4 FORMAT(/,I4,6F14.5)
     5 FORMAT(//,10H DEPENDENT)
     6 FORMAT(///10H INTERCEPT,13X,F13.5//23H MULTIPLE CORRELATION  ,F13.
      15//23H STD. ERROR OF ESTIMATE,F13.5/)
     7 FORMAT(//,21X,39HANALYSIS OF VARIANCE FOR THE REGRESSION//5X,19HSO
      1URCE OF VARIATION,7X,7HDEGREES,7X,6HSUM OF,10X,4HMEAN,13X,7HF VALU
      2E/30X,10HOF FREEDOM,4X,7HSQUARES,9X,7HSQUARES)
     8 FORMAT(/,30H ATTRIBUTABLE TO REGRESSION   ,I6,3F16.5/30H DEVIATION
      1 FROM REGRESSION    ,I6,2F16.5)
     9 FORMAT(/,5X,5HTOTAL,19X,I6,F16.5)
    10 FORMAT(16I2)
    11 FORMAT(/,15X,18HTABLE OF RESIDUALS//9H CASE NO.,5X,7HY VALUE,5X,10
      1HY ESTIMATE,6X,8HRESIDUAL)
    12 FORMAT(I6,F15.5,2F14.5)
    13 FORMAT(////53H NUMBER OF SELECTIONS NOT SPECIFIED.  JOB TERMINATED
      1.)
    14 FORMAT(//52H THE MATRIX IS SINGULAR.  THIS SELECTION IS SKIPPED.)
    15 FORMAT(2I2)
    16 FORMAT('1')
       WRITE(MX,16)
C      READ PROBLEM PARAMETER CARDS
   100 READ (MY,1) PR,PR1,N,M,NS
C      PR.......PROBLEM NUMBER (MAY BE ALPHAMERIC)
C      PR1......PROBLEM NUMBER (CONTINUED)
C      N........NUMBER OF OBSERVATIONS
C      M........NUMBER OF VARIABLES
C      NS.......NUMBER OF SELECTIONS
       IO=0
       X=0.0
       CALL CORRE (N,M,IO,X,XBAR,STD,RX,R,D,B,T)
C        TEST NUMBER OF SELECTIONS
       IF(NS) 108,108,109
   108 WRITE(MX,13)
       GO TO 300
   109 DO 200 I=1,NS
       WRITE(MX,2) PR,PR1,I
C      READ SUBSET SELECTION CARD
       READ(MY,10) NRESI,NDEP,K,(ISAVE(J),J=1,K)
C         NRESI.....OPTION CODE FOR TABLE OF RESIDUALS
C         0 IF IT IS NOT DESIRED
C         1 IF IT IS DESIRED
C        NDEP.....DEPENDENT VARIABLE
C         NUMBER OF INDEPENDENT VARIABLES INCLUDED
C         ISAVE.....A VECTOR CONTAINING THE INDEPENDENT VARIABLES INCLUDED
```

```
      CALL ORDER (M,R,NDEP ,K,ISAVE,RX,RY)
      CALL MINV (RX,K,DET,B,T)
C     TEST SINGULARITY OF THE MATRIX INVERTED
      IF(DET) 112,110,112
  110 WRITE(MX,14)
      GO TO 200
  112 CALL MULTR(N,K,XBAR,STD,D,RX,RY,ISAVE,B,SB,T,ANS)
C     PRINT NAMES, STANDARD DEVIATIONS, INTERCORRELATIONS BETWEEN
C     X AND Y, REGRESSION COEFFICIENTS, STANDARD DEVIATIONS OF
C     REGRESSION COEFFICIENTS, AND COMPUTED T VALUES
      MM=K+1
      WRITE(MX,3)
      DO 115 J=1,K
      L=ISAVE(J)
  115 WRITE(MX,4) L,XBAR(L),STD(L),RY(J),B(J),SB(J),T(J)
      WRITE(MX,5)
      L=ISAVE(MM)
      WRITE(MX,4) L,XBAR(L),STD(L)
C     PRINT INTERCEPT, MULTIPLE CORELATION COEFFICIENT, AND
C     STANDARD ERROR OF ESTIMATE
      AANS=EXP(ANS(1))
      WRITE(MX,6)   AANS,ANS(2),ANS(3)
C     PRINT ANALYSIS OF VARIANCE FOR THE REGRSSION
      WRITE(MX,7)
      L=ANS(8)
      WRITE(MX,8) K,ANS(4),ANS(6),ANS(10),L,ANS(7),ANS(9)
      L=N-1
      SUM=ANS(4)+ANS(7)
      WRITE(MX,9) L, SUM
      WRITE(MX,16)
      IF(NRESI) 200,200,120
C         PRINT TABLE OF RESIDUALS
  120 WRITE(MX,2) PR,PR1,I
      WRITE(MX,11)
      MM=ISAVE(K+1)
      DO 140 II=1,N
      CALL DATA(M,D)
      DO 333 I=1,M
      W(I)=EXP(D(I))
  333 CONTINUE
      SUM=EXP(ANS(1))
      DO 130 J=1,K
      L=ISAVE(J)
  130 SUM=SUM*EXP(D(L))**B(J)
      RESI=W(MM)-SUM
  140 WRITE(MX,12) II,W(MM),SUM,RESI
  200 CONTINUE
      GO TO 100
  300 STOP
      END
```

Note that CORRE, ORDER, MINV, AND MULTR are the IBM SSP subroutine.

MULTIPLE REGRESSION .....LIQUID HOLD UP IN LIQUID * GAS BEDS

VARIABLE	MEAN	STANDARD DEVIATION	CORRELATION X VS Y	REGRESSION COEFFICIENT	STD. ERROR OF REG. COEF.	COMPUTED T VALUES
V_ℓ	0.21117	0.06549	-0.06485	-0.02941	0.00687	-4.27951
V_g	0.30177	0.23992	-0.88023	-0.08475	0.00230	-36.71589
γ	0.00803	0.01098	0.33044	0.01547	0.00211	7.30139
σ	0.15224	0.02139	0.17484	0.06876	0.01537	4.47158
DEPENDENT						
ε_{ℓ_1}	0.86314	0.08055				
INTERCEPT		0.88854				

MULTIPLE CORRELATION 0.92936

STD. ERROR OF ESTIMATE 0.0296

ANALYSIS OF VARIANCE FOR THE REGRESSION

SOURCE OF VARIATION	DEGREES OF FREEDOM	SUM OF SQUARES	MEAN SQUARES	F VALUES
ATTRIBUTABLE TO REGRESSION	4	1.94471	0.48617	388.18188
DEVIATION FROM REGRESSION	245	0.30685	0.00125	
TOTAL	249	2.25157		

TABLE D.1

MULTIPLE REGRESSION ..... LIQUID HOLD UP IN LIQUID * GAS BEDS

VARIABLE	MEAN	STANDARD DEVIATION	CORRELATION X VS Y	REGRESSION COEFFICIENT	STD. ERROR OF REG. COEF.	COMPUTED T VALUES
We_m	10.100	0.1345	-0.89284	-0.04331	0.00138	-31.28254

DEPENDENT

$\epsilon_{\ell 1}$ 0.86314 0.08055

INTERCEPT -0.89916

MULTIPLE CORRELATION 0.89284

STD. ERROR OF ESTIMATE 0.0356

ANALYSIS OF VARIANCE FOR THE REGRESSION

SOURCE OF VARIATION	DEGREES OF FREEDOM	SUM OF SQUARES	MEAN SQUARES	F VALUES
ATTRIBUTABLE TO REGRESSION	1	1.79495	1.79495	978.59741
DEVIATION FROM REGRESSION	249	0.45671	0.00183	
TOTAL	250	2.25167		

TABLE D.2

MULTIPLE REGRESSION ..... LIQUID PHASE HMU IN LIQUID * GAS BEDS

VARIABLE	MEAN	STANDARD DEVIATION	CORRELATION X VS Y	REGRESSION COEFFICIENT	STD. ERROR OF REG. COEF.	COMPUTED T VALUES
V_l	0.24081	0.07877	-0.66823	-0.54298	0.04324	-12.55736
V_g	0.31733	0.27711	0.68434	0.18544	0.01442	12.85995

DEPENDENT

HMU 2.38908 0.72717

INTERCEPT 1.38531

MULTIPLE CORRELATION 0.95656

STD. ERROR OF ESTIMATE 0.03376

ANALYSIS OF VARIANCE FOR THE REGRESSION

SOURCE OF VARIATION	DEGREES OF FREEDOM	SUM OF SQUARES	MEAN SQUARES	F VALUES
ATTRIBUTABLE TO REGRESSION	2	2.57427	1.28713	161.50738
DEVIATION FROM REGRESSION	30	0.23908	0.00796	
TOTAL	32			

TABLE D.3

MULTIPLE REGRESSION ..... BUBBLE RISING VELOCITY IN LIQUID-GAS BEDS

VARIABLE	MEAN	STANDARD DEVIATION	CORRELATION X VS Y	REGRESSION COEFFICIENT	STD. ERROR OF REG. COEF.	COMPUTED T VALUES
v_ℓ	0.19075	0.06044	-0.17744	-0.23704	0.04994	-4.74649
v_g	0.26166	0.17996	0.80767	0.27506	0.01772	15.56820
μ	0.01034	0.01453	-0.03391	0.00854	0.01182	0.72253
σ	0.14657	0.02941	-0.13588	-0.18252	0.07608	-2.39912
DEPENDENT						
V_{br}	3.8048	1.2340				

INTERCEPT 0.11918

MULTIPLE CORRELATION 0.86149

STD. ERROR OF ESTIMATE 0:5132

ANALYSIS OF VARIANCE FOR THE REGRESSION

SOURCE OF VARIATION	DEGREES OF FREEDOM	SUM OF SQUARES	MEAN SQUARES	F VALUES
ATTRIBUTABLE TO REGRESSION	4	5.64644	1.41161	64.76528
DEVIATION FROM REGRESSION	90	1.96162	0.02179	
TOTAL	94	7.60806		

TABLE D.4

MULTIPLE REGRESSION ..... BUBBLE RISING VELOCITY IN LIQUID * GAS BEDS

VARIABLE	MEAN	STANDARD DEVIATION	CORRELATION X VS Y	REGRESSION COEFFICIENT	STD. ERROR OF REG. COEF.	COMPUTED T VALUES
d_b	0.1603	0.0482	0.83700	0.96263	0.06525	14.7510

DEPENDENT

V_{br}	3.8048	1.2340
INTERCEPT		21.88475

MULTIPLE CORRELATION 0.8370

STD. ERROR OF ESTIMATE 0.6813

ANALYSIS OF VARIANCE FOR THE REGRESSION

SOURCE OF VARIATION	DEGREES OF FREEDOM	SUM OF SQUARES	MEAN SQUARES	F VALUES
ATTRIBUTABLE TO REGRESSION	1	7.05010	7.05010	217.59384
DEVIATION FROM REGRESSION	93	3.01322	0.03240	
TOTAL	94	10.06332		

TABLE D.5

MULTIPLE REGRESSION ..... BUBBLE SIZE IN LIQUID-GAS BEDS

VARIABLE	MEAN	STANDARD DEVIATION	CORRELATION X VS Y	REGRESSION COEFFICIENT	STD. ERROR OF REG. COEF.	COMPUTED T VALUES
v_ℓ	0.19075	0.06044	-0.17744	-0.23704	0.04994	-4.74660
v_g	0.26166	0.17996	0.80767	0.27596	0.01772	15.56816
μ	0.01034	0.01453	-0.03392	0.00854	0.01182	0.72253
σ	0.14657	0.02941	-0.13588	-0.18253	0.07607	-2.39922
DEPENDENT						
d_b	0.16030	0.04822				

INTERCEPT 0.11918

MULTIPLE CORRELATION 0.86149

STD. ERROR OF ESTIMATE 0.0259

ANALYSIS OF VARIANCE FOR THE REGRESSION

SOURCE OF VARIATION	DEGREES OF FREEDOM	SUM OF SQUARES	MEAN SQUARES	F VALUES
ATTRIBUTABLE TO REGRESSION	4	5.64642	1.41160	64.76510
DEVIATION FROM REGRESSION	90	1.96162	0.02179	
TOTAL	94	7.60804		

TABLE D.6

MULTIPLE REGRESSION .... LIQUID HOLD UP IN LIQUID * SOLID BEDS

VARIABLE	MEAN	STANDARD DEVIATION	CORRELATION X VS Y	REGRESSION COEFFICIENT	STD. ERROR OF REG. COEF.	COMPUTED T VALUES
V_l	0.19643	0.06892	0.31249	0.38062	0.01189	31.98972
d_p	0.01114	0.00726	-0.60541	-0.28499	0.00612	-46.50689
γ	0.00463	0.00725	0.22731	0.11490	0.00403	28.44330
DEPENDENT						
ε_{l_2}	0.61307	0.13008				

INTERCEPT 0.58881

MULTIPLE CORRELATION 0.97343

STD. ERROR OF ESTIMATE 0.02804

ANALYSIS OF VARIANCE FOR THE REGRESSION

SOURCE OF VARIATION	DEGREES OF FREEDOM	SUM OF SQUARES	MEAN SQUARES	F VALUES
ATTRIBUTABLE TO REGRESSION	3	6.44318	2.14772	861.46264
DEVIATION FROM REGRESSION	143	0.35651	0.00249	
TOTAL	146	6.79970		

TABLE D.7

MULTIPLE REGRESSION ..... LIQUID HOLD UP IN LIQUID*SOLID FLUIDIZED BEDS

VARIABLE	MEAN	STANDARD DEVIATION	CORRELATION X VS Y	REGRESSION COEFFICIENT	STD. ERROR OF REG. COEF.	COMPUTED T VALUES
Fr_ℓ	0.17261	0.13974	0.78974	0.20255	0.00626	32.33750
Re_ℓ	89.57705	117.7229	-0.47891	-0.09595	0.00459	-20.90277
DEPENDENT						
ε_{ℓ_2}	0.61307	0.13008				

INTERCEPT 1.32100

MULTIPLE CORRELATION 0.95222

STD. ERROR OF ESTIMATE 0.0381

ANALYSIS OF VARIANCE FOR THE REGRESSION

SOURCE OF VARIATION	DEGREES OF FREEDOM	SUM OF SQUARES	MEAN SQUARES	F VALUES
ATTRIBUTABLE TO REGRESSION	2	6.16545	3.08272	699.90075
DEVIATION FROM REGRESSION	144	0.63425	0.00440	
TOTAL	146	6.79970		

TABLE D.8

MULTIPLE REGRESSION ..... LIQUID PHASE HMU IN LIQUID-SOLID FLUIDIZED BEDS

VARIABLE	MEAN	STANDARD DEVIATION	CORRELATION X VS Y	REGRESSION COEFFICIENT	STD. ERROR OF REG. COEF.	COMPUTED T VALUES
V_ℓ	0.22822	0.08096	0.54144	1.37232	0.27255	5.03506
d_p	0.01202	0.00707	-0.45708	-0.69434	0.15287	-4.54191
DEPENDENT HMU/Ho	0.19011	0.13159				

INTERCEPT	0.04908
MULTIPLE CORRELATION	0.81308
STD. ERROR OF ESTIMATE	0.0892

ANALYSIS OF VARIANCE FOR THE REGRESSION

SOURCE OF VARIATION	DEGREES OF FREEDOM	SUM OF SQUARES	MEAN SQUARES	F VALUES
ATTRIBUTABLE TO REGRESSION	2	8.69397	4.34698	18.53262
DEVIATION FROM REGRESSION	19	4.45661	0.23455	
TOTAL	21	13.15058		

TABLE D.9

MULTIPLE REGRESSION ..... LIQUID PHASE AXIAL MIXING(HMU) IN LIQUID-SOLID FLUIDIZED BEDS

VARIABLE	MEAN	STANDARD DEVIATION	CORRELATION X VS Y	REGRESSION COEFFICIENT	STD. ERROR OF REG. COEF.	COMPUTED T VALUES
Fr_ℓ	0.20546	0.15915	0.81294	0.68923	0.11040	6.24306

DEPENDENT

HMU/Ho	0.19011	0.13159

INTERCEPT	0.55512
MULTIPLE CORRELATION	0.81294
STD. ERROR OF ESTIMATE	0.08709

ANALYSIS OF VARIANCE FOR THE REGRESSION

SOURCE OF VARIATION	DEGREES OF FREEDOM	SUM OF SQUARES	MEAN SQUARES	F VALUES
ATTRIBUTABLE TO REGRESSION	1	8.69987	8.69987	38.97586
DEVIATION FROM REGRESSION	20	4.46424	0.22321	
TOTAL	21	13.16411		

TABLE D.10

MULTIPLE REGRESSION ..... LIQUID HOLD UP IN THREE PHASE FLUIDIZED BEDS

VARIABLE	MEAN	STANDARD DEVIATION	CORRELATION X VS Y	REGRESSION COEFFICIENT	STD. ERROR OF REG. COEF.	COMPUTED T VALUES
V_ℓ	0.10992	1.16592	0.27706	0.41183	0.01000	41.15078
V_g	0.14244	0.14511	-0.52406	-0.07841	0.00412	-19.00622
d_p *	0.01059	0.00737	0.46316	0.14682	0.00383	40.36898
γ	0.00477	0.00704	0.46316	0.14682	0.00383	38.30701
σ	0.14830	0.02477	0.37390	0.19870	0.02027	9.80154
DEPENDENT						
ε_{ℓ_3}	0.50785	0.12395				
INTERCEPT		1.03582				
MULTIPLE CORRELATION		0.95600				
STD. ERROR OF ESTIMATE		0.0351				

ANALYSIS OF VARIANCE FOR THE REGRESSION

SOURCE OF VARIATION	DEGREES OF FREEDOM	SUM OF SQUARES	MEAN SQUARES	F VALUES
ATTRIBUTABLE TO REGRESSION	5	32.23255	6.44651	1106.66845
DEVIATION FROM REGRESSION	521	3.03490	0.00582	
TOTAL	526	35.26746		

TABLE D.11

MULTIPLE REGRESSION ..... LIQUID HOLD UP IN THREE PHASE FLUIDIZED BEDS

VARIABLE	MEAN	STANDARD DEVIATION	CORRELATION X VS Y	REGRESSION COEFFICIENT	STD. ERROR OF REG. COEF.	COMPUTED T VALUES
Fr_ℓ	0.16653	0.13663	0.60408	0.23486	0.00532	44.10346
Fr_g	0.10562	0.15491	-0.39118	-0.08627	0.00301	-28.62768
Re_ℓ	83.19662	111.95306	-0.55165	-0.08190	0.00354	-23.09130
We	0.00422	0.00854	0.04243	0.09242	0.00414	22.30493
DEPENDENT						
ε_ℓ	0.51188	0.12275				
INTERCEPT		1.5044				

MULTIPLE CORRELATION 0.93630

STD. ERROR OF ESTIMATE 0.03911

ANALYSIS OF VARIANCE FOR THE REGRESSION

SOURCE OF VARIATION	DEGREES OF FREEDOM	SUM OF SQUARES	MEAN SQUARES	F VALUES
ATTRIBUTABLE TO REGRESSION	4	31.03749	7.75937	927.61657
DEVIATION FROM REGRESSION	522	4.36645	0.00836	
TOTAL	526	35.40394		

TABLE D.12

MULTIPLE REGRESSION ..... BED POROSITY IN BUBBLE DISINTEGRATING BEDS IN THREE PHASE BEDS

VARIABLE	MEAN	STANDARD DEVIATION	CORRELATION X VS Y	REGRESSION COEFFICIENT	STD. ERROR OF REG. COEF.	COMPUTED T VALUES
V_ℓ	0.20544	0.06929	0.60755	0.33005	0.00929	35.51506
V_g	0.18819	0.17144	0.07399	0.05907	0.00390	15.11799
d_p	0.01533	0.00565	-0.17816	-0.18169	0.00858	-21.15788
γ	0.00412	0.00350	0.46761	0.08826	0.00378	23.31769
σ	0.14788	0.02485	0.32169	0.05358	0.01941	2.75967
DEPENDENT						
$\varepsilon_\ell + \varepsilon_g$	0.57406	0.08816				
INTERCEPT		0.95392				

MULTIPLE CORRELATION 0.93327

STD. ERROR OF ESTIMATE 0.0325

ANALYSIS OF VARIANCE FOR THE REGRESSION

SOURCE OF VARIATION	DEGREES OF FREEDOM	SUM OF SQUARES	MEAN SQUARES	F VALUES
ATTRIBUTABLE TO REGRESSION	5	6.33659	1.26731	405.10870
DEVIATION FROM REGRESSION	300	0.93850	0.00312	
TOTAL	305	7.27509		

TABLE D.13

MULTIPLE REGRESSION ..... BUBBLE DISINTEGRATING BEDS IN THREE PHASE FLUIDIZED BEDS

VARIABLE	MEAN	STANDARD DEVIATION	CORRELATION X VS Y	REGRESSION COEFFICIENT	STD. ERROR OF REG. COEF.	COMPUTED T VALUES
Fr_ℓ	0.10817	0.08199	0.66333	0.17025	0.00535	31.77367
We	0.00447	0.00584	0.39416	0.07861	0.00330	23.80947
DEPENDENT						
$(\epsilon_\ell + \epsilon_g)$	0.57365	0.08787				

INTERCEPT	1.40187
MULTIPLE CORRELATION	0.89695
STD. ERROR OF ESTIMATE	0.04062

ANALYSIS OF VARIANCE FOR THE REGRESSION

SOURCE OF VARIATION	DEGREES OF FREEDOM	SUM OF SQUARES	MEAN SQUARES	F VALUES
ATTRIBUTABLE TO REGRESSION	2	5.85301	2.92650	625.59387
DEVIATION FROM REGRESSION	304	1.42210	0.00467	
TOTAL	306	7.27511		

TABLE D.14

MULTIPLE REGRESSION ..... BUBBLE COALESCENCING BEDS IN THREE PHASE FLUIDIZED BEDS

VARIABLE	MEAN	STANDARD DEVIATION	CORRELATION X VS Y	REGRESSION COEFFICIENT	STD. ERROR OF REG. COEF.	COMPUTED T VALUES
V_ℓ	0.10530	0.72479	0.68507	0.34787	0.00713	48.76810
V_g	0.08601	0.06692	-0.02372	0.00345	0.00282	1.22220
d_p	0.00463	0.00451	0.007369	-0.27010	0.00783	-34.45423
γ	0.00566	0.01005	0.32061	0.13180	0.00363	36.27822
σ	0.14980	0.02464	0.04486	-0.03843	0.01394	-2.75597
DEPENDENT						
$(\varepsilon_\ell + \varepsilon_g)$	0.69258	0.10530				

INTERCEPT 0.61207

MULTIPLE CORRELATION 0.96730

STD. ERROR OF ESTIMATE 0.0213

ANALYSIS OF VARIANCE FOR THE REGRESSION

SOURCE OF VARIATION	DEGREES OF FREEDOM	SUM OF SQUARES	MEAN SQUARES	F VALUES
ATTRIBUTABLE TO REGRESSION	5	3.23531	0.64706	625.61084
DEVIATION FROM REGRESSION	215	0.22237	0.00103	
TOTAL	220	3.45768		

TABLE D.15

MULTIPLE REGRESSION ..... BED POROSITY IN THE CONTRACTED BEDS IN THREE PHASE BEDS

VARIABLE	MEAN	STANDARD DEVIATION	CORRELATION X VS Y	REGRESSION COEFFICIENT	STD. ERROR OF REG. COEF.	COMPUTED T VALUES
Fr_ℓ	0.24726	0.15505	0.57939	0.12828	0.00559	22.92699
We	0.00383	0.01125	0.24210	0.07294	0.00306	23.80992
$e^{(V_\ell/V_g)\varepsilon_{\ell_2}}$	144.444	486.059	0.39694	0.03098	0.00210	14.70266
DEPENDENT ($\varepsilon_\ell + \varepsilon_g$)	0.69258	0.08443				
INTERCEPT		1.30164				

MULTIPLE CORRELATION 0.90838

STD. ERROR OF ESTIMATE 0.03539

ANALYSIS OF VARIANCE FOR THE REGRESSION

SOURCE OF VARIATION	DEGREES OF FREEDOM	SUM OF SQUARES	MEAN SQUARES	F VALUES
ATTRIBUTABLE TO REGRESSION	3	2.85316	0.95105	341.38275
DEVIATION FROM REGRESSION	217	0.60453	0.00278	
TOTAL	220	3.45770		

TABLE D.16

MULTIPLE REGRESSION ..... LIQUID PHASE HMU IN THREE PHASE FLUIDIZED BEDS

VARIABLE	MEAN	STANDARD DEVIATION	CORRELATION X VS Y	REGRESSION COEFFICIENT	STD. ERROR OF REG. COEF.	COMPUTED T VALUES
V_ℓ	0.21550	0.08003	0.64940	0.81546	0.07954	10.25194
V_g	0.24976	0.27341	0.68446	0.30895	0.02814	10.97770
DEPENDENT						
HMU/Ho	0.47651	0.24816				
INTERCEPT			2.81591			
MULTIPLE CORRELATION			0.88742			
STD. ERROR OF ESTIMATE			0.10249			

ANALYSIS OF VARIANCE FOR THE REGRESSION

SOURCE OF VARIATION	DEGREES OF FREEDOM	SUM OF SQUARES	MEAN SQUARES	F VALUES
ATTRIBUTABLE TO REGRESSION	2	18.60194	9.30097	129.72247
DEVIATION FROM REGRESSION	70	5.01892	0.07169	
TOTAL	72	23.62086		

TABLE D.17

MULTIPLE REGRESSION ..... RELATIVE BUBBLE RISING VELOCITY IN THREE PHASE FLUIDIZED BEDS

VARIABLE	MEAN	STANDARD DEVIATION	CORRELATION X VS Y	REGRESSION COEFFICIENT	STD. ERROR OF REG. COEF.	COMPUTED T VALUES
V_ℓ	0.18335	0.05814	0.18221	0.06544	0.03904	1.67628
V_g	0.19335	0.16623	0.83066	0.33971	0.01589	21.37594
μ	0.00726	0.01045	0.00387	0.02524	0.01216	2.07573
σ	0.14649	0.02791	0.10034	0.17931	0.06759	2.65271
DEPENDENT						
V_{br}	2.91107	0.99151				

INTERCEPT 9.85894

MULTIPLE CORRELATION 0.85796

STD. ERROR OF ESTIMATE 0.538

ANALYSIS OF VARIANCE FOR THE REGRESSION

SOURCE OF VARIATION	DEGREES OF FREEDOM	SUM OF SQUARES	MEAN SQUARES	F VALUES
ATTRIBUTABLE TO REGRESSION	4	13.35401	3.33850	122.29583
DEVIATION FROM REGRESSION	176	4.80455	0.02729	
TOTAL	180	18.15856		

TABLE D. 18

MULTIPLE REGRESSION ..... BUBBLE RISING VELOCITY IN THREE PHASE FLUIDIZED BEDS

VARIABLE	MEAN	STANDARD DEVIATION	CORRELATION X VS Y	REGRESSION COEFFICIENT	STD. ERROR OF REG. COEF.	COMPUTED T VALUES
d_b	0.17399	0.04349	0.77714	0.98965	0.05990	16.52148
DEPENDENT						
V_{br}	2.79069	1.00840				
INTERCEPT		16.93171				
MULTIPLE CORRELATION		0.77714				
STD. ERROR OF ESTIMATE		0.5851				

ANALYSIS OF VARIANCE FOR THE REGRESSION

SOURCE OF VARIATION	DEGREES OF FREEDOM	SUM OF SQUARES	MEAN SQUARES	F VALUES
ATTRIBUTABLE TO REGRESSION	1	10.74265	10.74265	272.95959
DEVIATION FROM REGRESSION	179	7.04476	0.03935	
TOTAL	180	17.78741		

TABLE D.19

MULTIPLE REGRESSION ..... BUBBLE SIZE IN THREE PHASE FLUIDIZED BEDS

VARIABLE	MEAN	STANDARD DEVIATION	CORRELATION X VS Y	REGRESSION COEFFICIENT	STD. ERROR OF REG. COEF.	COMPUTED T VALUES
V_ℓ	0.18335	0.05814	0.17057	0.05281	0.03516	1.50193
V_g	0.19335	0.16623	0.79875	0.24858	0.01431	17.36589
μ	0.00726	0.01045	0.09707	0.00837	0.01095	0.76461
d	0.14649	0.02791	-0.02230	0.03388	0.06088	0.55647
DEPENDENT						
d_b	0.16498	0.04267				

INTERCEPT	0.31958
MULTIPLE CORRELATION	0.80464
STD. ERROR OF ESTIMATE	0.02358

ANALYSIS OF VARIANCE FOR THE REGRESSION

SOURCE OF VARIATION	DEGREES OF FREEDOM	SUM OF SQUARES	MEAN SQUARES	F VALUES
ATTRIBUTABLE TO REGRESSION	4	7.15828	1.78957	80.80340
DEVIATION FROM REGRESSION	176	3.89791	0.02214	
TOTAL	180	11.05620		

TABLE D.20

APPENDIX E

LIQUID AND GAS PHASE HOLD-UPS DATA IN LIQUID-GAS BEDS

HOLD-UPS OF LIQUID AND GAS PHASE IN LIQUID-GAS BEDS

LIQUID VELOCITY (FT/SEC)	GAS VELOCITY (FT/SEC)	VISCOSITY (CP)	SURFACE TENSION (DYNE/CM)	LIQUID DENSITY (GR/CU.CM)	LIQUID HOLD-UP	GAS HOLD-UP
0.125	0.046	1.430	39.800	0.960	0.954	0.045
0.125	0.185	1.430	39.800	0.960	0.866	0.133
0.125	0.360	1.430	39.800	0.960	0.813	0.186
0.125	0.527	1.430	39.800	0.960	0.732	0.267
0.177	0.046	1.430	39.800	0.960	0.938	0.061
0.177	0.185	1.430	39.800	0.960	0.849	0.150
0.177	0.360	1.430	39.800	0.960	0.795	0.204
0.177	0.527	1.430	39.800	0.960	0.718	0.281
0.252	0.046	1.430	39.800	0.960	0.933	0.066
0.252	0.185	1.430	39.800	0.960	0.846	0.153
0.252	0.360	1.430	39.800	0.960	0.764	0.235
0.252	0.527	1.430	39.800	0.960	0.699	0.300
0.312	0.046	1.430	39.800	0.960	0.923	0.076
0.312	0.185	1.430	39.800	0.960	0.843	0.156
0.312	0.360	1.430	39.800	0.960	0.721	0.278
0.125	0.046	1.260	50.200	0.980	0.966	0.033
0.125	0.185	1.260	50.200	0.980	0.870	0.129
0.125	0.360	1.260	50.200	0.980	0.795	0.204
0.125	0.527	1.260	50.200	0.980	0.736	0.263
0.177	0.046	1.260	50.200	0.980	0.958	0.041
0.177	0.185	1.260	50.200	0.980	0.866	0.133
0.177	0.360	1.260	50.200	0.980	0.767	0.232
0.177	0.527	1.260	50.200	0.980	0.717	0.282
0.252	0.046	1.260	50.200	0.980	0.952	0.047
0.252	0.185	1.260	50.200	0.980	0.845	0.154
0.252	0.360	1.260	50.200	0.980	0.745	0.254
0.252	0.527	1.260	50.200	0.980	0.704	0.295
0.312	0.046	1.260	50.200	0.980	0.930	0.069
0.312	0.185	1.260	50.200	0.980	0.832	0.167
0.312	0.360	1.260	50.200	0.980	0.699	0.300
0.125	0.046	1.110	60.000	0.990	0.955	0.044
0.125	0.185	1.110	60.000	0.990	0.849	0.150
0.125	0.360	1.110	60.000	0.990	0.764	0.235
0.125	0.527	1.110	60.000	0.990	0.705	0.294
0.177	0.046	1.110	60.000	0.990	0.941	0.058
0.177	0.185	1.110	60.000	0.990	0.833	0.166
0.177	0.360	1.110	60.000	0.990	0.745	0.254
0.177	0.527	1.110	60.000	0.990	0.702	0.297
0.252	0.046	1.110	60.000	0.990	0.921	0.078
0.252	0.185	1.110	60.000	0.990	0.818	0.181
0.252	0.360	1.110	60.000	0.990	0.734	0.265
0.252	0.527	1.110	60.000	0.990	0.698	0.301
0.312	0.046	1.110	60.000	0.990	0.911	0.088
0.312	0.185	1.110	60.000	0.990	0.802	0.197
0.125	0.046	1.000	72.800	1.000	0.985	0.014
0.125	0.185	1.000	72.800	1.000	0.921	0.078
0.125	0.360	1.000	72.800	1.000	0.839	0.160
0.125	0.527	1.000	72.800	1.000	0.826	0.173
0.125	0.854	1.000	72.800	1.000	0.780	0.219

0.177	0.046	1.000	72.800	1.000	0.977	0.022
0.177	0.185	1.000	72.800	1.000	0.916	0.083
0.177	0.360	1.000	72.800	1.000	0.833	0.166
0.177	0.527	1.000	72.800	1.000	0.820	0.179
0.177	0.854	1.000	72.800	1.000	0.771	0.228
0.252	0.046	1.000	72.800	1.000	0.973	0.026
0.252	0.185	1.000	72.800	1.000	0.877	0.122
0.252	0.360	1.000	72.800	1.000	0.820	0.179
0.252	0.527	1.000	72.800	1.000	0.805	0.194
0.252	0.854	1.000	72.800	1.000	0.743	0.256
0.312	0.046	1.000	72.800	1.000	0.972	0.027
0.312	0.185	1.000	72.800	1.000	0.855	0.144
0.312	0.360	1.000	72.800	1.000	0.801	0.198
0.312	0.527	1.000	72.800	1.000	0.776	0.223
0.312	0.854	1.000	72.800	1.000	0.733	0.266
0.335	0.046	1.000	72.800	1.000	0.970	0.029
0.335	0.185	1.000	72.800	1.000	0.849	0.150
0.335	0.527	1.000	72.800	1.000	0.771	0.228
0.125	0.046	2.370	72.900	1.094	0.960	0.039
0.125	0.185	2.370	72.900	1.094	0.925	0.074
0.125	0.360	2.370	72.900	1.094	0.841	0.158
0.125	0.527	2.370	72.900	1.094	0.809	0.190
0.125	0.854	2.370	72.900	1.094	0.730	0.269
0.174	0.046	2.370	72.900	1.094	0.974	0.025
0.174	0.185	2.370	72.900	1.094	0.920	0.079
0.174	0.360	2.370	72.900	1.094	0.814	0.185
0.174	0.527	2.370	72.900	1.094	0.797	0.202
0.174	0.854	2.370	72.900	1.094	0.733	0.266
0.246	0.046	2.370	72.900	1.094	0.978	0.021
0.246	0.185	2.370	72.900	1.094	0.890	0.109
0.246	0.360	2.370	72.900	1.094	0.808	0.191
0.246	0.527	2.370	72.900	1.094	0.738	0.261
0.246	0.854	2.370	72.900	1.094	0.702	0.297
0.290	0.046	2.370	72.900	1.094	0.927	0.072
0.290	0.185	2.370	72.900	1.094	0.865	0.134
0.290	0.360	2.370	72.900	1.094	0.789	0.210
0.290	0.527	2.370	72.900	1.094	0.751	0.248
0.125	0.046	4.640	75.500	1.152	0.963	0.036
0.125	0.185	4.640	75.500	1.152	0.909	0.090
0.125	0.360	4.640	75.500	1.152	0.845	0.154
0.125	0.527	4.640	75.500	1.152	0.803	0.196
0.125	0.854	4.640	75.500	1.152	0.721	0.278
0.174	0.046	4.640	75.500	1.152	0.993	0.006
0.174	0.185	4.640	75.500	1.152	0.904	0.095
0.174	0.360	4.640	75.500	1.152	0.821	0.178
0.174	0.527	4.640	75.500	1.152	0.786	0.213
0.174	0.854	4.640	75.500	1.152	0.729	0.270
0.264	0.046	4.640	75.500	1.152	0.980	0.019
0.264	0.185	4.640	75.500	1.152	0.880	0.119
0.264	0.360	4.640	75.500	1.152	0.798	0.201
0.264	0.527	4.640	75.500	1.152	0.784	0.215
0.264	0.854	4.640	75.500	1.152	0.715	0.284
0.303	0.046	4.640	75.500	1.152	0.928	0.071
0.303	0.185	4.640	75.500	1.152	0.880	0.119
0.303	0.360	4.640	75.500	1.152	0.787	0.212
0.303	0.527	4.640	75.500	1.152	0.720	0.279
0.125	0.046	7.600	75.900	1.172	0.949	0.050
0.125	0.185	7.600	75.900	1.172	0.891	0.108
0.125	0.360	7.600	75.900	1.172	0.837	0.162
0.125	0.527	7.600	75.900	1.172	0.785	0.214
0.125	0.854	7.600	75.900	1.172	0.742	0.257

0.174	0.046	7.600	75.900	1.172	0.941	0.058
0.174	0.185	7.600	75.900	1.172	0.906	0.093
0.174	0.360	7.600	75.900	1.172	0.825	0.174
0.174	0.527	7.600	75.900	1.172	0.805	0.194
0.174	0.854	7.600	75.900	1.172	0.739	0.260
0.265	0.046	7.600	75.900	1.172	0.954	0.045
0.265	0.185	7.600	75.900	1.172	0.855	0.144
0.265	0.360	7.600	75.900	1.172	0.780	0.219
0.265	0.527	7.600	75.900	1.172	0.754	0.245
0.265	0.854	7.600	75.900	1.172	0.736	0.263
0.307	0.046	7.600	75.900	1.172	0.943	0.056
0.307	0.185	7.600	75.900	1.172	0.841	0.158
0.307	0.360	7.600	75.900	1.172	0.789	0.210
0.307	0.527	7.600	75.900	1.172	0.754	0.245
0.125	0.046	12.770	68.900	1.230	0.992	0.007
0.125	0.092	12.770	68.900	1.230	0.969	0.030
0.125	0.185	12.770	68.900	1.230	0.928	0.071
0.125	0.360	12.770	68.900	1.230	0.890	0.109
0.177	0.046	12.770	68.900	1.230	0.984	0.015
0.177	0.092	12.770	68.900	1.230	0.968	0.031
0.177	0.185	12.770	68.900	1.230	0.928	0.071
0.177	0.360	12.770	68.900	1.230	0.874	0.125
0.230	0.046	12.770	68.900	1.230	0.977	0.022
0.230	0.092	12.770	68.900	1.230	0.962	0.037
0.230	0.185	12.770	68.900	1.230	0.934	0.065
0.230	0.360	12.770	68.900	1.230	0.852	0.147
0.280	0.046	12.770	68.900	1.230	0.974	0.025
0.280	0.092	12.770	68.900	1.230	0.966	0.033
0.280	0.185	12.770	68.900	1.230	0.924	0.075
0.280	0.360	12.770	68.900	1.230	0.840	0.159
0.315	0.046	12.770	68.900	1.230	0.977	0.022
0.315	0.092	12.770	68.900	1.230	0.960	0.039
0.315	0.185	12.770	68.900	1.230	0.933	0.066
0.315	0.360	12.770	68.900	1.230	0.833	0.166
0.125	0.046	6.300	72.800	1.004	0.955	0.044
0.125	0.092	6.300	72.800	1.004	0.930	0.069
0.125	0.185	6.300	72.800	1.004	0.896	0.103
0.125	0.360	6.300	72.800	1.004	0.840	0.159
0.125	0.527	6.300	72.800	1.004	0.798	0.201
0.177	0.046	6.300	72.800	1.004	0.961	0.038
0.177	0.092	6.300	72.800	1.004	0.924	0.075
0.177	0.185	6.300	72.800	1.004	0.866	0.133
0.177	0.360	6.300	72.800	1.004	0.829	0.170
0.177	0.527	6.300	72.800	1.004	0.804	0.195
0.218	0.046	6.300	72.800	1.004	0.939	0.060
0.218	0.092	6.300	72.800	1.004	0.910	0.089
0.218	0.185	6.300	72.800	1.004	0.836	0.163
0.218	0.360	6.300	72.800	1.004	0.796	0.203
0.125	0.046	8.500	72.800	1.004	0.966	0.033
0.125	0.185	8.500	72.800	1.004	0.911	0.088
0.125	0.527	8.500	72.800	1.004	0.818	0.181
0.125	0.854	8.500	72.800	1.004	0.767	0.232
0.177	0.046	8.500	72.800	1.004	0.961	0.038
0.177	0.185	8.530	72.800	1.004	0.901	0.098
0.177	0.527	8.500	72.800	1.004	0.814	0.185
0.177	0.854	8.500	72.800	1.004	0.765	0.234
0.252	0.046	8.500	72.800	1.004	0.955	0.044
0.252	0.185	8.500	72.800	1.004	0.889	0.110
0.252	0.527	8.500	72.800	1.004	0.808	0.191
0.252	0.854	8.500	72.800	1.004	0.758	0.241
0.270	0.046	8.500	72.800	1.004	0.933	0.066

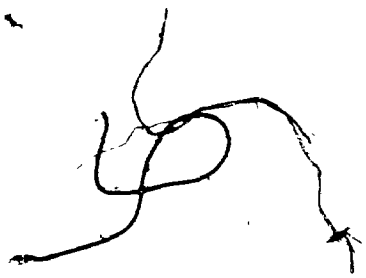

0.270	0.185	8.500	72.000	1.004	0.885	0.114
0.270	0.527	8.500	72.800	1.004	0.795	0.204
0.270	0.854	8.500	72.800	1.004	0.754	0.245
0.125	0.046	13.000	73.000	1.003	0.964	0.035
0.125	0.092	13.000	73.000	1.003	0.944	0.055
0.125	0.185	13.000	73.000	1.003	0.904	0.095
0.125	0.360	13.000	73.000	1.003	0.851	0.148
0.125	0.527	13.000	73.000	1.003	0.807	0.192
0.177	0.046	13.000	73.000	1.003	0.961	0.038
0.177	0.092	13.000	73.000	1.003	0.917	0.082
0.177	0.185	13.000	73.000	1.003	0.898	0.101
0.177	0.360	13.000	73.000	1.003	0.843	0.156
0.177	0.527	13.000	73.000	1.003	0.814	0.185
0.218	0.046	13.000	73.000	1.003	0.961	0.038
0.218	0.092	13.000	73.000	1.003	0.911	0.088
0.218	0.185	13.000	73.000	1.003	0.908	0.091
0.218	0.360	13.000	73.000	1.003	0.871	0.128
0.218	0.527	13.000	73.000	1.003	0.813	0.186
0.252	0.046	13.000	73.000	1.003	0.955	0.044
0.252	0.185	13.000	73.000	1.003	0.907	0.092
0.252	0.360	13.000	73.000	1.003	0.858	0.141
0.252	0.527	13.000	73.000	1.003	0.827	0.172
0.286	0.046	13.000	73.000	1.003	0.955	0.044
0.286	0.185	13.000	73.000	1.003	0.893	0.106
0.286	0.360	13.000	73.000	1.003	0.879	0.120
0.286	0.527	13.000	73.000	1.003	0.840	0.159
0.312	0.046	13.000	73.000	1.003	0.960	0.039
0.312	0.185	13.000	73.000	1.003	0.896	0.103
0.312	0.360	13.000	73.000	1.003	0.836	0.163
0.312	0.527	13.000	73.000	1.003	0.808	0.191
0.125	0.046	20.000	73.500	1.002	0.955	0.044
0.125	0.092	20.000	73.500	1.002	0.944	0.055
0.125	0.185	20.000	73.500	1.002	0.916	0.083
0.125	0.527	20.000	73.500	1.002	0.815	0.184
0.125	0.854	20.000	73.500	1.002	0.767	0.232
0.177	0.046	20.000	73.500	1.002	0.942	0.057
0.177	0.092	20.000	73.500	1.002	0.913	0.086
0.177	0.185	20.000	73.500	1.002	0.901	0.098
0.177	0.360	20.000	73.500	1.002	0.851	0.148
0.177	0.527	20.000	73.500	1.002	0.827	0.172
0.177	0.854	20.000	73.500	1.002	0.779	0.220
0.218	0.046	20.000	73.500	1.002	0.954	0.045
0.218	0.092	20.000	73.500	1.002	0.911	0.088
0.218	0.185	20.000	73.500	1.002	0.879	0.120
0.218	0.360	20.000	73.500	1.002	0.842	0.157
0.218	0.527	20.000	73.500	1.002	0.824	0.175
0.252	0.046	20.000	73.500	1.002	0.936	0.063
0.252	0.185	20.000	73.500	1.002	0.888	0.111
0.252	0.527	20.000	73.500	1.002	0.783	0.216
0.252	0.854	20.000	73.500	1.002	0.749	0.250
0.270	0.046	20.000	73.500	1.002	0.970	0.029
0.270	0.185	20.000	73.500	1.002	0.907	0.092
0.270	0.527	20.000	73.500	1.002	0.807	0.192
0.270	0.854	20.000	73.500	1.002	0.777	0.222
0.125	0.046	70.000	73.800	1.001	0.967	0.032
0.125	0.092	70.000	73.800	1.001	0.958	0.041
0.125	0.185	70.000	73.500	1.001	0.927	0.072
0.125	0.360	70.000	73.800	1.001	0.870	0.129
0.125	0.527	70.000	73.800	1.001	0.845	0.154
0.177	0.046	70.000	73.800	1.001	0.966	0.033
0.177	0.092	70.000	73.100	1.001	0.961	0.038

0.177	0.185	70.000	73.300	1.001	0.932	0.067
0.177	0.360	70.000	73.800	1.001	0.879	0.120
0.177	0.527	70.000	73.800	1.001	0.832	0.167
0.221	0.046	70.000	73.800	1.001	0.964	0.035
0.221	0.092	70.000	73.800	1.001	0.955	0.044
0.221	0.185	70.000	73.800	1.001	0.935	0.064
0.221	0.360	70.000	73.800	1.001	0.882	0.117
0.221	0.527	70.000	73.800	1.001	0.827	0.172
0.252	0.046	70.000	73.800	1.001	0.958	0.041
0.252	0.092	70.000	73.800	1.001	0.955	0.044
0.252	0.185	70.000	73.300	1.001	0.932	0.067
0.252	0.360	70.000	73.800	1.001	0.880	0.119
0.252	0.527	70.000	73.800	1.001	0.824	0.175
0.286	0.046	70.000	73.800	1.001	0.954	0.045
0.286	0.092	70.000	73.800	1.001	0.936	0.063
0.286	0.185	70.000	73.800	1.001	0.923	0.076
0.286	0.360	70.000	73.800	1.001	0.855	0.144

APPENDIX F

LIQUID HOLD-UP AND EXPANDED BED DATA IN LIQUID-SOLID BEDS

LIQUID HOLD-UP AND EXPANDED BED HEIGHT IN LIQUID-SOLID BEDS

SOLID = 6 MM GLASS BEADS

LIQUID VELOCITY (FT/SEC)	VISCOSITY (CP)	SURFACE TENSION (DYNE/CM)	LIQUID DENSITY (GR/CU.CM)	LIQUID HOLD-UP	BED HEIGHT (INCH)
0.125	1.430	39.800	0.960	0.389	21.600
0.177	1.430	39.800	0.960	0.446	23.800
0.252	1.430	39.800	0.960	0.509	26.600
0.312	1.430	39.800	0.960	0.541	28.300
0.125	1.260	50.200	0.980	0.384	21.600
0.177	1.260	50.200	0.980	0.426	22.800
0.252	1.260	50.200	0.980	0.484	25.500
0.312	1.260	50.200	0.980	0.504	26.800
0.125	1.110	60.000	0.990	0.380	21.600
0.177	1.110	60.000	0.990	0.428	23.000
0.252	1.110	60.000	0.990	0.490	25.800
0.312	1.110	60.000	0.990	0.515	27.000
0.125	1.000	72.800	1.000	0.380	21.600
0.177	1.000	72.800	1.000	0.428	23.000
0.252	1.000	72.800	1.000	0.500	26.200
0.312	1.000	72.800	1.000	0.536	28.700
0.335	1.000	72.800	1.000	0.550	29.600
0.125	2.370	72.900	1.094	0.385	22.000
0.174	2.370	72.900	1.094	0.456	24.200
0.246	2.370	72.900	1.094	0.502	27.000
0.290	2.370	72.900	1.094	0.526	27.800
0.125	4.640	75.500	1.152	0.425	22.700
0.174	4.640	75.500	1.152	0.482	25.200
0.264	4.640	75.500	1.152	0.524	27.000
0.303	4.640	75.500	1.152	0.557	28.600
0.125	7.600	75.900	1.172	0.459	24.600
0.174	7.600	75.900	1.172	0.507	26.800
0.265	7.600	75.900	1.172	0.563	30.200
0.307	7.600	75.900	1.172	0.603	32.800
0.080	12.770	68.900	1.230	0.412	22.700
0.125	12.770	68.900	1.230	0.460	24.700
0.177	12.770	68.900	1.230	0.544	29.300
0.230	12.770	68.900	1.230	0.555	30.000
0.280	12.770	68.900	1.230	0.597	33.100
0.315	12.770	68.900	1.230	0.627	35.500
0.125	8.500	72.800	1.004	0.493	26.000
0.177	8.500	72.800	1.004	0.541	27.900
0.252	8.500	72.800	1.004	0.594	32.300
0.298	8.500	72.800	1.004	0.638	36.400
0.125	13.000	73.500	1.003	0.450	24.200
0.177	13.000	73.500	1.003	0.505	27.500
0.218	13.000	73.500	1.003	0.512	28.100
0.252	13.000	73.500	1.003	0.555	30.600
0.281	13.000	73.500	1.003	0.586	33.300
0.312	13.000	73.500	1.003	0.620	34.800
0.335	13.000	73.500	1.003	0.653	37.500

0.125	20.000	72.800	1.002	0.514	27.200
0.177	20.000	72.800	1.002	0.547	30.200
0.252	20.000	72.800	1.002	0.657	39.500
0.270	20.000	72.800	1.002	0.670	42.000
0.298	20.000	72.800	1.002	0.703	45.800
0.125	70.000	73.800	1.000	0.604	33.800
0.177	70.000	73.800	1.000	0.685	42.500
0.218	70.000	73.800	1.000	0.734	50.100
0.252	70.000	73.800	1.000	0.770	59.000
0.281	70.000	73.800	1.000	0.772	66.500

LIQUID HOLD-UP AND EXPANDED BED HEIGHT IN LIQUID-SOLID BEDS

SOLID = 2.6 MM GRAVEL

LIQUID VELOCITY (FT/SEC)	VISCOSITY (CP)	SURFACE TENSION (DYNE/CM)	LIQUID DENSITY (GR/CU.CM)	LIQUID HOLD-UP	BED HEIGHT (INCH)
0.125	1.430	39.800	0.960	0.417	24.500
0.177	1.430	39.800	0.960	0.482	26.500
0.252	1.430	39.800	0.960	0.578	33.000
0.312	1.430	39.800	0.960	0.643	38.200
0.125	1.260	50.200	0.980	0.418	24.500
0.177	1.260	50.200	0.980	0.476	27.600
0.252	1.260	50.200	0.980	0.567	32.500
0.312	1.260	50.200	0.980	0.640	38.100
0.125	1.110	60.000	0.990	0.411	24.400
0.177	1.110	60.000	0.990	0.478	27.400
0.208	1.110	60.000	0.990	0.530	30.200
0.252	1.110	60.000	0.990	0.575	32.200
0.312	1.110	60.000	0.990	0.652	38.000
0.125	1.000	72.800	1.000	0.414	24.700
0.177	1.000	72.800	1.000	0.473	27.100
0.208	1.000	72.800	1.000	0.515	29.900
0.252	1.000	72.800	1.000	0.573	33.500
0.312	1.000	72.800	1.000	0.622	38.000
0.125	2.370	72.900	1.094	0.461	26.500
0.174	2.370	72.900	1.094	0.529	30.300
0.246	2.370	72.900	1.094	0.640	38.800
0.310	2.370	72.900	1.094	0.686	46.000
0.125	4.640	75.500	1.152	0.492	28.200
0.174	4.640	75.500	1.152	0.563	33.200
0.264	4.640	75.500	1.152	0.688	46.000
0.310	4.640	75.500	1.152	0.780	63.200
0.125	7.600	75.900	1.172	0.534	30.600
0.174	7.600	75.900	1.172	0.629	38.300
0.265	7.600	75.900	1.172	0.750	57.500
0.307	7.600	75.900	1.172	0.778	66.000
0.125	12.770	68.900	1.230	0.635	38.200
0.177	12.770	68.900	1.230	0.709	48.500
0.230	12.770	68.900	1.230	0.770	62.000
0.280	12.770	68.900	1.230	0.800	71.300
0.090	8.500	72.800	1.000	0.468	26.100
0.125	8.500	72.800	1.000	0.521	28.800
0.177	8.500	72.800	1.000	0.605	36.000
0.218	8.500	72.800	1.000	0.655	41.000
0.090	20.000	73.500	1.000	0.558	31.600
0.125	20.000	73.500	1.000	0.628	37.000
0.177	20.000	73.500	1.000	0.705	47.400
0.218	20.000	73.500	1.000	0.751	57.900

LIQUID HOLD-UP AND EXPANDED BED HEIGHT IN LIQUID-SOLID BEDS

SOLID = 1 MM GLASS BEADS

LIQUID VELOCITY (FT/SEC)	VISCOSITY (CP)	SURFACE TENSION (DYNE/CM)	LIQUID DENSITY (GR/CU.CM)	LIQUID HOLD-UP	BED HEIGHT (INCH)
0.125	1.430	39.800	0.960	0.639	36.100
0.177	1.430	39.800	0.960	0.715	45.200
0.208	1.430	39.800	0.960	0.785	58.000
0.252	1.430	39.800	0.960	0.820	73.300
0.125	1.260	50.200	0.980	0.587	32.200
0.177	1.260	50.200	0.980	0.692	42.200
0.208	1.260	50.200	0.980	0.757	52.300
0.252	1.260	50.200	0.980	0.797	63.000
0.125	1.110	60.000	0.990	0.590	32.800
0.177	1.110	60.000	0.990	0.687	41.500
0.208	1.110	60.000	0.990	0.736	49.500
0.252	1.110	60.000	0.990	0.783	59.200
0.125	1.000	72.800	1.000	0.591	32.100
0.177	1.000	72.800	1.000	0.686	41.700
0.208	1.000	72.800	1.000	0.751	52.500
0.252	1.000	72.800	1.000	0.795	62.800
0.090	2.370	72.900	1.094	0.549	29.700
0.125	2.370	72.900	1.094	0.658	39.500
0.174	2.370	72.900	1.094	0.756	53.700
0.200	2.370	72.900	1.094	0.797	64.200
0.090	1.000	72.800	1.000	0.499	12.100
0.125	1.000	72.800	1.000	0.578	14.000
0.177	1.000	72.800	1.000	0.672	18.000
0.200	1.000	72.800	1.000	0.725	20.000
0.218	1.000	72.800	1.000	0.757	21.800
0.252	1.000	72.800	1.000	0.793	24.800
0.090	2.370	72.900	1.094	0.567	14.300
0.125	2.370	72.900	1.094	0.656	17.700
0.174	2.370	72.900	1.094	0.764	25.500
0.200	2.370	72.900	1.094	0.790	28.200
0.090	4.640	75.500	1.152	0.613	15.900
0.125	4.640	75.500	1.152	0.712	21.200
0.174	4.640	75.500	1.152	0.827	34.200
0.200	4.640	75.500	1.152	0.864	38.700
0.090	7.600	75.900	1.172	0.652	18.200
0.125	7.600	75.900	1.172	0.757	25.000
0.174	7.600	75.900	1.172	0.869	44.000
0.200	7.600	75.900	1.172	0.889	48.200
0.090	3.700	72.800	1.006	0.599	14.600
0.125	3.700	72.800	1.006	0.627	16.800
0.177	3.700	72.800	1.006	0.752	23.800
0.218	3.700	72.800	1.006	0.824	34.300
0.090	5.700	72.800	1.004	0.634	16.800
0.125	5.700	72.800	1.004	0.708	20.500
0.177	5.700	72.800	1.004	0.864	39.500
0.200	5.700	72.800	1.004	0.905	53.400

0.090	6.300	72.800	1.004	0.673	18.000
0.125	6.300	72.800	1.004	0.746	23.600
0.177	6.300	72.800	1.004	0.902	52.000

APPENDIX G

LIQUID AND GAS HOLD-UPS, BED POROSITY, EXPANDED BED HEIGHT AND WAKE VOLUME TO GAS VOLUME DATA IN THREE PHASE FLUIDIZED BEDS

LIQUID AND GAS HOLD-UPS, BED POROSITY, EXPANDED BED HEIGHT, AND WAKE VOLUME TO GAS VOLUME

SOLID = 1 MM GLASS BEADS

LIQUID VELOCITY (FT/SEC)	GAS VELOCITY (FT/SEC)	VISCOSITY (CP)	SURFACE TENSION (DYNE/CM)	LIQUID HOLD-UP	GAS HOLD-UP	BED HEIGHT (INCH)	BED POROSITY	WAKE/GAS VOLUME
0.125	0.023	1.430	39.800	0.501	0.088	33.000	0.589	0.508
0.125	0.046	1.430	39.800	0.482	0.108	33.200	0.591	0.368
0.125	0.092	1.430	39.800	0.478	0.121	33.900	0.600	0.259
0.125	0.185	1.430	39.800	0.428	0.187	35.300	0.615	0.175
0.177	0.023	1.430	39.800	0.587	0.099	43.300	0.686	0.440
0.177	0.046	1.430	39.800	0.568	0.109	42.100	0.677	0.380
0.177	0.092	1.430	39.800	0.537	0.131	41.000	0.669	0.315
0.177	0.185	1.430	39.800	0.490	0.163	39.200	0.654	0.269
0.208	0.023	1.430	39.800	0.651	0.094	53.300	0.745	0.345
0.208	0.046	1.430	39.800	0.622	0.120	52.600	0.742	0.287
0.208	0.092	1.430	39.800	0.590	0.140	50.500	0.731	0.257
0.208	0.185	1.430	39.800	0.546	0.182	50.000	0.728	0.204
0.252	0.023	1.430	39.800	0.746	0.066	72.500	0.812	0.214
0.252	0.046	1.430	39.800	0.695	0.108	69.100	0.803	0.257
0.252	0.092	1.430	39.800	0.654	0.136	65.100	0.791	0.244
0.252	0.185	1.430	39.800	0.596	0.178	60.100	0.774	0.224
0.125	0.023	1.260	50.200	0.478	0.090	31.500	0.569	0.593
0.125	0.046	1.260	50.200	0.462	0.098	30.900	0.561	0.494
0.125	0.092	1.260	50.200	0.441	0.110	30.300	0.552	0.407
0.125	0.185	1.260	50.200	0.402	0.173	32.000	0.576	0.238
0.177	0.023	1.260	50.200	0.632	0.024	39.500	0.656	1.226
0.177	0.046	1.260	50.200	0.595	0.088	37.000	0.633	0.620
0.177	0.092	1.260	50.200	0.518	0.113	36.800	0.631	0.443
0.177	0.185	1.260	50.200	0.464	0.171	37.200	0.635	0.295
0.208	0.023	1.260	50.200	0.640	0.082	49.000	0.723	0.452
0.208	0.046	1.260	50.200	0.608	0.106	47.500	0.714	0.385
0.208	0.092	1.260	50.200	0.588	0.118	46.200	0.706	0.325
0.208	0.185	1.260	50.200	0.532	0.176	46.500	0.708	0.232
0.252	0.023	1.260	50.200	0.707	0.064	59.600	0.772	0.550
0.252	0.046	1.260	50.200	0.656	0.101	56.000	0.757	0.463
0.252	0.092	1.260	50.200	0.641	0.110	54.800	0.752	0.373
0.252	0.185	1.260	50.200	0.592	0.165	56.000	0.757	0.247
0.125	0.023	1.110	60.000	0.487	0.088	32.000	0.576	0.510
0.125	0.046	1.110	60.000	0.462	0.111	31.800	0.573	0.396
0.125	0.092	1.110	60.000	0.436	0.143	32.300	0.580	0.282
0.125	0.185	1.110	60.000	0.367	0.226	33.400	0.594	0.202
0.177	0.023	1.110	60.000	0.576	0.077	39.200	0.654	0.607
0.177	0.046	1.110	60.000	0.547	0.091	37.600	0.639	0.536
0.177	0.092	1.110	60.000	0.516	0.125	37.900	0.642	0.368
0.177	0.185	1.110	60.000	0.464	0.206	38.900	0.651	0.245
0.208	0.023	1.110	60.000	0.635	0.087	48.800	0.722	0.390
0.208	0.046	1.110	60.000	0.608	0.103	47.000	0.711	0.362
0.208	0.092	1.110	60.000	0.575	0.116	44.100	0.692	0.352
0.208	0.185	1.110	60.000	0.520	0.174	44.400	0.694	0.249
0.252	0.023	1.110	60.000	0.695	0.072	58.500	0.768	0.479
0.252	0.046	1.110	60.000	0.647	0.106	55.000	0.753	0.435

0.252	0.092	1.110	60.000	0.621	0.121	52.900	0.743	0.366
0.252	0.189	1.110	60.000	0.550	0.190	52.300	0.740	0.283
0.125	0.023	1.000	72.800	0.467	0.089	30.600	0.556	0.615
0.125	0.046	1.000	72.800	0.441	0.105	29.900	0.546	0.512
0.125	0.092	1.000	72.800	0.423	0.114	29.300	0.537	0.429
0.125	0.185	1.000	72.800	0.381	0.141	28.800	0.529	0.335
0.177	0.023	1.000	72.800	0.568	0.077	38.200	0.645	0.639
0.177	0.046	1.000	72.800	0.534	0.094	36.500	0.628	0.565
0.177	0.092	1.000	72.800	0.512	0.105	35.500	0.618	0.470
0.177	0.185	1.000	72.800	0.426	0.168	35.200	0.614	0.315
0.208	0.023	1.000	72.800	0.622	0.081	45.800	0.703	0.493
0.208	0.046	1.000	72.800	0.578	0.098	42.000	0.677	0.530
0.208	0.092	1.000	72.800	0.550	0.120	41.200	0.670	0.413
0.208	0.185	1.000	72.800	0.482	0.186	41.000	0.669	0.291
0.252	0.023	1.000	72.800	0.670	0.071	52.500	0.741	0.693
0.252	0.046	1.000	72.800	0.639	0.081	48.500	0.720	0.669
0.252	0.092	1.000	72.800	0.616	0.097	47.500	0.714	0.507
0.252	0.185	1.000	72.800	0.535	0.175	46.900	0.710	0.325
0.090	0.023	2.370	72.900	0.468	0.065	29.100	0.534	0.570
0.090	0.046	2.370	72.900	0.465	0.096	31.000	0.562	0.273
0.090	0.092	2.370	72.900	0.414	0.141	30.500	0.555	0.227
0.090	0.185	2.370	72.900	0.387	0.200	32.900	0.587	0.136
0.125	0.023	2.370	72.900	0.558	0.077	37.300	0.636	0.383
0.125	0.046	2.370	72.900	0.529	0.090	35.600	0.619	0.372
0.125	0.092	2.370	72.900	0.509	0.111	35.800	0.621	0.269
0.125	0.185	2.370	72.900	0.473	0.137	34.900	0.611	0.223
0.174	0.023	2.370	72.900	0.649	0.065	47.500	0.714	0.486
0.174	0.046	2.370	72.900	0.600	0.102	45.700	0.703	0.379
0.174	0.092	2.370	72.900	0.562	0.134	44.700	0.696	0.293
0.174	0.185	2.370	72.900	0.507	0.184	44.000	0.691	0.222
0.200	0.023	2.370	72.900	0.677	0.073	54.500	0.751	0.501
0.200	0.046	2.370	72.900	0.626	0.107	51.000	0.734	0.417
0.200	0.092	2.370	72.900	0.591	0.132	49.100	0.723	0.333
0.090	0.023	7.600	75.500	0.593	0.076	41.200	0.670	0.132
0.090	0.046	7.600	75.500	0.581	0.083	40.500	0.665	0.128
0.090	0.092	7.600	75.500	0.518	0.138	39.500	0.656	0.127
0.090	0.185	7.600	75.500	0.454	0.200	39.300	0.655	0.107
0.125	0.023	7.600	75.500	0.631	0.097	50.000	0.728	0.258
0.125	0.046	7.600	75.500	0.607	0.109	48.000	0.717	0.231
0.125	0.092	7.600	75.500	0.595	0.122	48.000	0.717	0.178
0.125	0.185	7.600	75.500	0.470	0.217	43.500	0.688	0.158
0.090	0.023	1.000	72.800	0.361	0.112	11.500	0.474	0.429
0.090	0.046	1.000	72.800	0.344	0.115	11.200	0.460	0.556
0.090	0.092	1.000	72.800	0.335	0.152	11.800	0.487	0.331
0.090	0.185	1.000	72.800	0.296	0.238	13.000	0.534	0.187
0.125	0.023	1.000	72.800	0.411	0.140	13.500	0.552	0.572
0.125	0.046	1.000	72.800	0.387	0.157	13.300	0.545	0.465
0.125	0.092	1.000	72.800	0.370	0.167	13.100	0.538	0.383
0.125	0.185	1.000	72.800	0.343	0.269	15.600	0.612	0.179
0.177	0.023	1.000	72.800	0.522	0.135	17.700	0.658	0.477
0.177	0.046	1.000	72.800	0.483	0.171	17.500	0.654	0.379
0.177	0.092	1.000	72.800	0.435	0.224	17.800	0.660	0.282
0.177	0.185	1.000	72.800	0.419	0.254	18.500	0.673	0.204
0.200	0.023	1.000	72.800	0.520	0.165	19.300	0.686	0.489
0.200	0.046	1.000	72.800	0.500	0.183	19.100	0.683	0.388
0.200	0.092	1.000	72.800	0.475	0.221	19.900	0.696	0.272
0.200	0.185	1.000	72.800	0.431	0.280	21.000	0.712	0.195
0.090	0.023	2.370	72.900	0.477	0.090	14.000	0.568	0.321
0.090	0.046	2.370	72.900	0.466	0.092	13.700	0.558	0.291
0.090	0.092	2.370	72.900	0.403	0.134	13.100	0.538	0.269
0.090	0.185	2.370	72.900	0.387	0.227	15.700	0.614	0.109

0.125	0.023	2.370	72.900	0.591	0.022	15.700	0.614	1.042
0.125	0.046	2.370	72.900	0.561	0.043	15.300	0.604	0.641
0.125	0.092	2.370	72.900	0.505	0.090	15.000	0.596	0.374
0.125	0.185	2.370	72.900	0.470	0.178	17.200	0.648	0.153
0.174	0.023	2.370	72.900	0.628	0.116	23.700	0.744	0.262
0.174	0.046	2.370	72.900	0.612	0.108	21.700	0.721	0.298
0.174	0.092	2.370	72.900	0.562	0.156	21.500	0.718	0.229
0.174	0.185	2.370	72.900	0.533	0.195	22.300	0.728	0.162
0.200	0.023	2.370	72.900	0.671	0.100	26.500	0.771	0.328
0.200	0.046	2.370	72.900	0.633	0.117	24.300	0.751	0.335
0.200	0.092	2.370	72.900	0.596	0.141	23.100	0.738	0.287
0.200	0.185	2.370	72.900	0.556	0.185	23.500	0.742	0.203
0.090	0.023	4.640	75.500	0.552	0.054	15.400	0.607	0.320
0.090	0.046	4.640	75.500	0.540	0.088	16.300	0.628	0.153
0.090	0.092	4.640	75.500	0.503	0.138	16.900	0.642	0.109
0.090	0.185	4.640	75.500	0.492	0.169	17.900	0.662	0.070
0.125	0.023	4.640	75.500	0.636	0.066	20.300	0.702	0.234
0.125	0.046	4.640	75.500	0.614	0.097	21.000	0.712	0.152
0.125	0.092	4.640	75.500	0.579	0.140	21.600	0.720	0.114
0.125	0.185	4.640	75.500	0.543	0.182	22.100	0.726	0.091
0.174	0.023	4.640	75.500	0.725	0.069	29.500	0.794	0.239
0.174	0.046	4.640	75.500	0.680	0.102	27.800	0.782	0.234
0.174	0.092	4.640	75.500	0.664	0.096	25.300	0.760	0.253
0.174	0.185	4.640	75.500	0.648	0.129	27.300	0.778	0.148
0.200	0.023	4.640	75.500	0.737	0.101	37.700	0.839	0.231
0.200	0.046	4.640	75.500	0.694	0.129	34.400	0.824	0.229
0.200	0.092	4.640	75.500	0.671	0.141	32.200	0.812	0.204
0.200	0.185	4.640	75.500	0.641	0.177	33.500	0.819	0.143
0.090	0.023	7.600	75.900	0.562	0.066	16.300	0.628	0.342
0.090	0.046	7.600	75.900	0.554	0.087	16.900	0.642	0.203
0.090	0.092	7.600	75.900	0.523	0.177	20.200	0.700	0.072
0.090	0.185	7.600	75.900	0.512	0.199	21.000	0.712	0.052
0.125	0.023	7.600	75.900	0.662	0.069	22.600	0.732	0.257
0.125	0.046	7.600	75.900	0.632	0.097	22.400	0.730	0.199
0.125	0.092	7.600	75.900	0.615	0.126	23.500	0.742	0.127
0.125	0.185	7.600	75.900	0.592	0.143	22.900	0.735	0.111
0.174	0.023	7.600	75.900	0.791	0.056	40.000	0.848	0.145
0.174	0.046	7.600	75.900	0.757	0.083	38.000	0.840	0.159
0.174	0.092	7.600	75.900	0.737	0.104	38.200	0.841	0.123
0.200	0.023	7.600	75.900	0.804	0.062	45.700	0.867	0.333
0.200	0.046	7.600	75.900	0.775	0.089	44.600	0.864	0.242
0.200	0.092	7.600	75.900	0.747	0.103	40.500	0.850	0.218
0.090	0.023	3.700	72.800	0.542	0.040	14.500	0.582	0.433
0.090	0.046	3.700	72.800	0.547	0.052	15.100	0.599	0.207
0.090	0.092	3.700	72.800	0.560	0.056	15.800	0.617	0.082
0.090	0.185	3.700	72.800	0.452	0.181	16.500	0.633	0.093
0.125	0.023	3.700	72.800	0.608	0.017	16.200	0.626	1.619
0.125	0.046	3.700	72.800	0.591	0.041	16.500	0.633	0.606
0.125	0.092	3.700	72.800	0.541	0.104	17.100	0.646	0.259
0.125	0.185	3.700	72.800	0.492	0.182	18.600	0.674	0.141
0.177	0.023	3.700	72.800	0.681	0.040	21.800	0.722	0.927
0.177	0.046	3.700	72.800	0.630	0.084	21.200	0.714	0.500
0.177	0.092	3.700	72.800	0.590	0.129	21.600	0.720	0.305
0.177	0.185	3.700	72.800	0.519	0.219	23.200	0.739	0.178
0.218	0.023	3.700	72.800	0.717	0.072	28.800	0.790	0.637
0.218	0.046	3.700	72.800	0.698	0.087	28.300	0.786	0.465
0.218	0.092	3.700	72.800	0.625	0.118	23.600	0.743	0.442
0.218	0.185	3.700	72.800	0.573	0.186	25.200	0.760	0.250
0.090	0.023	5.700	72.800	0.612	0.013	16.200	0.626	0.318
0.090	0.046	5.700	72.800	0.542	0.082	16.100	0.624	0.201
0.090	0.092	5.700	72.800	0.477	0.158	16.600	0.635	0.138

0.090	0.185	5.700	72.800	0.429	0.221	17.300	0.650	0.100
0.125	0.023	5.700	72.800	0.626	0.058	19.200	0.685	0.433
0.125	0.046	5.700	72.800	0.596	0.093	19.500	0.689	0.266
0.125	0.092	5.700	72.800	0.558	0.140	20.100	0.699	0.173
0.125	0.185	5.700	72.800	0.544	0.189	22.800	0.734	0.092
0.177	0.023	5.700	72.800	0.742	0.054	29.800	0.797	0.375
0.177	0.046	5.700	72.800	0.700	0.088	28.600	0.788	0.285
0.177	0.092	5.700	72.800	0.681	0.103	28.200	0.785	0.221
0.177	0.185	5.700	72.800	0.637	0.181	33.300	0.818	0.106
0.210	0.023	5.700	72.800	0.744	0.095	37.800	0.840	0.373
0.210	0.046	5.700	72.800	0.716	0.096	32.400	0.813	0.398
0.210	0.092	5.700	72.800	0.699	0.112	32.200	0.812	0.292
0.210	0.185	5.700	72.800	0.661	0.164	34.800	0.826	0.173
0.090	0.023	6.300	72.800	0.579	0.060	16.800	0.640	0.200
0.090	0.046	6.300	72.800	0.565	0.068	16.500	0.633	0.188
0.090	0.092	6.300	72.800	0.542	0.101	17.000	0.644	0.121
0.090	0.185	6.300	72.800	0.517	0.157	18.600	0.674	0.066
0.125	0.023	6.300	72.800	0.632	0.073	20.600	0.706	0.304
0.125	0.046	6.300	72.800	0.611	0.097	20.800	0.709	0.215
0.125	0.092	6.300	72.800	0.607	0.118	22.100	0.726	0.128
0.125	0.185	6.300	72.800	0.567	0.180	24.000	0.748	0.080
0.177	0.023	6.300	72.800	0.749	0.062	32.200	0.812	0.297
0.177	0.046	6.300	72.800	0.709	0.078	28.500	0.787	0.332
0.177	0.092	6.300	72.800	0.669	0.114	28.100	0.784	0.231
0.177	0.185	6.300	72.800	0.640	0.187	35.300	0.828	0.101
0.200	0.023	6.300	72.800	0.787	0.065	41.300	0.853	0.278
0.200	0.046	6.300	72.800	0.737	0.085	34.200	0.823	0.337
0.200	0.092	6.300	72.800	0.697	0.111	31.700	0.809	0.274
0.200	0.185	6.300	72.800	0.671	0.159	35.900	0.831	0.151

LIQUID AND GAS HOLD-UPS, BED POROSITY, EXPANDED BED HEIGHT, AND WAKE VOLUME TO GAS VOLUME

SOLID = 2.6 MM GRAVEL

LIQUID VELOCITY (FT/SEC)	GAS VELOCITY (FT/SEC)	VISCOSITY (CP)	SURFACE TENSION (DYNE/CM)	LIQUID HOLD-UP	GAS HOLD-UP	BED HEIGHT (INCH)	BED POROSITY	WAKE/GAS VOLUME
0.125	0.046	1.430	39.800	0.298	0.138	25.500	0.437	0.775
0.125	0.092	1.430	39.800	0.277	0.170	26.000	0.447	0.555
0.125	0.185	1.430	39.800	0.259	0.208	27.000	0.468	0.383
0.177	0.046	1.430	39.800	0.337	0.136	27.300	0.474	1.022
0.177	0.092	1.430	39.800	0.327	0.155	27.800	0.483	0.727
0.177	0.185	1.430	39.800	0.291	0.209	28.800	0.501	0.493
0.252	0.046	1.430	39.800	0.421	0.150	33.500	0.571	0.899
0.252	0.092	1.430	39.800	0.380	0.199	34.200	0.580	0.627
0.252	0.185	1.430	39.800	0.340	0.256	35.600	0.596	0.441
0.312	0.046	1.430	39.800	0.503	0.148	41.300	0.652	0.716
0.312	0.092	1.430	39.800	0.478	0.194	43.900	0.672	0.452
0.125	0.046	1.260	50.200	0.355	0.070	25.000	0.425	0.996
0.125	0.092	1.260	50.200	0.341	0.106	26.000	0.447	0.546
0.125	0.185	1.260	50.200	0.336	0.131	27.000	0.468	0.341
0.177	0.046	1.260	50.200	0.385	0.102	28.000	0.487	0.974
0.177	0.092	1.260	50.200	0.366	0.131	28.600	0.498	0.650
0.177	0.185	1.260	50.200	0.364	0.145	29.300	0.510	0.453
0.252	0.046	1.260	50.200	0.459	0.112	33.500	0.571	0.929
0.252	0.092	1.260	50.200	0.434	0.143	34.000	0.577	0.645
0.252	0.185	1.260	50.200	0.399	0.192	35.200	0.592	0.437
0.312	0.046	1.260	50.200	0.526	0.116	40.200	0.642	0.760
0.312	0.092	1.260	50.200	0.507	0.146	41.500	0.654	0.505
0.125	0.046	1.110	60.000	0.404	0.023	25.100	0.428	1.518
0.125	0.092	1.110	60.000	0.394	0.053	26.000	0.447	0.546
0.125	0.185	1.110	60.000	0.378	0.085	26.800	0.464	0.311
0.177	0.046	1.110	60.000	0.423	0.063	28.000	0.487	1.093
0.177	0.092	1.110	60.000	0.413	0.077	28.200	0.490	0.760
0.177	0.185	1.110	60.000	0.394	0.115	29.300	0.510	0.439
0.208	0.092	1.110	60.000	0.463	0.095	32.500	0.558	0.449
0.208	0.185	1.110	60.000	0.432	0.144	33.900	0.576	0.293
0.252	0.046	1.110	60.000	0.515	0.053	33.300	0.568	1.139
0.252	0.092	1.110	60.000	0.482	0.096	34.100	0.579	0.639
0.252	0.185	1.110	60.000	0.458	0.133	35.200	0.592	0.413
0.312	0.046	1.110	60.000	0.548	0.092	40.000	0.641	0.717
0.312	0.092	1.110	60.000	0.524	0.126	41.100	0.650	0.200
0.125	0.046	1.000	72.800	0.408	0.026	25.300	0.432	2.468
0.125	0.092	1.000	72.800	0.400	0.036	25.500	0.437	0.799
0.125	0.185	1.000	72.800	0.393	0.054	26.000	0.447	0.391
0.177	0.046	1.000	72.800	0.444	0.033	27.500	0.477	1.630
0.177	0.092	1.000	72.800	0.440	0.047	28.000	0.487	0.905
0.177	0.185	1.000	72.800	0.425	0.085	29.400	0.511	0.407
0.208	0.046	1.000	72.800	0.481	0.052	30.800	0.533	0.880
0.208	0.092	1.000	72.800	0.472	0.070	31.400	0.542	0.543
0.208	0.185	1.000	72.800	0.451	0.105	32.400	0.556	0.339
0.252	0.046	1.000	72.800	0.524	0.053	34.000	0.577	0.858
0.252	0.092	1.000	72.800	0.509	0.075	34.600	0.585	0.544

0.252	0.185	1.000	72.800	0.477	0.127	36.300	0.604	0.323
0.312	0.046	1.000	72.800	0.562	0.067	38.800	0.630	0.813
0.312	0.092	1.000	72.800	0.542	0.092	39.300	0.634	0.558
0.312	0.185	1.000	72.800	0.530	0.118	40.900	0.649	0.346
0.125	0.046	2.370	72.900	0.436	0.030	26.900	0.466	1.151
0.125	0.092	2.370	72.900	0.419	0.061	27.700	0.481	0.503
0.125	0.185	2.370	72.900	0.409	0.093	28.900	0.503	0.266
0.174	0.046	2.370	72.900	0.486	0.043	30.500	0.529	1.088
0.174	0.092	2.370	72.900	0.458	0.086	31.500	0.544	0.523
0.174	0.185	2.370	72.900	0.445	0.125	33.500	0.571	0.277
0.246	0.046	2.370	72.900	0.559	0.090	41.000	0.649	0.441
0.246	0.092	2.370	72.900	0.544	0.116	42.300	0.660	0.294
0.246	0.185	2.370	72.900	0.537	0.139	44.500	0.677	0.180
0.303	0.046	2.370	72.900	0.624	0.088	50.000	0.712	0.334
0.303	0.092	2.370	72.900	0.606	0.123	53.000	0.729	0.203
0.125	0.046	4.640	75.500	0.482	0.025	29.200	0.508	1.012
0.125	0.092	4.640	75.500	0.478	0.047	30.300	0.526	0.398
0.125	0.185	4.640	75.500	0.449	0.109	32.500	0.558	0.169
0.174	0.046	4.640	75.500	0.574	0.018	35.300	0.593	0.893
0.174	0.092	4.640	75.500	0.566	0.039	36.500	0.606	0.323
0.174	0.185	4.640	75.500	0.537	0.087	38.300	0.625	0.167
0.264	0.046	4.640	75.500	0.660	0.040	48.000	0.700	0.613
0.264	0.092	4.640	75.500	0.639	0.073	50.000	0.712	0.314
0.264	0.185	4.640	75.500	0.619	0.099	51.000	0.718	0.222
0.310	0.046	4.640	75.500	0.742	0.030	63.200	0.772	-0.010
0.310	0.092	4.640	75.500	0.715	0.064	65.500	0.780	0.090
0.310	0.185	4.640	75.500	0.691	0.106	71.000	0.797	0.063
0.125	0.046	7.600	75.900	0.548	0.012	32.700	0.560	0.574
0.125	0.092	7.600	75.900	0.534	0.044	34.100	0.579	0.152
0.125	0.185	7.600	75.900	0.526	0.077	36.300	0.604	0.051
0.174	0.046	7.600	75.900	0.606	0.037	40.300	0.643	0.330
0.174	0.092	7.600	75.900	0.591	0.060	41.300	0.652	0.199
0.174	0.185	7.600	75.900	0.577	0.095	44.000	0.673	0.098
0.265	0.046	7.600	75.900	0.710	0.046	58.900	0.756	0.322
0.265	0.092	7.600	75.900	0.674	0.086	60.200	0.761	0.230
0.265	0.185	7.600	75.900	0.664	0.103	62.000	0.768	0.158
0.307	0.046	7.600	75.900	0.742	0.055	71.000	0.797	0.349
0.307	0.092	7.600	75.900	0.707	0.093	72.000	0.800	0.256
0.125	0.023	12.770	68.900	0.597	0.025	38.000	0.622	-0.110
0.125	0.046	12.770	68.900	0.581	0.069	41.100	0.650	-0.038
0.125	0.092	12.770	68.900	0.575	0.088	42.700	0.663	-0.031
0.125	0.185	12.770	68.900	0.532	0.137	43.500	0.669	0.034
0.177	0.023	12.770	68.900	0.632	0.051	45.500	0.684	0.406
0.177	0.046	12.770	68.900	0.625	0.079	48.600	0.704	0.178
0.177	0.092	12.770	68.900	0.611	0.115	52.500	0.726	0.090
0.177	0.185	12.770	68.900	0.578	0.165	56.000	0.743	0.071
0.230	0.023	12.770	68.900	0.693	0.068	60.500	0.762	0.339
0.230	0.046	12.770	68.900	0.675	0.087	60.400	0.762	0.272
0.230	0.092	12.770	68.900	0.666	0.100	61.500	0.766	0.196
0.230	0.185	12.770	68.900	0.634	0.141	64.000	0.775	0.140
0.280	0.023	12.770	68.900	0.731	0.061	69.300	0.792	0.694
0.280	0.046	12.770	68.900	0.722	0.068	68.500	0.790	0.532
0.280	0.092	12.770	68.900	0.718	0.070	67.800	0.788	0.422
0.090	0.023	8.500	72.800	0.415	0.012	25.100	0.428	3.809
0.090	0.046	8.500	72.800	0.407	0.032	25.600	0.439	1.237
0.090	0.092	8.500	72.800	0.394	0.071	26.900	0.466	0.445
0.090	0.185	8.500	72.800	0.361	0.111	27.200	0.472	0.292
0.125	0.023	8.500	72.800	0.484	0.007	28.300	0.492	6.685
0.125	0.046	8.500	72.800	0.477	0.041	29.800	0.518	0.955
0.125	0.092	8.500	72.800	0.471	0.056	30.400	0.527	0.553
0.125	0.185	8.500	72.800	0.427	0.127	32.300	0.555	0.246

0.177	0.023	8.500	72.800	0.580	0.006	35.400	0.594	6.580
0.177	0.046	8.500	72.800	0.577	0.033	36.900	0.610	0.965
0.177	0.092	8.500	72.800	0.489	0.126	37.400	0.616	0.392
0.177	0.185	8.500	72.800	0.539	0.082	38.000	0.622	0.323
0.218	0.023	8.500	72.800	0.619	0.022	40.100	0.642	2.449
0.218	0.046	8.500	72.800	0.604	0.053	41.900	0.657	0.848
0.218	0.092	8.500	72.800	0.568	0.092	42.400	0.661	0.481
0.218	0.185	8.500	72.800	0.537	0.135	43.900	0.672	0.298
0.090	0.023	20.000	73.500	0.504	0.024	30.500	0.529	0.705
0.090	0.046	20.000	73.500	0.490	0.049	31.200	0.539	0.324
0.090	0.092	20.000	73.500	0.479	0.073	32.100	0.552	0.186
0.090	0.185	20.000	73.500	0.446	0.117	32.900	0.563	0.132
0.125	0.023	20.000	73.500	0.594	0.009	36.300	0.604	1.267
0.125	0.046	20.000	73.500	0.563	0.032	35.500	0.595	0.601
0.125	0.092	20.000	73.500	0.541	0.057	35.800	0.599	0.342
0.125	0.185	20.000	73.500	0.529	0.084	37.200	0.614	0.189
0.177	0.023	20.000	73.500	0.648	0.036	45.600	0.685	0.743
0.177	0.046	20.000	73.500	0.638	0.048	46.000	0.687	0.472
0.177	0.092	20.000	73.500	0.628	0.063	46.600	0.691	0.311
0.177	0.185	20.000	73.500	0.594	0.104	47.600	0.698	0.197
0.218	0.023	20.000	73.500	0.703	0.040	56.000	0.743	0.730
0.218	0.046	20.000	73.500	0.675	0.063	54.800	0.738	0.506
0.218	0.092	20.000	73.500	0.658	0.067	52.500	0.726	0.453
0.218	0.185	20.000	73.500	0.644	0.096	55.500	0.741	0.252

LIQUID AND GAS HOLD-UPS, BED POROSITY, EXPANDED BED HEIGHT, AND WAKE VOLUME TO GAS VOLUME

SOLID = 6 MM GLASS BEADS

LIQUID VELOCITY (FT/SEC)	GAS VELOCITY (FT/SEC)	VISCOSITY (CP)	SURFACE TENSION (DYNE/CM)	LIQUID HOLD-UP	GAS HOLD-UP	BED HEIGHT (INCH)	BED POROSITY	WAKE/GAS VOLUME
0.125	0.046	1.430	39.800	0.313	0.088	22.200	0.401	0.504
0.125	0.185	1.430	39.800	0.290	0.146	23.600	0.436	0.240
0.125	0.360	1.430	39.800	0.249	0.209	24.600	0.459	0.205
0.125	0.527	1.430	39.800	0.243	0.228	25.200	0.472	0.183
0.177	0.046	1.430	39.800	0.363	0.095	24.600	0.459	0.465
0.177	0.185	1.430	39.800	0.326	0.172	26.500	0.498	0.250
0.177	0.360	1.430	39.800	0.295	0.223	27.600	0.518	0.214
0.177	0.527	1.430	39.800	0.298	0.239	28.200	0.528	0.180
0.252	0.046	1.430	39.800	0.403	0.102	26.900	0.505	0.754
0.252	0.185	1.430	39.800	0.351	0.183	28.600	0.535	0.407
0.252	0.360	1.430	39.800	0.327	0.239	30.700	0.567	0.273
0.252	0.527	1.430	39.800	0.314	0.288	33.500	0.603	0.193
0.312	0.046	1.430	39.800	0.455	0.085	28.900	0.540	0.814
0.312	0.185	1.430	39.800	0.379	0.198	31.500	0.578	0.422
0.312	0.360	1.430	39.800	0.347	0.255	33.500	0.603	0.306
0.312	0.527	1.430	39.800	0.342	0.283	35.500	0.625	0.230
0.125	0.046	1.260	50.200	0.304	0.091	22.000	0.395	0.542
0.125	0.185	1.260	50.200	0.281	0.143	23.100	0.424	0.281
0.125	0.360	1.260	50.200	0.239	0.211	24.200	0.450	0.245
0.125	0.527	1.260	50.200	0.197	0.287	25.800	0.484	0.222
0.177	0.046	1.260	50.200	0.329	0.130	24.600	0.459	0.593
0.177	0.185	1.260	50.200	0.307	0.181	26.000	0.488	0.304
0.177	0.360	1.260	50.200	0.264	0.234	26.500	0.498	0.291
0.177	0.527	1.260	50.200	0.238	0.295	28.500	0.583	0.230
0.252	0.046	1.260	50.200	0.373	0.115	26.000	0.488	0.993
0.252	0.185	1.260	50.200	0.329	0.178	27.000	0.507	0.541
0.252	0.360	1.260	50.200	0.310	0.235	29.300	0.546	0.333
0.252	0.527	1.260	50.200	0.296	0.264	30.300	0.561	0.276
0.312	0.046	1.260	50.200	0.413	0.099	27.300	0.513	1.288
0.312	0.185	1.260	50.200	0.362	0.181	29.200	0.544	0.573
0.312	0.360	1.260	50.200	0.334	0.265	33.200	0.599	0.318
0.312	0.527	1.260	50.200	0.315	0.299	34.500	0.614	0.269
0.125	0.046	1.110	60.000	0.305	0.090	22.000	0.395	0.477
0.125	0.185	1.110	60.000	0.262	0.146	22.500	0.409	0.366
0.125	0.360	1.110	60.000	0.249	0.198	24.100	0.443	0.222
0.125	0.527	1.110	60.000	0.206	0.265	25.200	0.472	0.222
0.177	0.046	1.110	60.000	0.360	0.090	24.200	0.450	0.408
0.177	0.185	1.110	60.000	0.332	0.135	25.000	0.468	0.279
0.177	0.360	1.110	60.000	0.273	0.215	26.000	0.488	0.287
0.177	0.527	1.110	60.000	0.261	0.249	27.200	0.511	0.228
0.252	0.046	1.110	60.000	0.393	0.098	26.200	0.492	0.788
0.252	0.185	1.110	60.000	0.342	0.168	27.200	0.511	0.478
0.252	0.360	1.110	60.000	0.321	0.234	29.900	0.555	0.281
0.252	0.527	1.110	60.000	0.304	0.265	30.900	0.569	0.241
0.312	0.046	1.110	60.000	0.421	0.100	27.800	0.521	1.025
0.312	0.185	1.110	60.000	0.383	0.158	29.000	0.541	0.528

0.312	0.360	1.110	60.000	0.356	0.228	32.000	0.584	0.308
0.125	0.046	1.000	72.800	0.322	0.084	22.400	0.406	0.184
0.125	0.185	1.000	72.800	0.283	0.138	23.000	0.422	0.243
0.125	0.527	1.000	72.800	0.262	0.195	24.500	0.457	0.150
0.125	0.854	1.000	72.800	0.241	0.273	27.400	0.514	0.098
0.177	0.046	1.000	72.800	0.394	0.049	23.900	0.443	-0.184
0.177	0.185	1.000	72.800	0.363	0.100	24.800	0.464	0.120
0.177	0.527	1.000	72.800	0.346	0.175	27.800	0.521	0.040
0.177	0.854	1.000	72.800	0.328	0.255	32.000	0.584	0.013
0.252	0.046	1.000	72.800	0.467	0.040	27.000	0.507	-0.987
0.252	0.185	1.000	72.800	0.439	0.091	28.300	0.530	-0.080
0.252	0.527	1.000	72.800	0.424	0.161	32.100	0.585	-0.062
0.252	0.854	1.000	72.800	0.394	0.239	36.300	0.633	-0.020
0.312	0.046	1.000	72.800	0.519	0.026	29.300	0.546	-2.476
0.312	0.185	1.000	72.800	0.477	0.118	32.900	0.595	-0.184
0.312	0.527	1.000	72.800	0.450	0.209	39.100	0.660	-0.084
0.335	0.046	1.000	72.800	0.532	0.029	30.300	0.561	-2.353
0.125	0.046	2.370	75.500	0.365	0.046	22.600	0.411	0.299
0.125	0.185	2.370	75.500	0.334	0.092	23.200	0.427	0.246
0.125	0.360	2.370	75.500	0.329	0.187	27.500	0.516	0.039
0.125	0.527	2.370	75.500	0.292	0.266	30.200	0.559	0.055
0.174	0.046	2.370	75.500	0.428	0.042	25.100	0.470	0.014
0.174	0.185	2.370	75.500	0.379	0.112	26.200	0.492	0.208
0.174	0.360	2.370	75.500	0.358	0.166	28.000	0.525	0.135
0.174	0.527	2.370	75.500	0.332	0.239	31.100	0.572	0.095
0.246	0.046	2.370	75.500	0.477	0.063	29.000	0.541	0.108
0.246	0.185	2.370	75.500	0.453	0.117	31.000	0.571	0.088
0.246	0.360	2.370	75.500	0.432	0.158	32.500	0.591	0.086
0.290	0.046	2.370	75.500	0.510	0.039	29.500	0.549	0.473
0.290	0.185	2.370	75.500	0.495	0.089	32.000	0.584	0.099
0.290	0.360	2.370	75.500	0.481	0.118	33.300	0.600	0.079
0.125	0.046	4.640	75.500	0.411	0.010	23.000	0.422	0.497
0.125	0.185	4.640	75.500	0.402	0.055	24.500	0.457	0.029
0.125	0.360	4.640	75.500	0.380	0.144	28.000	0.525	0.000
0.125	0.527	4.640	75.500	0.343	0.239	31.900	0.583	0.019
0.174	0.046	4.640	75.500	0.451	0.029	25.600	0.480	0.588
0.174	0.185	4.640	75.500	0.430	0.079	27.100	0.509	0.186
0.174	0.360	4.640	75.500	0.398	0.135	28.500	0.533	0.147
0.174	0.527	4.640	75.500	0.375	0.210	32.100	0.585	0.083
0.264	0.046	4.640	75.500	0.498	0.043	29.000	0.541	1.313
0.264	0.185	4.640	75.500	0.477	0.124	33.400	0.602	0.226
0.264	0.360	4.640	75.500	0.458	0.163	35.200	0.622	0.154
0.264	0.527	4.640	75.500	0.445	0.218	39.600	0.664	0.083
0.303	0.046	4.640	75.500	0.532	0.021	29.800	0.553	2.935
0.303	0.185	4.640	75.500	0.504	0.113	34.800	0.618	0.294
0.303	0.360	4.640	75.500	0.498	0.154	38.000	0.650	0.142
0.125	0.046	7.600	75.900	0.448	0.019	25.000	0.468	-0.436
0.125	0.185	7.600	75.900	0.419	0.112	28.400	0.531	-0.033
0.125	0.360	7.600	75.900	0.394	0.214	34.000	0.609	-0.025
0.125	0.527	7.600	75.900	0.361	0.274	36.500	0.635	0.003
0.174	0.046	7.600	75.900	0.506	0.003	27.100	0.509	-0.991
0.174	0.185	7.600	75.900	0.461	0.087	29.500	0.549	0.097
0.174	0.360	7.600	75.900	0.438	0.178	34.700	0.616	0.020
0.174	0.527	7.600	75.900	0.405	0.240	37.500	0.645	0.002
0.265	0.046	7.600	75.900	0.525	0.050	31.400	0.576	1.038
0.265	0.185	7.600	75.900	0.498	0.134	36.300	0.633	0.214
0.265	0.360	7.600	75.900	0.480	0.189	40.200	0.669	0.115
0.265	0.527	7.600	75.900	0.476	0.259	50.200	0.735	0.028
0.307	0.046	7.600	75.900	0.542	0.086	35.800	0.628	0.688
0.307	0.185	7.600	75.900	0.529	0.137	39.900	0.666	0.219
0.307	0.360	7.600	75.900	0.516	0.196	46.300	0.712	0.088

0.125	0.046	12.770	68.900	0.418	0.015	23.500	0.434	2.381
0.125	0.092	12.770	68.900	0.422	0.039	24.700	0.461	0.577
0.125	0.185	12.770	68.900	0.413	0.065	25.500	0.478	0.285
0.177	0.046	12.770	68.900	0.543	0.008	29.700	0.552	-0.813
0.177	0.092	12.770	68.900	0.535	0.018	29.800	0.553	-0.113
0.177	0.185	12.770	68.900	0.507	0.063	31.000	0.571	0.074
0.230	0.046	12.770	68.900	0.562	0.002	30.500	0.564	14.232
0.230	0.092	12.770	68.900	0.553	0.024	31.500	0.578	0.954
0.230	0.185	12.770	68.900	0.544	0.056	33.300	0.600	0.294
0.280	0.046	12.770	68.900	0.596	0.013	34.100	0.610	2.861
0.280	0.092	12.770	68.900	0.576	0.039	34.600	0.615	0.962
0.280	0.185	12.770	68.900	0.535	0.084	35.000	0.620	0.517
0.315	0.046	12.770	68.900	0.598	0.021	35.000	0.620	3.009
0.315	0.092	12.770	68.900	0.576	0.047	35.300	0.623	1.279
0.315	0.185	12.770	68.900	0.531	0.096	35.800	0.628	0.647
0.125	0.046	8.500	72.800	0.473	0.021	26.300	0.494	-1.478
0.125	0.185	8.500	72.800	0.438	0.069	26.900	0.505	-0.097
0.125	0.360	8.500	72.800	0.405	0.139	29.200	0.544	-0.004
0.125	0.527	8.500	72.800	0.383	0.224	32.300	0.588	0.027
0.125	0.854	8.500	72.800	0.258	0.362	35.000	0.620	0.079
0.177	0.046	8.500	72.800	0.506	0.036	29.100	0.543	-0.330
0.177	0.185	8.500	72.800	0.450	0.108	30.100	0.558	0.121
0.177	0.360	8.500	72.800	0.434	0.132	30.700	0.567	0.106
0.177	0.527	8.500	72.800	0.406	0.194	33.300	0.600	0.081
0.252	0.046	8.500	72.800	0.556	0.054	34.200	0.611	0.047
0.252	0.185	8.500	72.800	0.542	0.081	35.300	0.623	0.058
0.252	0.360	8.500	72.800	0.487	0.143	36.000	0.630	0.147
0.252	0.527	8.500	72.800	0.443	0.208	38.200	0.652	0.135
0.298	0.046	8.500	72.800	0.603	0.046	38.000	0.650	-0.124
0.298	0.185	8.500	72.800	0.556	0.109	39.800	0.666	0.117
0.298	0.360	8.500	72.800	0.518	0.157	41.000	0.675	0.134
0.125	0.046	13.000	73.000	0.469	0.003	25.200	0.472	-1.285
0.125	0.092	13.000	73.000	0.451	0.027	25.500	0.478	0.109
0.125	0.185	13.000	73.000	0.441	0.049	26.100	0.490	0.085
0.125	0.360	13.000	73.000	0.415	0.113	28.200	0.528	0.054
0.125	0.527	13.000	73.000	0.387	0.164	29.700	0.552	0.060
0.177	0.046	13.000	73.000	0.516	0.010	28.100	0.526	0.847
0.177	0.092	13.000	73.000	0.528	0.006	28.600	0.535	0.095
0.177	0.185	13.000	73.000	0.512	0.036	29.500	0.549	0.076
0.177	0.360	13.000	73.000	0.468	0.089	30.100	0.558	0.152
0.177	0.527	13.000	73.000	0.436	0.149	32.100	0.585	0.112
0.218	0.046	13.000	73.000	0.539	0.006	29.300	0.546	4.623
0.218	0.092	13.000	73.000	0.528	0.088	30.700	0.567	0.602
0.218	0.185	13.000	73.000	0.515	0.057	31.100	0.572	0.383
0.218	0.360	13.000	73.000	0.458	0.127	32.100	0.585	0.256
0.218	0.527	13.000	73.000	0.370	0.247	34.800	0.618	0.198
0.252	0.046	13.000	73.000	0.562	0.006	30.800	0.568	6.752
0.252	0.092	13.000	73.000	0.574	0.009	31.900	0.583	3.267
0.252	0.185	13.000	73.000	0.565	0.035	33.300	0.600	0.561
0.252	0.360	13.000	73.000	0.552	0.060	34.400	0.613	0.239
0.281	0.046	13.000	73.000	0.592	0.020	34.300	0.612	1.637
0.281	0.092	13.000	73.000	0.560	0.062	35.200	0.622	0.614
0.281	0.185	13.000	73.000	0.541	0.103	37.500	0.645	0.299
0.281	0.360	13.000	73.000	0.526	0.131	38.800	0.657	0.205
0.312	0.046	13.000	73.000	0.621	0.023	37.500	0.645	1.189
0.312	0.092	13.000	73.000	0.602	0.060	39.500	0.663	0.411
0.312	0.185	13.000	73.000	0.597	0.077	41.000	0.675	0.229
0.335	0.046	13.000	73.000	0.631	0.037	40.100	0.668	0.861
0.335	0.092	13.000	73.000	0.603	0.072	41.100	0.676	0.486
0.335	0.185	13.000	73.000	0.597	0.108	45.200	0.705	0.197
0.129	0.046	20.000	73.900	0.510	0.014	28.000	0.525	-1.353

0.125	0.185	20.000	73.500	0.474	0.078	29.700	0.552	-0.066
0.125	0.360	20.000	73.500	0.431	0.156	32.200	0.587	0.016
0.125	0.527	20.000	73.500	0.397	0.202	33.200	0.599	0.042
0.177	0.046	20.000	73.500	0.550	0.023	31.200	0.573	-0.123
0.177	0.185	20.000	73.500	0.498	0.093	32.500	0.591	0.133
0.177	0.360	20.000	73.500	0.454	0.149	33.600	0.604	0.129
0.177	0.527	20.000	73.500	0.410	0.209	35.000	0.620	0.121
0.252	0.046	20.000	73.500	0.642	0.030	40.600	0.672	-0.593
0.252	0.185	20.000	73.500	0.617	0.072	42.900	0.690	-0.086
0.252	0.360	20.000	73.500	0.556	0.141	44.000	0.697	0.068
0.270	0.046	20.000	73.500	0.651	0.045	44.000	0.697	-0.388
0.270	0.185	20.000	73.500	0.635	0.074	45.900	0.710	-0.110
0.270	0.360	20.000	73.500	0.578	0.138	47.000	0.717	0.052
0.298	0.046	20.000	73.500	0.691	0.027	47.300	0.718	-0.917
0.125	0.046	70.000	73.800	0.599	0.007	33.800	0.606	-2.867
0.125	0.092	70.000	73.800	0.566	0.034	33.300	0.600	-0.200
0.125	0.185	70.000	73.800	0.534	0.056	32.500	0.591	0.044
0.125	0.360	70.000	73.800	0.517	0.087	33.700	0.605	0.038
0.177	0.046	70.000	73.800	0.660	0.020	41.600	0.680	-0.784
0.177	0.092	70.000	73.800	0.647	0.030	41.200	0.677	-0.275
0.177	0.185	70.000	73.800	0.584	0.089	40.800	0.674	0.083
0.177	0.360	70.000	73.800	0.512	0.154	39.900	0.666	0.128
0.221	0.046	70.000	73.800	0.707	0.025	49.800	0.733	-0.542
0.221	0.092	70.000	73.800	0.700	0.027	48.900	0.728	-0.269
0.221	0.185	70.000	73.800	0.643	0.075	47.200	0.718	0.112
0.221	0.290	70.000	73.800	0.608	0.106	46.600	0.714	0.135
0.252	0.046	70.000	73.800	0.765	0.007	58.600	0.773	-3.109
0.252	0.092	70.000	73.800	0.732	0.032	54.600	0.765	-0.225
0.252	0.138	70.000	73.800	0.684	0.073	55.000	0.758	0.090
0.281	0.046	70.000	73.800	0.764	0.030	64.700	0.794	-0.336
0.281	0.092	70.000	73.800	0.731	0.054	62.000	0.785	0.068

APPENDIX H

LIQUID PHASE AXIAL MIXING DATA IN TWO AND THREE PHASE FLUIDIZED BEDS.

LIQUID PHASE AXIAL MIXING IN LIQUID-GAS BEDS

TRACER INJECTION = PULSE

LIQUID VELOCITY (FT/SEC)	GAS VELOCITY (FT/SEC)	LIQUID HMU (FT)
0.125	0.046	2.319
0.125	0.185	2.759
0.125	0.527	3.729
0.125	0.854	4.620
0.177	0.046	2.069
0.177	0.185	2.049
0.177	0.527	3.180
0.177	0.854	3.480
0.252	0.046	1.789
0.252	0.185	2.139
0.252	0.527	2.639
0.252	0.854	2.819
0.312	0.046	1.620
0.312	0.185	1.899
0.312	0.527	2.499
0.312	0.854	2.499
0.335	0.046	1.500
0.335	0.185	1.819
0.335	0.527	2.599

LIQUID PHASE AXIAL MIXING IN LIQUID-GAS BEDS

TRACER INJECTION = STEP

LIQUID VELOCITY (FT/SEC)	GAS VELOCITY (FT/SEC)	LIQUID HMU (FT)
0.125	0.046	2.789
0.125	0.185	3.000
0.177	0.046	2.289
0.177	0.185	2.529
0.177	0.527	3.199
0.252	0.046	1.669
0.252	0.185	2.049
0.252	0.527	2.789
0.312	0.046	1.199
0.312	0.185	1.889
0.312	0.527	2.259
0.335	0.046	1.359
0.335	0.185	1.769
0.335	0.527	1.999

4 4

OF/DE

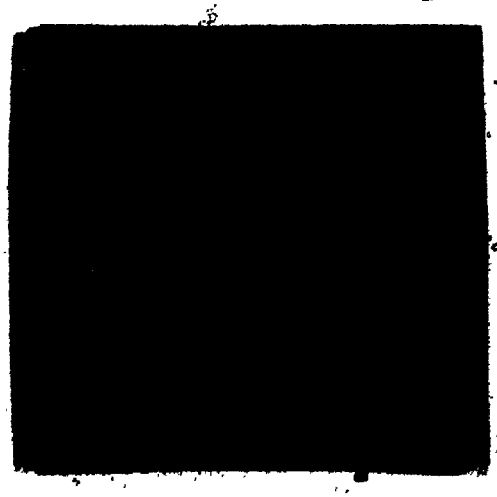

LIQUID PHASE AXIAL MIXING IN LIQUID*SOLID BEDS

****

TRACER TECHNIQUE: PULSE

LIQUID VELOCITY (FT/SEC)	PARTICLE SIZE (mm)	LIQUID HMU (FT)	HMU/Ho
0.125	6.0	0.1259	0.0703
0.177	6.0	0.1349	0.0753
0.252	6.0	0.2239	0.1250
0.312	6.0	0.3249	0.1813
0.335	6.0	0.3499	0.1953
0.125	2.6	0.2309	0.1289
0.177	2.6	0.3469	0.1936
0.252	2.6	0.4669	0.2606
0.312	2.6	0.6489	0.3622
0.335	2.6	0.7369	0.4113

TRACER TECHNIQUE: STEP

0.125	6.0	0.0492	0.0275
0.177	6.0	0.0626	0.0349
0.252	6.0	0.0989	0.0552
0.312	6.0	0.1149	0.0641
0.125	2.6	0.2119	0.1183
0.177	2.6	0.3509	0.1958
0.252	2.6	0.5229	0.2919
0.312	2.6	0.7899	0.4409
0.335	2.6	0.8399	0.4688
0.090	1.0	0.1009	0.1212
0.125	1.0	0.1169	0.1404
0.177	1.0	0.1289	0.1547
0.210	1.0	0.1449	0.1739
0.252	1.0	0.1710	0.2052

LIQUID PHASE AXIAL MIXING IN THREE PHASE FLUIDIZED BED

SOLID = 6 MM GLASS BEADS --- PULSE

LIQUID VELOCITY (FT/SEC)	GAS VELOCITY (FT/SEC)	LIQUID HMU (FT)	HMU/HO
0.125	0.046	0.270	0.150
0.125	0.185	0.603	0.336
0.125	0.527	0.880	0.491
0.125	0.854	1.140	0.636
0.177	0.046	0.357	0.199
0.177	0.185	0.735	0.410
0.177	0.527	1.040	0.580
0.177	0.854	1.300	0.725
0.252	0.046	0.476	0.265
0.252	0.185	0.869	0.485
0.252	0.527	1.270	0.708
0.252	0.854	1.530	0.853
0.312	0.046	0.652	0.363
0.312	0.185	1.200	0.669
0.312	0.527	1.560	0.870
0.312	0.854	1.800	1.004
0.335	0.046	0.681	0.380
0.335	0.185	1.300	0.725
0.335	0.527	1.710	0.954
0.335	0.854	2.000	1.116

LIQUID PHASE AXIAL MIXING IN THREE PHASE FLUIDIZED BED

SOLID = 6 MM GLASS BEADS --- STEP

LIQUID VELOCITY (FT/SEC)	GAS VELOCITY (FT/SEC)	LIQUID HMU (FT)	HMU/HO
0.125	C.046	0.303	0.169
0.125	0.185	0.532	0.296
0.125	C.527	0.725	0.404
0.125	0.854	0.952	0.531
0.177	C.046	0.437	0.243
0.177	0.185	0.640	0.357
0.177	0.527	0.869	0.485
0.177	0.854	1.150	0.641
0.252	C.046	0.540	0.301
0.252	0.185	0.833	0.464
0.252	0.527	1.270	0.708
0.252	0.854	1.400	0.781
0.312	C.046	0.610	0.340
0.312	0.185	0.882	0.492
0.312	0.527	1.400	0.781
C.312	C.854	1.700	0.948

LIQUID PHASE AXIAL MIXING IN THREE PHASE FLUIDIZED BED

SOLID = 2.6 MM GRAVEL --- PULSE

LIQUID VELOCITY (FT/SEC)	GAS VELOCITY (FT/SEC)	LIQUID HMU (FT)	HMU/HO
0.125	0.046	0.581	0.324
0.125	0.185	0.833	0.464
0.177	0.046	0.697	0.389
0.177	0.185	1.030	0.574
0.252	0.046	0.880	0.491
0.252	0.185	1.130	0.630
0.312	0.046	0.985	0.549
0.312	0.185	1.340	0.747
0.335	0.046	1.050	0.586
0.335	0.185	1.400	0.781

LIQUID PHASE AXIAL MIXING IN THREE PHASE FLUIDIZED BED

SOLID = 2.6 MM GRAVEL --- STEP

LIQUID VELOCITY (FT/SEC)	GAS VELOCITY (FT/SEC)	LIQUID HMU (FT)	HMU/HO
0.125	0.046	0.704	0.392
0.125	0.185	0.810	0.452
0.177	0.046	0.820	0.457
0.177	0.185	0.944	0.526
0.252	0.046	0.956	0.533
0.252	0.185	1.190	0.664
0.312	0.046	1.150	0.641
0.312	0.185	1.400	0.781
0.335	0.046	1.250	0.697

LIQUIC PHASE AXIAL MIXING IN THREE PHASE FLUIDIZED BED

SOLID = 1 MM GLASS BEADS --- STEP

LIQUIC VELOCITY (FT/SEC)	GAS VELOCITY (FT/SEC)	LIQUID HMU (FT)	HMU/HO
0.090	0.023	0.124	0.148
0.090	0.046	0.132	0.158
0.090	0.092	0.137	0.164
0.090	0.185	0.170	0.204
0.125	0.023	0.134	0.160
0.125	0.046	0.138	0.165
0.125	0.092	0.143	0.171
0.125	0.185	0.188	0.225
0.177	0.023	0.148	0.177
0.177	0.046	0.164	0.196
0.177	0.092	0.173	0.207
0.177	0.185	0.222	0.266
0.210	0.023	0.158	0.189
0.210	0.046	0.176	0.211
0.210	0.092	0.188	0.225
0.210	0.185	0.236	0.283
0.252	0.023	0.173	0.207

APPENDIX I

BUBBLE SIZE AND RISING VELOCITY DATA IN LIQUID-GAS AND THREE PHASE FLUIDIZED BEDS.

BUBBLE SIZE AND RISING VELOCITY IN LIQUID•GAS BEDS

LIQUID VELOCITY (FT/SEC)	GAS VELOCITY (FT/SEC)	LIQUID VISCOSITY (CP)	SURFACE TENSION (DYNE/CM)	BUBBLE SIZE (FT)	ABS. BUBBLE VELOCITY (FT/SEC)	RELATIVE BUBBLE VELO. (FT/SEC)
0.125	0.046	1.460	39.800	0.132	2.450	2.320
0.125	0.092	1.460	39.800	0.157	2.730	2.590
0.125	0.185	1.460	39.800	0.228	4.020	3.870
0.125	0.360	1.460	39.800	0.234	4.840	4.690
0.125	0.527	1.460	39.800	0.307	6.090	5.920
0.177	0.046	1.460	39.800	0.105	2.430	2.380
0.177	0.092	1.460	39.800	0.119	2.968	2.780
0.177	0.185	1.460	39.800	0.152	3.267	3.060
0.177	0.360	1.460	39.800	0.214	5.250	5.030
0.177	0.527	1.460	39.800	0.309	6.720	6.470
0.252	0.185	1.460	39.800	0.140	3.350	3.050
0.252	0.360	1.460	39.800	0.199	3.960	3.630
0.312	0.185	1.460	39.800	0.096	3.560	3.200
0.125	0.046	1.260	50.200	0.117	2.550	2.420
0.125	0.185	1.260	50.200	0.168	3.520	3.380
0.125	0.360	1.260	50.200	0.197	2.480	5.320
0.125	0.527	1.260	50.200	0.228	6.140	5.970
0.177	0.046	1.260	50.200	0.107	2.430	2.250
0.177	0.185	1.260	50.200	0.154	3.410	3.200
0.177	0.527	1.260	50.200	0.233	5.060	4.810
0.252	0.092	1.260	50.200	0.106	2.600	2.330
0.252	0.185	1.260	50.200	0.135	3.350	3.050
0.252	0.360	1.260	50.200	0.166	3.770	3.430
0.252	0.527	1.260	50.200	0.203	5.220	4.860
0.312	0.185	1.260	50.200	0.100	2.750	2.380
0.125	0.046	1.000	72.800	0.099	3.000	2.870
0.125	0.185	1.000	72.800	0.137	4.580	4.440
0.125	0.527	1.000	72.800	0.219	6.380	6.230
0.177	0.046	1.000	72.800	0.094	2.770	2.590
0.177	0.185	1.000	72.800	0.135	4.250	4.050
0.177	0.527	1.000	72.800	0.206	6.230	6.010
0.252	0.046	1.000	72.800	0.084	2.880	2.620
0.252	0.185	1.000	72.800	0.131	4.030	3.740
0.252	0.527	1.000	72.800	0.185	6.120	5.800
0.312	0.185	1.000	72.800	0.121	3.680	3.310
0.312	0.527	1.000	72.800	0.160	6.000	5.600
0.335	0.185	1.000	72.800	0.116	4.010	3.620
0.335	0.527	1.000	72.800	0.144	5.950	5.510
0.125	0.046	2.370	72.900	0.119	2.190	2.060
0.125	0.185	2.370	72.900	0.160	4.130	3.990
0.125	0.360	2.370	72.900	0.255	5.250	5.100
0.125	0.527	2.370	72.900	0.265	5.960	5.800
0.174	0.046	2.370	72.900	0.099	2.900	2.730
0.174	0.092	2.370	72.900	0.125	2.720	2.544
0.174	0.185	2.370	72.900	0.145	3.560	3.384
0.174	0.527	2.370	72.900	0.280	6.200	5.980
0.246	0.185	2.370	72.900	0.141	3.320	3.050
0.246	0.360	2.370	72.900	0.218	5.350	5.020
0.246	0.527	2.370	72.900	0.244	5.680	5.330

0.310	0.185	2.370	72.9C0	0.145	3.450	3.090
0.125	C.046	7.600	75.9C0	0.118	2.670	2.540
0.125	0.185	7.600	75.900	0.133	3.430	3.290
0.125	0.360	7.600	75.9C0	0.155	4.490	4.340
0.125	0.527	7.600	75.9C0	0.177	5.880	5.720
C.174	C.046	7.600	75.9C0	0.129	2.680	2.500
0.174	0.092	7.600	75.9C0	0.131	2.750	2.560
0.174	0.185	7.600	75.9C0	0.151	3.980	3.790
C.174	C.360	7.600	75.9C0	0.183	5.240	5.030
0.174	0.527	7.600	75.9C0	0.214	6.150	5.940
0.265	0.092	7.600	75.9C0	0.117	2.530	2.240
C.265	0.185	7.600	75.9C0	0.151	3.300	2.990
0.265	0.527	7.600	75.9C0	0.206	5.430	5.090
0.307	C.185	7.600	75.9C0	0.135	4.210	3.850
0.125	C.046	20.000	73.5C0	0.112	1.850	1.720
0.125	0.C92	20.000	73.500	0.114	2.400	2.270
0.125	0.185	20.000	73.5C0	0.139	2.930	2.790
0.125	0.360	20.000	73.5C0	0.165	4.420	4.270
C.125	C.527	20.CC0	73.5C0	0.185	5.520	5.370
0.177	0.046	20.000	73.5C0	0.114	2.330	2.150
0.177	0.092	20.000	73.5C0	0.119	2.540	2.350
C.177	C.185	20.000	73.5C0	0.133	3.160	2.960
0.177	0.360	20.000	73.5C0	0.[illegible]	4.630	4.420
C.177	C.527	20.000	73.5C0	0.212	5.380	5.160
0.218	C.092	20.000	73.5C0	0.107	2.230	1.990
C.218	0.185	20.000	73.5C0	0.115	3.150	2.910
0.218	0.360	20.000	73.5C0	0.155	4.120	3.870
0.218	0.527	20.CC0	73.5C0	0.188	5.380	5.110
C.125	C.046	70.000	73.8C0	0.118	2.830	2.700
0.125	0.092	70.000	73.8C0	0.135	3.230	3.100
0.125	0.185	7C.000	73.8C0	0.141	3.580	3.450
C.125	C.360	70.000	73.8C0	0.151	3.750	3.610
0.125	0.527	70.000	73.8C0	0.188	4.580	4.430
0.177	0.046	70.000	73.8C0	0.143	2.990	2.800
0.177	0.185	70.000	73.8C0	0.166	3.430	3.240
C.177	0.360	70.000	73.8C0	0.185	4.420	4.220
0.177	0.527	70.000	73.8C0	0.194	5.720	5.500
0.210	C.046	70.000	73.8C0	0.119	3.130	2.900
C.210	C.092	70.000	73.8C0	0.135	3.610	3.380
0.210	0.185	70.000	73.8C0	0.145	3.590	3.360
0.210	0.360	70.000	73.8C0	0.165	4.820	4.570
C.210	C.527	70.000	73.8C0	0.212	5.160	4.890
0.252	0.046	70.000	73.8C0	0.117	2.990	2.730
0.252	0.185	70.000	73.8C0	0.140	3.920	3.650
C.252	0.360	70.000	73.8C0	0.180	4.610	4.320
0.252	0.527	70.000	73.8C0	0.205	4.830	4.530

BUBBLE SIZE AND RISING VELOCITY IN THREE PHASE FLUIDIZED BEDS

SOLID = 1 MM GLASS BEADS

LIQUID VELOCITY (FT/SEC)	GAS VELOCITY (FT/SEC)	LIQUID VISCOSITY (CP)	SURFACE TENSION (DYNE/CM)	BUBBLE SIZE (FT)	ABS. BUBBLE VELOCITY (FT/SEC)	RELATIVE BUBBLE VELO. (FT/SEC)
0.125	C.046	1.430	39.800	0.140	1.970	1.710
0.125	0.092	1.430	39.800	0.148	2.790	2.530
0.125	0.185	1.430	39.800	0.192	4.150	3.860
0.177	0.092	1.430	39.800	0.137	2.390	2.060
0.177	0.185	1.430	39.800	0.199	3.739	3.376
0.218	0.185	1.430	39.800	0.186	3.079	2.696
0.125	C.046	1.260	50.200	0.125	2.010	1.740
0.125	C.092	1.260	50.200	0.145	2.350	2.070
C.125	0.185	1.260	50.200	0.177	2.885	2.577
0.177	C.046	1.260	50.200	0.113	1.600	1.280
0.177	0.092	1.260	50.200	0.149	2.360	2.020
0.177	0.185	1.260	50.200	0.169	2.746	2.362
0.218	0.092	1.260	50.200	0.107	2.020	1.670
0.218	0.185	1.260	50.200	0.143	2.512	2.127
0.125	C.023	1.000	72.800	0.139	1.980	1.680
0.125	0.046	1.000	72.800	0.140	2.180	1.860
0.125	C.092	1.000	72.800	0.149	2.230	1.890
0.125	0.185	1.000	72.800	0.168	2.360	2.000
0.177	0.023	1.000	72.800	0.114	2.090	1.760
0.177	C.046	1.000	72.800	0.141	2.390	2.030
0.177	0.092	1.000	72.800	0.156	2.670	2.270
0.177	0.185	1.000	72.800	0.163	2.810	2.400
0.252	C.046	1.000	72.800	0.147	2.590	2.200
0.252	C.092	1.000	72.800	0.168	2.940	2.530
0.252	0.185	1.000	72.800	0.203	3.290	2.820
0.125	0.185	4.640	75.500	0.192	1.940	1.710
0.200	0.185	4.640	75.500	0.116	2.780	2.470
0.125	0.046	5.700	72.800	0.145	2.190	1.980
0.125	0.092	5.700	72.800	0.155	2.230	2.010
0.125	0.185	5.700	72.800	0.166	3.003	2.771
0.177	C.046	5.700	72.800	0.149	2.280	2.030
0.177	0.092	5.700	72.800	0.152	3.308	3.043
0.177	0.185	5.700	72.800	0.158	3.500	3.220
0.207	0.046	5.700	72.800	0.114	2.450	2.160
0.207	0.092	5.700	72.800	0.150	3.060	2.760
0.207	0.185	5.700	72.800	0.165	4.230	3.910
C.090	0.046	6.300	72.800	0.134	1.980	1.820
C.090	C.092	6.300	72.800	0.140	2.130	1.960
C.090	0.185	6.300	72.800	0.163	2.730	2.560
C.125	0.046	6.300	72.800	0.122	1.910	1.710
0.125	0.092	6.300	72.800	0.145	2.350	2.150
0.125	0.185	6.300	72.800	0.177	2.910	2.690
0.090	0.046	6.300	72.800	0.127	1.680	1.520
0.090	0.092	6.300	72.800	0.137	2.190	2.020
C.125	0.046	6.300	72.800	0.133	2.220	2.020
0.125	C.092	6.300	72.800	0.136	2.610	2.410

0.125	0.185	6.300	72.800	0.150	3.210	3.005
0.174	0.046	6.300	72.800	0.136	2.100	1.870
0.174	0.092	6.300	72.800	0.141	2.790	2.560
0.174	0.185	6.300	72.800	0.156	4.000	3.760
0.200	0.046	6.300	72.800	0.115	2.430	2.170
0.200	0.092	6.300	72.800	0.136	2.560	2.290
0.200	0.185	6.300	72.800	0.159	3.070	2.790

BUBBLE SIZE AND RISING VELOCITY IN THREE PHASE FLUIDIZED BEDS

SOLID = 2.6 MM GRAVEL

LIQUID VELOCITY (FT/SEC)	GAS VELOCITY (FT/SEC)	LIQUID VISCOSITY (CP)	SURFACE TENSION (DYNE/CM)	BUBBLE SIZE (FT)	ABS. BUBBLE VELOCITY (FT/SEC)	RELATIVE BUBBLE VELO. (FT/SEC)
0.125	0.092	1.430	39.800	0.121	2.878	2.420
0.125	0.185	1.430	39.800	0.172	3.550	3.070
0.177	0.092	1.430	39.800	0.126	2.610	2.070
0.177	0.185	1.430	39.800	0.159	3.070	2.460
0.252	0.092	1.430	39.800	0.100	1.990	1.330
0.252	0.185	1.430	39.800	0.163	3.290	2.550
0.312	0.185	1.430	39.800	0.175	4.470	3.780
0.125	0.046	1.260	50.200	0.103	2.300	1.950
0.125	0.092	1.260	50.200	0.121	3.000	2.640
0.125	0.185	1.260	50.200	0.160	3.570	3.200
0.177	0.046	1.260	50.200	0.107	2.410	1.950
0.177	0.092	1.260	50.200	0.121	2.690	2.200
0.177	0.185	1.260	50.200	0.142	3.300	2.820
0.252	0.092	1.260	50.200	0.107	2.720	2.140
0.252	0.185	1.260	50.200	0.155	3.590	2.960
0.312	0.185	1.260	50.200	0.175	3.860	3.220
0.125	0.046	1.000	72.800	0.047	2.730	2.420
0.125	0.185	1.000	72.800	0.078	3.770	3.450
0.177	0.046	1.000	72.800	0.054	2.810	2.410
0.177	0.185	1.000	72.800	0.094	3.890	3.480
0.252	0.046	1.000	72.800	0.067	2.890	2.410
0.252	0.185	1.000	72.800	0.094	3.830	3.300
0.280	0.046	1.000	72.800	0.069	2.950	2.400
0.280	0.185	1.000	72.800	0.107	4.150	3.560
0.125	0.046	2.370	72.900	0.093	2.388	2.090
0.125	0.092	2.370	72.900	0.139	2.840	2.540
0.125	0.185	2.370	72.900	0.159	3.340	3.040
0.174	0.046	2.370	72.900	0.135	2.320	1.960
0.174	0.092	2.370	72.900	0.140	2.800	2.420
0.174	0.185	2.370	72.900	0.173	3.190	2.800
0.246	0.092	2.370	72.900	0.140	2.010	1.560
0.246	0.185	2.370	72.900	0.142	2.810	2.350
0.303	0.185	2.370	72.900	0.187	2.820	2.370
0.125	0.046	7.600	75.900	0.140	2.500	2.270
0.125	0.092	7.600	75.900	0.147	2.600	2.370
0.125	0.185	7.600	75.900	0.169	3.400	3.160
0.174	0.046	7.600	75.900	0.133	2.700	2.410
0.174	0.092	7.600	75.900	0.146	3.210	2.920
0.174	0.185	7.600	75.900	0.175	3.480	3.180
0.265	0.046	7.600	75.900	0.123	2.630	2.260
0.265	0.185	7.600	75.900	0.185	3.840	3.440
0.307	0.185	7.600	75.900	0.185	3.750	3.300
0.125	0.046	12.770	68.900	0.133	2.600	2.390
0.125	0.092	12.770	68.900	0.154	2.700	2.480
0.125	0.185	12.770	68.900	0.187	3.350	3.120
0.177	0.046	12.770	68.900	0.141	2.130	1.850

0.177	0.092	12.770	68.900	0.145	2.420	2.130
0.177	0.185	12.770	68.900	0.187	3.630	3.320
0.237	0.046	12.770	68.900	0.141	2.030	1.690
0.237	0.092	12.770	68.900	0.157	2.540	2.200
0.237	0.185	12.770	68.900	0.188	3.770	3.410
0.092	0.092	8.500	72.800	0.102	2.440	2.210
0.092	0.185	8.500	72.800	0.115	2.760	2.510
0.125	0.185	8.500	72.800	0.123	3.300	3.000
0.218	0.092	8.500	72.800	0.107	2.500	2.120
0.218	0.185	8.500	72.800	0.120	2.980	2.580
0.092	0.185	20.000	73.500	0.119	2.910	2.710
0.177	0.046	20.000	73.500	0.105	2.300	2.020
0.177	0.092	20.000	73.500	0.123	2.730	2.450
0.177	0.185	20.000	73.500	0.145	3.930	3.630
0.218	0.046	20.000	73.500	0.107	2.370	2.050
0.218	0.092	20.000	73.500	0.118	2.890	2.560
0.218	0.185	20.000	73.500	0.141	3.580	3.240
0.257	0.046	20.000	73.500	0.099	2.410	2.200
0.257	0.092	20.000	73.500	0.125	2.950	2.740

BUBBLE SIZE AND RISING VELOCITY IN THREE PHASE FLUIDIZED BEDS

SOLID = 6 MM GLASS BEADS

LIQUID VELOCITY (FT/SEC)	GAS VELOCITY (FT/SEC)	LIQUID VISCOSITY (CP)	SURFACE TENSION (DYNE/CM)	BUBBLE SIZE (FT)	ABS. BUBBLE VELOCITY (FT/SEC)	RELATIVE BUBBLE VELO. (FT/SEC)
0.125	0.185	1.430	39.800	0.128	3.340	2.910
0.125	0.360	1.430	39.800	0.189	3.960	3.460
0.125	0.527	1.430	39.800	0.250	4.630	4.120
0.177	0.185	1.430	39.800	0.180	2.540	2.000
0.177	0.360	1.430	39.800	0.220	3.910	3.310
0.177	0.527	1.430	39.800	0.262	4.700	4.090
0.252	0.185	1.430	39.800	0.179	3.390	2.670
0.252	0.360	1.430	39.800	0.238	4.050	3.280
0.125	0.185	1.260	50.200	0.167	3.080	2.640
0.125	0.360	1.260	50.200	0.216	4.150	3.630
0.125	0.527	1.260	50.200	0.235	4.740	4.110
0.177	0.185	1.260	50.200	0.174	3.500	2.930
0.177	0.360	1.260	50.200	0.210	4.320	3.650
0.177	0.527	1.260	50.200	0.248	5.070	4.330
0.252	0.185	1.260	50.200	0.144	2.590	1.830
0.252	0.360	1.260	50.200	0.194	4.090	3.280
0.125	0.185	1.000	72.800	0.117	3.110	2.675
0.125	0.527	1.000	72.800	0.136	4.310	3.830
0.125	0.854	1.000	72.800	0.252	4.760	4.240
0.177	0.185	1.000	72.800	0.125	3.340	2.857
0.177	0.854	1.000	72.800	0.253	5.150	4.610
0.252	0.854	1.000	72.800	0.253	5.850	5.210
0.312	0.527	1.000	72.800	0.181	5.300	4.600
0.312	0.854	1.000	72.800	0.263	5.950	5.220
0.335	0.527	1.000	72.800	0.175	5.560	4.850
0.125	0.185	2.370	72.900	0.156	3.200	2.820
0.125	0.360	2.370	72.900	0.219	5.640	5.260
0.125	0.527	2.370	72.900	0.259	6.710	6.280
0.174	0.185	2.370	72.900	0.172	3.440	2.980
0.174	0.360	2.370	72.900	0.225	4.910	4.420
0.174	0.527	2.370	72.900	0.241	6.700	6.170
0.246	0.185	2.370	72.900	0.170	3.760	3.220
0.246	0.360	2.370	72.900	0.220	5.220	4.650
0.246	0.527	2.370	72.900	0.262	5.890	5.320
0.174	0.046	7.600	75.900	0.143	2.600	2.260
0.174	0.185	7.600	75.900	0.185	4.700	2.790
0.174	0.360	7.600	75.900	0.214	3.170	4.300
0.174	0.527	7.600	75.900	0.290	6.710	6.280
0.265	0.046	7.600	75.900	0.135	2.460	1.960
0.265	0.185	7.600	75.900	0.195	3.140	2.610
0.265	0.360	7.600	75.900	0.252	4.910	4.360
0.307	0.185	7.600	75.900	0.182	3.890	3.310
0.307	0.360	7.600	75.900	0.249	5.490	4.900
0.125	0.046	13.000	73.000	0.128	2.860	2.590
0.125	0.092	13.000	73.000	0.140	3.210	2.930
0.125	0.185	13.000	73.000	0.164	3.930	3.050

0.125	0.360	13.000	73.000	0.225	4.540	4.240
0.125	0.527	13.000	73.000	0.241	5.760	5.440
0.177	0.185	13.000	73.000	0.204	3.670	3.300
0.177	0.360	13.000	73.000	0.234	3.940	3.540
0.177	0.527	13.000	73.000	0.269	5.010	4.580
0.218	0.185	13.000	73.000	0.185	3.540	3.120
0.218	0.360	13.000	73.000	0.244	4.460	3.990
0.252	0.185	13.000	73.000	0.210	3.410	2.970
0.252	0.360	13.000	73.000	0.220	4.150	3.700
0.252	0.527	13.000	73.000	0.243	6.160	5.700
0.286	0.360	13.000	73.000	0.226	5.620	5.090
0.125	0.185	70.000	73.800	0.151	3.140	2.900
0.125	0.360	70.000	73.800	0.175	4.230	3.990
0.177	0.046	70.000	73.800	0.155	2.690	2.420
0.177	0.092	70.000	73.800	0.180	2.790	2.520
0.177	0.185	70.000	73.800	0.189	2.980	2.680
0.177	0.360	70.000	73.800	0.249	3.590	3.250
0.218	0.046	70.000	73.800	0.134	2.540	2.230
0.218	0.092	70.000	73.800	0.143	2.960	2.650
0.218	0.185	70.000	73.800	0.191	4.420	4.070
0.218	0.290	70.000	73.800	0.218	4.730	4.370
0.252	0.046	70.000	73.800	0.130	3.240	3.130
0.252	0.092	70.000	73.800	0.142	3.480	3.130
0.252	0.138	70.000	73.800	0.163	3.670	3.300
0.286	0.046	70.000	73.800	0.122	2.530	2.160
0.286	0.092	70.000	73.800	0.139	3.030	2.650

BIBLIOGRAPHY

1. Adlington,D.,and Thompson,E.,(1965),"Desulphurization in Fixed and Fluidized Bed Catalyst Systems.", Proc. 3rd. European Symp. React. Eng., 203-210
2. Afschar, A.S.,and Schügerl, K.,(1968),"Eigmschaften von Dreiphasen-Fließbetten mit Gleichstrom von Wasser und Luft.", Chem. Eng. Sci., 23, 267-278
3. Angelino, H.,(1966),"Hydrodynamique des grosses bulles dans les liquides Visqueux.", Chem. Eng. Sci.,21, 541-550
4. Bailey,A.E.,(1951),"Encyclopedia of Chemical Technology.", 1st. ed., Vol. 6, P. 140, Wiely (interscience), New York
5. Bankoff, S.G.,(1960),"A Variable Density Single-Fluid Model for Two Phase Flow with Particular Reference to Steam-Water Flow.", Trans. Amer. Soc. Mech. Engrs. C82, 265-272
6. Bhaga,D.,and Weber,M.E.,(1972),"Hold-up in Vertical Two and Three Phase Flow.", Can. J. Chem. Eng., 50, 323-336
7. Bhatia,V.K.,Evans,K.A., and Epstein,N.,(1972),"Effect of Solid Wettability on Expansion of Gas-Liquid Fluidized Beds.", Ind. Eng. Chem. Process Des. Develop., 11, 151-152
8. Bhatia,V.K.,and Epstein, N.,(1973),"Three Phase Fluidization: A Generalized Wake Model.", Presented at Int. Symp. on Fluidization, Toulouse, France
9. Bhatia, V.K.,(1972),"Hold-up Studies in Three Phase Fluidized Beds.", Ph.D. Thesis, Univ. of British Columbia
10. Cairns,E.J., and Prausnitz,J.M.,(1960),"Longitudinal

Mixing in Fluidization.", A.I.Ch.E.J., 6, 400-405

11. Calderbank,P.H., Moo-Young,M.B., and Ribby,R.,(1965), "Coalescence in Bubble Reactors and Absorbers.", Proc. 3rd European Symp. React. Eng., 91-113
12. Chervenak, M.C.,Johanson,C.A.,Johnson,C.A.,Schuman,S.C., and Sze,M.,(1960),"H-Oil process promises to improve quality of Distillate Feed.", Oil Gas J., 58, 80-87
13. Chervenak, M.C.,Wolk,R.,Byrd,C.R.,Hellwig,L.R.,and Van Driesen,R.P.,(1963),"Hy-C Cracking.", Chem. Eng. Progr., 59, 53-59
14. Chervenak,M.C.,Feigelman,S.,Wolk,R.,Byrd,C.R., and Gellwig, L.R.,(1963),"Hy-C Cracking: a new hydrocracking process.", Oil Gas J., 14, 227-230
15. Dakshinamurty,P.,Scbrahamanyam,V., and Rao,J.N.,(1971), "Bed Prosities in Liquid-Gas Fluidization.", Ind. Eng. Chem. Process Des. Develop., 10, 322-328
16. Dakshinamurty,P.,Rao,K.V.,Subbaraju,R.V., and Subrahmanyam, V.,(1972),"Bed Porosities in Gas-Liquid Fluidization.", Ind. Eng. Chem. Process Des. Develop., 11, 318-319
17. Dakshinamurty,P.,Chiranjevi,C.,Subrahmanyam,V.,and Rao, P.K.,(1973),"Studies of Gas-Liquid Mass Transfer in Gas-Liquid Fluidized Beds.", Presented at Int. Symp. on Fluidization, Toulouse, France
18. Davenport,W.G.,Richardson,F.D.,and Bradshaw,A.V.,(1967), "Spherical cap Bubbles in low Density Liquids.", Chem. Eng. Sci., , 1221-1234

19. Davies, R.M.,and Taylor, Sir Geoffrey,(1950),"The Mechanics of large Bubbles rising through extended liquids and through liquids in tubes.", Proc. Roy.Soc.A, 200, 375-390

20. Diboun,M.,and Schügerl,K.,(1967),"Eine Blasensaüle mit Gleichstrom von Wasser und Luft-II-Mischungsvorgange in der Flussigkeitsphase.", Chem. Eng. Sci., 22, 161-169

21. Douglas,W.J.M.,(1964),"Heat and Mass transfer in a Turbulent Bed Contactor.", Chem. Eng. Progr., 60, 66-71

22. Douglas,H.R.,Snider,I.W.A.,and Thomlinson,G.H.,(1963), "The Turbulent Contact Absorber.", Chem. Eng.Progr., 59, 85-89

23. Efremov,G.I., and Vakhrushev,I.V.,(1970),"A Study of the Hydrodynamics of Three Phase Fluidized Beds.", Int. Chem. Eng., 10, 37-41

24. Glasstone,S.,(1960),"Text Book of Physical Chemistry.", 2nd. Edit., Macmillan, London

25. Griffith,P., and Wallis,G.B.,(1961),"Two Phase Slug Flow.", Trans. Amer. Soc. Mech. Engrs., Heat transfer, 83, Ser.C, 307-320

26. Griswold,C.R.,and Van Driesen,R.P.,(1966),"Commercial Experience With H-Oil.", Hydrocarbon Proc., 45, 153-158

27. Hanratty,T.J.,Latinen,G.,and Wilhelm,R.H.,(1956), "Turbulent Diffusion in Particulately Fluidized Beds of Particles.", A.I.Ch.E.J., 2, 372-380

28. Karolyi,J.,Zalai,A.,Birthler,R.,and Spitzner,H.,(1963), "Results of the Second Large Scale Test of the Varga Process.", Int. Chem. Eng., 3, 597-603

29. Kim, S.D., Baker,C.G.J., and Bergougnou,M.A.,(1972), "Hold-up and Axial Mixing Characteristics of Two and Three Phase Fluidized Beds.", Can. J. Chem. Eng., 50, 6, 695-701

30. Kunii, D., and Levenspiel,O.,(1969),"Fluidization Engineering.", Wiely & Sons Inc., New York

31. Letan,R., and Elgin,J.C.,(1972),"Fluid Mixing in Particulate Fluidized Beds.", Chem. Eng. J., 3, 136-144

32. Leva, M.,(1959), "Fluidization.", McGraw Hill, New York

33. Massimilla, L.,Solimando,A.,and Squillace, E.,(1961), "Gas Dispersion in Solid-Liquid Fluidized Beds.", Brit. Chem. Eng., 6, 232-239

34. Massimilla,L.,Majuri,N.,and Signorini,P.,(1959), "Gas Absorption in Solid-Liquid Fluidized Systems.", Ricerca Sci., 29, 1934-1940

35. Metzner,A.B., and Reed,J.C.,(1955),"Flow of Non-Newtonian Fluids-Correlation of the Larminar,Transition, and Turbulent Flow Regions.", A.I.Ch.E.J., 1, 434-440

36. Michelson,M.L.,and Østergaard,K.,(1968),"Hold-up and Axial Dispersion in Liquid-Gas Fluidized Beds.", Preprint 31d, 2nd Joint A.I.Ch.E.-I.I.Q.P.R. Meeting, Chem. Eng. Progr. Series.

37. Michelson,M.L.,and Østergaard, K.,(1970),"Hold-up and Fluid Mixing in Gas-Liquid Fluidized Beds.", Chem. Eng. J., 1, 37-46

38. Nicklin,D.J.,(1962),"Two Phase Bubble Flow.", Chem. Eng. Sci., 17, 693-702

39. Ohki, Y., and Inoue, H.,(1970), "Longitudinal Mixing of the Liquid Phase in Bubble Columns.", Chem. Eng. Sci., 25, 1-16

40. Østergaard, K.,(1971), "Three Phase Fluidization.", Fluidization, Chapter 18, Wiely & Sons Inc., New York

41. Østergard, K.,(1968), Advances in Chemical Engineering, 7, 71-137, Academic Press, New York

42. Østergaard, K.,(1966), "On the Growth of Air Bubbles formed at A Single Orifice in A Water Fluidized Bed.", Chem. Eng. Sci., 21, 470-472

43. Østergaard,K.,and Theisen,P.I.,(1966),"The effect of Particle Size and Bed Height on the Expansion of Mixed Phase (gas-liquid) Fluidized Beds.", Chem. Eng. Sci., 21, 413-417

44. Østergaard, K.,(1965), "On Bed Porosity in Gas-Liquid Fluidization.", Chem. Eng. Sci., 20, 165-167

45. Østergaard,K., and Suchozebrski,W.,(1969),"Gas-Liquid Mass Transfer in Gas-Liquid Fluidized Beds.", Proc. 4th European Symp. Chem. React. Eng., Pergamon Press, 21-29

46. Østergaard,K., and Fosbøl,P.,(1972),"Transfer of Oxygen Across the Gas-Liquid Interface in Gas-Liquid Fluidized Beds.", Chem. Eng. J., 3, 105-111

47. Østergaard, K.,(1964), In "Fluidization.", 58-60, Soc. Chem. Ind., London

48. Page, R.E., and Harrison, D.,(1972),"The Size Distribution of Gas Bubbles Leaving A Three Phase Fluidized Bed.",

Powder Technol., 6, 245-249

49. Perry, J.H.,(1963),"Chemical Engineers' Handbook.", McGraw Hill, New York

50. Razumov,I.M.,Manshilin,V.V.,and Nemets,L.L.,(1973), "The Structure of Three Phase Fluidized Beds.", Int. Chem. Eng., 13, 57-61

51. Richardson, J.F.,and Zaki, W.N.,(1954), "Sedimentation and Fluidization:Part I.", Trans. Instn. Chem. Engrs., 32, 35-51

52. Rigby,G.R.,Van Blockland,G.P.,Park, W:H.,and Capes,C.E., (1970), "Properties of Bubbles in Three Phase Fluidized Beds as measured by an Electroresistivity Probe.", Chem. Eng. Sci., 25, 1729-1741

53. Rigby, G.R.,and Capes, C.E.,(1970),"Bed Expansion and Bubble Wakes in Three Phase Fluidized Beds.", Can. J. Chem. Eng., 48, 343-348

54. Sater,V.E., and Levenspiel, O.,(1966),"Two Phase Flow in Paked Beds.", Ind. Eng. Chem. Fund., 5, 86-92

55. Schügerl, K.,(1967),"Experimental Comparison of Mixing Processes in Two and Three Phase Fluidized Beds.",Proc. Intern. Symp. on Fluidization, Netherland Univ. Press, Amsterdam, 782-794

56. Schuman, S.C.,(1961), "Hydrogen Consumption in the H-Oil Process.", Chem. Eng. Progr., 57, 49-54

57. Sherrard,A.J.,(1966), "Three Phase Fluidized Beds.", Ph.D. Thesis, University of College of Swansea

58. Simpson,H.C.,and Rodger,B.W.,(1962),"The Fluidization of light solids by Gases under Pressure and heavy solids by Water.", Chem. Eng. Sci., 16, 153-180

59. Stewart,P.S.B.,and Davidson,J.F.,(1964), "Three Phase Fluidization: Water, Particles and Air.", Chem. Eng. Sci., 19, 319-322

60. Turner, R.,(1964),"Fluidization in the Petroleum Industry.", In Fluidization, Soc. Chem. Ind. London, 47-61

61. Vail, Yu. K.,Manakov,N.Kh.,and Manshilin,V.V.,(1970), "The Gas Content of Three Phase Fluidized Beds.", Int. Chem. Eng., 10, 244-247

62. Vail,Yu.K.,Manakov,N.kh.,and Manshilin,V.V.,(1968), "Turbulent Mixing in A Three Phase Bed.", Int. Chem. Eng., 8, 293-296

63. Van Deemter,J.J.,(1965),"Trickle Hydrosulphrization-A case History.", Proc. 3rd European Symp. React. Eng., 215-223

64. Van der Laan, E.Th.,(1958),"Notes on the Diffusion Type Model for the Longitudinal Mixing in Flow.", Chem. Eng. Sci., 7, 187-191

65. Van Driesen, R.P.,and Stewart,N.C.,(1964),"How Cities Service's H-Oil Unit in Performing.", Oil Gas J.,62, 20, 100-105

66. Viswanathan,S.,Kaker,A.S.,and Murti,P.S.,(1965), "Effect of Dispersing Bubbles into Liquid Fluidized Beds on Heat Transfer and Hold-up at Constant Bed Expansion.",

Chem. Eng. Sci., 20, 903-910

67. Volpicelli,G.,and Massimilla,L.,(1965),"Application of Three Phase Fluidization to Calcium Bisulphite Acid Production.", Pulp Paper Mag. Can., 66, T512-T514

68. Volpicelli,G., and Massimilla,L.,(1970),"Three Phase Fluidized Bed Reactors An Application to the Production of Calcium Bisulphite Acid Solutions.", Chem. Eng. Sci., 25, 1361-1373

69. Vukovic,D.V.,Zdanski,F.K.,and Tunjak,G.V.,(1973), "The Three Phase Spouted Bed - A New System in Chemical Engineering Processing.", Presented at the 75th AIChE Meeting, Detroit

70. Wallis, G.B.,(1969),"One-Dimensional Two Phase Flow.", McGraw Hill, New York

71. Wilhelm,R.H.,and Kwauk,M.,(1948),"Fluidization of Solid Particles.", Chem. Eng. Progr., 44, 201-218